



**UNIVERSITÀ
DEGLI STUDI
DI TRIESTE**

UNIVERSITÀ DEGLI STUDI DI TRIESTE

**XXXIII CICLO DEL DOTTORATO DI RICERCA IN
NANOTECNOLOGIE**

**THERMORESPONSIVE CHITOSAN AND POLY-N-
VINYLCAPROLACTAM MICROGELS FOR DRUG
EMBEDDED CHEMOEMBOLIZATION**

Settore scientifico-disciplinare: CHIM/02

DOTTORANDO / A

LORENZO MARSILI

COORDINATORE

ALBERTO MORGANTE

SUPERVISORE DI TESI

DOTT. GIUSEPPE TOFFOLI

ANNO ACCADEMICO 2020/2021

Abstract	7
Sommario	10
Abbreviation list	13
Chapter 1: Introduction	17
1.1 Nanotechnology: a multidisciplinary approach	19
1.2 The reproducibility crisis	20
1.3 Biocompatible polymers	23
1.4 Synthetic polymers as biomaterials	26
1.5 Thermoresponsivity	27
1.6 Thermoresponsive polymers for biomedical applications	34
1.7 The determination of LCST	39
1.8 Poly-N-Vinyl caprolactam	44
1.9 Polysaccharides: natural biocompatible polymers	47
1.10 Chitosan	50
1.11 Microgels: polymeric microparticles	53
1.12 Ionotropic gelation	58
1.13 Chitosan-Poly-N-Vinylcaprolactam (CP) microgels	63
1.14 The interaction between doxorubicin and chitosan	72
1.15 Chemoembolization	75
Chapter 2: My project	78
2.1 Initial aim of the project	78
2.2 Development of the project	79
2.3 Brief overview of the thesis	81
Chapter 3: Synthesis and characterization of PNVCL-COOH polymers	83
3.1 Spectroscopic characterization	84
3.2 Determination of -COOH end groups	89
3.3 Analysis of the thermoresponsive behaviour	90

3.3.1	Spectroscopic determination of LCST	90
3.3.2	Scattering determination of LCST	92
3.4	Molecular weight determination.....	93
3.4.1	Size exclusion chromatography	93
3.4.2	Dynamic light scattering	94
3.4.3	Viscosimetry	96
3.5	Differential Scanning Calorimetry	98
3.5	Summary	99
Chapter 4: Characterization of chitosan		100
4.1	NMR characterization	100
4.2	Viscosimetric determination of the molecular weight.....	101
4.3	X-ray diffraction analysis	103
4.4	Summary	104
Chapter 5: Synthesis and characterization of Chitosan-g-Poly-N-Vinylcaprolactam polymers		104
5.1	Spectroscopic characterization	105
5.2	Estimation of the degree of substitution.....	109
5.3	Analysis of the thermoresponsive behaviour.....	110
5.4	Summary	112
Chapter 6: Preparation and characterization of chitosan microgels.....		113
6.1	Preparation and optimization.....	113
6.1.1	Effect of polymer concentration.....	113
6.1.2	Effect of molecular weight and DDA	114
6.1.3	Effect of CS/TPP mass ratio	114
6.1.4	Effect of temperature	115
6.1.5	Effect of NaCl concentration	116
6.1.6	Optimization of DLS measurements.....	117
6.2	Nanoparticle tracking analysis	118
6.3	Purification method	119
6.4	pH-responsivity	123
6.5	Summary	124
Chapter 7: Preparation of chitosan-grafted-poly-N-vinylcaprolactam microgels.....		124
7.1	Preparation and optimization.....	124

7.1.1	Evolution of particle formation.....	126
7.1.2	Particle purification.....	129
7.1.3	pH stability.....	129
7.2	Particle storage	130
7.2.1	Lyophilization.....	131
7.3	Nanoparticle tracking analysis	134
7.4	Transmission electron microscopy	135
7.5	Thermoresponsive behaviour	136
7.6	Summary	140
Chapter 8: Preparation and characterization of thermoresponsive magnetic microgels		141
8.1	Preparation and characterization of iron oxide magnetic nanoparticles	141
8.2	Preparation and characterization of CP magnetic nanoparticles.....	144
8.3	Summary	145
Chapter 9: DOX loading and release.....		146
9.1	Encapsulation of DOX	146
9.1.1	Thermoinduced drug encapsulation	150
9.2	DOX release and uptake.....	150
9.2.1	Cumulative release and uptake	150
9.2.2	DOX release and uptake	152
9.3	Summary	155
Chapter 10: Assessment of biocompatibility.....		156
10.1	Determination of LCST in plasma	156
10.2	In-vitro cytotoxicity assays	158
10.2.1	MTT test	159
10.2.2	Cell-Titer	160
10.2.3	Immunofluorescence	161
10.4	Summary	163
Chapter 11: Materials and methods		163
11.1	Materials.....	163
11.2	Preparation protocols.....	164
11.2.1	Recrystallization of AIBN	164
11.2.2	Synthesis of PNVCL-COOH.....	165
11.2.3	Synthesis of Chitosan-g-PNVCL (CP)	165

11.2.3	Preparation of Fe ₃ O ₄ magnetic nanoparticles (MNPs)	166
11.2.4	Preparation of CP and CS microgels via ionotropic gelation	166
11.3	Methods.....	166
11.3.1	UV-Visible spectroscopy.....	166
11.3.2	Fluorescence spectroscopy	166
11.3.3	Calibration of DOX measurements.....	167
11.3.3	UV-VIS determination of LCST	167
11.3.4	DLS determination of LCST/VPTT	167
11.3.5	Temperature dependent DOX release and uptake.....	168
11.3.6	FT-IR spectroscopy	169
11.3.7	NMR spectroscopy	169
11.3.8	Size exclusion chromatography	170
11.3.9	Viscosimetry	171
11.3.10	X-Ray Diffraction (XRD).....	172
11.3.11	Differential Scanning Calorimetry (DSC)	172
11.3.12	Dynamic Light Scattering (DLS).....	172
11.3.13	Zeta potential	175
11.3.14	Nanoparticle tracking analysis (NTA).....	175
11.3.15	MTT test	176
11.3.16	Cell Titer.....	177
11.3.17	Immunofluorescence	178
11.3.18	Optical microscopy.....	178
11.3.19	Fluorescence microscopy.....	179
11.3.20	Transmission electron microscopy	179
Chapter 12: Conclusions		179
Appendices		182
I:	Free radical polymerization of PNVCL	182
II:	Polymer conjugation with EDC/NHS	185
III:	Mathematical models for drug release.....	186
III.I	Zero order kinetics	186
III.II	First order kinetics	187
III.III	Higuchi model	187
III.IV	Korsmeyer-Peppas model	188
III.V	Double exponential models.....	188
References.....		190

Alle mie nonne, Fiorella e Silvana

Abstract

Transarterial chemoembolization is a common procedure for the treatment hepatocellular carcinoma. During the treatment, chemotherapy drugs are injected into a blood vessel feeding the tumour with the addition of an embolic agent that blocks blood flow. This prevents the rapid washout of the drug, leading to higher locoregional concentrations, which increases efficacy and reduces toxicity. In recent times, the treatment has been improved by the utilization of microparticles that interacts with the drug with ionic bonds. This relatively new approach, called drug-eluting beads transarterial chemoembolization, increases the exposure of the tumour to the drug and decreases toxicity due to reduced systemic drug circulation¹⁻⁵. With the advent of nanotechnologies, scientist have pointed out that the utilization of sub-micrometric particles may result in less invasive therapies for the treatment of advanced tumours⁶. In the present thesis, we describe the design of a chitosan-*grafted*-Poly-N-Vinylcaprolactam polymeric nanostructured responsive system for transarterial chemoembolization for the treatment of hepatocellular carcinoma. Specifically, the aim of this study was the fabrication of sub-micrometric chitosan thermoresponsive particles (microgels) with a size around 200 nm for the release of doxorubicin. Thermoresponsive microgels were fabricated by using a copolymer of chitosan-N-*grafted*-poly-vinylcaprolactam and microgels were designed in order to undergo a critical change in size and conformation in a range of temperature between 37 and 42 °C. Chitosan was selected as a model polymer due to its biodegradability, non-toxicity, tissue-adhesive activity and drug permeation enhancing capability. Poly-N-Vinylcaprolactam is a non-ionic, biocompatible and non-adhesive polymer that has a lower critical solution temperature between 25 and 50 °C^{7,8}. In the first part of the study (chapter 3), a special focus was devoted to the characterization of poly-N-vinylcaprolactam thermoresponsive behaviour, by assessing how the lower critical solution temperature is affected by environmental and structural factors such as salinity, pH, polymer concentration and molecular mass by synthesizing and characterizing a series of poly-N-vinylcaprolactam with different chain length using free radical polymerization. The structure of the polymers was characterized using nuclear magnetic resonance, infrared spectroscopy and conductimetric titration and the polymers exhibited lower critical solution temperature between 33 and 42 °C. Molecular mass determination showed that the lower solution temperature diminishes as the molecular mass increases. Furthermore, the results demonstrated that ionic environment has a stronger effect in relation to the pH of

the solution. In the following section (chapter 5), poly-N-vinylcaprolactam were grafted on two different type of chitosan and the lower critical solution temperature of the resulting copolymers were related with the ratio between the two polymers, the molecular mass and degree of deacetylation. This allowed to select chitosan-N-*grafted*-poly-vinylcaprolactam with a lower critical solution temperature between 37 and 42 °C for the fabrication of thermoresponsive microgels. Microgels were fabricated using ionotropic gelation, using tripolyphosphate as an anionic cross-linker. Formulations were characterized in terms of size distribution and surface charge and their storage stabilities were examined. Microgels preparation was optimized in terms of several parameters, including pH, concentration, and polymer/linker ratio. Chitosan-N-*grafted*-poly-vinylcaprolactam microgels exhibited an average diameter between 110 and 180 nm and surface charge between 10 and 25 mV. Their thermoresponsive behaviour was studied using dynamic light scattering. Upon heating, chitosan-N-*grafted*-poly-vinylcaprolactam microgels were able to grow into bigger particles in a reversible way at a specific volume phase transition temperature. In chapter 8, we evaluated the preparation of dual-responsive magneto- and thermoresponsive microgels for the fabrication of a remote-triggered delivery device. Fe₃O₄ magnetic nanoparticles were synthesized and encapsulated by dissolving them with tripolyphosphate during ionotropic gelation. Transmission electron micrographs demonstrated that magnetic nanoparticles were encapsulated, but the formulations exhibited poor stability. In chapter 9, release and uptake of doxorubicin is discussed. Release test showed that the loading of doxorubicin can be achieved by incubating chitosan-N-*grafted*-poly-vinylcaprolactam microgels with doxorubicin for a few hours above their critical volume phase transition temperature, which also resulted in particle aggregation. Finally, a preliminary evaluation of the cytotoxicity of CP microgels and the synthesized polymers is provided in chapter 10. The tests (MTT, Cell Titer, immunofluorescence) were performed *in-vitro* on human carcinoma cell lines (HUH7) and showed mild toxicity. This confirmed the importance of the screening of the behavior of poly-N-vinylcaprolactam based polymers due to the dependence of critical temperatures towards environmental factors (pH, types of ions dissolved in the solution and polymer concentration). In another experiment, the lower solution temperature of poly-N-vinylcaprolactam was measured in human plasma and resulted in the lowering of the LCST by about 10°C. Accordingly, the lowering the lower critical solution temperature may diminish biocompatibility in biologically relevant environments. Similarly, the utilization of aggregated doxorubicin-loaded chitosan-N-*grafted*-poly-vinylcaprolactam gels resulted in a significant increase in drug toxicity. In

conclusion, in the present thesis, we described the development of a protocol for the fabrication of chitosan-*N-grafted*-poly-vinylcaprolactam thermoresponsive microgels and we evaluated the encapsulation of doxorubicin for the treatment of hepatocellular carcinoma with transarterial chemoembolization. We demonstrated that microgels undergo a reversible thermoinduced transition which is concentration dependent, but the weak interaction between chitosan and doxorubicine did not allow drug encapsulation. Since doxorubicin encapsulation was achieved within aggregated Chitosan-*N-grafted*-poly-vinylcaprolactam gels, the low stability of magnetic microgels does not necessarily represent a limitation for the fabrication of magnetoresponse micrometric doxorubicin-eluting microparticles. Thus, we provided evidence that the proposed thermoresponsive microgel could be used for a type of drug-eluting beads based on the release of doxorubicin by exposing them to alternating magnetic fields.

Sommario

La chemioembolizzazione arteriosa rappresenta una procedura comune per il trattamento del carcinoma epatocellulare nel quale un chemioterapico viene iniettato in un vaso sanguigno collegato al tumore con l'aggiunta di un agente embolico che blocca il flusso di sangue. Questo impedisce l'eliminazione rapida del farmaco e ne aumenta la concentrazione a livello locoregionale, diminuendone l'efficacia e riducendone la tossicità. In tempi recenti, il trattamento è stato migliorato mediante l'utilizzo di microparticelle emboliche in grado di interagire col farmaco tramite legami ionici. Questa terapia relativamente innovativa, chiamata DEB-TACE, permette di aumentare l'esposizione del tumore e diminuirne la tossicità, riducendone la concentrazione nella circolazione sistemica. Con l'avvento delle nanotecnologie, alcuni scienziati hanno osservato che l'utilizzo di particelle sub-micrometriche potrebbe essere in grado di offrire terapie meno invasive per il trattamento del carcinoma epatocellulare in stato avanzato. Nella presente tesi viene descritto lo sviluppo di sistemi polimerici termoresponsivi nanostrutturati per la chemoembolizzazione arteriosa a base di chitosano-*graft*-poli-N-vinilcaprolattame. In particolare, l'obiettivo di questo studio è stato quello di fabbricare particelle sub-micrometriche (microgels) a base di chitosano circa 200 nm per il rilascio di doxorubicina. I microgels termoresponsivi sono stati fabbricati usando dei copolimeri di chitosano-*graft*-poli-N-vinilcaprolattame ed i microgels sono stati ottimizzati in modo da esibire un cambio conformazionale e dimensionale in un intervallo di temperatura compreso tra 37 e 42 °C. Il chitosano è stato scelto come modello per la fabbricazione di microgels per le caratteristiche di biodegradabilità, non tossicità, adesività ai tessuti. Il poli-N-vinilcaprolattame è un polimero non ionico, biocompatibile e non adesivo che ha la peculiarità di esibire una temperatura inferiore di miscibilità in acqua (LCST) compreso tra 25 e 50 °C. Nella prima parte dello studio (capitolo 3), un'attenzione particolare è stata dedicata alla caratterizzazione del comportamento termoresponsivo dei polimeri di poli-N-vinilcaprolattame, verificando come la LCST viene influenzata da fattori ambientali e strutturali quali salinità, pH, concentrazione del polimero e massa molecolare sintetizzando e caratterizzando una serie di poli-N-vinilcaprolattame con diversa massa molecolare mediante sintesi radicalica libera. Tutti i polimeri sono stati caratterizzati utilizzando spettroscopia NMR, FT-IR e titolazione conduttimetrica e la LCST dei polimeri è stata osservata tra i 33 ed i 42 °C. La determinazione della massa molecolare ha dimostrato che la LCST diminuisce all'aumentare della massa molecolare. Inoltre, i risultati hanno

dimostrato che l'ambiente ionico ha un'influenza molto più marcata rispetto al pH delle soluzioni. Nella sezione successiva (capitolo 5), i polimeri di poli-N-vinilcaprolattame sono stati grafitati su due tipi differenti di polimeri di chitosano e la LCST delle soluzioni di copolimero è stata relazionata al rapporto tra i due polimeri, alla massa molecolare ed al grado di deacetilazione. Ciò ha permesso di selezionare i polimeri di chitosano-N-graft-poli-N-vinilcaprolattame con una LCST compresa tra 37 e 42 °C per la fabbricazione dei microgels termoresponsivi. I microgels sono stati preparati mediante gelazione ionotropica, utilizzando il TPP come linker polianionico. Le formulazioni sono state caratterizzate in termini di distribuzione dimensionale, morfologia e capacità di conservazione, e la loro produzione è stata ottimizzata in relazione a condizioni di pH, concentrazione e rapporto polimero/linker. Le formulazioni di CP mostrano un diametro medio di circa 110-180 nm ed una carica superficiale tra 10 e 15 mV. Il comportamento termoresponsivo è stato caratterizzato utilizzando il DLS. Riscaldando le sospensioni acquose, i microgels sono in grado di aumentare la loro dimensione ad una specifica temperatura di transizione volumetrica (VPTT). I test effettuati hanno dimostrato che la transizione è reversibile. Nel capitolo 8, è stata valutata la possibilità di preparare dei microgels a doppia responsività, magneto e termoresponsivi, per la fabbricazione di un dispositivo di rilascio controllabile da remoto. Le nanoparticelle di Fe₃O₄ magnetiche sono state sintetizzate e disperse nella soluzione di tripolifosfato durante il processo di gelazione ionotropica. Le micrografie effettuate al TEM hanno confermato l'incapsulazione delle particelle magnetiche all'interno dei microgels, ma le sospensioni si sono mostrate instabili. Nel capitolo 9, è stato studiato il rilascio e l'uptake di doxorubicina da parte dei microgels. I test di rilascio effettuati hanno dimostrato che il loading di doxorubicina è possibile incubando i microgels di chitosano-graft-poli-N-vinilcaprolattame in una soluzione di doxorubicina alcune ore al di sopra della loro VPTT, in modo da indurre anche l'aggregazione dei microgels stessi. Infine, nel capitolo 10 viene fornita una valutazione preliminare della citotossicità dei microgels e dei polimeri sintetizzati. I test (MTT, Cell Titer, immunofluorescenza) sono stati effettuati in-vitro su linee cellulari di carcinoma umano (HUH7) ed hanno mostrato una tossicità lieve. Questo ha confermato l'importanza della verifica del comportamento dei polimeri a base di poli-N-vinilcaprolattame a causa della dipendenza della LCST di questi polimeri da fattori ambientali (pH, tipi di ioni presenti in soluzione e concentrazione di polimero). In un altro esperimento, la LCST del poli-N-vinilcaprolattame è stata misurata in plasma umano e la presenza del plasma ha portato alla riduzione della LCST del polimero di circa 10 °C. Di conseguenza, la riduzione della

LCST può diminuire la biocompatibilità in ambienti rilevanti dal punto di vista fisiologico. In modo simile, i microgels micrometrici aggregati caricati con doxorubicina sono in grado di aumentare significativamente la tossicità del farmaco. In conclusione, nella presente tesi viene descritto lo sviluppo di un protocollo per la fabbricazione di microgels di chitosano-*graft*-poli-N-vinilcaprolattame termoresponsivi ed è stata valutata la possibilità di incapsulare doxorubicina al loro interno per il trattamento del carcinoma epatocellulare mediante chemioembolizzazione arteriosa. È stato dimostrato che i microgels attraversano una transizione termoindotta in modo reversibile, e che la temperatura di tale transizione dipende dalla concentrazione dei microgels. Tuttavia, a causa delle deboli interazioni tra doxorubicina e chitosano, non è stato possibile caricare il farmaco all'interno dei microgels. Dal momento che la doxorubicina è in grado di entrare dentro ai microgels di chitosano-*graft*-poli-N-vinilcaprolattame in forma aggregata, la bassa stabilità dei microgels magnetici e termoresponsivi non rappresenta necessariamente una limitazione al loro utilizzo per applicazioni di DEB-TACE. In questo modo, abbiamo dimostrato che i modelli proposti di microgels termoresponsivi potrebbero essere utilizzati per applicazioni di DEB-TACE basati sul rilascio della doxorubicina attraverso l'esposizione ad un campo magnetico alternato.

Abbreviation list

+CS	HMC+ Chitosan
AIBN	2,2'-azobisisobutyronitrile
Ar	Argon
ATP	Adenosine triphosphate
CP	Chitosan-N-grafted-Poly-N-Vinylcaprolactam
CP-MAS	Cross Polarization/Magic Angle Spinning
CP NPs	Chitosan-N-grafted-Poly-N-Vinylcaprolactam microgels/nanogels
CRO	Centro di Riferimento Oncologico
CS	Chitosan
CT	Computed tomography
Da	Dalton
DDA	Degree of deacetylation
DEB-TACE	Drug-eluting beads transarterial chemoembolization
D _h	Hydrodynamic diameter
DLS	Dynamic light scattering
DLVO	Derjaguin–Landau–Verwey–Overbeek
DMEM	Dulbecco's Modified Eagle's Medium
DMF	N,N'-Dimethylformamide
DMSO	Dimethylsulfoxide
DOX	Doxorubicine
DSC	Differential Scanning Calorimetry
<i>e.g.</i>	<i>exempli gratia</i>
EDC	1-Ethyl-3-(3-dimethylaminopropyl)carbodiimide

EPR	Enhanced permeation and retention
Et	Ethyl
<i>et al.</i>	<i>et alii, et alia</i>
EtOH	Ethanol
FAL	Float-A-Lyzer™
FH	Flory-Huggins theory
FRP	Free radical polymerization
FT-IR	Fourier-Transmission Infrared Spectroscopy
g	grams
h	hour(s)
HCC	Hepatocellular carcinoma
HMW	High molecular weight
HP-DEC	High-power Decoupling
HP-SEC-TDA	High Performance Size Exclusion Chromatography Triple Detector Array
HUH7	Human hepatoma cell line
IF	Impact Factor
JHF	Journal Impact Factor
L	millilitre(s)
LCST	Lower critical solution temperature
LMW	Low molecular weight
MES	2-morpholin-4-ylethanesulfonic acid
MHS	Mark-Howink Sakurada
min	minute(s)
MNPs	Magnetic nanoparticles
mol	mole(s)

MPA	Mercaptopropionic acid
mPEG	Methyl poly(ethylene glycol)
MRI	Magnetic resonance imaging
MTT	3-(4,5-dimethylthiazol-2-yl)-2,5-diphenyltetrazolium bromide
MW	Molecular weight
MWCO	Molecular weight cut-off
M_{η}	Viscosimetric molecular mass
NHS	N-hydroxy succinimide
NMR	Nuclear magnetic resonance
NPs	Nanoparticles/microgels
NTA	Nanoparticle tracking analysis
NVCL	N-Vinyl Caprolactam
PBS	Phosphate-buffered saline
PDI	Polydispersity index
PEG	Poly(ethylene glycol)
PET	Positron emission tomography
PLGA	Poly(lactic-co-glycolic acid)
PMMA	Poly-methyl-methacrylate
PNIPAM	Poly-N-isopropylamide
PNVCL	Poly-N-vinylcaprolactam
R_g	Radius of gyration
R_h	Hydrodynamic radius
SAL	Slide-A-Lyzer™
SEC	Size exclusion chromatography
TACE	Transarterial chemoembolization

TEM	Transmission electron microscope/microscopy
THF	Tetrahydrofuran
TPP	Tripolyphosphate
TRITC	Tetramethylrhodamine
UCST	Upper critical solution temperature
UV-VIS	UV-Visible
V	Volt(s)
VPTT	Volume phase transition temperature
vs.	verses
XRD	X-Ray Diffraction
ζ	Zeta potential

Chapter 1: Introduction

A drug delivery system represents the method or the process in which a pharmaceutical compound is administered in order to achieve a therapeutic effect.⁹ There are different types of drugs, formulations and route of administration that span from traditional tablets to micro- and nanoparticle-based formulations. Nanoparticle formulations possess unique properties due to their large surface area, which bulk materials do not possess. Nanoparticles can be fabricated and engineered with different compositions, shapes, sizes and surface chemistry. In the drug delivery area, they have been used primarily to increase drug bioavailability, usually by increasing their solubility. The first nanostructured material that was used in drug delivery was poly(methyl methacrylate), in 1976.¹⁰ Since then, thousands of different studies about nanoparticle-based drug delivery systems have been published. According to their IUPAC definition, nanoparticles are defined as “particles with any shape with dimensions between 1 and 100 nm”, even though the term is commonly used for bigger particles¹¹. In general, nanoparticles comprehend all these particles that exhibit novel properties due to their reduced size, in comparison to bulk materials.¹² In oncological research, nanoparticles-based therapies have been developed for the treatment of carcinomas through a variety of methods of administration^{13–23}. Current research on nanoparticles for cancer diagnosis and application has established its advantages within contemporary oncology as well as its intrinsic limitations^{15,24–26}. As a consequence, though the astonishing technological progress made in the field of nanomedicine, standard oncological treatments still rely on conventional methods, such as surgery, radiotherapy and chemotherapy^{27–34}. To this date, clinical application of nanoparticles is still hindered by the lack of understanding of the mechanism of interaction between nanoparticles and the complex biological matrix and by the lack of trials and standardizations^{13,15,16,18,19,28,35–44}. The interest towards nano-based therapies in oncological research is to develop minimally invasive treatments that can enhance the selectivity towards tumour tissues. The utilization of metal and polymeric particles with well-defined size and shape may improve the process of drugs delivery, resulting in the reduction of the strong side effects associated with the utilization of chemotherapy drugs, such as vomiting^{45,46}, diarrhea^{47–49}, hair loss^{50–52} and weakening of the immune system^{34,53–58}. Due to their reduced size, nanoparticles have been considered ideal vectors for the release of drugs as they are theoretically able to accumulate in the tumour tissue by passing through the discontinuous epithelium of the tumour neovasculature^{59,60}. This phenomenon, called

“passive accumulation”, along with the lack of a proper lymphatic drainage into cancer tissues, led to the development of the “enhanced permeation and retention” effect^{37,39,61–66}, which is commonly found in literature but still controversial^{24,25,67}. A remarkable amount of in-vivo studies have outlined that these vectors are rapidly subjected to a metabolic fate depending on its size^{60,68–71} in the absence of an active targeting system, which recognizes a specific characteristic of the tumour^{59,72–74}, though active targeting doesn’t necessarily represent the best choice for tumour targeting⁶³. Most of the metal particles developed for theranostic purposes usually exhibit the interesting properties in a dimensional range inferior to 10 nm, since surface properties arise from the exponential increase of the number of surface atoms that occurs under a critical size threshold^{75–78}. However, due to their small size, these nanoparticles are rapidly disposed by the body of through the kidneys^{79–84}. In order to overcome these limitations, polymer particles and hydrogels have been extensively studied as they can provide biocompatible scaffolds for the application of nanoparticles^{85–87}. Polymeric systems have also been investigated for the possibility of creating “smart” drug delivery systems^{13,88–90} capable of responding to external stimuli such as variations in pH^{85,90–94}, temperature^{7,90,91,95–104}, magnetic fields^{20,84,98,105–109} and concentration.^{110–112} Some of these systems have proved to be particularly promising due to the possibility of providing drug and nanoparticles encapsulation along with the sensitivity for an external trigger.^{99,100,106,113} The application of such nanosized-smart systems is of particles interest as the development of dual-triggered therapies^{99,106,113,114} in a biocompatible fashion could provide the basis for new therapies with reduced toxicity and improve drug efficiency improvement. A better understanding on the behaviour of these systems is crucial in order to adapt them for the utilization in conventional cancer therapies. In the present thesis, we describe the design of a polymeric nanostructured responsive system for chemoembolization, which is a standard procedure for the treatment of liver cancer, or hepatocellular carcinoma (HCC)^{1,3,5}.

1.1 Nanotechnology: a multidisciplinary approach

Nanotechnologies utilize the physical, chemical, mechanical and optical properties that occur at the nanoscale, when the percentage of surface atoms is still relevant to define the final properties of the object under consideration⁷⁵⁻⁷⁸. Over the course of the twentieth century, this revolutionary approach has brought together experts within different scientific areas. In this way, the advent of the nanotechnologies allowed to create a common paradigm to different scientific areas and brought people from different fields to abandon some of the dogmas of their disciplines. To date, the figure of nanotechnologist refers person able to translate the phenomena of the nanoscale to applications that can bring benefits in the real world, without any reference to a specific scientific field of expertise. The nanotechnological approach is therefore, by definition, multidisciplinary. In the opinion of the writer, multidisciplinary is the only way that allows a branch of science to go beyond its intrinsic limits. To this day, we would never have been able to land a robot on Mars, or to photograph the farthest galaxies, or even to attempt spinal cord regeneration, had it not been through the cooperation of scientists who put aside their differences in terms of ethnicity, language and academic training. A multidisciplinary approach allows thousands of scientists around the globe to unite around the same purpose but, at the same time, it requires addition effort for efficient dissemination work. In this way, knowledges are passed from one discipline to another and, finally, they can be translated into competences. Nevertheless, this poses two fundamental problems. From the epistemological point of view, it is crucial to develop a common knowledge base which could be accessible to experts from different sectors. There is also a procedural problem, which consist of the development of a standardized approach in the applications of such knowledges in different fields. Every single scientific work has a history that has its own precise historical and geographical location, which results in a scientific paradigm that has been developed over decades of research by the individual institute or research group. A multidisciplinary approach can create problems when it is impossible to understand whether the approach of a discipline is suitable for the interpretation a certain behaviour or an experimental result. On the other hand, an excessive sectorialisation of individual scientific field can make it difficult to transmit important concepts from one discipline to another.

1.2 The reproducibility crisis

Entering the merits of the study of this thesis, this work is a collaboration between the oncological centre of Aviano (Centro di Riferimento Oncologico, C.R.O.) and the University of Trieste. The aim of this study is the development of a nanostructured system for the treatment of liver cancer, or hepatocellular carcinoma (HCC). For the development of this drug delivery system, our research started from the premises of *Indulekha et al.*^{91,93,96,99}, which combined the properties of two polymers with promising properties from the biological point of view: chitosan (CS), a polysaccharide of natural origin, and a thermoresponsive synthetic polymer, poly-N-Vinylcaprolactam (PNVCL). In view of the difficulties encountered in the first phase of this study, it was necessary to consider some aspects of basic thermodynamics characterizing the behaviour of these polymers, to which some subsequent sections of this introduction have been dedicated. The knowledge of some basic thermodynamic concepts is, in fact, fundamental to evaluate possible applications of thermoresponsive polymers in the biological field. As a matter of fact, the lack of consideration of the thermodynamic behaviour of the polymeric solutions inevitably leads to issues with standardization and reproducibility. In the following chapters of this introduction, a brief overview of the Flory-Huggins theory and its progressive modifications is provided, as it has a profound relationship on the theoretical premises of this study. At this point, it is appropriate to engage a reflection on scientific literature in order to understand the perspective that has been used within this work. Due to the sectorialisation of scientific journals and publications, it is common to assume that the reader already possesses the fundamentals of the discipline. In most publications, the introduction is usually dedicated to a “state of the art” that provides an overview of the most recent achievements rather than a dissertation of the fundamental concepts. According to this dynamic, over the course of the last 50 years, scientific literature has progressively moved further away from popular periodicals. This continuous process of sectorialisation has created an elite marked linked to the prestige of high-impact publications. From this point of view, the utilization of the journal impact factor (JIF) has had dramatic consequences on the scientific community, by creating a real race towards high-impact research fields. In a brilliant editorial from *Science*, may 2013, Bruce Alberts called this phenomenon “*me-too science*”¹¹⁵ and defined JIF as “*highly destructive*”, stating that it blocks innovation as it encourage researchers in working in popular areas of science, in which every article is expected to obtain a high number of citations independently from

its quality. Many other studies have already pointed out that the factor does not necessarily represent the scientific value or scientific publications¹¹⁶⁻¹¹⁹. In 2012, with the purpose of stopping the utilization the impact factor, the San Francisco declaration on research assessments (DORA), stated that impact factor must not be used as: *“a surrogate measure of the quality of individual research articles, to assess an individual scientist's contributions, or in hiring, promotion, or funding decisions.”*

Despite the importance of the DORA statement, the scientific community has been continuing using the JIF as a main parameter for decision of economic order. To date, the “impact factor production” is widely used to evaluate the activity of a department within a research institute. At the same time, due to the increase of the number of PhDs student interested in pursuing an academic career, the institutional pressure inside research University has been frequently described by the expression “publish or perish”. Consequently, the impact factor has become the criterion on which doctoral and academic courses, funding and hiring decision are based. In few cases, this phenomenon led to unexpected tragic consequences, as in the case of Norman Zarcone, the researcher whose loss has shocked the Italian academic system in 2009. As a phenomenon, the race for impact-factor, or “scientific hype”, it is very alike to the phenomena that created financial bubbles and the success of influencers on social networks. One way to visualize the scientific race for high-impact research fields is by using website databases such as Scopus, which show the exponential increase in the number of publications linked to a specific topic over the years, starting from 1988. The comparison between two widely studied topics in nanotechnology, such as “gold nanoparticles” and “graphene”, provides a good case in point. By the end of 2010, the year in which graphene was discovered, the word was already present in the title of 9543 publications. In the same year, “gold nanoparticles” were featured in 19’482 publications. Ten years later, the number of publications featuring the word “graphene” (172’529) in the title is about twice the number of publications featuring “gold nanoparticles” (85’746). However, these data are not necessarily representative of the goodness or the quality of these systems, nor of that of the publications, but they give a good picture of the current trend of scientific research. Statistically, in 2020, graphene studies have more possibilities of getting cited than papers about gold nanoparticles. Furthermore, the JHF factor system shows its fallacy when a study is frequently mentioned because of its misconceptions. Paradoxically, in this case, the JHF seems to reward those publications that fail in the rigorous application of the scientific method. Due to their low average JIF, scientific journals dedicated to polymeric

Chapter 1: Introduction

sciences are heavily penalized by this metrics and, therefore, they fall into the category of the "least reliable" regardless of the quality of the publications. The average JIF for polymer publications, calculated from a sample of 75 periodicals, is 2.806 (source: journal-if.com, Figure 1). In contrast, other science fields are characterized by higher average indexes, such as nanotechnology (5,079, calculated from 56 periodicals) or oncology (6.486; calculated from 196 periodicals, source: journal-if.com). Understandably, a researcher who devote his life to studying the thermodynamic behaviour of polymers cannot have the same career expectations in the research field in respect to an oncologist or a graphene specialist. From a gnoseological point of view, the impact does not necessarily represent an index of reliability. Since new and promising materials attract citations, citations enhance the IF and IF leads to

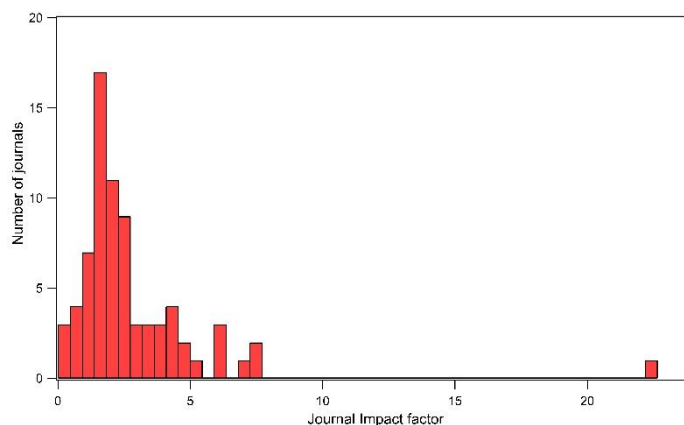


Figure 1 Journal impact factors for polymeric journals. Source: journal-if.com

funding. Consequently, the “me-too science” phenomenon has frequently buried the old scientific principle of “do not use what you do not know” in favour of “use what it is popular”. In the early 2010s, the term “replication crisis” or “reproducibility crisis” was introduced in psychology and in medicine to describe that many scientific studies are difficult or impossible to reproduce. The methodological crisis became evident when Nobel Prize in Chemistry Frances H. Arnold made the news announcing that she retracted a Science publication (JIF = 41.845) in 2019 due to the impossibility of reproducing the published work.

In the case of studies related to the utilization of polymeric materials in the biological or medical field, the issue of reproducibility is usually linked to little acquaintance with the chemical-physical laws that govern the behaviour of the materials. The difficulty of replicating the results of these works can be linked to the lack of information related to the morphology, the size, the length of the chain, the minority presence of a comonomer (e.g., CS and derivatives) etc. When dealing with such biases, the task of a scientist is to use an informative and interdisciplinary approach, in order to allow those unfamiliar with the subject to develop a critical sensitivity towards the matter. In this way, the transmitted knowledge will easily develop into a competence outside his own discipline. A question as

simple as: "what is a polymer" has an answer that is far from obvious. When setting up a polymeric study, it is mandatory to refer to the concept of "distribution" and "dispersity". The concept of monodispersed polymer, with unique and well-defined characteristics, is nothing but an abstract entity and the properties of a polymeric specimen cannot be described without resorting to statistics. Similarly, it is essential to refer to the appropriate characterization techniques, which allow to reduce the degree of uncertainty of the measurement of each of the macromolecular properties. Therefore, as scientists, we must not underestimate the importance of polymeric publications, even if they are penalized by the impact factor.

From an ethical point of view, every scientist should take responsibility for every single published work. According to this principle, a work that is not reproducible should not be published. However, this is incompatible with market demands for scientific publications. According to the ruthless reality of the "public or perish" paradigm, a less reliable work is usually published in a periodical with lower JIF. In this way, paradoxically, a decision that we could simply decide using our conscience is delegated to a number.

In the course of this work, we often found ourselves dealing with procedures that were difficult to reproduce. In other situation, we found conflicting information in the literature that we relied on. In the following chapters of this introduction, some theoretical concepts will be provided that will allow, in the following chapters, to get to the root of the problem and to relate our experimental data with those present in the literature.

1.3 Biocompatible polymers

From a physiological point of view, only few materials can be considered totally inert. Almost every known material contains different toxic components or irritating properties. A biomaterial is defined as a substance that can function as a part of a system that aims to treat or replace any tissue, organ or body function during a certain amount of time¹²⁰. Moreover, during the setting of such materials, harmful effects can be provided by chemical reaction¹²¹. Williams provides a useful definition of biocompatibility, which is:

“the ability of a biomaterial to perform its desired function with respect to a medical therapy, without eliciting any undesirable local or systemic effects in the recipient or beneficiary of that therapy, but generating the most appropriate beneficial cellular or tissue response to that specific situation, and optimizing the clinically relevant performance of that therapy¹²².”

Chapter 1: Introduction

The biocompatibility of a material is assessed by establishing the relationship between the material and the organism, so that neither of them produce undesirable effects. In order to accommodate a substance in the class of biomaterials, it has to satisfy various prerequisites, including biocompatibility. The verification of this feature implies that its components must undergo different testing procedures which are performed as recommended by different federations and organizations¹²³. In general, for the appropriate evaluation of experimental material, the safety for clinical application in humans is established throughout a sequence of research protocols that are described and regulated in many countries¹²⁰.

Considering that the term “biocompatibility” incorporates many different aspects, including its physical, chemical and mechanical properties, as well as potential allergenic, mutagenic and cytotoxic effects, these evaluation protocols involve different areas such as chemistry, biology, pharmaceuticals and include different studies ranging from virtual simulations to in vitro and in vivo assays to clinical trials¹²⁴. Most medical studies focus on the toxicity of degradation byproducts and the inflammatory reaction or immune response of the body when dealing with local implants or regional therapies. In the field of nanomedicine, surface properties such as roughness and surface energy are of major interest as they play a fundamental role in cell–material interactions since they define the pattern of adsorption onto the biological surface and their spatial orientation. Before the approval, it is of major importance to monitor the interaction between the biomaterial and the proteins present in physiological fluids, such as albumin, immunoglobulin, fibrinogen and fibronectin, that guide the inflammatory response.¹²⁵

Among biomaterials, there is a variety of polymers that can be used for biological and medical applications, including drug delivery scaffolds and replacement of tissues, which are referred as polymeric biomaterials.^{126–131} These polymers can be of synthetic or natural origin, and they behave mechanically in a way that resemble natural tissues.^{128–130,132} Natural polymers, such as polynucleotides, polypeptides and polysaccharides, are produced by living cells and are commonly used in medical applications as they allow for cellular adhesion and recognition, cell growth and differentiation¹³³. Nonetheless, their biological application is hindered by the lack of control over their properties, which are not easily modified with processing. Synthetic polymers, on the contrary, can be produced in an industrial fashion with control over several parameters, including morphology, mechanical properties and solubility. Regardless the promising properties of polymers that are

Chapter 1: Introduction

continuously prepared for biological applications, their utilization is usually prevented by low rates of cellular adhesion and recognition.¹³²

1.4 Synthetic polymers as biomaterials

Synthetic polymers represent the broadest and most diverse class of biomaterials and they are available in a variety of compositions for any kind of application¹³⁴. During the last three decades, technological progress has made significant steps in the development of biodegradable polymeric materials for biomedical applications. Degradable polymeric biomaterials are suitable candidates for the development of drug delivery vehicles, scaffolds for tissue engineering and temporary prostheses devices. In order to provide efficacy, these polymers require specific biological, chemical, physical, biomechanical and degradation properties. In relation to natural polymers, synthetic biomaterials have more batch-to-batch uniformity, and their properties are more predictable. Their main advantage is that they provide tailored property profiles for specific applications. Some of these properties include the ability to respond to an external stimulus, such as a change in concentration, pH or a change in temperature, and can be tuned by controlling their chemical structure and conformation through the manufacturing process. The first synthetic polymer used in biological application was poly(-glycolic acid) in 1967¹³⁵. Since then, technological and scientific advance had led to the design and development of a new variety of biodegradable polymers for drug and gene delivery vehicles, scaffolds for tissue engineering and transient implants for orthopaedic and related medical applications. In more recent times, natural and synthetic materials have been combined into hybrid materials in order to enhance the biological activity of these polymers¹³⁶.

1.5 Thermoresponsivity

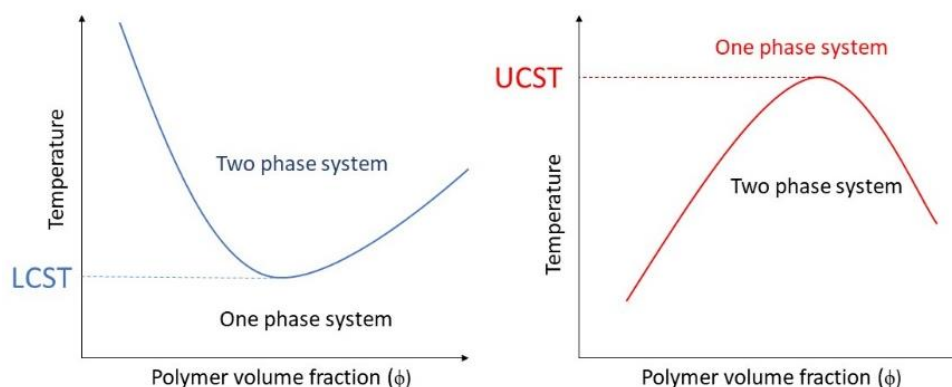
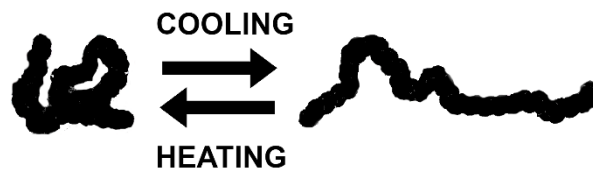


Figure 2 Temperature vs. polymer volume fraction (ϕ). Schematic illustration of phase diagrams for polymer solution lower critical solution temperature (left) and upper critical solution temperature (right).

Stimuli-responsive materials can alter their physicochemical properties upon exposure to external stimuli. Among these, thermoresponsive or temperature-responsive polymers, are characterized by a drastic and discontinuous change of their physical properties with temperature. Accordingly, thermoresponsive polymers display a miscibility gap in their temperature-composition diagram at a critical solution temperature (Figure 2). If solubility is reached upon heating, this point is called upper critical solution temperature (UCST). If the polymer becomes insoluble over a critical temperature, the point is called lower critical solution temperature (LCST)¹³⁷. However, their behaviour can be quite complex to describe as a polymer can exhibit both behaviour depending on many different factors, including molecular mass, polymer concentration, termination groups and the presence of co-solutes. A summary of the different types of thermoresponsive polymer is included in the following chapter. Most of the thermoresponsive polymers are amphiphilic and possess both hydrophobic and hydrophilic segments and are able to self-organize in solution. As a result, the solvent-polymer mixture can result in a self-organized micelle, a gel, a globule a coil or a two-phase system, depending on the conditions¹³⁸. In water, these conformational changes arise from the balance between the intra- and intermolecular hydrophobic attraction of the polymeric backbones and the hydrophilic interaction between the hydrophilic groups and the solvent⁹⁰. When a thermoresponsive polymer is completely dissolved, the hydrophilic groups (carboxylic acid, hydroxyl and amines) interact with the solvent molecules via hydrogen bonding. As a result, the polymer is solvated, and the system appears as a clear solution. However, hydrogen bonding is only effective at low temperatures. When temperature is increased, the water is partially displaced from the

polymer coil and the interaction is weakened. On the contrary, hydrophobic interactions follow the opposite trend as they tend to increase at higher temperature¹³⁹. If the interactions between the polymers becomes more favourable, the polymer undergo a LCST transition and its conformation changes from (Figure 3)^{138,140}. At this point, particle



aggregation usually results in visible turbidity. For this reason, the critical

Figure 3 Schematic representation of a coil-to-globule LCST transition.

LCST point is also referred as “cloud point”¹⁴¹. When the polymeric chains cause the complete displacement of the solvent, phase separation occurs. The free enthalpy of mixing ($\Delta G_{mix} = \Delta H_{mix} - T\Delta S_{mix}$), which accounts enthalpic (ΔH_{mix}) and entropic (ΔS_{mix}) contributions, establishes whether UCST or LCST miscibility gaps occur. LCST transitions are associated with an unfavourable entropic effect. A decrease in solubility with a rise in temperature is originated with a negative, exothermic enthalpy of mixing. At a critical point (T_c), phase separation occurs if the favourable energy effect overcome is overcome by a negative entropy term¹⁴². On the contrary, it is agreed that an UCST arises from strong polymer-polymer and solvent-solvent interactions compared to weak polymer-solvent interactions. Accordingly, the hydrophobic effect is more dominant in LCST transition. According to *Seuring et al.*, UCST behaviour in water is quite common but was rarely observed in physiological conditions¹⁴³. Since hydrophobic effect is largely accounted as an entropic effect, UCST behaviour is usually considered an enthalpy driven transition¹⁴⁴. However, recent study has described the hydrophobic effect as a far more complicated process, which is more challenging to interpret¹⁴⁵. The hydration shell of small hydrophobic solutes is commonly described as a clathrate, ice-like structure, characterized by strong hydrogen bonding interactions between water molecules, which account for favourable enthalpic contributions and a distinct loss in entropy. However, the hydration of extended nonpolar planar surfaces involve the formation of different structures of the hydration shells, in which unsatisfied hydrogen bonds are directed towards the hydrophobic surface¹⁴⁶. The overall positive entropic contribution is generally assigned to the demixing between the two phases systems that breaks the organized water structures around the hydrophobic surfaces. In more recent times, computational simulations have demonstrated that some hydrophobic interactions between ligand and receptors are actually

enthalpy-driven, as the main contributions comes from the expulsion of the disorganized water from the receptor cavity¹⁴⁷.

A starting approach to describe the behaviour of polymer solution is the method developed by Flory and Huggins in 1942, known as the Flory-Huggins theory^{148,149}. This theory employs a lattice model of the thermodynamics of polymer solutions that takes into account the great dissimilarity in molecular sizes. The thermodynamic quantities of the solution are derived from a reduced Gibbs energy parameter, χ , and a simple concept of combinational entropy of mixing¹⁵⁰. The χ parameter is calculated from this equation:

$$\chi = \frac{z}{k_B T} \left(w_{12} - \frac{w_{11} + w_{22}}{2} \right) \quad (1)$$

In which the left term is the energy increment for every monomer-solvent contact and involves there are three enthalpic contributions: solvent-solvent interaction (w_{11}), monomer-monomer interaction between different chains (w_{22}) and monomer-solvent (w_{12}) interaction. In the right term, z is the coordination number, k_B is the Boltzmann constant and T is the temperature of the system. Consequently, the χ parameter is a dimensionless quantity that takes into account the reduced solubility of polymers at low temperature. The FH theory led to this equation of the free energy of mixing:

$$\Delta G_{mix} = RT[n_1 \ln \phi_1 + n_2 \ln \phi_2 + n_1 \phi_2 \chi] \quad (2)$$

And led to the following equation for the ΔG_{mix} normalized per lattice site:

$$\frac{\Delta G_{mix}}{N k_B T} = \chi \phi_1 \phi_2 + \frac{\phi_1}{x_1} \ln \phi_1 + \frac{\phi_2}{x_2} \ln \phi_2 \quad (3)$$

In which ϕ and x are, respectively, the volume and the molar fractions of the two-component system. From a qualitative point of view, the Flory-Huggins expression provided an adequate description of the main phenomena associated with the thermodynamic behaviour of polymeric solutions¹⁴². As we already pointed out, χ parameter considers the dramatical change of solubility with the lowering of temperatures, which can result in phase separation. In addition, it is suitable for the description of the phase separation observed at an UCST critical point. Since the FH does not involve steric interactions, the temperature in which polymer-solvents interactions are balanced by long-range forces between polymer molecular segments is called Flory or theta temperature θ . In this condition, the polymer is at the edge of solubility and exist in the form of statistical coil, the solution is considered ideal and there is no enthalpy of mixing. Consequently, there is no excluded volume effect due to polymer expansion. The solvent at the theta temperature is also called theta solvent¹⁵¹. At temperature θ , the second virial coefficient (B) of the osmotic pressure is zero:

$$\frac{\Pi}{RT} = \frac{c}{M} + Bc^2 + B_3c^3 + \dots \quad (4)$$

Virial coefficients are functions that describes the deviations from the ideal gas law. If we consider that the chemical potential is related to the osmotic pressure by this simple relation:

$$\Delta\mu = -v_s \frac{\Pi}{RT} \quad (5)$$

We can conclude B is connected to the excess chemical potential and depends on the square polymer concentration. Its value gives a representation of the deviation of the solution behaviour from ideality due to polymer-solvent interaction:

$$B = -\frac{\Delta\mu_{exc}}{v_1c^2} \quad (6)$$

Since B reflects the binary interactions between solvent molecules and segment of the polymeric chains, it is connected to the behaviour of the polymer in solution. When $B > 0$, polymer-solvent interactions are favourable, and the solvent is referred as "good". In this condition, repulsive forces between the polymer segment promote the swelling of the chains into the solution. When $B < 0$, solvent-polymer interactions are unfavourable, and the solvent is referred as "poor". As a consequence, the polymeric chains shrink as they attract to each other. The Huggins constant χ is also dependent to the quality of the solvent according to the following relation:

$$\ln a_1 = \frac{\Delta\mu_1}{RT} = \ln(1 - \phi_2) + \left(1 - \frac{1}{N}\right)\phi_2 + \chi\phi_2^2 \quad (7)$$

In which N is the degree of polymerization of the polymer. θ is evaluated by plotting the value of second virial coefficient in order to find the zero value, according to this relation:

$$B = \frac{(1/2 - \chi)}{v_1\rho_2^2} \quad (8)$$

In which ρ_2 represent the density of the polymer. According to these equations, good solvents are obtained if $\chi > 1/2$ and poor solvent are obtained if $\chi < 1/2$. The FH parameter for polymer-solvent pairs is extracted at infinite dilution¹⁵².

For his fundamental achievements, Flory was awarded with the Nobel Prize in Chemistry in 1974. However, despite the remarkable achievements of the FH theory, the assumption of ideal polymeric chains has demonstrated to be reason for its limited application. The FH approach does not account for the change in conformation nor for the volume change of the polymer associated with different phenomena, including LCST transitions. From a

quantitative point of view, the main limit of the theory was the overestimation of the value for χ , that were in contrast with the definition in terms of contact energy. Moreover, the theory was based on the regular solution assumption, for which the entropy of mixing is equal to that of an ideal solution of the same composition, but it is non-ideal due to a non-zero enthalpy of mixing. This assumption was not compatible with the dependency of χ with temperature. During the sixties, the free energy parameter was redefined with a contribution of a non-combinatorial entropy of mixing: $\chi = \chi_H + \chi_S$. A further advance in the theory was provided by *Patterson et al.*¹⁵³, who provided a simple explanation for LCST, by considering the free volume into the FH theory. The free volume (v_f) is measure of the quantity of space available in which polymer chains can change their conformation. The free volume can be formulated as $v_f = v - v_o$, where v is the volume occupied by the polymer at a certain temperature and v_o is the limiting occupied volume, or the incompressible molecular volume, and depends on temperature, pressure, and concentration. The new theory provided suitable explanation for the calculation of the parameter χ under different conditions, including its dependence from the concentration and the related heats of mixing ΔH_{mix} .¹⁴² The new formulations include a new expression of the χ parameter which included a solubility parameter:

$$\delta_2 = \left(\frac{\Delta E_2^{vap}}{v_2} \right)^{\frac{1}{2}} \quad (9)$$

which included the energy of evaporation ΔE_2^{vap} and the molar volume of the polymer. The free energy parameter became:

$$\chi = v_2 \frac{(\delta_1 - \delta_2)^2}{RT} = \frac{z\Delta w}{k_B T} \quad (10)$$

According to this formula, the change of χ with rising temperature is caused by the rapid decrease of δ_1 in comparison to the slow decrease of the polymeric δ_2 . If the temperature is sufficiently high, χ follows an opposite trend as indicated by the FH theory, and increases with increasing temperature. In this condition, when the system reaches the T_c , a LCST transition is produced. The inherent ΔH_{mix} , derived from the Gibbs-Helmoltz equation, with the assumption that all temperature variations are caused by δ_1 , is the following:

$$\Delta H_{mix} \cong 2V_{mix} \delta_1 \delta_2 (\delta_1 - \delta_2) T \frac{\partial \delta_1}{\partial T} \quad (11)$$

and predicts that ΔH_{mix} can be positive or negative according to the difference between δ_1 and δ_2 . According to this model, negative enthalpies of mixing are expected even for chemically similar systems. This should be considered as the opposite of “like dissolves

like rule”, as a chemically similar solvent is not expected to be the best solvent for the dissolution of a polymer¹⁵³. Another formulation which includes the result of Patterson and Flory is the following:

$$\chi = v_{12} \frac{\Delta E_1^{vap}}{RT} + \frac{C_{p1}}{2R} \tau_{12} \quad (12)$$

In which C_{p1} represent the configurational heat capacity of the solvent, v_{12} is a term related to the molecular differences in cohesive energy and size between polymer and solvent and τ_{12} is the expansivity, or the difference in free volume between polymer and solvent. While first term decreases with increasing temperature, the second temperature follows an opposite trend. The free volume term contributes to ΔG_{mix} and always led to a LCST transition, even when v is zero. According to the free volume theory, since χ is increased by both lowering or increasing the temperature, phase separation can be reached by exceeding a χ critical value. Accordingly, two-phase polymer-solvent systems can display both LCST and UCST. The free volume theory of liquids predicts that all systems exhibit LCST while UCST is caused by unfavourable positive heats of mixing. For a polymer-solvent system displaying both LCST and UCST, the minimum value of χ provides the best quality of the solvent¹⁴². A more recent phenomenological analysis of the miscibility behaviour, although general, differentiates between three types of limiting critical miscibility behaviour. This approach is based on the definition of an interaction parameter $g(T, \phi)$ that can be modified to account both concentration and temperature dependence of the miscibility gaps. The g parameter is derived from the Flory-Huggins-Staverman (FHS) expression for the Gibbs free energy of mixing:

$$\frac{\Delta G_{mix}}{NRT} = \frac{\phi_1}{m_1} \ln \phi_1 + \sum \frac{\phi_{2i}}{m_{2i}} \phi_{2i} + \phi_1 \phi_2 g(T, \phi_2) \quad (13)$$

In this equation, the first two terms represent the ideal part of the entropy of mixing. This combinatorial part is based on a similar lattice model in which m represents the number of lattice site occupied by a molecule. The FHS model shows that the combinatorial entropy of mixing is smaller for the polymers in relation to small molecules. In this condition, miscibility gaps can form easily due to small interaction. For this reason, it is standard practice to use the interaction parameter g for phase-diagram modeling. In Equation 14 ϕ_1 and ϕ_{2i} represent the volume fractions of the solvent and the number of species present in the polymer, respectively $\phi_2 = \sum \phi_{2i}$ ¹⁵⁴⁻¹⁵⁶. The interaction g is generally represented by a second order polynomial in ϕ_2 :

$$g(T, \phi_2) = g_0 + g_1 \phi_2 + g_2 \phi_2^2 \quad (14)$$

And the dependency from temperature¹⁵⁶ can be described with a similar equation:

$$g(T, \phi_2) = g_0 + \frac{g_1}{T} + g_2 T \quad (15)$$

In some cases, a polymer can show both UCST and LCST due to complex temperature dependence of the interaction parameter, as shown in Figure 4. The values of g_1 and g_2 at the consolute point determine the type of phase behaviour¹⁵⁴. The classical Flory-Huggins miscibility behaviour (Type I) is observed if the following conditions are satisfied:

$$g_0 \leq \frac{1}{2} + g_1 \text{ and } g_2 \geq g_1 - \frac{1}{6} \quad (16)$$

A complete description of the theory is reported by *Solc et al.*¹⁵⁷. In general, it is a strong assumption to assume polymer solution as strictly binary. Even with a small narrow distribution, it is impossible to produce polymers with uniform molar mass. A polymer solution should be considered as a quasi-binary mixture of polymers with different molecular mass. The FHS has been previously extended for accounting polydispersity¹⁵⁸. In this condition, the miscibility gap is shifted towards different values of temperature and polymer concentration. In addition, three-phase equilibria can appear and the curvature of the LCST curve can change sign. However, for the sake of simplicity, polymer-solvent mixtures will be referred as binary mixtures in this work.

In organic solvent, the g parameter is calculated on the assumption that most of the molecules interacts via simple van der Waals forces. In water, these assumptions are not valid since the polymer need to contain polar groups that interact via polar interaction and hydrogen bonding.

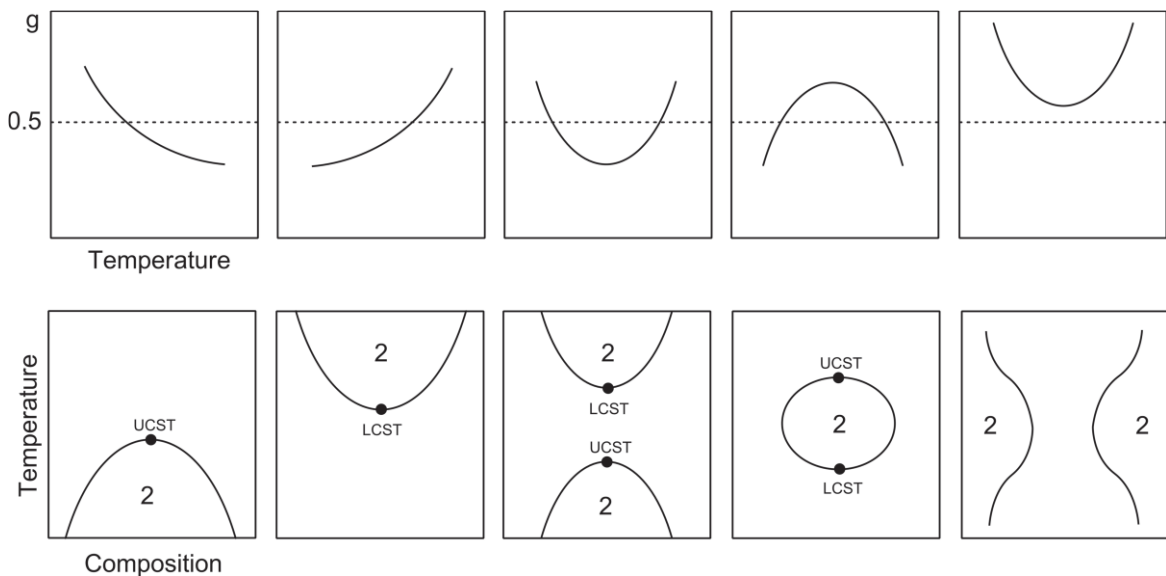


Figure 4 Correlation between the temperature dependence of the interaction parameter g and the type of miscibility gap. The number 2 indicates the presence of a two-phase region.

These interactions exhibit a stronger and non-monotonic temperature and concentration dependence. In some cases, the strong concentration dependence can lead to off-zero critical point for infinite molar masses. Since this discovery, polymers have been divided into three different types according to their phase behaviour (Table 1). For Type I polymers, also known as the “classical” type, the position of T_c is shifted with the increase of the polymer chain length - and, consequently, with the increase of the average molecular mass - towards lower polymer concentration. In the limit of infinite chain length ($N \rightarrow \infty$, or $m \rightarrow \infty$), the critical polymeric concentration at the ϑ temperature is zero. On the other hand, Type II is characterized by a single off-zero critical polymeric concentration, $\phi_c \neq 0$ that occurs at non ϑ conditions. For a polymer characterized by a type II behaviour, the LCST critical point it is almost independent on the polymer chain length. Finally, Type III exhibits one zero limiting critical concentration and two off-zero limiting critical concentrations. The first critical point is usually exhibited at low polymer concentrations and the polymer behaves as described by the Flory–Huggins. The critical point shifts to zero concentration and to the ϑ temperature for $N \rightarrow \infty$. The other points are not influenced by the length of the polymeric chains at high polymer concentration^{154–157}. Examples are the LCST of poly-N-vinylcaprolactam (PNVCL, type I), poly-N-isopropilacrylamide (PNIPAM, type II) and poly(vinylmethyl ether) (PVME, type III).

Miscibility behaviour	LCST dependence on molecular weight
Type I	Dependent
Type II	Independent
Type III	Dependent for diluted solution, independent for concentrated solution

Table 1 Molecular weight dependency of LCST based on the type of miscibility behaviour.

1.6 Thermoresponsive polymers for biomedical applications

From a purely theoretical point of view, a cloud point could be determined for every existing polymer with a zwitterionic character. In general, LCST-type polymers are easily solvated in water through hydrogen bonding and polar interactions. On the contrary, UCST behaviour is less common in water^{143,159} and it has been observed more frequently in organic or organic/water solutions^{160–167}. Since UCST polymers relies mainly on non-polar interaction, their behaviour can be influenced greatly by the presence of salts. UCST in organic solvent has been observed for common industrial polymers, such as polypropylene

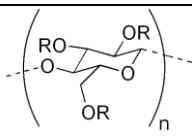
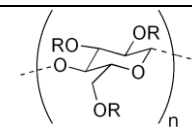
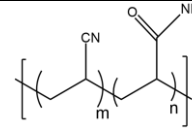
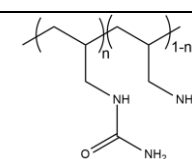
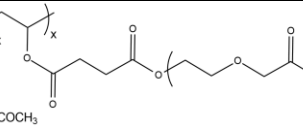
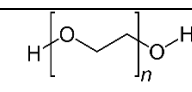
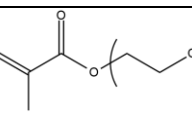
in n-hexane, polystyrene in butylacetate or polyethylene in diphenylether¹⁶⁸. In some cases, both LCST and UCST has been observed in polymer of industrial relevance, such as polyethylene oxide (PEO), polyhydroxymethylmethacrylate (PHEMA) and polyvinylmethylether (PVME). However, the UCST of those polymers is usually observed outside the region between 0 and 100 °C. In other cases, cloud point were determined under extreme experimental condition or by exploiting salting out effects using high salt concentrations (e.g. polyacrylic acid (PAA) in water)¹⁶⁹.

Due to their ability to respond to a change in temperature, thermoresponsive polymer are considered a “smart” class of materials that can be useful in a wide range of applications. Their biological interest relies in the present of a desirable sharp transition. However, in order to be used in the biological field, a thermoresponsive polymer must possess a cloud point at a temperature close to the normal human physiological temperature, which it is usually comprised between 36.5 and 37.5 °C, but can oscillate in a wider range between 33.2 and 38.2 °C¹⁷⁰. The synthesis of the polymer must therefore be finely optimized, in order to ensure control over chemical structure, chain desired and the desired morphology (linear, branched, star-shaped, comb, brush, network, dendrimer). In some cases, the possibility of combining different polymers together has allowed to provide thermoresponsive properties to other polymers of biological interest. Additionally, by combining two or more desirable properties of different species, hybrid molecular devices were synthesized in order to provide dual-combinational therapies. To this date, there are hundreds of thermoresponsive polymers developed for various applications in the biological field, which include tissue engineering, bioseparation and drug and gene delivery. Among those, N-alkylated poly(acrylamides) have been extensively studied for their thermoresponsive behaviour, such as PNIPAM, PNIPMAM, PNCPAL, PNEAM, PNAGA, PNCPAL or PNVCL. The most popular poly(acrylamide) is poly-N-isopropylamide, PNIPAM, which has a 32-34 °C LCST with a type II transition behaviour^{7,8,171}. Another important example of water-soluble material with LCST properties is polymethylvinylether, or PMVE, which usually exhibits LCST between around 33 and 37 °C with a typical type III demixing behaviour⁸⁹. LCST properties were found also in polymers of natural origins, such as hydroxypropyl cellulose (HMC), methylcellulose (HPC) and elastine⁸⁹. It should be noted that the cloud points are affected by chain modification and end groups. Polyethylene glycol (PEG), also known as polyethylene oxide (PEO) at higher molecular weight ($M_w > 20,000$), is a highly biocompatible polyester used in biomedical applications with thermoresponsive properties.

PEG methacrylate polymers, or PEGMA, possess a lower LCST that depends on the number of ethylene oxide units¹⁷². Poly(N-ethyl oxazoline)s represent another important class of polymers with a transition temperature too high for any biological application, but their modification with other polymers have shown some potentials in drug delivery⁸⁹. Polymers like PNIPAM have been extensively used in combination with pH-responsive polymer for the fabrication of double-responsive copolymers. PNIPAM-based copolymers usually exhibit LCST close to physiological temperature. This ability has been demonstrated in combination with polymers that do not exhibit thermoresponsive properties close to the physiological range, such as polyvinylalcohol (PVA) or PEO, and even in combination with UCST polymers such as polyacrylamide (PAAM). Copolymerization or grafting is also an excellent strategy to bring the cloud point closer to human temperature, such in the case of poly(acrylamide-co-acrylonitrile) (PAAM-co-PAN), poly(allylamine-co-allylurea) (PAA-co-PAU) or poly(vinylalcohol)-co-vinylbutyrate) (PVA-co-PVB). Another important class of thermoresponsive copolymers of biological industrial interest are polaxamers, also commercially known as Pluronic[®], Synperonic[®] or Kolliphor[®], which consist in a three-block copolymer of PEO and polypropylene oxide (PPO). In some cases, it was possible to observe both UCST and LCST, depending on the ratio between the two copolymers. In the case of poly(p-dioxanone)-g-poly(vinylalcohol) (PPDO-g-PVA), the ability to switch between UCST and LCST behaviour is controlled by adjusting the chain length of the PPDO block. Among UCST polymers, poly(acrylic acid) and poly(sulfobetaine) represent two of the most studied examples for industrial and biological applications. UCST in water and water mixtures have been studied for drug delivery applications in linear and cross-linked polymers and copolymers such as poly(acrylic acid)¹⁶⁹, poly(sulfobetaine)s and poly(oxazoline)s polymers^{161,173,174}. A list of polymers with thermoresponsive properties in water is provided in table 2. The table is very generic and does not provide guidance as to the architecture and chain length of the individual polymers mentioned. A more complete list is provided by the Handbook of Chemistry and Physics list of LCST and UCST value, in which the molecular length and the proportion of co-monomers is reported for every polymer listed as well as the solvent. Far from providing a complete list, the handbook provides excellent indications of how thermoresponsive properties should be reported in order to ensure maximum reproducibility. Since it is impossible to prepare a perfectly monodispersed polymer, it is always necessary to consider the intrinsic limit of absolute models that allow us to predict the behaviour of a polymer. For example, during an LCST

Chapter 1: Introduction

transition, a polymer will go through a fractional precipitation process in which the various portions will precipitate depending on their different structural characteristics. This is also valid for Type II polymers, such as PNIPAM, whose behaviour is substantially, but not entirely independent of the molecular mass. Given the importance of experimental evidence, it is easy to find discrepancies in the literature. This is the case, for example, of the PMVE, the LCST of which is reported, respectively, to occur at 33¹⁷⁵, 35¹⁷⁶ or 37 °C¹⁷⁷, or of the PEO, whose LCST oscillate between 85 and 175 °C^{89,175}. In the case of biological applications, however, a difference of just one degree can make a huge difference. In addition, it is fundamental to indicate if the polymer belongs to one of the three classes of the phase type behaviour (I, II or III), as this information is crucial to provide control over the cloud point through synthesis. The problem of the reproducibility will be dealt more thoroughly in the next chapters.

Name	Structure	UCST (°C)	LCST (°C)	Ref.
<i>Hydroxypropyl cellulose (HPC)</i>	 $R = H \text{ or } CH_2CH(OH)CH_3$		45.3 – 58.1	168
<i>methylcellulose</i>	 $R = H \text{ or } CH_3$		51.6	168
<i>poly(acrylamide-co-acrylonitrile) (PAAm-co-PAN)</i>		6.4 – 57		178
<i>poly(allylamine-co-allylurea) (PAA-co-PAU)</i>		25 - 54		144,179
<i>poly(p-dioxanone)-g-poly(vinylalcohol) (PPDO-g-PVA)</i>	 $R=OH \text{ or } OCOCH_3$	30 – 80	30 – 80	174
<i>Poly(ethylene oxide) (PEO)</i>			100 – 175	175
<i>Poly(ethylene glycol) methacrylate (PEGMA/OEGMA)</i>			26-90	180

Chapter 1: Introduction

<i>poly(ethylene oxide)-b-poly(propylene oxide)-b-poly(ethylene oxide) (PEO-PPO-PEO or Pluronic or Polaxamer)</i>			12.5 – 52.5	177
<i>poly(hydroxyethylmethacrylate) (PHEMA)</i>		22		175
<i>poly(methacryl amide) (PMAAm)</i>		60		175
<i>Poly(propylene glycol)</i>			15 – 42	175
<i>poly(vinyl methyl ether) (PMVE)</i>			33 – 37	168,175,177
<i>poly(vinylalcohol) (PVA)</i>			241	168
<i>Poly(vinylalcohol)-co-vinylbutyrate (PVA-co-PVB)</i>		131	25	168
<i>poly[2-(dimethylamino)ethyl methacrylate] (PDMAEMA)</i>			32 - 53	181
<i>poly-2-isopropyl-2-oxazoline (PiPrOx)</i>			26 – 34	182,183
<i>Poly-3-dimethyl(methacryloyloxyethyl)ammonium propane sulfonate (PDMAPS)</i>		60		175
<i>(PNAGA)</i>			22	175
<i>Poly(6-(acryloyloxymethyl) uracil) (PAU)</i>		80		175
<i>Poly-N-cyclopropylacrylamide (PNCPAL)</i>			40 – 50	177

Chapter 1: Introduction

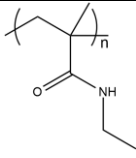
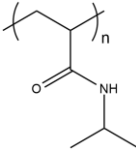
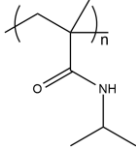
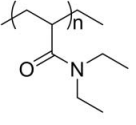
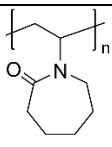
<i>Poly-N-ethylacrylamide (PNEMAM)</i>			82	175
<i>poly-N-isopropylamide (PNIPAM)</i>			32 – 34	7,168,184
<i>poly-N-isopropylmethacrylamide (PNIPMAM)</i>			42 - 46	177
<i>Poly-N,N-diethylacrylamide (PDEAAM)</i>			25 – 32	172
<i>Poly-N-vinylcaprolactam (PNVCL)</i>			25 – 50	7,8,156

Table 2 List of polymers with thermoresponsive properties.

1.7 The determination of LCST

One of the most important aspects of the demonstration reported by *Solc et al.* in 1995 is the determining role played by the length of the polymer and by the concentration in defining the critical miscibility behaviour^{154–157}. Due to the sectorialisation of scientific publications, this thermodynamic concept, although apparently basic, is not necessarily considered, or explained, in many works that evaluate the possible applications of thermoresponsive polymers in a biological environment^{91,93,99,185}

In most cases, the behaviour of polymers in aqueous solutions had been described many years before the biomedical community started showing an interest towards these materials. The first phase behaviour diagram of the most studied thermoresponsive polymer, PNIPAM, was reported in 1968 by Heskins and Guillet^{184,186}. The thermoresponsivity of another polymer, poly-N-vinylcaprolactam (PNVCL), was observed in 1952¹⁸⁷, although the first application of the material was only reported in 1996¹⁸⁸. Although the miscibility behaviour of the polymer had been previously described, a detailed description of the behaviour of PNVCL in aqueous environment was reported by *Meeussen et al.* in 2000¹⁵⁶. However, despite the two polymers have been investigated for more than 50 years, PNVCL is still described as a novelty in biological and

nanotechnological-related publications. PNVCL and PNIPAM are usually presented together as they both exhibit LCST behaviour at 32 °C and PNVCL is usually introduced as a biocompatible alternative to PNIPAM^{91,99,140,185,189–192}. However, this information can be misleading if it is neglected that the two polymers exhibit opposite critical miscibility behaviour and their LCST depends on very different conditions. PNIPAM belongs to type II and its main advantage is to have a LCST which is almost completely independent of the chain length and from other factors such as concentration, salinity and pH of the aqueous environment. PNVCL, on the other hand, has a very variable temperature (between 25 and 50 °C), as it belongs to type I and its behaviour in water can be described by the Flory-Huggins theory. However, it is essential to consider that these thermodynamic models have an intrinsic limited range of applications. An accurate description of the polymeric properties is therefore required to ensure reproducibility. It is essential to establish whether a certain property is “independent” or “substantially independent” from a certain factor. This consideration is even more important when evaluating a polymeric application in a physiological environment. The properties of polymer solutions are generally characterized in ideal environments, such as two-component systems. However, when facing the complexity of biological matrices, one must expect substantial variation from the theoretical predictions. In this sense, the knowledge of the thermodynamic behaviour of a polymer is fundamental for any application in the biological field and the models that are used should be as complete as possible. According to these principles, instead of reporting a single LCST value, some studies prefer to report a temperature range. In the case of PNIPAM, the LCST is usually reported in a thin temperature interval (31-34 °C). According to these considerations, we should not be considering any “type II” behaviour as completely independent from the length of the polymer. Nonetheless, the small variation accounts for the fact that the length of the polymer has only a light influence over the value of the LCST. In the case of “type I” polymers such as PNVCL, it is of crucial importance to consider that the miscibility behaviour is concentration and molecular mass dependent in order to avoid loss in reproducibility in the synthetic process^{156,193–197}. In the specific experience of this work, we discovered that PNVCL dissolved in DMF cannot be precipitated by the utilization of diethyl ether under a certain critical molecular mass. By increasing the chain length, we were able to reproduce the results of reported in literature^{91,93,96,99}, but we were not able to reproduce the synthetic protocol in the same exact conditions.

Another particularly important issue related to the utilization of thermoresponsive polymers in biological environment is the accurate determination of the LCST. Typically, the determination of the LCST relies on the definition of the transition temperature as “cloud point”. The measurement is performed by exploiting the scattering properties of the globular aggregates that form in solution during the transition. The most easily available techniques for the determination of the LCST are UV-VIS spectroscopy and DLS. However, these methods provide an "indirect" measure of the phenomenon, as the information is extrapolated through the saturation of the instrument signal. Since the temperature is not the direct output of the instrument, the LCST measurement should be considered qualitative rather than quantitative. In an UV-VIS measurement, the value of the LCST is extrapolated the curve of solubility in which the transmittance of the solution is plotted against the temperature. Due to the cloudiness of the solution, the transmittance drops dramatically to zero in a certain temperature range. However, in order to plot the points of the solubility curve in which the transmittance value is lower than 1, absorbance values are necessarily higher than 2, due to the simple relation: $T (\%) = 10^{(2-A)}$. When performing a UV-VIS measurement, the general habit is to use dilute solutions in order to keep the absorbance value below 1. In modern UV-VIS spectrophotometers, the measurement is automatically compensated in the range of absorbance values between 1 and 2 and values in these range are generally considered acceptable for quantitative measurements. In any case, higher values are never used as they come out of the linear range of Lambert-Law. However, when performing a LCST measurement, the determination requires the utilization of UV-VIS light spectrophotometers outside their linearity range. In general, the LCST is attributed to the point where the transmittance drops dramatically to zero. From a conceptual point of view, this is imprecise, as the LCST represents an equilibrium temperature and, therefore, the correct temperature must be correlated with the inflection point of the curve. Furthermore, the choice of the wavelength (λ) for the determination of the LCST is not usually discussed. Ideally, the transmittance should be calculated in a spectral range where the absorption below the LCST is zero but changes rapidly during the transition. The assumption that the LCST should be obtained from the point in which the transmittance drops to zero is not suitable for the accurate description of concentration-dependent cloud points. In the case of diluted solutions, it is very difficult, if not impossible, to reach the desired value of $A = 2$. In concentrated solutions, the baseline is shifted to higher absorbance values. In the present thesis, the LCST was determined by fitting each solubility curve with a sigmoidal model:

$$y = A_{max} + \frac{(A_{max} - A_{min})}{1 + e^{\frac{(T-T_C)}{dT}}} \quad (17)$$

In which A represent the transmittance and T is the temperature of the system. In this way, the two constants, A_{max} and A_{min} , are related to the optical properties of the systems before and after the transition. The LCST correspond to the value of the inflection point T_C , which is provided by the fitting of the curve along with the uncertainty and the correlation factor r^2 . The sigmoidal model is useful for the interpretation of the thermoresponsive behaviour of diluted systems, in order to study the dependence of the LCST from the concentration. In this way, the inflection point can be determined even if the transmittance does not drop to zero. In addition, the model is suitable for the study of the behaviour of the polymer in a complex matrix and the baseline signal is represented by the constant A_{min} . Accordingly, the behaviour of PNVCL in human plasma is described at page 142.

DLS determination of the LCST relies on the possibility of measuring the dimension of the polymeric globules that are formed during the transition, although the newly formed particles are unstable, and they rapidly undergo aggregation if the system is composed only by the polymer and the solvent. As a result, due to their increased dimension and polydispersity, the relative dimensional distributions curves do not provide any useful information about the system in analysis. A more appropriate use of the DLS is to report the correlation function $g^2(t)$ instead of dynamic diameters distribution, as g^2 represent the analytical output of the analysis. LCST can be easily associated to the temperature in which dramatic change or displacement of the normalized correlation curves is observed.

Another way to determine the LCST is through DSC. DSC is a thermoanalytical technique in which the difference in the amount of heat required to increase the temperature of a sample and reference is measured as a function of temperature. DSC is commonly used to determine thermal transitions of polymeric materials. The analysis of an aqueous solutions of a thermoresponsive polymer usually provides an endothermic peak related to the LCST transition. The analysis of the peak provides the energy of the transition and the value of LCST. However, in order to study the behaviour of aqueous solutions, DSC requires special sealed pans that guarantees that prevent the solvent from the evaporation during the analysis. When the solvent starts to evaporate, the mass of the system changes and the instrument records the energy related to the process. In this condition, the LCST peak is hidden under the evaporation curve, and it is difficult to establish the accurate value even through the utilization of multi-peak fitting analysis. The LCST of a polymer can be determined by means of other techniques, such as viscosimetry and turbidimetry. if the

Chapter 1: Introduction

polymer has acidic or basic properties, the LCST can also be established through pH measurements. However, the discussion of these techniques is outside the interest of this study.

1.8 Poly-N-Vinyl caprolactam

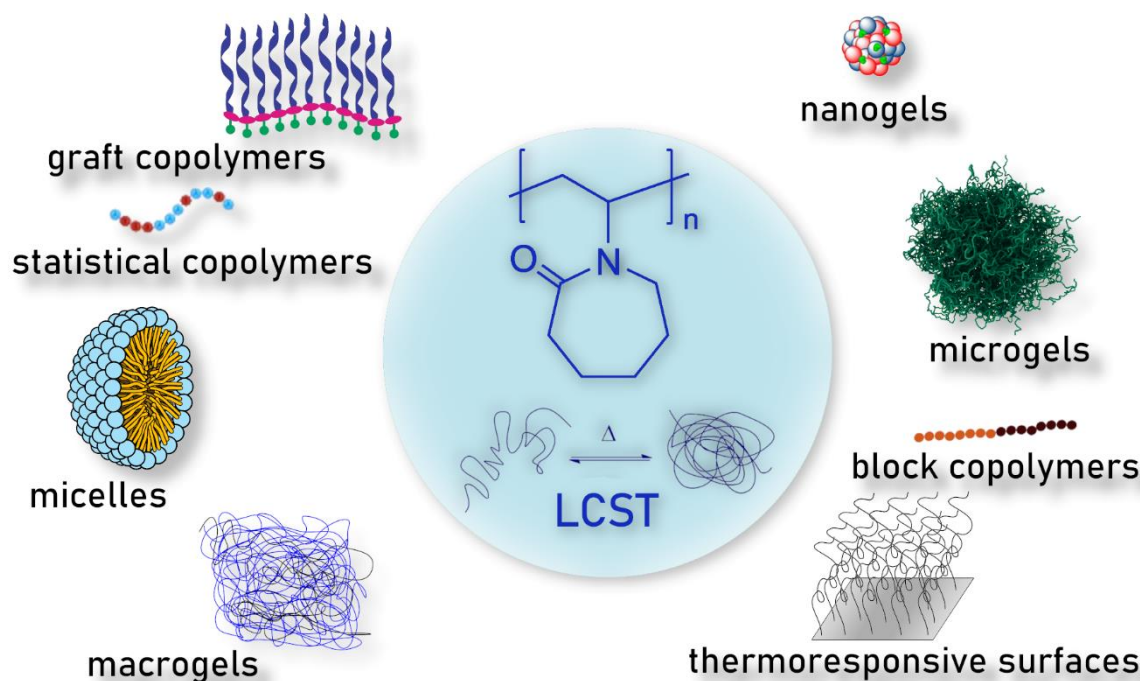


Figure 5 Schematic representation of PNVCCL and its possible applications.

Poly(N-vinylcaprolactam) (PNVCCL) is a temperature-responsive polymer which has been applied in biomedical applications, environmental applications, in cosmetics and as an anticlogging agent in pipelines. The polymer possesses exceptional film forming properties, is able to inhibit crystal growth and it interacts as a complexing molecule with organic substances. The monomer, NVCL is an amphiphilic compound that is soluble in both polar and non-polar solvents. The first polymerization of NVCL was described by *Shostakovski et al.* and published in the Russian language in 1952¹⁹⁸. The synthesis and the bulk polymerization PNVCCL was later described in English by *Solomon et al.* in 1968¹⁹³. The free-radical synthesis of PNVCCL has been performed in many different solvent over the years, including benzene^{199–201}, toluene¹⁹³, isopropanol¹⁹⁰, DMF^{91,93,96,99,202}, DMSO and water mixture¹⁹¹ and *p*-dioxane^{196,203}. Recently, the synthesis of the polymer has been reported in water¹⁹⁵ and alcohol/water²⁰⁴. The polymer is soluble in both polar and non-polar solvents, such as alcohols, DMSO, DMF, THF, *p*-dioxane, chloroform, and dichloromethane. In water, the polymer exhibit thermoresponsivity and it is soluble under its critical miscibility point (LCST). As previously mentioned, PNVCCL has been usually compared to PNIPAM for its thermoresponsive behaviour since both polymers exhibit a LCST close to the physiological temperature. However, their miscibility behaviour is completely different. PNIPAM belongs to type II and exhibit a LCST at ~32 °C, which is

almost independent from the molecular weight, while PNVCL belongs to type I and its LCST depends on molecular weight and polymer concentration^{7,8}. The LCST of PNVCL is also lowered by the presence of salts^{201,205–207}. It has also been reported that the addition of small quantity of alcohol decreases the LCST in water^{7,140}. On the contrary, the presence of compounds that increase the hydrophilicity of the polymer is known to increase the LCST. In solution, PNVCL behaves as a polyelectrolyte and interacts with surfactants via hydrophobic interactions. Upon heating, the polymer undergoes a coil-to-globule transition when the critical point is reached. During the transition, the shrinkage of the polymeric coils is accompanied by dehydration^{7,8,189,194}. This has been observed through the reduction in the intrinsic viscosity near LCST²⁰⁸. The presence of anionic and cationic surfactants prevents the aggregation of the polymeric chains, thereby increasing the LCST²⁰¹. This has been also reported for proteins, such as insulin and bovine serum albumin²⁰⁹. The type I critical behaviour of PNVCL in water was confirmed and elucidated by *Maeda et al.* through infrared spectroscopy measurements²¹⁰. The coil to globule transition in water was reported by light scattering²¹¹, small angle neutron scattering²¹² (SANS) and fluorescence investigations²¹³. The lack of popularity of PNVCL in relation to PNIPAAm has been often associated to the difficulty of polymerizing NVCL in a controlled fashion^{7,8,140,189}. Since the thermoresponsivity of PNVCL is molecular weight dependent, the control of both molecular weight and dispersity is of crucial importance^{156,193–197}. In recent times, the possibility of controlling the polymerization and copolymerization of the monomer through controlled free-radical polymerization have resulted in an increasing number of publications. The polymer has also earned some fame to its alleged biocompatibility, whereas many studies have addressed that PNIPAAm is inconvenient for biomedical applications^{7,8,214–216}. The hydrolysis of PNVCL under acidic condition has been described in detail by *Imaz et al.*²¹⁷. Unlike PNIPAAm, the cyclic amide group present in the structure of PNVCL prevents the formation of toxic amide compounds²¹⁶. The utilization of strong acid provokes the opening of the lactam ring and produce a polymeric carboxylic acid and acetaldehyde as a side product. Despite the potential of the polymer for biomedical application has been described for several years, the first “in vitro” evaluation of PNVCL cytotoxicity was published only in 2005²¹⁶. The study observed the behaviour of two cell lines, intestinal Caco-2 and pulmonary Calu-3, in relation to the exposure to PNVCL and PNVCL-grafted-PEO (PNVCL-g-PEO). The test demonstrated great cell tolerance towards the polymers but, at the same time, it demonstrated the polymer exhibits toxic effects above its LCST²¹⁶. To date, the polymer has been tested in different cell lines, including

human endothelial cells and different types of human carcinomas^{7,218-220}. All studies showed that the polymer is fundamentally biocompatible. Nevertheless, it is still necessary to assess the polymer toxicity at the specific condition of the specific biomedical application. The biocompatibility of the polymer, combined with thermoresponsive properties, makes PNVCL a perfect candidate for biomedical and environmental applications. Due to its biocompatibility, the polymer has been commercialized as a hair setting product by the name of Luviscol® Plus²²¹. To date, the non-biodegradable nature of PNVCL represents its major drawback. PNVCL absorbs numerous organic compounds from water^{208,211,222}. As reported by *Makhaeva et al.*, charged surfactants binds to PNVCL due to hydrophobic interaction²²². In recent years, *Rejinold et al.* developed degradable nanoparticles with low-toxicity and efficient cell uptake by combining PNVCL with CS^{104,223}.

Since PNVCL exhibits an LCST point in the proximity of physiological temperature, the polymer has been studied for applications in biochemistry and medicine. Due to its filming properties, the polymer has been studied for the fabrication of responsive surfaces. The polymer has been successfully applied for the bioseparation of proteins and tissue engineering²²⁴⁻²²⁷. The precipitation of trypsin using thermoresponsive PNVCL-based membrane was first reported in 1992²²⁵. Most of these applications relies on the ability of transforming the polymer backbone to an insoluble state upon temperature exposure. Upon covalent modification, the polymer is covalently coupled with ligands that are specific to a target protein. By raising the temperature, the protein-polymer complex is precipitated. PNVCL was also investigated as a suitable environment for cell proliferation and manipulation. The implantation of PNVCL cryogels in C57B1/10 mice has been studied by *Shakya et al*²²⁷. The study demonstrated that the gel degraded rapidly and excluded local or systemic toxicities. Another aspect that makes PNVCL so interesting from the biomedical point of view is the possibility of realizing thermoresponsive hydrogels. Hydrogels represent a class of materials that exhibit a three-dimensional and elastic network, which is formed from polymers crosslinked chemically or physically to form insoluble polymer matrices. In aqueous solutions, PNVCL hydrogels can swell or shrink with as a response to a temperature change. A more detailed description on the application of hydrogels in biomedical applications will be provided later in the section entitled “Microgels: polymeric nanoparticles” .PNVCL hydrogels have been successfully applied the entrapment of various enzymes, such as trypsin and carboxypeptidase B, and for animal cell immobilization^{7,8,228}. The hydrogel scaffold increases the stability of enzymes without

affecting their enzymatic activity²²⁸. PNVCL-based hydrogels have been studied as systems for controlled drug delivery, especially in conjunction with other polymers. The utilization of copolymers containing PNVCL grafted onto polysaccharides have been reported for the preparation of hydrogels, microspheres, microgels and nanoparticles. The presence of a high content of functional groups in macromolecules such as CS, alginate or dextran has allowed to create many different biocompatible copolymers. The synthesis is usually started by generating free radicals on the polysaccharide backbone, which are subsequently used as macroinitiators for the monomers. In other cases, the two polymers are attached with a condensation reaction. In most of these syntheses, PNVCL is provided with a carboxyl group at the end of the polymeric chain.^{7,8}

1.9 Polysaccharides: natural biocompatible polymers

Polysaccharides, also known as polymeric carbohydrates, are natural polymers built from monosaccharides via O-glycosidic bonds that can be isolated from different sources, including animals, plants, algae and other microorganisms, such as bacteria and fungi²²⁹. Polysaccharides represent a broad class of materials with wide structural diversity and functional versatility, which derives from the abundant presence of functional groups along the molecular chains. The abundant presence of hydrophilic groups, mainly hydroxyl, carboxyl, carbonyl and amines, provides aqueous solubility and allows the possibility of adhesion and recognition between biological tissues via non-covalent interactions.⁶⁷ Due to their excellent adaptability to the cellular physiology, polysaccharides fall into the category “generally recognised as safe” (GRAS) defined under sections 201(s) and 409 by the Federal Food, Drug and Cosmetic Act, meaning that they are considered biocompatible, biodegradable and non-toxic materials^{67,126,229}.

Polysaccharide can be classified according to their chemical structure or composition, source, solubility and applications. Based on their chemical structure, polysaccharides are divided into homoglycans, which consist of a polymer made by the repetition of a single type of monosaccharide, and heteroglycans. Another useful way to classify the polymers is by considering their positive charge, as it defines the interactions between the polymer and the biological tissues. Due to recent advances in technology and processes, polysaccharides have been established as important alternative materials in various applications for their versatility, low cost and ease of use.²³⁰ On account of these advantages, many polysaccharides such as CS, hyaluronan, dextran, cellulose, starch, pectins and pullulan

Chapter 1: Introduction

have been extensively used as drug-delivery materials.²³¹ Their inherent bioactivities allow to modulate the response of the immune systems and include receptor recognition and binding, site specific enzymatic degradation, mucoadhesion and transport and environmental triggering²²⁹. A list of polysaccharide biomedical application is reported in Table 3^{232,233}. In addition, upon contact with water, hydrophilic polymers can form hydrogels, which are solid-like materials composed by water and a three-dimensional polymer network. Due to their high water content, which can be up to 99% of their total mass, hydrogels provide tissue-like properties that have been studied extensively as drug delivery systems for their biocompatibility and the ability to encapsulate drugs²³⁴. By means of chemical modifications, polysaccharides that undergo gelification can be modified in order to provide the desired properties as a building block for the development of drug delivery systems. Recent advances led to the development of smart platforms, provided by both bulk and nano-sized hydrogels (micro- and nanogels), which are able to respond to a specific internal or external trigger due to their chemical structure. Due to their ability to respond to different and multiple stimuli, these systems cover a wide range of applications. These promising structures are usually referred as “smart drug delivery systems” and their application is still confined in pre-clinical trials for the lack of toxicity assessments and standardized manufacturing methods.²³⁵

Source	Name	Structure	Biological activity
Plants	Cellulose	β -(1 \rightarrow 4) linked D-glucopyranose	Bowel movement regulator, stool bulk increaser
	Hemicellulose	Xylans, mannans, mixed linkage β -glucans and xyloglucans	Bowel movement and cholesterol level regulator, free radicals scavenger, immunomodulator and antithrombotic
	Starch	α -(1 \rightarrow 4) and/or (1 \rightarrow 6) linked D-glucopyranose	Prebiotic agent, regulation of blood glucose levels, enhancement of mineral absorption, prevention of colorectal cancer
	β -glucans	β -(1 \rightarrow 4) and β -(1 \rightarrow 3) linked D-Glucopyranose	Cholesterol and blood glucose levels regulator, immunostimulator, antihypertensive
	Glucomannan	β -(1 \rightarrow 4) linked-D-glucopyranose and β -(1 \rightarrow 4)-linked D-mannose	Cholesterol level regulator, anti-constipation agent
	Inulin	β -(1 \rightarrow 2) linked D-Fructofuranose	Hypolipidemic and prebiotic agent, mineral absorption enhancer
	Pectins	α -(1 \rightarrow 4) linked D-galacturonic acid and rhamnose backbone, arabinose, galactose, xylose side chains, partially O-methyl/acetylated	Cholesterol level regulator, intestinal immunomodulator, gastric and small-intestine and cholesterol-lowering effect, gastric emptying decreaser
	Guar, arabic and locust ben gum	Galactan, xylan, xyloglucan, glucuronic mannan, galacturonic rhamnosan type	Hypocholesterolemic and hypotriglyceridemic agent, gastric emptying decreaser

Chapter 1: Introduction

Animals	Chitin and chitosan	β -(1 \rightarrow 4) linked D-glucosamine, partially N-acetylated	Tablet component, absorption enhancing agent
	Hyaluronic acid (hyaluronan)	β -(1 \rightarrow 4) and β -(1 \rightarrow 3) linked glucuronic acid and N-acetylglucosamine	Useful in cancer, wound repair, inflammation, granulation, cell migration, skin healing, fetal wound healing
	Heparin	2-O-sulphated- α -L-iduronic acid, β -D-glucuronic acid and N-sulfated or 6-O-sulfated- α -D-glucosamine	Anticoagulant, used in cancer treatment, tissue engineering, and biosensors
Algae	Alginates	B-(1 \rightarrow 4) linked D-mannuronate and α -L-guluronate	Controlled drug release, cells encapsulation, tissue engineering and for preparation of dental molds
	Carrageenan	α -(1 \rightarrow 4) and β -(1 \rightarrow 3) linked D-galactose and D-anhydrogalactose, partially substituted by ester sulphates	Buccal, ophthalmic, and vaginal drug delivery systems
	Red algae sulphated polysaccharides, porphyran,	Backbone of alternating β -(1 \rightarrow 3) linked D-galactosyl units and α -(1 \rightarrow 4) linked L-galactosyl, (1 \rightarrow 6) 3,6-anhydro or sulphate- α -L galactosyl units	Antiviral (herpes simplex virus types 1 and 2)
	Green algae sulphated polysaccharides	(1 \rightarrow 3) linked galactose, (1 \rightarrow 3) linked arabinose, partially 6-O and 3-O sulphated, (1 \rightarrow 4)-linked glucopyranose and terminal (1 \rightarrow 4)-linked xylose	Antioxidant and anticoagulant
Microorganisms	Dextran	α -(1 \rightarrow 6) linked D-Glucopyranose with α -1,3 branches	Plasma expander
	Pullulan	α -(1 \rightarrow 4) and α -(1 \rightarrow 6) linked glucan or maltotriose	Anticoagulant and plasma expander
	Xantan gum	α -(1 \rightarrow 3) linked glucopyranose backbone with trisaccharide side chains containing D-mannose- β -(1 \rightarrow 4)-D-glucuronic acid- β -(1 \rightarrow 2)-D-mannose	Carrier for drug and proteins
	Gellan gum	D-glucopyranose- β -(1 \rightarrow 4)-D-glucuronic acid- β -(1 \rightarrow 4)-glucopyranose- β -(1 \rightarrow 2)-L-rhamnose α -(1 \rightarrow 4)	Multifunctional excipient for pharmaceutical formulation

Table 3 List of polymeric biomaterials related to their sources and applications.

In a drug delivery system based on polysaccharide particles, the polymeric biomaterial provides the scaffold in which the drug is absorbed or bound to the internal or to the external surface. This increase the stability of the drug in an unsuitable environment and can also enhance its solubility, therefore providing enhanced permeation and retention at the site of interest²²⁹. Furthermore, the functional moieties on the carbohydrate backbone can be modified chemically in order to conjugate imaging probes and targeting agents, such as antibodies, in order to provide prolonged circulation time and site-specific accumulation activities⁶⁷.

To the present date, one of the main drawbacks to the utilization of polysaccharides in drug delivery comes from the variability of their properties. Natural sourced polymers usually have broad molecular weight distributions that can significantly vary between each batch¹²⁶ and their properties cannot be changed easily due to the lack of solubility in most organic solvent²³⁶. The molecular weight, along with molecular composition, is one of the main determinant factors of the polysaccharide behaviour in a physiological environment and determines chain flexibility, intra- and intermolecular interactions, scaffold shape, surface charge, drug loading capacity and polymer solubility in blood and plasma. Moreover, this set of physicochemical properties establishes the type of interactions with the proteins and its immunogenicity. As a consequence, the controls concerning the development of polysaccharide drugs or drug scaffold start from the standardization of the synthesis process and product characterization since the preliminary stages of development in the laboratory. The need for improvement in the quantification and the standardization of their physicochemical properties has posed considerable problems for the development of polysaccharide-based drug delivery systems with well-defined characteristics that can reach a clinical approval. In general, their translation into clinical studies requires more insight on their drug release properties, targeting and therapeutic efficacy and a more detailed description of their degradation profile. Despite this, some formulations have entered clinical trials with different types of delivery routes, including percutaneous or intracoronary injection, intravenous infusion, inhalation, xenotransplantation, intravesical instillation and topical skin application²³⁷.

The first polysaccharide that entered phase I of clinical trial was dextran, in 1993, under the name of AD-70, and was developed in Germany in 1993 by *Danhauser-Riedl et al.* for the treatment of refractory solid tumors.²³⁸ Over the years, CS (Millican, 2006, small HCC)²³⁹, hyaluronic acid (Radiaplex, 2007, radiation dermatitis)²⁴⁰, cyclodextrins (CALAA-01, 2008, solid tumours)²⁴¹ and alginate (DIABECCELL, 2009, type I diabetes)²⁴² have also reached the clinical trial stage, although the development stage of treatment has never advanced beyond phase III.

1.10 Chitosan

Chitosan (CS) is a biodegradable and biocompatible polysaccharide consisting of a linear polymer of β -(1 \rightarrow 4) linked glucosamine (2-amino-2-deoxy-glucopyranose). The polymer is obtained through N-deacetylation of chitin, which is a natural polymer contained in the

cell walls of fungi and arthropods such crabs and shrimps (Figure 6). Initially, CS was thought to be an easily accessible substance from seafood industry waste. Another natural source for CS is mushrooms, and it is considered to be safer for biomedical application as it usually exhibits narrower molecular weight distribution compared to CS obtained from animal sources²⁴³. To this date, CS is one of the most cited polymers in a very extended scientific range which includes food science, environmental, biopharmaceutical and biomedical applications²⁴⁴. The polymer first appears in a study by Clark and Smith that described the X-Ray investigation of N-deacetylated chitin fibres extracted from lobster tendons²⁴⁵. By early 2020, the polymer is mentioned in about 75,000 papers (source: Scopus, November 2020). Among all the natural polymers, its uniqueness is represented by the presence of the glucosamine monomer, partially or fully deacetylated. This structural characteristic is the basis of its remarkable biophysical properties. In aqueous solution, the polymer behaves like a linear polysaccharide with positive charge density at low pH, making it the only positively charged high molecular weight polysaccharide produced on

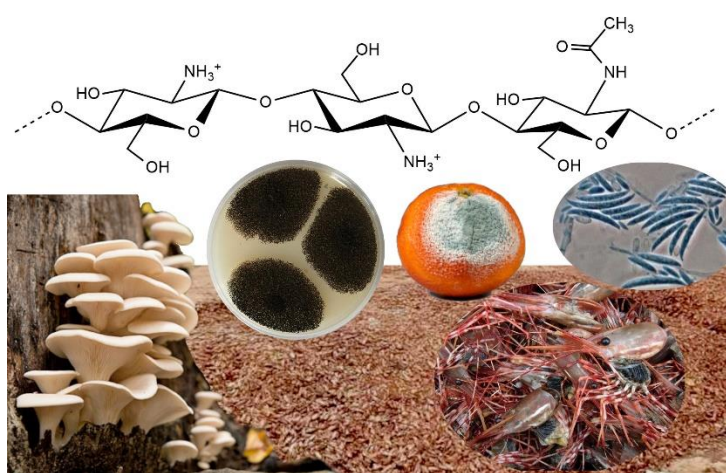


Figure 6 Natural source of chitosans: animals (seafood waste, mainly crabs and shrimps) and mushrooms (from left to right: *Pleurotus Ostreatus*, *Aspergillus Niger*, *Penicillium Citrinum*, *Fusarium Oxysporum*).

an industrial scale²⁴⁴. Commercial CSs are produced in high yields with average molecular weights between 3.8 and 2,000 kDA and have a degree of deacetylation (DDA) between 66 and 95%^{244,246}. For this reason, its more appropriate to talk about “chitosans” whether than chitosan, as the term implies a series of copolymers that differs in the percentage of fractions (the deacetylated degree, DDA), but also in the distribution and the length of the comonomer sequences (Figure 7). Unfortunately, this copolymer character has been strongly underestimated in literature,

an industrial scale²⁴⁴. Commercial CSs are produced in high yields with average molecular weights between 3.8 and 2,000 kDA and have a degree of deacetylation (DDA) between 66 and 95%^{244,246}. For this reason, its more appropriate

to talk about “chitosans” whether than chitosan, as the term implies a series of

where it has been extensively studied for close natural polymers, such as alginates. The two monomers, glucosamine and N-acetylglucosamine, display different solution properties as the first provides the ionic character and the second is slightly hydrophobic. This difference is amplified by the presence of block-type sequence and can have dramatic consequences on chain conformation and aggregation²⁴⁴. Due to the presence of amino groups, CS has intrinsic acidic properties and its pKa is between 6.17 and 6.51, depending mainly on the molecular weight and the DDA²⁴⁷. Consequently, the polymer is not soluble at neutral pH and its solubility is troublesome when the pH is kept over 6, especially at high

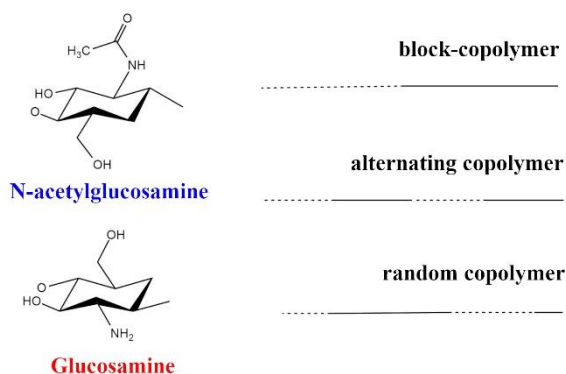


Figure 7 Schematic representations of three possible conformations for chitosan copolymers. The chemical structures of the two repetitive units are represented on the left.

molar masses.²⁴⁴ Many studies have reported the utilization of derivatives, such as 6-O-Pegylated CS^{248,249} and trimethylammonium derivatives^{244,250,251}, for the utilization of CS at physiological pH. Other studies report chemical and physical treatments in order to achieve low molecular weight (LMW) CS for enhanced solubility and faster degradation²⁵². CS has been extensively studied as a polycationic biomaterial for its ability to adhere to negatively charged surfaces. It was originally conceived as an excipient for solid dosage form and it has been used in coating, tablet binder, lubricant, viscosity-increasing agent, disintegrant and mucoadhesive. In relation to synthetic cationic polymers, CS has very low immunogenicity and can be used as a bioadhesive for negatively charged mucosal cells and increase transport and retention properties²⁵³. The first study reporting the utilization of CS for drug delivery was published by Henriksen in 1993²⁵⁴. The mucoadhesive properties of CS have been demonstrated by its ability to adhere to porcine gastric mucosa in vitro²⁵⁵. It is believed that the positive charge enables to enhance the opening of the epithelial junctions and to widen paracellular pathways²⁵¹. Basing on these considerations, CS have been studied has a scaffold polymer for both hydrophilic and hydrophobic drugs^{256,257}. Although the initial attention was focused on the formulation of microparticles^{244,251}, the attention has rapidly shifted towards the fabrication of nanoparticles along with the rising of nanomedicine. The choice between a nano- or micrometric based formulation is defined by the type of application. For the case of

pulmonary delivery, microparticles have better efficacy²⁴⁴, while nanoparticles are usually preferred for intravenous administration, unless the formation of an embolus is intentional, such as in chemoembolic treatment¹. The pathways for the fabrication of CS micro- and nanoparticles are discussed in the “Ionotropic Gelation” section. Furthermore, it has been suggested that CS is a valuable polymer for gastrointestinal and small intestine drug delivery²⁵⁰. Up to date, thanks to the opportunities provided by the developing of nanostructure systems and by modifying the polymer backbone with ionic or hydrophobic moieties, there are thousands of different formulations for dental, buccal, gastrointestinal, colon, mucosal and gene delivery²⁵⁸. There are also studies on the utilization of CS particles for cancer treatment, most importantly Millican, which has entered clinical trials for the treatment of small HCC²³⁹. Chemotherapy drugs are conjugated involving the several free amine groups. The interaction with the drug could be by means of weak interactions or covalent bonds, depending on the required flexibility of the system and the application. For examples, many studies report the conjugation of DOX to CS via a succinic anhydride spacer²⁵⁶. Another approach involves the formation of micelles, or core-shell nanoparticles, for the encapsulation of chemotherapeutics, which can be applicable for both hydrophilic drugs (es. DOX) or hydrophobic drug with low water solubility, such as 5-fluorouracil or paclitaxel²⁵⁶. Other properties include bioactivity as antioxidant, antimicrobial and antifungal²⁵¹. The killing potential is based on the electrostatic interaction with the negatively charged microbial surface, that dramatically affects the bacterial vitality²⁴⁴.

1.11 Microgels: polymeric microparticles

One of the main efforts in biomedical research focus on the design of new nano- and microstructured, biocompatible materials that does not necessarily come from natural origin. In this field, gels, microgels and nanogels have become popular due to their high biocompatibility and the significant progress in the field of polymer synthesis. As we already reported, gels are defined as three-dimensional polymeric networks that are swollen by the presence of a solvent. The type of crosslinking can be of physical or chemical origin, depending on the type of the interaction between the different chains. If the water is the dispersion medium, a gel is commonly referred as hydrogel. Over the years, cross-linked polymers have been prepared in a wide range of compositions, structures and topologies. Furthermore, numerous efforts have focused on the development

of finely dispersed cross-linked polymeric particles with a size range that span from few nm to several μm . When the size is reduced to the colloidal regime, a gel is generally referred to as a nanogels if the overall size is below 100 nm. According to the IUPAC definition, larger objects, from 100 nm up to several microns, are called “microgels”, even though the two designations are not always used strictly²⁵⁹. On the other hand, the growing interest in nanotechnologies and the phenomenon of "me too science" resulted in a general preference for the utilization of the term nanogels, however inappropriate, for particles with size inferior to 1000 nm. This semantic problem is similar to the definition of nanoparticle that was previously mentioned. Normally, biomedical or oncological research institutes are not necessarily involved in the synthesis of nanoparticle systems. In these research fields, the primary interest in the utilization of such systems is linked to their biological potential and the definition of “nanoparticle” or “nanogel” is commonly used inappropriately. In clinical applications, particles larger than 100 nm represent the majority of the colloidal systems used for clinical applications. Although it is true that small particles are used in some formulations, they are always enclosed within systems that easily fit within the scale of the "micro". The utilization of bigger enclosures prevents small nanoparticles from being easily removed from the body and improves their therapeutic effectiveness⁷⁹⁻⁸⁷. In the case of microgels, however, the IUPAC definition is particularly important as it spans a very wide range of dimensions. This is related to the fact that it is easy to assume that a material of 100 nm, having a very low percentage of surface atoms, has surface properties that are closer a bulk material than a material of a few nm in size⁷⁵⁻⁷⁸. Nevertheless, while it is easier to think that a particle of a few nm may have superficial properties similar to those of a polymer chain, being in the same dimensional range, it is easy to see why materials between 100 and 1000 nm have been so successful in the medical field. Their reduced surface activity makes them more biomimetic materials than smaller nanostructures and they additionally have the same size range of cell vesicles and proteins. Another important feature of microparticles with an overall size around 100 nm is that they provide long-lasting circulation. This increase the possibility of the microparticle to extravasate through fenestration tissues present in tumours, which are usually between 380 and 780 nm in size. However, non-continuous epithelia are also present also in the liver, with vascular fenestrations measuring between 50 and 100 nm, and in the spleen, due to the presence of interendothelial cell slits between 200 and 500 nm²⁶⁰. For these reasons, some studies reported that particles between 70 and 200 nm have the ideal size to accumulate passively within tumour tissues^{59,60,261}. A "golden

dimension", in fact, does not exist and the ideal size threshold is often subject to interpretation. It is likely that the reference to this "ideal size" was originated by a breakthrough study published in 1990 study by *Klibanov et al.*, which described the long circulation times of PEG-grafted liposomes²⁶². However, although the advantages of the utilization of liposomes in drug delivery have been extensively demonstrated, it cannot be excluded a priori that these size thresholds can change depending on the materials and the type of particle used. Also, the ability of the nanoparticle to accumulate in the target tissues can depend on the tumour type and it is influenced by many microenvironmental factors. Particles between 70 and 200 nm exhibit surface properties that resembles those of bulk materials (Figure 8), even though there are few studies that focus on the utilization of microgels for catalysis applications²⁶³. However, while falling within the "nano" range, the interest towards microgels in biomedical applications is primarily related to their metabolic fate. Initially, the miniaturization of the delivery devices was focused on the development of micrometric particles ($>1 \mu\text{m}$)^{264,265}. In fact, many commercial formulations and "innovative" therapies are still based on this principle. For some applications, such as chemoembolization, which is a common strategy for the treatment of HCC, this paradigm

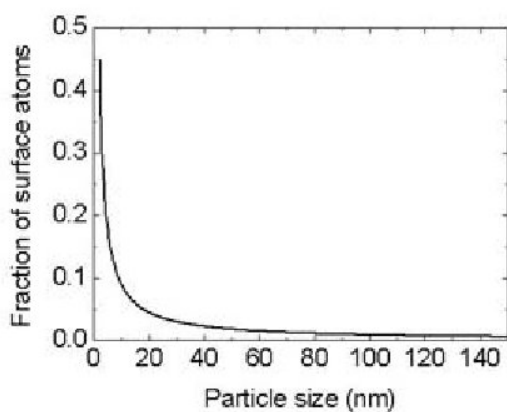


Figure 8 Fractions of surface atoms as a function of the particle size for cubic shape ($\alpha = 6$) and interatomic distance $a = 1.5 \text{ \AA}$. Over 100 nm, the percentage of surface atoms is close to zero. Picture available by CC by 3.0 license (right and sharing of the material for any purpose).

has not yet changed, and micrometric particles are used^{1,4}. However, by further miniaturizing the medical devices, it is possible to overcome some limitations that are related with the utilization of bigger particles. One of these important limitations is the treatment of advanced tumors¹. In addition to oncology, the ability to produce smaller nano- and microgels has opened up new possibilities for the treatment of other pathologies (e.g. osteoarthritis²⁶⁶, schizophrenia²⁶⁷, bacterial infections²⁶⁸, vaccine delivery^{42,269}) and for cosmetic applications. Systems of such

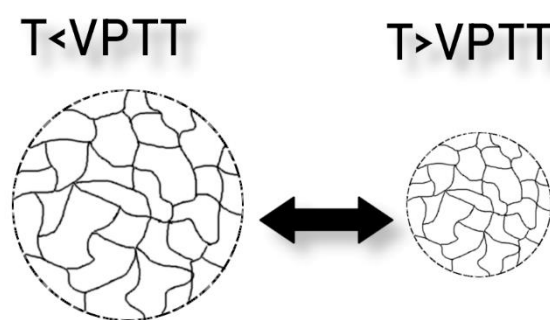
dimensions, such as the aforementioned liposomes, are similar in size to microgels and are usually prepared in a range between 50 and 250 nm. To date, they are present in many commercial formulations and are present in most drugs based on "nanotechnologies" that widely used in oncological hospitals (e.g. Liposil²⁶⁰). Another recent example of these

drugs is Pfizer's Covid-Sars-19 vaccine, consisting of mRNA filaments encapsulated inside a liposomal envelope²⁷⁰.

Nano- and microgels can be considered as soft and deformable particles with an internal gel structure that is swollen by a solvent. The presence of the three-dimensional polymeric network makes them hollow particles and they can be used for drug encapsulation. Due to their softness, their behaviour resembles the one of macromolecules and they exhibit a quick response to changes in solvent quality by changing their local conformation. They also behave like surfactants, and they reduce the interfacial tension by adsorbing to interfaces. Nanogels and microgels are highly regarded for the unique dynamicity and permeability of their architecture and their deformability and they are emerging as important candidates for biocatalysis, sensing and drug delivery systems. Basing on their different composition, micro- and nanogels facilitate the delivery of therapeutics in various applications due to their tunable porosity, elasticity, composition and colloidal stability²⁶³. In clinical applications, the current challenges focus on the identification of suitable substances that can be loaded into their core in order to be delivered on purpose to the target of interest. The research of responsive microgels is aimed to determine the conditions under which the mesh of the micro or nanogels can swell or shrink, in order to provide a suitable trigger for the release of the therapeutic. Drug-triggered releases are of particular interest in the oncologic field as they allow the release of the drug to be gradual. Their unique properties make them perfect candidates to provide the so-called "enhanced permeation and retention" (EPR) effect, which consist in an effective reduction the chemotherapeutic toxicity along with the increase of its effectiveness²⁴. The lack of degradability of some of the materials used for the production of nano- and microgels has limited the potential of the utilization of such materials for *in vivo* applications. Recent achievements in the fabrication of biodegradable alternatives have provided new appealing strategies for the design of new polymeric delivery systems, such as the combination of synthetic polymers with polymer of natural origins²⁶³. However, what could really make this type of technology a breakthrough in oncology is the ability to "drive" the release and control it remotely. Over the years, microgels that are able to respond to different types of triggers (temperature^{7,90,91,95-104}, magnetic fields^{20,84,98,105-109}, concentration gradients¹¹⁰⁻¹¹², etc...) have been prepared in various sizes and compositions, depending on the application for which they were designed. The development of dual-responsive microgels provided a step forward in this direction^{99,106,113,114}. CS, which is usually described as a responsive pH material, has been combined with various polymers for the fabrication of multi-responsive

microgels. By combining CS with a thermoresponsive material such as PNIPAM or PNVCL, pH and thermoresponsive microgels can be fabricated^{91,93,96,99,100,271}. These types of systems are of particular interest in oncology, as they provide an opportunity to exploit the mild acid environment that surround tumours. Gold Nanoparticles (Au NPs) and superparamagnetic iron oxide nanoparticles (SPIONs) have also been encapsulated within double-responsive polymeric microgels in order to fabricate hybrid materials that exhibit multi-responsivity^{96,99,272}. Au NPs provide local heating upon exposure to near-infrared (NIR) frequencies. As the particles heat, the thermoresponsive network reacts and the drug is released by the core of the microgel. In this way, it is possible to carry out a combinational therapy based on both drug release and thermal-induced apoptosis. On the other hand, magnetic microgels can produce local heating upon the exposure to an alternating magnetic field. This causes a relaxation or collapse of the gel chains, which induces the release of the drug contained within the gel.

The transition temperature of a thermoresponsive gel is usually referred as the volume phase transition temperature (VPTT) and it describes the behaviour of the polymeric meshes (Figure 9). A gel can shrink or swell, depending on the type of thermoresponsivity. Although there are some studies focus on the mechanistic aspect of these devices^{101,171}, their mechanism is not always entirely clear. Usually, microgels are easily characterized by using DLS equipment that are accessible within biological laboratories and their response is characterized by a dramatic change in their size distributions. However, by using DLS, the aggregation processes of microgels are similar, if not indistinguishable, to the ones of polymeric solutions. This usually occurs if the VPTT is close to the LCST, and their vicinity have been demonstrated for many formulations^{99,171,273}. Another limit of the DLS is also to assume that the objects detected are spheres. From the IUPAC definition of microgels, it can be inferred that microgels can be spherical, but they can have different shapes. Even if we put a spherical microgels under consideration, the Gaussian distribution provides the D_h , which is different from the real diameter of the microgels. DLS provides the measurement of hypothetical hard sphere that diffuses with the same speed as the particle under examination. In practice, polymeric microgels are non- or quasi-spherical particles with a



big solvation shell. Therefore, the size calculated from their diffusional properties represents the apparent size of the solvated particle. In this condition, it is very difficult, if not impossible, to establish the actual shape of a nano- or a microparticle with the means available in a biological laboratory, especially if the particle is made of amorphous material. However, it is possible to relate the data to the other values reported in literature. In fact, one of the problems in standardizing polymer particles is due to the difficulty of controlling their shape, and this is particularly evident for microgels that are formed by self-assembly reactions. The form these aggregates depends primarily on whether the solvent is a good solvent at a certain temperature. Microgels shape can be estimated through computer simulations that considers the interactions that take place in a certain environment. When the shape of the microgel particle is known, a sample can be analysed via small angle X-Ray scattering (SAXS) by using its form factor. By fitting the spectral information, the dispersity and the average dimension is provided with high statistical significance. On the other hand, despite the growing interest in the application of this technique for the detailed study of self-assembled microgels^{274,275}, this approach was considered outside the interest of the project. In any case, it should be noted that the main aim of this research was to develop thermoresponsive particles of a target size of about 200 nm, regardless of their shape. The interest towards this size range is motivated by the necessity to develop of a device for the treatment of liver cancer, or HCC. Also, particles in this size range allow to avoid cytotoxic effects that are usually related to the presence of large aggregates (>500 nm) and to avoid the production of small nanogels (<50 nm) that are not subjected to rapid renal excretion for *in-vivo* applications. The process of formation of microgels will be explained in the next chapter.

1.12 Ionotropic gelation

Ionotropic gelation probably represents the most studied preparation for CS-based microparticles and nanoparticles (Figure 10). The process exploits the sol-gel transition of CS polymers in the presence of a polyanionic crosslinking agent, such as sodium triphosphate (TPP). Due to the absence of toxic reagents, the low energy requirements and the presence mild and aqueous processing conditions simplicity, the process has received a remarkable amount of research attention and has become one of the standard encapsulation methods for the preparation of CS nanoparticles. CS-based particles have been prepared with ionotropic gelation for drug delivery, gene therapy application and

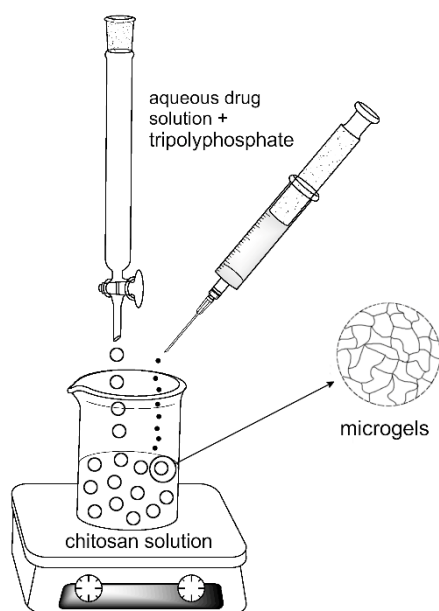


Figure 10 Schematic representation of ionotropic gelation setup.

protein formulation²⁷⁶. The formation of micro- and nanoparticles through ionotropic gelation is based on the weak basic properties of the CS molecule. Due to the presence of D-glucosamine residues, CS behaves a polyelectrolyte with a strong positive surface charge in acidic conditions and interact strongly with polyanionic molecules such as TPP. In neutral and alkaline pH, CS is insoluble unless it is chemically modified. The first production of CS microparticle via ionotropic gelation was reported by Calvo *et al.* in 1997²⁷⁷. The approach described by Calvo provided microparticles in the 200-1000 nm range. By the time of the study was published, CS beads were already studied for their ability to respond pH changes and their positive charge, but

due to their large size (1-2 mm), they were not suitable for deposition on nasal and mucosal mucous membranes. Also, Calvo's contribution provided an alternative to the utilization of glutaraldehyde, a covalent crosslinker that allowed to produce microparticles with a good degree of monodispersity, but possibly antigenic. In addition, the procedure offered for the first time the possibility for the incorporation of proteins or peptides that would suffer from covalent crosslinking. The study demonstrated that ionotropic gelation prepared CS microparticles allow to encapsulate proteins with high efficiency and laid the foundations for future studies on gene and antigens therapies²⁷⁷. Over the years, ionotropic gelation has also been extensively studied for the delivery of both small drugs and macromolecules²⁷⁸. Despite the apparent simplicity of the process, the interaction of the CS polycation with a polyanion cannot be completely explained by the electro-neutrality principle. The gelation process involves the formation of a three-dimensional network that occurs due to both inter and intra-molecular cross linking of the positively charged CS chains^{278,279}. The TPP anion can possess up to five negative charges depending on the pH of the solution. Consequently, the crosslink can occur either between two protonated amine groups belonging to the same polymer chains (intra-molecular) or between groups that belongs to different polymer chains (inter-molecular)²⁸⁰. By changing the preparation parameters, it is possible to influence the interaction between CS and TPP in order to produce micro- and nanoparticles and reduce their dispersity. It has been reported that the

fabrication of nanoparticles requires dilute polymer concentrations, in order to ensure that local gelation process take place within small polymer coils. In a semi-dilute regime, the probability of polymer chains overlaps increases, and the formation of much larger particles is most likely to occur. One of the first correlations between the concentration of TPP and the polymer and the formation of nanoparticles was reported by *Pan et al.*, although it was based on a limited number of attempts and the use of a single type of CS with high molecular weight (HMW) and an 89% DD²⁸¹. In general, polymer particles are produced in a concentration range of 0.5 to 2 mg/ml, although some examples of higher concentrations have also been reported²⁷⁹. In any case, a direct correlation between the properties of nanoparticles and the polymer should be established for each individual batch of polymer considered. The lack of batch-to-batch uniformity associated to the polymer often results in poor control over size distribution, high dispersity and inconsistent results²⁸². In some cases, the associated variables are such that the correlation should be done on a single weight of the polymer. Under these conditions, it is naturally difficult to guarantee total reproducibility of the experiments. In fact, despite the abundance of empirical data about the preparation of micro- and nanogels through ionotropic gelation, their preparation mainly relies on trial and error and the correlations between their formation process, interaction and structure are not totally understood^{278,282,283}. CS chains can originate very different particles based on their structural properties, including molecular weight (MW), index of polydispersity, deacetylation degree (DDA), and D-glucosamine distribution along the polymer backbone. These parameters can affect both the stiffness and flexibility of the polymer and the viscosity of the solutions that are used for the preparation of the particles²⁵². The most crucial parameter for the formation of particles with low dispersity is the CS/TPP ratio. This ratio usually defines the microgel average diameter and the drug release properties. Lower CS/TPP ratios have generally resulted in smaller particles with lower zeta potential, while higher CS/TPP ratio have been employed to form bigger particles and, in some cases, to induce the precipitation of micrometric particles. In general, particles are prepared using a ratio between 1.75:1 and 6:1, although each individual sample needs be evaluated separately^{277-279,283,284}. For chemically modified CS, such as N-grafted polymers, these ratios may vary greatly as ionotropic gelation requires free amine sites to take place⁹⁹. The utilization of different pH during particle preparation has also a moderate effect on the size of the particles, as the pH influences the number of charges on the TPP molecules²⁸⁰. By decreasing the pH, the interaction between CS and TPP is strengthened, and smaller particles are produced. In

general, CS nano- and microparticles are prepared in a range of pH between 4.5 and 5.5. According to some studies, the increase in molecular weight has a similar effect to the increase in concentration^{252,282,285}. This consideration is in accordance with the fact that higher molecular weights result in an increase in the viscosity of the solution. Based on this consideration, *Zhang et al.* prepared particles between 90 and 200 nm by fractionating the polymer to reduce its molecular mass distribution. The study showed that the particles had low polydispersity (<0.1) compared to other formulations (0.3-0.4), although the particles were not suitable for encapsulation of macromolecules due to the reduced molecular weight²⁸⁵. However, some studies argue that lower molecular weights results in bigger particles due to the reduced flexibility of shorter polymer chains²⁵². Other efforts have been made in order to tune the characteristics of CS-TPP nano- and microparticles, including adjusting the salinity of the solvent^{278,282}, changing the temperature²⁸⁶, and increasing the mechanical energy during their preparation²⁸⁷. *Fan et al.* reported a preparation in which the polydispersity (PDI) of microparticles was narrowed to 0.026 by diluting the quantity of acetic acid and reducing the ambient temperature during cross-linking. The microgels had a mean D_h of 138 nm and a positive zeta potential. In its hypothesis, the lower thermal agitation favours the formation of particles in a more orderly way and reduces the overlapping of polymer chains, thus reducing the polydispersity of the particles²⁸⁶. Interestingly, it has been demonstrated that dispersion and size of nanoparticles can be reduced by using monovalent salt solutions^{278,282}. *Huang et al.* demonstrated that the strength of the CS/TPP interactions can be strengthened through the addition of a monovalent salt, such as NaCl. The study revealed that small amounts of salt (150 mM) enhance the colloidal stability of microgels during their formation, while the binding is weakened at high ionic strength (500 mM). This suggested the hypothesis of an optimal concentration for the preparation of CS/TPP microgels with narrow size distribution. The hypothesis of *Huang et al.* was that the presence of NaCl inhibits the bridging between microgels and prevent their aggregation. This remarkable result demonstrated that CS microgels behave differently from other colloidal systems²⁸². Normally, the colloidal stability is determined by the sum of the potential energy of the attractive van der Waals forces and the repulsive electrostatic interactions. This description is the basis of the DLVO theory and is considered valid for the description of the behaviour of inorganic particles in solution²⁸⁸. However, when the particles in consideration are fully or partially covered with polymers, their behaviour is more complex to describe. If the polymer layer on the colloid exceeds a minimum thickness, dispersion forces are unimportant. At

moderate surface coverage, a critical point exists and depends on the theta point of the polymer²⁸⁹. In the case of CS nano- and microgels, it can be roughly assumed that the behaviour of the microgel is similar to that of a particle entirely covered with a polymer. Otherwise, it could be imagined that the behaviour of a microgels resembles the one of a “hollow” polymer particle which is exclusively formed by the polymeric coverage. Therefore, microgels should not be considered "nanoparticles" in the same way as we consider inorganic nanoparticles. Inside the microgel, the polymer chains can move within a series of constraints imposed by the three-dimensional structure of the gel, unlike inorganic particles in which all the atoms are condensed on the surface of a nanoparticle. Also, given the size of the only CS macromolecules in solution, which can reach up to 20 nm for high molecular weights, we can easily assume that small CS aggregates (<100 nm) are made of few macromolecules and their behaviour can be close to that of the single macromolecule in solution. The aqueous behaviour of microgels has a direct impact on the release profile. More specifically, drug release occurs mainly by three mechanisms: diffusion, swelling and erosion (Figure 11). The type of mechanism is strictly dependent on the type (ionic, covalent) and the degree of crosslinking. Covalent cross-linked microgels, such as CS-glutaraldehyde²⁹⁰, usually provides diffusion-controlled drug release, with the overall release profile depending on the cross-linking degree. Similarly, the swelling capacity is generally influenced by cross-linking density and environmental pH²⁹¹. The utilization of ionic cross-linkers, such as TPP, may result in erosion release profiles. In the initial part of the release profile, the kinetic of swelling and erosion determines a characteristic lag phase. Model equations for the interpretations of several different studies have been proposed by a huge number of studies^{244,292,293}. In general, diffusion-controlled behaviour can be interpreted with exponential functions, erosion-controlled release curves have a characteristic sigmoidal shape. Swelling-controlled behaviour may depend on the square root of time, as proposed by *Higuchi et al.*^{293,294}. The mathematical models that were used in this thesis are explained in the “Materials and methods” section.

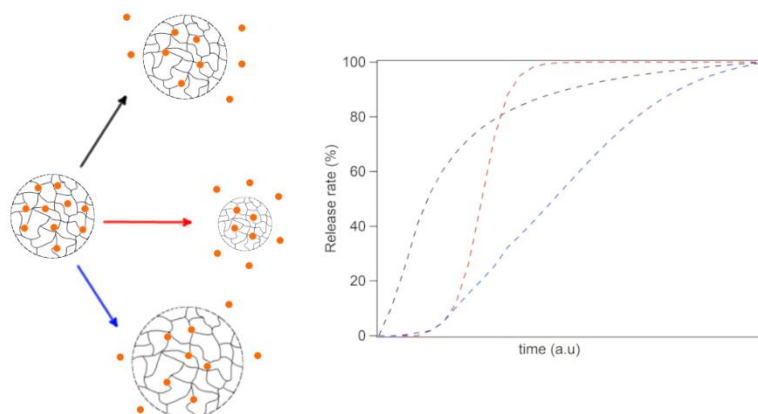


Figure 11 Representation of release mechanisms: diffusion (black), erosion (red) and swelling (blue) and related release curve according to different mathematical models.

1.13 Chitosan-Poly-N-Vinylcaprolactam (CP) microgels

In the previous chapters, it has been observed that the poor biodegradability of thermoresponsive polymers, such as PNIPAM and PNVCL, represents the main limit for their biological application^{7,8,295}. The solution of this problem was provided by the development of hybrid materials that were prepared by combining synthetic thermoresponsive polymers with biopolymers of natural origins^{104,223,243,296}. The synthesis of these hybrid materials has led to the development of thermoresponsive and biodegradable devices for drug delivery, such as gels and particles in the nano-, micro- and macroscale. Among the various natural biopolymers that can be combined with a synthetic thermoresponsive polymer, CS has proven to be an incredibly useful and versatile for its high compatibility and pH-responsiveness. The preparation of the first hydrogel that combined PNIPAM and CS was reported by *Wang et al.* in 2000²⁹⁰. The gel exhibited thermoresponsivity and the transition temperature was determined at 32° C, close to the LCST of the starting PNIPAM (31 ° C). For the preparation of the CS-based thermoresponsive gel, PNIPAM was modified with carboxyl termination groups prior to the preparation of the gel and gelation was achieved using glutaraldehyde²⁹⁰. To date, thermoresponsive polymer with carboxyl group terminations represents the most common way to prepare CS thermoresponsive copolymers. These pre-modified polymers are generally referred to as -COOH polymers for simplicity (*e.g.*, PEG-COOH, PNVCL-COOH, PNIPAM-COOH). The carboxyl end groups allow to create an amide bond with the amine sites present on the D-glucosamines distributed along the skeleton of CS. The coupling between the two functional groups results in the formation of a graft copolymer.

The reaction is commonly carried out through the activation of the carboxyl end group by using NHS and EDC. The initial procedure reported by Wang *et al.* did not require the synthesis of a copolymer prior to gelification. The synthesis of a thermoresponsive CS-g-PNIPAM copolymer was later described in 2006 by Chen *et al.*²⁹⁷, while the first CS-g-PNVCL copolymer (CP) was prepared by Prabakaran *et al.* in 2008⁹³. Over the years, numerous types of graft-copolymers have been prepared with CS using the coupling reaction between the amino and carboxyl groups. This type of reaction falls within the field of click chemistry, as it is relatively fast, requires mild conditions and produce inoffensive byproducts. On the contrary, the preparation of CS copolymers with different architectures (e.g. star, comb, brush, ring block) requires complex and expensive synthetic procedures²⁹⁸. In addition, the utilization of CS as a reagent entails some limitations for multi-step reactions due to its extremely low solubility in organic solvents. Due to the huge number of functional groups, chemical modification of CS is usually time consuming. Depending on the mass of the polymer, the initial protection reaction of the functional groups that are not involved in the reaction can take up to several days, depending on the molecular mass of the polymer²⁴³. Similarly, the determination of chemical structure through simple spectroscopic techniques such as ¹H-NMR can become very complex due to long-lasting spectral acquisition. Although a single polymer ¹H-NMR spectrum with sufficient resolution can be acquired within a single day, the acquisition of a ¹³C-NMR spectrum or a two-dimensional spectrum may take up to one week due to the high number of functional groups and the viscosity of the solutions²⁹⁹. For these reasons, these synthetic procedures are rarely accomplished inside university facilities and they are carried out on a larger scale by research institutes that are specialised in the study and the development of few specific polymers. For simplicity, scientists have turned their attention to the utilization of LMW CS with low dispersity for synthetic purposes^{252,278}. Also, the utilization of LMW CS for drug delivery systems has been promoted for its better solubility, biocompatibility, bioactivity, biodegradability and less toxicity in relation to HMW CS²⁸⁶. Nevertheless, the mild conditions required for the formation of graft copolymers allow the utilization of both LMW and HMW CS for the preparation of thermoresponsive copolymers. This allow to maintain some interesting biological properties that are connected to the high molecular weight of the polysaccharide. Both LMW and HMW CS are highly regarded for drug delivery, but only HMW have shown high encapsulation efficacy towards proteins^{285,300}. Furthermore, HMW CS require less chemical processing. In relation to LMW CS, HMW CS is generally cheaper and generally

regarded as a “greener” reagent. To this date, CP copolymers have been prepared with both HMW and LMW CS for the release of both hydrophilic and hydrophobic drugs. The first CP copolymer was prepared by using LMW CS (~30 kDa). In his work, *Prabaharan et al.* described CP as promising for possible applications of dual-responsive therapies. The study reported a protocol for the encapsulation of a hydrophobic drug, ketoprofen, during the preparation of CP beads via ionotropic gelation. The size of the beads was not determined, which suggests that the particles were at least micrometric in size. In fact, the term beads is commonly used as an abbreviation for the term microbeads, which are defined as uniform polymeric particles with a size between 0.5 and 500 μm in diameter³⁰¹. The ability of the copolymer beads to respond to both pH and temperature stimuli was demonstrated by swelling studies and release tests⁹³. The cytotoxicity of the CP beads was assessed using an MTT assay against e EA.hy 926 endothelial cell lines and the researched demonstrated that CP would have provided a safe and effective drug-delivery carrier within the living body. Despite being not nanotechnology-related research, the work of *Prabaharan et al.* paved the way for the development of CP-based nanoformulations^{91,96,99,104,223}. However, the discussion on the behaviour of PNVCL-COOH by *Prabaharan et al.* remains controversial. In its introduction, *Prabaharan* described PNVCL as a “*well-studied polymer with a lower critical solution temperature (LCST) at about 32 °C, which shows a well-defined response towards temperature*”⁹³ while not considering that PNVCL is a type I thermoresponsive polymer. As we already pointed out, PNVCL can exhibit a LCST between 25 and 50 °C as it depends on PNVCL molecular weight, concentration and the presence of salts. In addition, the characterization of the polymer in GPC-SEC was carried out in THF⁹³, a solvent which has later been described as unsuitable for molecular determination of PNVCL^{7,189}. Furthermore, few technical details on the analysis were reported. The molecular mass, which was established to be around 1 kDa⁹³, appears to be too low in relation to the LCST value. The data disagreed with the LCST-molecular mass dependence that were previously reported by Meeussen^{155,156} and later by Cortez-Lemus⁷. According to Meeuseen’s predictions, PNVCL must be at least 20 KDa to exhibit LCST lower than 35 °C¹⁵⁶, even though Meeusen study did not account for PNVCL with carboxyl group terminations. Nevertheless, the negligible effect of PNVCL terminations to LCST was demonstrated by *Shao et al.* in 2012³⁰². Another important consideration is that the molecular weight value reported by *Prabaharan* correspond to a small oligomer made of 8 repetitive units of NVCL. This seems apparently unrelated to the high molar ratio (122:1) that was used for

the synthesis of PNVCL-COOH⁹³. During the development of this project, we have shown that PNVCL-COOH of ~1 kDa exhibits higher LCST. In addition, it has been demonstrated that it is not possible to precipitate the polymer dissolved in DMF using diethyl ether below a critical molecular mass. Although this experimental evidence has not yet been discussed by any study, the solubility of a type I polymer is expected to be affected by the molecular mass in any solvent. The description of the miscibility behaviour of PNVCL-COOH in diethyl ether is pivotal to ensure the reproducibility of the synthetic procedure, since the solvent is used to obtain the polymer as a solid-state product⁹³. However, the following works on the development of CP-based delivery systems seems to neglect the problematic aspects of Prabakaran's work^{91,96,99,104,223}. In the following years, the work of Prabakaran on CP-related systems was continued by the research group of *Indulekha et al.* Instead of reporting the procedure for the synthesis of PNVCL-COOH, Indulekha referred directly to the preparation previously reported by Prabakaran^{91,96,99}. Similarly, other authors reported a very similar procedure for the synthesis of a PNVCL-COOH polymer with a LCST of 32 °C^{104,223}. None of these studies mentioned the different chemical-physical properties that exist between PNVCL polymers of different lengths, nor did they provide detailed guidance for the characterization of their molecular mass. In this way, these works have contributed on passing down the misconception that PNVCL possesses a well-defined LCST at 32 °C. Due to the difficulty of replicating the results of the published works, the research on CP-related nanodevices remained confined to a few research groups. To this date, there are almost 25 published papers on CP.

The first CP-related study that falls within the field of nanotechnology was published by Rejinold in 2011²²³. The study described a protocol for the preparation of microparticles for the release of 5-fluoruracil. Since 5-fluoruracil is a chemotherapeutic, the study opened up the possibility of using CP of material for oncological applications. Rejinold reported that the polymer was prepared with different ratios between CS and PNVCL-COOH in order to achieve a desired transition temperature of 38 °C for the drug release. The LCST of the copolymer increased as the percentage of thermoresponsive polymer decreases. The encapsulation of the drug was achieved by synthesizing nanoparticles by dissolving the drug into a concentrated CP solution (5mg/ml). The synthesis of the microparticles was achieved via ionotropic gelation. Interestingly, the concentration of acetic acid was rather high (1%) in comparison to what has been reported for the preparation of monodisperse CS nanoparticles²⁸⁶. The average D_h of the particles was reported to be between 180 and 220 nm and the polydispersity of the sample was not reported. Furthermore, the complete

distribution curve between 1 and 4000 nm is not available in the publication. Instead, the histogram related to the distribution focused only on the interval 100 and 300 nm. The main peak of the histogram is at 1% intensity, suggesting that the sample could have been highly polydisperse. We calculated that the integration of the size range provided by Rejinold provides a total percentage inferior to 5% of the reported intensity. Alternatively, it may be thought that the peak distribution was located at higher values. In addition, the number of measurements that was reported (3) is too low compared to the average standard of DLS analyses. Typically, a DLS analysis using a Malvern Z-Sizer, which is one of the most common instruments for the determination of the D_h , requires three cycles of analysis, each of which usually includes between 10 and 17 measurements. The particles were purified by centrifugation and lyophilized using sucrose as a cryoprotectant. The release tests were carried out by the lyophilized particles in phosphate buffer (pH 7.4) and show a dramatic change in the behaviour of the particles in relation to temperature. Despite the promising results of this research group, there is not enough evidence to establish that the elution profile of a CP nanoparticle is similar to that of the particles described by Rejinold. In another work published in the same year, Rejinold proposed a similar preparation for the preparation of curcumin-loaded CP microgels¹⁰⁴. The particles undergo thermal induced aggregation at 38 °C and their blood compatibility was demonstrated via an haemolysis assay. Curcumin-loaded microgels showed specific toxicity to cancer cells at above their LCST and the analysis of JC-1 mitochondrial membrane confirmed that the apoptosis was mitochondrial-mediated¹⁰⁴. A few years later, the same research group introduced for the first time the synthesis of CP hybrid particles consisting of CP microgels loaded with both Au nanoparticles and curcumin^{303,304}. Microgels were prepared using the ionotropic gelation by mixing the Au NPs with the copolymer prior gelation. The study was based on the premise that Au-NPS are heated by the exposure of radiofrequencies (RF). Since Au-NPs are RF-heatable, the release of the encapsulated curcumin from the microgels was induced by the presence of the Au-NPs at optimum RF conditions. Microgels had an average D_h of 160 ± 20 nm and a positive surface charge and showed excellent and selective efficacy towards breast cancer cells and enhanced circulation and biodistribution in relation to the free drug. For anti-cancer assessment, MCF-7 and T47D cells were used. The cells were washed with metal-free solutions and maintained under a RF chamber at 40 W for 5 min. The samples exposed to RF showed higher apoptosis in relation to that without exposure³⁰⁴. The *in-vivo* test on 5-6 weeks old naked mice demonstrated the gels were retained at the colon tumour for 2 weeks³⁰³. Interestingly, the

same study was published in a short period of time on two very similar articles that differed only for the in-vitro experimentation part. One study was focused more on primary and secondary breast tumours, while the second study was directed to the treatment of colon cancer. The first study, originally published in 2014, was recently retracted (24th July 2020) by the journal RSC Advance due to duplication of six images, which included important results related to cytotoxicity, in vitro tests, mice tumour growth and haemolysis tests^{304,305}. Nevertheless, the procedure related to the synthesis of Au NPs and their characterization has only been reported in the retracted study, in which Au NPs of 10, 20 and 50 nm were synthesized in the presence of starch and D-glucose³⁰⁴. However, the details for the preparation of Au NPs of a specific diameter are not provided. Furthermore, there are no information related to which size of Au NPs were used for the preparation of microgels^{303,304}. In 2016, Rejinold reported the first preparation of a hybrid system consisting of CP particles and Fe₃O₄ nanoparticles for the release of curcumin. The magnetic nanoparticles and the drug were added to the CP solution prior to ionotropic gelation. In a similar way, indocyanine green and rhodamine-123 were added to the solution for labelling purpose, as previously reported for the preparation of Au-CP NPs³⁰³. The hybrid particles were able to respond to the application of an alternating magnetic field and were tested in vitro on 4T1 breast cancer cells and in vivo on Normal Swiss Albino Mice. Microgels possessed an average D_h of 180 ± 20 nm and showed cellular internalization on 4T1 breast cancer cells, and radiofrequency (RF) dependent curcumin release *in vitro*. The exposure to RF induced local heating within the microgels that induced the release of the drug. The *in vivo* studies demonstrated the feasibility of the system as a nanotherapeutics for the treatment of breast tumours as the particles prolonged the circulation of curcumin and showed significant tumour localization. A similar work was published by Indulekha in 2017, which also featured the contribution of Prabakaran. In their study, pH-, temperature-, and RF responsive particles were prepared using microgels of CP loaded with DOX and Fe₃O₄ nanoparticles for the treatment of breast cancer cells. The particles were prepared accordingly, by simply mixing the magnetic nanoparticles and DOX with the polymer before gelation. The microparticles were purified through dialysis against distilled water. The study showed the different behaviour of microparticles in relation different pH and temperature conditions and under alternating magnetic field exposure. Interestingly, the application of an alternating magnetic field resulted a step-like elution profile of the chemotherapy drug. From this point of view, this study represents the first example of remote control of the elution of a CP-based drug nanoformulation. In

comparison to the previous works published by Rejinold, the research team of Indulekha reported a more complete description of the size distribution of the samples and showed the change of the D_h of microgels a function of temperature. It can be observed that above the critical temperature, the average D_h is shifted to higher values. This may suggest that temperature-induced drug release is provoked by the swelling of the microgels, as it was already hypothesized by Rejinold²²³. However, the mechanism of the drug release mechanism is not described. Although it is evident that the change of pH or temperature accelerates drug release, the similar profiles of the release curves suggests that the release dynamics do not change during the transition. In addition, this work, as well as the previous ones, does not distinguish between the thermoresponsive behaviour of the polymer (LCST) and that of microgels (VPTT). According to the results of Indulekha, the magnetic-pH-thermoresponsive particles could encapsulate DOX with a very high efficiency (~57%). This value is in disagreement with what has been previously reported³⁰⁶, since it is well known that DOX interacts very weakly with CS-based polymers. The release behaviour of Indulekha's particles resembled the release mechanism reported by Rejinold¹⁰⁸. The absence of the use of a cryoprotector during freeze-drying suggests the hypothesis that the release tests were carried out using aggregates formed as a result of the lyophilization process that were different from the nanoparticles measured with DLS³⁰⁷. One element in favour of this hypothesis is the fact that the size of the freeze-dried nanoparticles is not reported in the study. The reduced *in vitro* toxicity of the encapsulated DOX has been described as a promising element for the utilization of CP-based devices for the treatment of breast cancer. In another work, Indulekha developed a thermoresponsive transdermal drug delivery system consisting in a CP macrogels for the treatment of local pain with on-demand localized drug delivery system. The drug was tested at three different temperatures (25, 32 and 39 °C) at two different pH (5.5 and 7) in order to demonstrate that the drug release was enhanced above the polymer LCST (39 °C) in mild acidic pH (5.5). The system was tested for the release of two hydrophobic drugs, acetamidophenol and etoricoxib. The biocompatibility of the gel was demonstrated by *in vitro* studies in rat skin⁹¹. Among the other contributions, Indulekha reported a preparation of microgels of CP loaded with Au NPs for the treatment of breast cancer with photothermal therapy. Although the utilization of Au NPs with CP microgels for the treatment of breast cancer was already reported by Rejinold, the work of Indulekha had a completely different approach and provide an accurate characterization of the Au-CP hybrid nanodevices. Furthermore, Indulekha used bigger Au NPs that are prepared in

presence of a CP dispersion. The Au NPs were nucleated directly on the surface of the CP microgels using ascorbic acid as a reducing agent, as it is suggested by both UV-VIS and TEM characterizations. Due to their “*ruffled*” morphology, Indulekha improperly used the term “core” and “shell” in reference to the morphology of microgels. However, their behaviour was similar to core-shell nanoparticles and microgels exhibited a tunable absorption in relation to the ratio between the amount of CP and the Au NPs. This allowed to tune the device in order to ensure absorption in the NIR (750 nm). The cytotoxicity tests on normal mouse fibroblast L929 showed a substantial reduction on the toxicity of Au NPs. The CP-Au devices was demonstrated to be biocompatible with both L929 and human breast adenocarcinoma cells MC-F. The exposition to a 750 nm laser reduced the viability of MCF-7 cells from 90% to approximately 5%. Furthermore, the study demonstrated that the nanodevice can be used as a biocompatible X-Ray contrast agent. In relation to commercially, iodine based, Omnipaque, Au/CP microgels gives greater contrast and require less concentrated samples due to the high electron density of Au. Thus, the study suggested the utilization of Au-CP based microgels disintegrable theranostic nanoprobe for image-guided triple therapy consisting in photothermal, chemo and radiotherapy treatment¹⁸⁵.

In more recent years, other CP-related systems have been developed and the polymer has started to show some promising properties for environmental applications. In 2019, Bahmani developed CP/ZIF-8 (zeolitic imidazolate framework) nanofibers to remove As (V) and Cr(VI) from aqueous solutions. Similarly, in 2021 a tri-block polymer PAA, PNVCL and CS was developed and used as a biocompatible flocculant for water remediation³⁰⁸. The polymer provided an excellent device for the removal of turbidity, ciprofloxacin and Cd(II) from aqueous solutions and its ability to bind pollutants increased above the LCST. The tri-block polymer was prepared by polymerizing acrylic acid in presence of CP³⁰⁸. The synthesis of another tri-block polymer is reported by Durkut, who prepared a biocompatible polymer of CS-g-galactosilate-g-PNVCL that shows pH- and temperature dependent responsivity⁸⁵. The polymer was tested for bovine serine album (BSA). In the field of nanotechnology, some authors have reported the synthesis of other hybrid nanodevices based on polymeric and inorganic nanoparticles. Niu and his coworkers reported a brilliant strategy for the preparation of a CP-peptide self-assembled nanoformulation for DOX release for the treatment of breast cancer³⁰⁹. The study reported a multi-step synthesis of the CP-peptide which involves the protection of the amine residues through phtaloylation²⁹⁸. For simplicity, the synthesis was carried out with a

LMW CS (10 kDa). NVCL was conjugated to CS by reversible addition fragmentation chain transfer was then conjugated (RAFT) polymerization using S-1-dodecyl-S'-(α,α' -dimethyl- α'' -acetic acid) trithiocarbonate (DDACT). In this way, after the removal of the phthaloyl residues, the amide residues were used to conjugate a peptide that allowed the device to recognise selectively MCF-7 breast tumour cells. Unlike the previous work, the particles are not formed through ionotropic gelation. Nia reported that the polymer self-assembled in aqueous solutions in ~200 nm microparticles. The results *in vivo* and *in vitro* on MCF-7 cells and xenografted mice demonstrated that the microparticles are taken up by cancerous cells with a substantial reduction of DOX toxicity and a significant reduction in tumour volume that resulted in a prolongation of the life span³⁰⁹. In 2020, Banihashem published a work similar to that of Indulekha and Rejinold, that reported the preparation of another Au/CP nanocarriers for the treatment of MCF cells with cisplatin. This work introduced the hypothesis that the utilization of thioglycolic acid as a ligand for Au NPs stabilization may strengthens the interaction between CP and Au NPs during ionotropic gelation. Similarly, Baninashem also reported a study for the development of CS nanofibers coated with Au-Au sulphide nanoparticles. A new method for the preparation of CP-Fe₃O₄ was reported by Sahebi. In his work, polymer is prepared through a step synthesis that involves the polymerization of NVCL in the presence of Fe₃O₄ nanoparticles. The PNVCL-capped NPs are subsequently conjugated to CS with EDC/NHS. The hybrid magnetic particles were used for the selective recognition of Imatinib mesylate from biological samples.

To date, thanks to their multi-responsivity, CP-based polymers and their hybrid derivatives represent an absolute novelty for the development of cascade-responsive delivery systems for oncological applications. Despite the astonishing progress in the development of CP delivery systems, there are still many aspects that needs to be clarified in order to expect a clinical translation of these studies. Despite the good quality of some publications, the swelling-mediated drug release of CP microgels is still nothing more than a hypothesis¹⁰⁴ and there are only few information about drug uptake mechanism during their preparation. Furthermore, there is still the need for a better understanding of the lyophilisation protocols of chitosan-based microgels³⁰⁷. For clinical applications, it is fundamental to investigate how mechanical and chemical-physical properties are modified by lyophilisation, as well as the ability of freeze-dried particles to maintain properties over time. In the future, we may expect that CP-based systems will also find their application in the same fields in

which CS-based systems have already been used, such as ocular delivery systems³¹⁰ and the treatment of prostate³¹¹ and liver cancer (HCC)²³⁹.

1.14 The interaction between doxorubicin and chitosan

Doxorubicin, also known as Adriamycin®, is an anthracycline that belongs to the family of anticancer antibiotics. The molecule can be described as a tetracenequinone with a sugar attached by a glycosidic bond. Due to the tetracyclic structure of anthraquinone, the molecule can intercalate between two DNA bases, while the sugar enters the minor groove and interacts with the adjacent base pair. Within its structure, DOX has five hydroxyl groups, two phenolic and three alcoholic, and one amino group. Consequently, DOX is slightly soluble in water and is a weakly acidic compound. The estimated values for pKas are 7.34 (phenolic group), 8.46 (amino group) and 9.46 (source: Sparc), respectively. These values indicate that DOX exists in cationic form in a pH range between 5 and 9. In aqueous solution, DOX molecules tends to self-associate via $\pi - \pi$ interactions³¹² and form gel-type structures. In addition, DOX chelates strongly di- and trivalent ions³¹³ and is subject to photolytic decomposition^{314–316} and oxidation³¹⁷. The use of DOX in

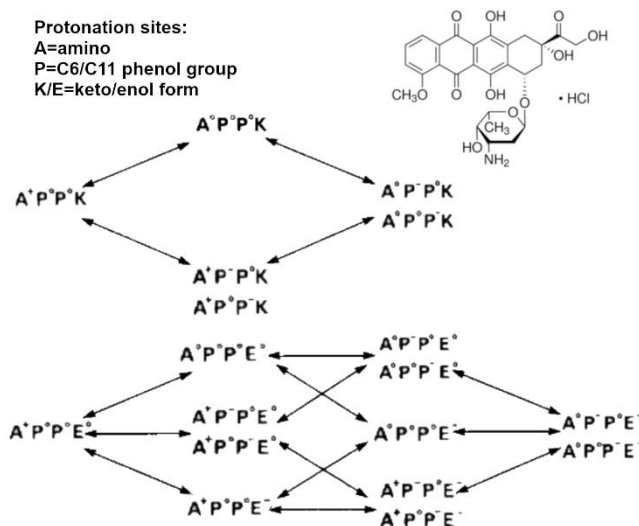


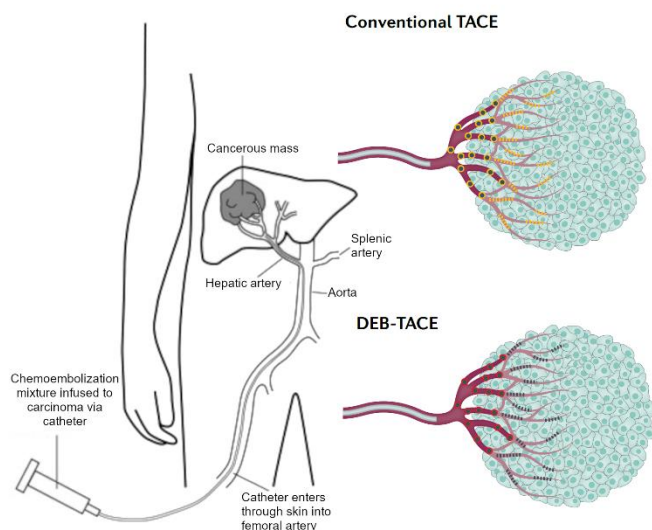
Figure 12 Protolytic equilibrium of DOX between pH 1 and 12.

chemotherapy has therefore placed the need to develop pharmaceutical formulations that increase both drug solubility and effectiveness. In particular, the molecule in aqueous solution undergoes conversion to doxorubicinone and daunosamine³¹⁸. This process is initiated by a tautomeric equilibrium and is catalysed by the presence of buffers and the increase of temperature. According to a study by *Beijnen et al.*, the best condition to stabilize a DOX solution is by using a diluted acetate buffer at pH 4,00, while conversion constants increase dramatically for pH above 6 and pH below 3^{318,319}. CS solutions are also generally prepared in low-concentration acetate buffers (1% w/v) in a pH range between 4 and 5.5. Since the polymer and the drug are prepared in similar conditions, many studies focused on the development of DOX-delivery systems based on CS-based

polymers^{99,106,309,320–322}. Nonetheless, the interaction between the two compounds it is difficult to explain due to the complexity of the equilibria that arise in solution. In a pH range between 4 and 6, it is necessary to consider that the DOX molecule can exist in neutral or zwitterionic form and that each type can undergo a degradation process catalysed by the solvent or the presence of protons in solution^{318,319} (Figure 12). At pH 4.00, since the pH is well below the pKa of the first phenolic dissociation (7.34), it can be assumed that both the DOX and the CS behave as cations. The overall interaction between the two species is influenced by the DDA of the polymer, as the presence of deacetylated residues lowers the positive surface charge of the polymer, thereby decreasing the ionic repulsion. Accordingly, the encapsulation of DOX in a CS nanoparticle would require the chemical modification of the structure of the drug or polymer³²³. Alternatively, non-modified DOX can be trapped by dissolving the drug in a different phase and the encapsulation is achieved via the formation of emulsions or microemulsions³²⁴. During ionotropic gelation, the drug can be entrapped by the formation of the microgel cage around them. Eventually, the drug can elute outside the three-dimensional network of the gel into the external solution. In this condition, the drug require a strong driving force in order to remain anchored inside the cavity of the microgel. In 2001, only four years after the development of ionotropic-gelated CS NPs by *Calvo et al.*²⁸⁴, a study by *Janes et al.* already pointed out that CS-based particles were a poor substrate for DOX encapsulation³²⁰. The study reported that DOX loading efficiency of non-modified CS NPs could not exceed 2%. Nevertheless, CS NPs has been widely used for the encapsulation of DOX and some studies reports loading efficacy higher than 50%. However, these promising results are rarely accompanied by an accurate description of the encapsulation phenomenon^{91,96,99,106}. In a few cases, some of these studies were retracted from publication journals^{304,305}. In fact, one of the possible mistakes of the authors may be related to the utilization of the molecule in a drug formulation. DOX standards are generally expensive and pharmaceutical formulations are often used, even if they may contain excipients and other components, such as methyl 4-hydroxybenzoate (methylparaben), which prevents self-association between DOX molecules. For instance, lyophilized Adriamycin[®] powder contains methylparaben and lactose and the mass percentage of DOX corresponds to about 10% of the formulation. In this case, if the encapsulation efficiency is calculated via UV-VIS, the calibration curve must be based on the extinction coefficient of the drug formulation. In general, DOX content in water is estimated by using an extinction coefficient between 10410⁹⁹ and 125000 L mol⁻¹ cm⁻¹³²⁵.

There is a possibility that some studies did not consider that the coefficient value is affected by the solvent. In a study by *Etrich et al.*³²⁶, the aqueous content of DOX was determined by using the value of extinction coefficient of DOX calculated in ethyl acetate by *Subr et al.*³²⁷. Although inaccurate, such values may be close that of expectation. However, the utilization of drug formulation can lead to strong overestimation of the quantity of DOX. The encapsulation coefficient is calculated from the absorbance value of the solution, so that lower values of absorbance correspond to higher encapsulation values. If not properly calibrated, the value can be overestimated. According to the previous example of lyophilized Adryamicine[®], since the content of DOX correspond to only 10% of the product, a non-calibrated estimation would lead to establish that the encapsulation efficacy is ten times higher than its real value. If not correctly calibrated, the value can be strongly overestimated. A brief explanation of the possible interaction between DOX and CS was provided by *Sadighian et al.*¹⁰⁶ DOX can interact with CS only via weak forces, such as hydrogen bonds and electrostatic interactions. DOX and CS interact by a polar “imine bond” that is sensitive to pH, which is developed between the carbonyl group of the DOX and the amino group of the polymer. According to this hypothesis, CS NPs can retain the drug for few days¹⁰⁶. In another study by *Sanyakamdhorn et al.*, the overall (non-covalent) interaction between CS and DOX was studied using molecular modeling³²¹. According to the reported results, the overall interaction was -3.89 kJ/mol for a CS made of 19 repeating units (about 3.4 KDa). The study also suggested that CS with higher molecular masses are better candidates for DOX encapsulation. Finally, another possibility is that the utilization of aggregated CS NPs increases the encapsulation DOX. Many studies do not mention the procedural difficulties associated with the lyophilization of CS particles^{96,99,104,106,108,304,305}. Since the characterization of CS NPs is reported prior to the freeze-drying process, they provide no evidence about the structure or size of the freeze-dried particles. However, as reported by *Rampino et al.*³⁰⁷, the lyophilization of CS NPS require to be treated with cryoprotectors and freeze-dried particles usually exhibit different size, surface charge and morphology. The differences between the chemico-physical properties of CS NPs and lyophilized CS NPs can have a strong influence on the release mechanism of the drug.

1.15 Chemoembolization



As of today, hepatocellular carcinoma (HCC) represents the second most common cause of cancer-related deaths worldwide³²⁸. In the last 15 years, HCC incidence had risen in developed country and it represent the most common cause of death in people with cirrhosis³²⁹. The only existing curative treatments for HCC are resection and transplantation, but

only a small percentage of patients are candidates.

Figure 13 Comparison between conventional TACE and DEB-TACE.

Small lesions can be treated with regional ablative

therapies, but the benefits are limited if the tumour is bigger than 3 cm³³⁰. The current standard care for patients with intermediate-stage HCC and still preserved liver function is transarterial chemoembolization (TACE). TACE is an image-guided catheter therapy that rely on the differences in the blood supply between HCC and normal liver tissue. In a patient with HCC, the majority of the blood flow supplied by the hepatic arteries is directed to HCC instead of normal liver tissues. The treatment involves the utilization of chemotherapeutics and synthetic materials called embolic agents that are injected into a blood vessel (Figure 13). The embolic agents cut off the blood supply of HCC and trap the chemotherapeutic within the tumour. TACE can be used as a standalone treatment or in combination with ablation, surgery, chemotherapy or radiotherapy^{1,5}. In general, TACE has been used as a palliative treatment for patients with unresectable HCC⁶. As reported by *Lencioni et al.*, TACE had shown to improve median survival from 16 to 20 months³³¹. However, the long-term survival is still not considered fully satisfactory due to the high rates of tumour recurrence. The progress is usually seen only in the treated tissues, while new tumours can form, and undetected HCC can progress. Furthermore, the treatment of a pathology via the formation of an embolus (embolotherapy) may result in different contraindications, such as: active systemic infection, bleeding disorder, leukopenia, renal insufficiency, hepatic encephalopathy and increased risk of hepatic ischemia^{1,331}. However, vein thrombosis is considered a minor contraindication to TACE, as it has been reported that the same conditions can be used safely for the embolization of hepatic artery

branches³³². Some studies also pointed out that TACE can encourage angiogenesis². For years, the most popular TACE technique has been represented by the administration of an anticancer-in-oil emulsion, followed by the injection of an embolic agent. The embolic agent usually consists in a solution of polymeric particles, or microgels, in a range of sizes that is commonly between 100 and 500 μm . In the last fifteen years, drug-eluting-beads (DEBs) provided a promising alternative to conventional chemoembolization. DEB treatment is based on the utilization of microspheres that interacts with the chemotherapeutic, mainly via ionic bonds. The beads can sequester the drug and to release it slowly inside the target tissue. This technique provides for more predictable pharmacokinetics of anticancer drugs and increases the control of the administrated drug. The slow elution results in the reduction of the associated toxicity due to reduced systemic drug circulation^{1,4}. Furthermore, the utilization of “small” particles (inferior to 100 μm) allows for deeper distal embolization of small vessels^{1,4,331}. In this way, it ensures the selective occlusion of the arteries connected to the tumour. DEB-TACE has the same clinical applications of conventional TACE. The technique is generally preferred for the treatment of liver lesion that can be selectively targetable. In general, the technique applies for asymptomatic patients without metastatic spreading, portal vein thrombosis or unpaired liver function⁴. One example of a commercial product for DEB-TACE is DC BeadTM. The product consists of a range of biocompatible, hydrophilic PVA hydrogels (100-500 μm) that are loaded with DOX or Irinotecan. These microgels provide high loading efficiency and allow for a sustained controlled release¹. Recent improvement in DEB-TACE were provided by the utilization of materials than can load more than one drug type and by the utilization of materials that can be detected by magnetic resonance (MRI) or computed tomography (CT)⁶. A recent example of pH-responsive DEBs is DOX-loaded-PLGA microspheres. Due to their polymeric structure, the beads can accelerate drug release at mild acidic pH (5.5 pH) and they reduce systemic exposure of DOX up to 29,9% of that of conventional hepatic arterial injection³³³. As of today, there are no commercial DEB formulation that provides microgels with dimensions inferior to 20 μm . In recent years, some studies started to point out the possible advantages of nanotechnology-based TACE. Due to their small size, the utilization of nanoparticles instead of micrometric particles would allow to extend the chemoembolic treatment to patients with advanced tumours⁶. In addition, the development of combinational therapies based on the utilization of modern nanocomposites may improve the outcomes of TACE procedures. In the future, scientist hopes that the introduction of nanotechnology-based approach would allow to combine

TACE with multimodal (MRI/CT/PET) imaging components and other therapeutic treatments such as immunotherapy, hyperthermia, and photodynamic therapies⁶. The perfect candidate for this type of applications are microgels, due to their biocompatibility, biodegradability and their ability to undergo dramatic change in their physico-chemical properties under the application of an external trigger. As we already pointed out, microgels provides an ideal platform as they can be used a biocompatible scaffold for the utilization of inorganic NPs inside the human body. In recent times, some studies suggested the utilization of photothermal materials, such as iron oxide nanoparticles (MNPs), in conjunction of pH-responsive materials for the delivery of DOX³³⁴. pH-responsive materials, such as CS or polydopamine (PDA) are regarded for their ability to respond to the acidic microenvironment of the tumour. Nevertheless, the utilization of the word "nanocomposite" is misleading as TACE studies are still based on the utilization of micrometric spheres. In most cases, the utilization of the word "nanocomposite" is only related to the properties of the materials used for TACE application and not to the actual dimension of the spheres. A further step towards a nanotechnology-based approach would be to replace microspheres with microgels with dimension inferior to 1 μm . The utilization of microparticles of these sizes would allow to exploit the passive accumulation (EPR)^{37,39,61-66}. The application of responsive microgels in DEB-TACE would provide a new frontier in chemoembolization, as the formation of the embolus would be provided by the application of an external trigger. In order to do this, it is necessary to find suitable materials that show stability in physiological conditions and that can undergo reversible aggregation in a controllable fashion. Furthermore, this approach would provide the possibility to reduce the systemic exposure of the body to the formation of the embolus. An ideal system would be to be able to provide a remote control over the elution of the drug as well as the possibility of acting as an image contrast agent. In the present thesis, we explore the possibility of introducing a relatively new approach based on reversible aggregation to develop a TACE treatment.

Chapter 2: My project

2.1 Initial aim of the project

The original aim of this project was the development of microgels with a cascade response mechanism, with a release mechanism that could be triggered by changes in pH, temperature and magnetic fields. In the first months of research at CRO of Aviano, we identified three main elements that could be assembled for the fabrication of the drug delivery device, by taking as a point of reference the work carried out by Indulekha^{96,99}, Prabakaran⁹³ and Rejinold^{104,108}. Such elements were chitosan (CS), which is a well-studied pH-responsive and biocompatible polymer, PNVCL, a thermoresponsive, non-adhesive and biocompatible polymer and superparamagnetic iron oxide nanoparticles (MNPS or SPIONs), which are FDA approved and can be obtained with simple synthetical procedures. Since the fabrication of similar devices has been previously described, the innovativeness of this project consisted in its application. To date, although chitosan has already been approved for the treatment of a small HCC²³⁹, nanostructured systems have not yet been proposed for TACE, nor DEB-TACE devices on remotely controllable thermosensitive or thermomagnetic materials.

In order to proceed with the fabrication of the nanostructured delivery devices, a collaboration was started with prof. Berti at the University of Trieste, which gave willingness to host me until the attention of the project was shifted to *in-vitro* and *in-vivo* experimentation. The project was conceived with a bottom-up approach, in which every single component of nanostructured microgels was built and then self-assembled for the fabrication of the drug-delivery device.

In the first phase, the objective was to synthesize a polymer of PNVCL-COOH based on the protocol reported by Prabakaran⁹³. The polymer should have exhibited LCST at 32°C. This would have allowed to prepare chitosan-grafted-PNVCL (CP) with higher LCST depending on PNVCL/CS ratio. CP and PNVCL would have required ¹H and ¹³C 1D-NMR and FT-IR for qualitative characterization and a thermostated UV-VIS for the determination of LCST. Eventually, conductimetric titration was considered for the determination of the number of end groups. At the beginning of the project, molecular mass characterization was not considered important as we assumed that PNVCL thermoresponsive behaviour was similar to PNIPAM and that the LCST was independent from the molecular mass, as mistakenly reported by many studies^{91,99,108,185,223,303,304}. In

parallel, MNPs would have been prepared using the coprecipitation method and characterized using DLS, Zeta potential, XRD and TEM.

In a second phase, CP microgels would have been prepared and purified by centrifugation, and a comparison between CP NPs and MNPs properties would have been compared using DLS, TEM, Zeta potential and XRD. According to the literature, DOX-loaded microgels should have formed by simply dissolving DOX inside TPP or CS solution during the formation of microgels via ionotropic gelation⁹⁹. At the end of this part of the project, freeze-dried microgels, loaded with DOX and MNPs, should have been stored for *in-vitro* and *in-vivo* experiments.

The first *in-vivo* experiment would have consisted in performing DOX release from freeze-dried DOX-loaded magnetic microgels at different pH, in order to emulate the behaviour of the microgels in physiological conditions (7.4 pH) and in the mild acidic environment that usually surrounds the tumour (5.5 pH). The tests would have been also performed and different temperatures, at 37°C and above the VPTT. Finally, the last release tests would have been performed with the use alternating magnetic fields generator, which would have provided the external trigger for remote-controlled release. Since this instrumentation was not available, this would have required the collaboration of an external institute and eventually open up the possibility of cooperating with another European research institute. The percentage of released drug would have been calculated by means of UV-VIS spectroscopy or LC-MS. In parallel, the biocompatibility of DOX, CS NPs, CP MNPs, DOX-loaded CP and DOX-loaded CP MNPs would have been compared by means of survival tests such as MTT and Cell Titer on HUH7 cells.

The final phase of the project would have involved the treatment of xenografted NOD/SCID immunodeficient mice with a human hepatocellular tumour with chemoembolization of DOX-loaded microgels. The biodistribution of DOX would have been verified by analysing blood samples from the various organs using LC-MS.

2.2 Development of the project

This thesis includes the results obtained in the development of CP multi-responsive microgels. During these years, the project has suffered several slowdowns due to experimental issues. Theoretically, the project may have benefitted from its interdisciplinary approach. A major disadvantage was represented by working outside a research group, being 128 km away from CRO hospital, in order to have the necessary

instrumentation for the realization of most part of the project. This led to a number of bureaucratic and administrative complications and difficulties in obtaining the reimbursements necessary for moving from one location to another. In some cases, the project was slowed down due to the use of irreproducible synthetic procedures, fragmentary literature and conflicting opinions. As a result, the project was stopped at a preliminary stage of *in-vitro* testing, but it was still possible to develop a reliable protocol for the synthesis of CP microgels and provide a detailed analysis of their thermoresponsive behaviour. Initially, the main difficulty was related to the inability to obtain PNVCL-COOH polymers. After months of unsuccessful attempts, the synthetic protocol was modified, by taking in account that the original study did not consider the dependence of the LCST of PNVCL and its solubility on the molecular mass. This significantly shifted the focus of the project from the development of microgels to a more in-depth investigation of the polymers, which comprehended extensive NMR characterization of PNVCL and CP polymers. Another important issue was the lack of possibility to significantly vary the acquisition parameters of NMR spectrometer available in Trieste. This led to months of unsuccessful characterization work with mere speculation on NMR data with very low resolution. In an attempt to solve this problem, a collaboration was commissioned to the Ronzoni Institute, but the cooperation took two years to develop, with a final six-month delay caused by the CoVid pandemic and the first results were received and discussed during April 2021. Despite the difficulties, the additional work on PNVCL polymer characterizations led to the publication of a study for *Polymers* in August 2021³³⁵. The outbreak of the Covid pandemic provided an important opportunity to reflect on the validity of the results and to restructure the subsequent work in a systematic way. However, due to the pandemic, we did not manage to perform TEM characterisation of +CP microgels in 2020. After returning to the CRO for the utilization of DLS and the realization of *in-vitro* experiments, the administration of the CRO reduced the access to the laboratories and excluded all PhD students from the hospital cafeteria and threatened to shut down the only kitchen available on the campus where I was staying for “security reasons”. The awkward situation that came out of it came out a bureaucratic gap that saw wavering both sides involved (CRO and University). After a long period of protest and complaints by doctoral and fellowship students, the administration of CRO finally granted swabs, vaccines and access to the cafeteria to doctoral students. Other important procedures that have slowed the progress of the project are the purification and lyophilization of microgels, the definition of the protocol for the realization of release tests

of DOX, the encapsulation of DOX and MNPs within the microgels. In my personal opinion, all these procedures are usually reported in a fragmentary way and perhaps this is related to a common standard approach for the writing of scientific publications. However, the information that are usually neglected in the scientific works, such as the relaxation delay for polymer NMR characterization, may actually represent the information the reader is looking for. In my limited personal experience, I found that scientific literature does provide interesting ideas for the development of the projects, but hardly gives important details on how to actually accomplish a specific task. This experience has certainly taught me the value of studies that criticize and underlines the most common mistakes in scientific publications. In the future, perhaps one day there will no longer be room for technological innovations, but there will always be room for critical reflection on what has been done previously.

2.3 Brief overview of the thesis

The thesis is articulated as follows.

In Chapter 3, the results of the synthesis of PNVCL-COOH polymers are described and a detailed characterization is provided. PNVCL-COOH were characterized by using NMR, FT-IR spectroscopy, viscosimetry, DLS and conductivity titration. The variation of the value of LCST is reported in relation to PNVCL molecular mass, PNVCL concentration, pH and NaCl concentration and the presence of different ions by using aqueous buffers (acetate, phosphate and citrate).

In Chapter 4, the characterization of the two CS polymers is reported, which included the determination of molecular mass and DDA. CS were characterized using NMR, viscosimeters and XRD techniques.

In Chapter 5, the results of the synthesis of CP copolymers are described and characterised by using NMR and FT-IR. The DS was estimated using conductimetric titration.

In Chapter 6, the results of the preparation of CS microgels are reported. DLS has been used to monitor the variation of the particle size distribution according to different parameters in order to find the optimal conditions for the fabrication via ionotropic gelation.

In Chapter 7, the results related to the preparation of CP thermoresponsive microgels are reported and their thermoresponsive behaviour is described in detail through the use of DLS. The chapter also provides an analysis of the evolution of particle size during

formation and storage. Microgels were also analysed by TEM, Zeta sizer and NTA. In Chapter 8, the results of the preparation of magnetic particles and CP magnetic microgels are reported. Nanoparticles and microgels were analysed using DLS, zeta sizer, TEM and XRD.

In Chapter 9, the results of the encapsulation of DOX within CP microgels are reported and the release tests of DOX are described. DOX-loaded CP aggregates were observed under optical and fluorescence microscopes in order to verify the presence of DOX. Finally, Chapter 10 illustrates a series of *in-vitro* tests which were used to provide a preliminary evaluation of the biocompatibility of polymers and microgels. The LCST of PNVCL-COOH was measured in human plasma and the lowering of the LCST was related to possible cytotoxic effect. The results obtained by MTT with Cell Titer survival test were compared, while cell morphology was observed by immunofluorescence.

Chapter 3: Synthesis and characterization of PNVCL-COOH polymers

PNVCL-COOH polymers were prepared via free radical polymerization by using the protocol that was previously described by Prabakaran⁹³. In any case, the utilization of the original procedure led to the formation of the polymer via precipitation in diethyl ether. Several experiments were performed, by paying attention to the utilization of anhydrous solvent and reagents and to the presence of oxygen. Eventually, a small amount of polymer was isolated (about 10 mg) in the form of white powder by keeping the diethyl ether solution at -20° C for 3d. The presence of the polymer was confirmed by NMR spectroscopy and the total yield of the process resulted inferior to 1%. The outcome of the initial attempts ruled out the possibility that the polymer was unable to precipitate into diethyl ether due to procedural errors. Since diethyl ether is a moderately polar solvent, the precipitation of the polymer was induced by increasing the chain length. Accordingly, the procedure was modified in order to produce PNVCL-COOH polymers with higher molecular weight. As previously explained, FRP provides little control over chain length and polydispersity, but there are few parameters that facilitate the formation of polymers with higher molecular mass. One of these parameters is the molar ratio between initiator and monomer (M/I). By increasing the number of NVCL molecules available, the number of repeating units for molecular chain increases. This number is commonly referred as degree of polymerization (\bar{X}_n). In free radical polymerization, \bar{X}_n is directly proportional to the square of the concentration of the monomer, according to the following equation:

$$\bar{X}_n = \alpha \frac{(k_p)^2}{2k_t v_p} [M]^2 \quad (18)$$

The utilization of different M/I ratios resulted in the preparation linear PNVCL-COOH polymers with different molecular weight and LCST. For this reason, PNVCL-COOH are distinguished within this work by the M/I number. The M/I were, respectively, 122 (equal to that reported by Prabakaran), 244, 305, 610, 1220 and 1690. The difference in the observed miscibility behaviour were related to a different hydrophobic-hydrophilic balance of the PNVCL-COOH macromolecule. According to Equation 18, the utilization of higher M/I ratios results in the elongation of hydrophobic portion of the PNVCL-COOH macromolecule. Accordingly, the LCST is lowered as the M/I ratio increases. The precipitation in diethyl ether was achieved from values of M/I above 610 (see Table 4).

Since PNVCL-COOH is a surfactant, the ideal hydrophilic-hydrophilic balance for the precipitation in diethyl ether lies between 305 and 610.

M/I	Precipitation in diethyl ether
122	No
244	No
244	No
610	Yes
1220	Yes
1690	Yes

Table 4 Solubility behaviour of PNVCL-COOH polymers in diethyl ether.

The yield of the polymers precipitated in diethyl ether was less than 20%. The average yield of the process was raised by purifying the polymer directly with dialysis using with membrane tubings (MWCO = 1 KDa) that were compatible with DMF solutions. In this way, PNVCL-COOH polymers were synthesized even if unable to precipitate in diethyl ether. To avoid possible side effects related to the utilization of DMF, PNVCL-COOH solutions were diluted 1:2 with milliQ water before dialysis. The main drawback of this alternative purification method is the inability to remove eventual traces of DMF that remains in water after dialysis. In few polymers, it was possible to identify a minor peak at 2.9 ppm (Figure 18, left) that demonstrates the presence of a residual DMF in freeze-dried products. The peak had been previously mistaken by Prabakaran for the methylene group (-C-S-CH₂) present in the terminal group⁹³. This hypothesis was excluded with the utilization of HSQC-DEPT heterocorrelated spectra (Figure 18, right). According to the low intensity of DMF signals showed, PNVCL-COOH polymers have a higher degree of purity than those described by Prabakaran.

3.1 Spectroscopic characterization

The polymerization of NVCL were confirmed by NMR and FT-IR and spectroscopy. NMR characterization was performed in D₂O and d₆-DMSO. In the ¹H spectrum of PNVCL-COOH, four main signals were observed. The formation of the polymer was confirmed by the formation of broad signals and from the disappearance of the vinylic signals at 7.36 ppm.. Assigned protons and carbon signals are reported in Table 5.

Chapter 3: Synthesis and characterization of PNVCL-COOH polymers

Proton Type	Shift (ppm)
H _a	0.8-2
H _b	2.0-2.6
H _c	2.6-3.5
H _d	4.0-4.5
H _e	1.55
H _f	2.4
Carbon type	Shift (ppm)
C ₁	25.13
C ₂	30.98
C ₃	32.12
C ₄	36.61
C ₅	39.52
C ₆	45.19
C ₇	49.65
C ₈	181.20
C ₉	30
C ₁₀	39

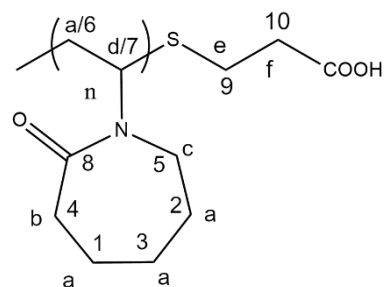


Table 5 NMR assignments of PNVCL-COOH polymers (solvent: D₂O).

PNVCL-COOH polymer structure was determined by the utilization of ¹H, 2D-COSY, 2D-HSQC, 2D-TOCSY, 2D-DOSY and ¹³C NMR. All the ¹H NMR PNVCL-COOH spectra exhibited the same characteristic independently from the different molecular mass of the polymers (Figure 16). Due to the thermoresponsivity of the polymer, it was not possible to acquire the spectra at higher temperatures in order to reduce spectral linewidth by decreasing the viscosity of the solutions. Consequently, the polymers were analysed at 25 °C. Preliminary data obtained using Varian 400 and 500 MHz spectrometers available in Trieste. The presence of -COOH end groups was confirmed by analysing PNVCL_244 and PNVCL_305 in d₆-DMSO using a high number of acquisitions. The signals were identified in small peaks observed at ~12 ppm in both spectra (figure 14).

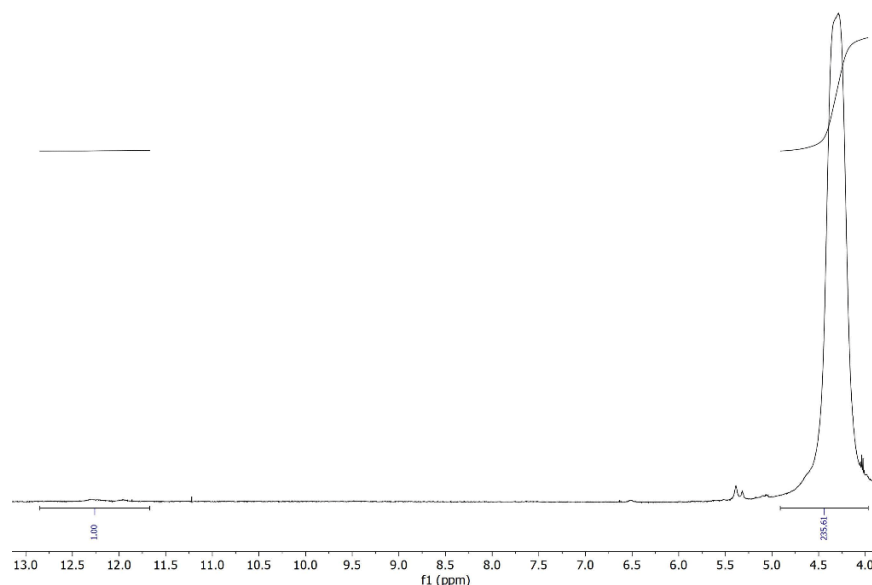


Figure 14 COOH- end group signals in ^1H NMR spectrum of PNVCL_305 dissolved in d_6 -DMSO. The spectrum was obtained with 2500 acquisition at 25 °C using a Varian 500Mhz spectrometer.

The integration of the $-\text{NCH}_2$ signal provided an initial rough estimation of the molecular mass around 32 kDa from the corresponding calculated degree of polymerization (235). Due to spectral linewidth of PNVCL-COOH signals, the value was overestimated by approximately ~ 10 kDa. The resolution of ^{13}C spectra acquired using Varian 400MHz and 500 MHz spectrometers did not allow to verify the presence of all structural groups despite the utilization of long acquisition times. To further investigate the structure of the polymers, the analyses was carried out with a high-resolution Bruker 500 MHz available at Istituto Ronzoni (Milan, IT). The utilization of the cryoprobe technology allowed to increase the signal to noise ratio by about four times. The ^{13}C spectra acquired with the Bruker spectrometer confirmed the structure of the polymers based on the previous literature³³⁶ (Figure 15 and 17). Heterocorrelated 2D-HSQC spectra (Figure 18) allowed the identification of two minor signals at 1.55 ppm/29 ppm and 2.4/38 ppm that were related to the presence of the sulphur-bonded aliphatic methylene and the methylene bonded to the carboxyl termination group. The utilization of HSQC-DEPT (Figure 18, right) allowed to distinguish CH/CH₃ signals from CH₂ signals. In this way, it was possible to establish that the two signals originated from the two $-\text{CH}_2$ groups present in the terminal segment of the polymers. The comparison between ^{13}C spectra of PNVCL_122, PNVCL_244 and PNCVL_1220 in the range between 50 and 25 ppm confirmed that the signals are associated to the aliphatic portion of the termination groups. The comparison between ^{13}C spectra is reported in Figure 15. As shown, the signal intensity decreases as M/I ratio increases.

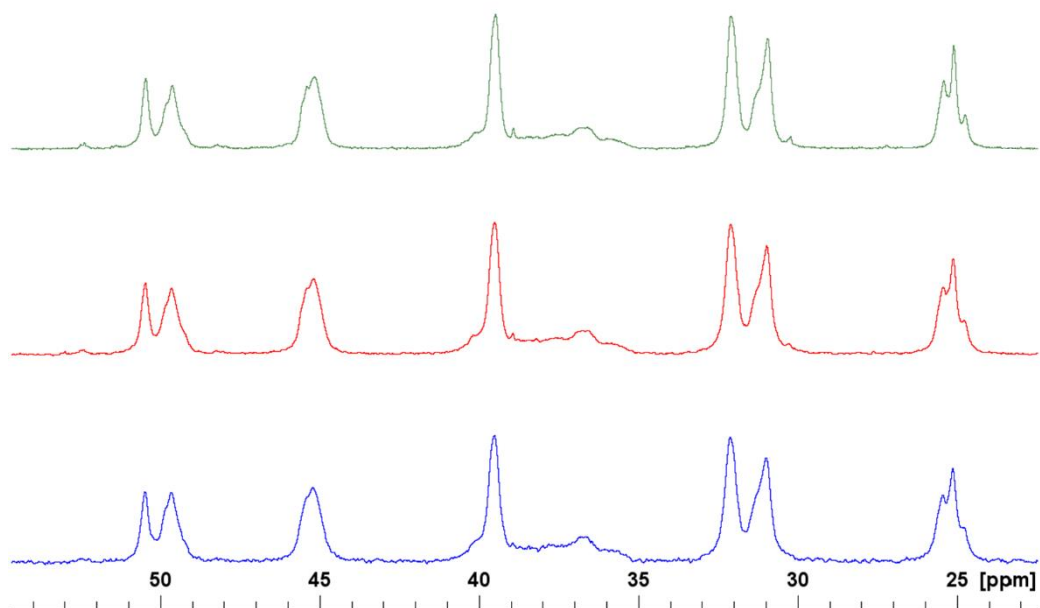


Figure 15 Comparison between ^{13}C spectra of PNVCL122 (green), PNVCL305 (red) and PNCL1220 (blue).

This observation is in accordance with the presence of different PNVCL-COOH polymer with increasing molecular mass with increasing M/I ratio. As mentioned above, HSQC-DEPT (Figure 18, right) also demonstrated the minority presence of residual solvent in few samples. The signals at 2.9/37 ppm originated from CH_3 residues of the DMF molecule.

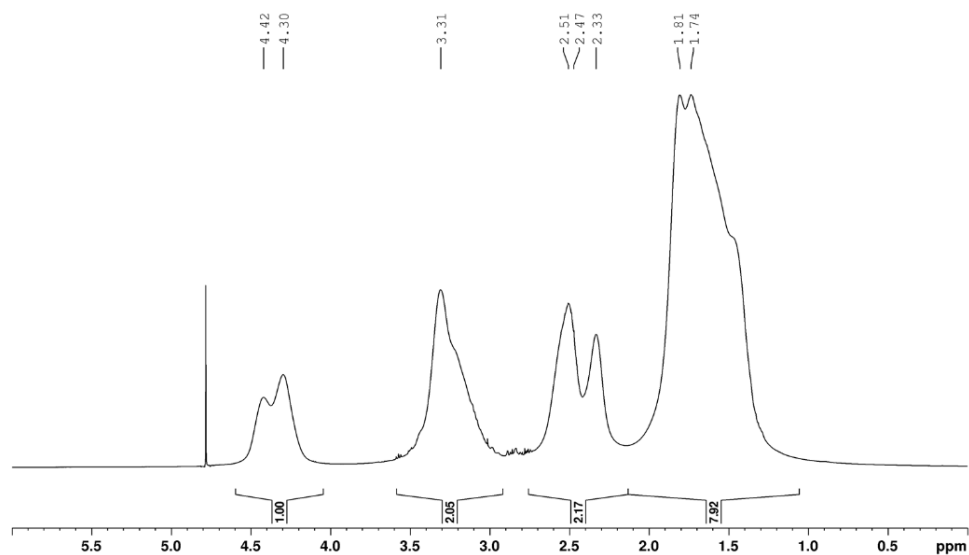


Figure 16 ^1H NMR spectrum of PNVCL_305 in D_2O .

Chapter 3: Synthesis and characterization of PNVCL-COOH polymers

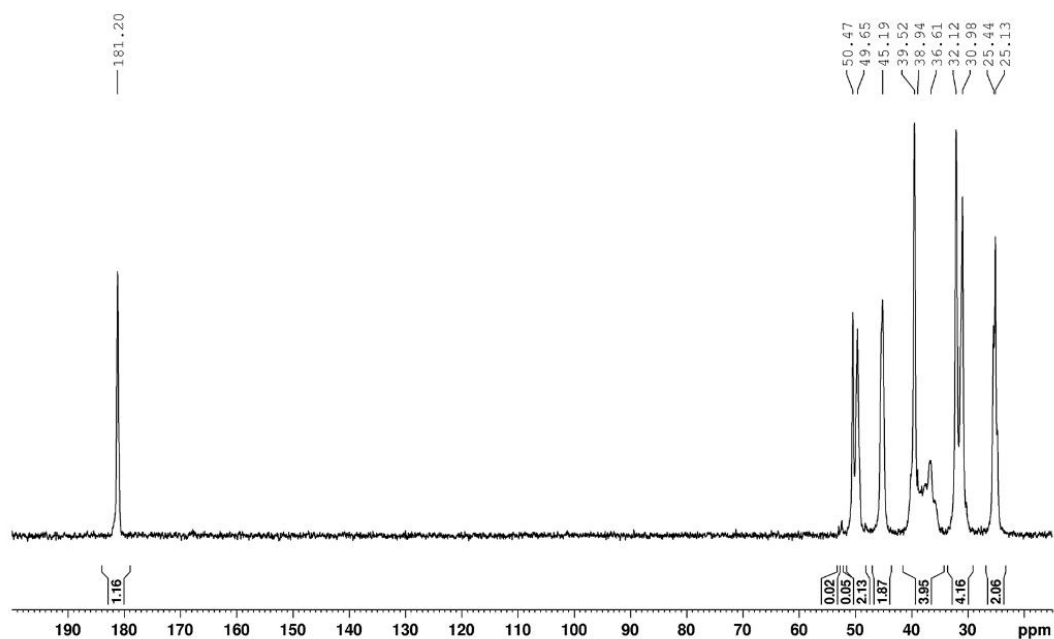


Figure 17 ^{13}C NMR spectrum of PNVCL₃₀₅ in D_2O .

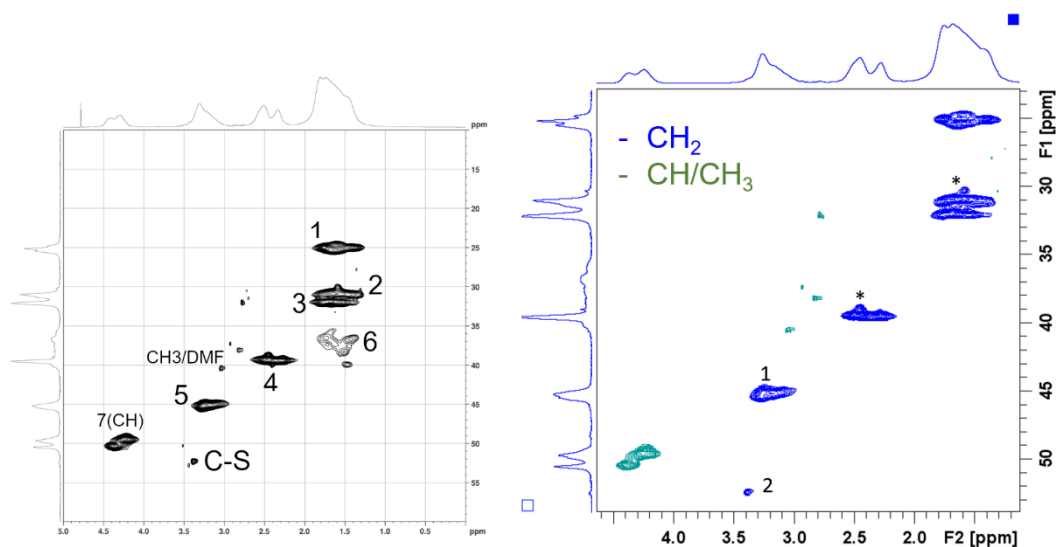


Figure 18 2D-HSQC spectrum of PNVCL₃₀₅ (left). 2D-HSQC-DEPT spectrum of PNVCL₁₂₂ (right). *signals were associated to the aliphatic portion of the termination groups.

FT-IR analysis was used as a complementary measurement to confirm polymerization. For all samples, it was possible to observe amide I signals at 1631 cm^{-1} and 1480 cm^{-1} (C-N stretching vibration), while the characteristic signals related to the monomer (C=C, 1658 cm^{-1} , CH= and CH₂=, 3000 and 3100 cm^{-1}) disappeared (Figure 32). The analyses allowed to establish the presence of -COOH signals (3450 cm^{-1}) related to the end-groups of the polymers.

3.2 Determination of -COOH end groups

The number of terminal carboxyl groups was determined via conductimetric titration. The polymers were dissolved using diluted HCl and the solutions were titrated using a standardised solution of NaOH 0.1M. The deprotonation of the -COOH end groups resulted in the formation of a small plateau in the conductimetric titration curve. The number of carboxyl groups was determined by the volume difference of added NaOH solution between the initial and the final point of the plateau. An example is reported in Figure 19. The results (Table 6) confirmed the presence of carboxyl groups. The analysis showed that polymer with higher M/I ratio, which results in higher molecular weight, have fewer -COOH end groups due to the presence of longer polymer chains.

Sample	Estimation of carboxyl group content (mmol/g)
PNVCL_122	0.96±0.25
PNVCL_244	0.73±0.17
PNVCL_610	0.63±0.18
PNVCL_1220	0.55±0.12
PNVCL_1690	0.45±0.13

Table 6 Results of the estimation of -COOH end groups via conductimetric titration.

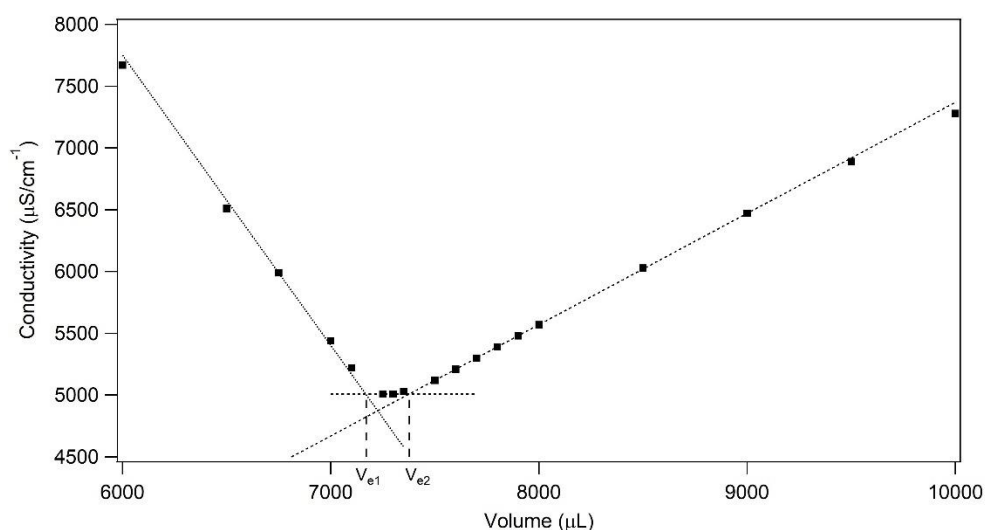


Figure 19 Conductimetric titration of PNVCL_305.

3.3 Analysis of the thermoresponsive behaviour

3.3.1 Spectroscopic determination of LCST

In this work, the LCST of thermoresponsive polymers was determined mainly via UV-Visible spectroscopy. The miscibility curves were represented by plotting the transmittance of the solutions as a function of temperature (Figure 20). The LCST was determined from the inflection point of the sigmoidal functions that were used to fit the miscibility curves (Equation 17). LCST values were associated to the behaviour of 5 mg/ml PNVCL-COOH aqueous solutions. PNVCL-COOH polymers exhibited LCST in a range between 33 and 42 °C. As previously mentioned, the LCST diminishes in relation to the M/I ratio that were used for the synthesis of the polymers (Table 7). This molecular mass-depended behaviour is in accordance with a “classical” type I miscibility behaviour. The results excluded the presence of "step" transitions, that are generally observed in highly polydispersed polymers with different LCSTs. As a result, the variation of the M/I ratio provided a reliable procedure for the control of the LCST.

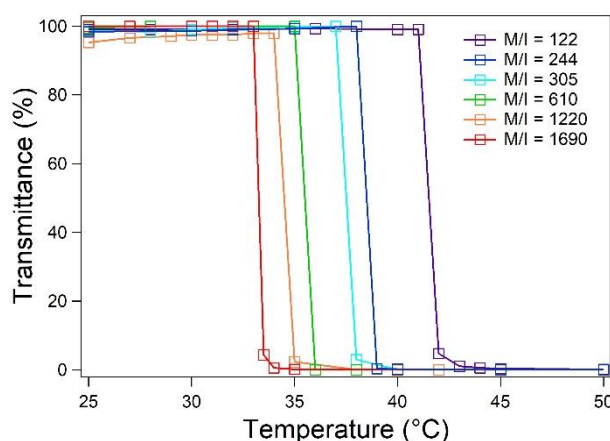


Figure 20 Solubility curves of PNVCL-COOH polymers.

Sample	LCST (°C)	r ²
PNVCL_122	41,71±0.17	0.99997
PNVCL_244	38,56±0.14	0.99972
PNVCL_305	37,23±0.63	0.99921
PNVCL_610	35,75±1.74	0.99601
PNVCL_1220	34,73±0.56	0.99929
PNVCL_1690	33,27±0.03	0.99728

Table 7 LCST calculated as the inflection point of a sigmoidal solubility curve. The correlation values of the fits are reported in the right column.

The type I behaviour of PNVCL-COOH was further validated by measuring the LCST in the presence of salt species. 5 mg/ml PNVCL-COOH solutions were prepared in citrate

(pH 3), acetate (pH 5) and phosphate buffer (pH 7). All buffers were prepared at the concentration of 0.1 M to compare the effect of the different ions on the LCSTs of the polymers. The results showed a strong dependence towards the types of ions dissolved in solution, as it was previously demonstrated by other studies on PNVCL polymers⁷. The effect of salts is more pronounced for short chain polymers, which have a higher LCST. The most evident effect was observed by dissolving PNVCL-COOH in phosphate buffer. This could be relevant from the biological point of view, since phosphate buffers solutions (e.g., PBS) are widely used in kits for cell treatment kits. The lowering of the LCST could result in the formation of aggregates that could reduce the biocompatibility of the polymer. PNVCL-COOH solutions were analysed in water at 5, 1, 0.5, 0.1 and 0.05 mg/ml. Dilution resulted in higher values of LCST and slower transition. Accordingly, PNVCL-COOH concentration affects the kinetics and the energy of LCST transition. Finally, the miscibility behaviour was characterized in presence of NaCl in range of concentration between 0 and 0.15 M. Results showed that LCST decreases proportionally in relation to NaCl concentration. LCST decreases by ~ 1 °C in a physiological solution (0.9% NaCl, or 0.15 M). Consequently, pharmaceutical applications of PNVCL-COOH polymer in a physiological solution would require a polymer with a LCST > 38 °C in order to avoid cytotoxic effects due to the polymer transition.

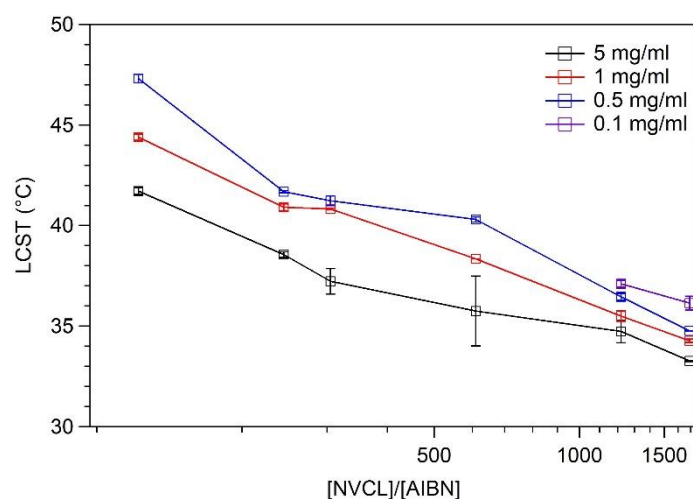


Figure 21 PNVCL-COOH LCST reported as a function of the concentration of the polymers.

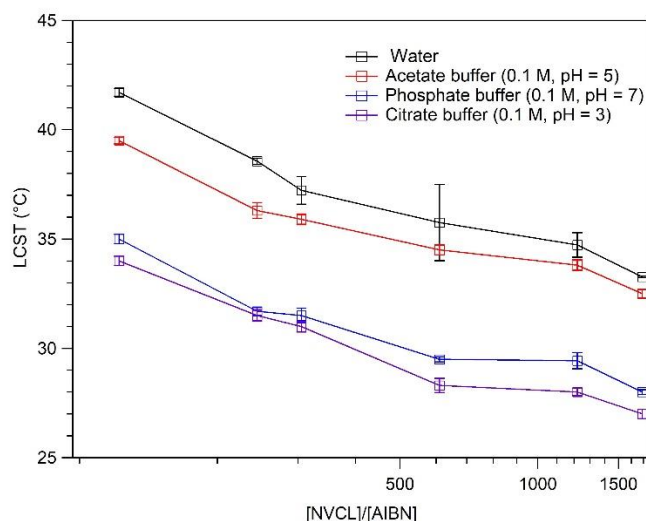


Figure 22 PNVCL-COOH (5mg/ml) LCST dependency towards the type of buffers present in aqueous solution.

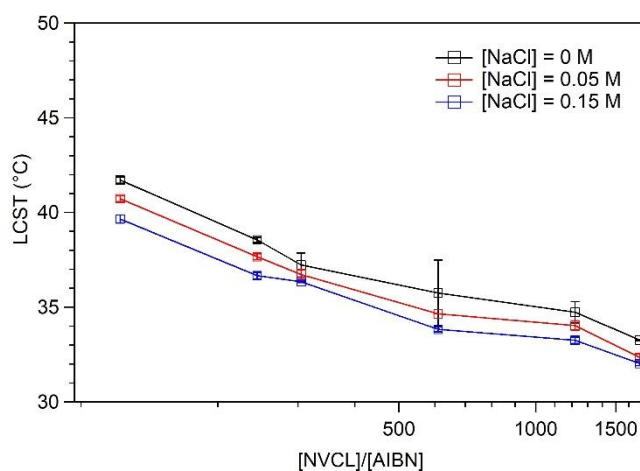


Figure 23 PNVCL-COOH LCST dependency towards the concentration of NaCl.

3.3.2 Scattering determination of LCST

PNVCL-COOH LCST was characterized using DLS. For each measurement, the sample was incubated at different temperatures for 5 minutes and the variation of the autocorrelation curve was monitored in the temperature range between 25 and 50 °C. DLS measurement proved an estimation of the average D_h of PNVCL-COOH polymer with higher molecular mass (PNVCL_610, PNVCL_1220 and PNVCL_1690). For these polymers, the LCST was attributed to the temperature at which a dramatic change in the shape of the autocorrelation curve was observed (Figure 24). For the samples with lower molecular mass, the value of LCST was related to the temperature at which the solution became turbid. Results are reported in Table 8.

Chapter 3: Synthesis and characterization of PNVCL-COOH polymers

Sample	LCST (°C)
PNVCL_122	41
PNVCL_244	37
PNVCL_305	37
PNVCL_610	34
PNVCL_1220	33.5
PNVCL_1690	32.5

Table 8 Results of LCST determination of PNVCL-COOH polymers via DLS.

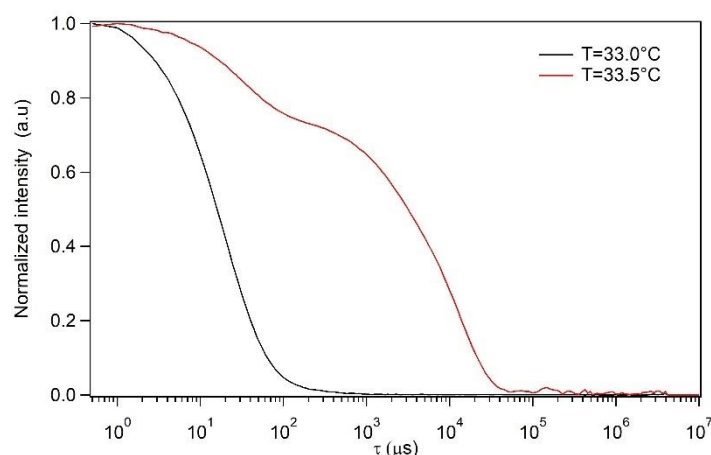


Figure 24 Correlation curve of a 5 mg/ml solution of PNVCL_1220 at different temperatures.

DLS provided lower values of LCST in relation to UV-VIS spectroscopy. The differences can be related to the different thermal conductivity of the cuvette materials and to the different efficiencies of the heating chambers. Another possible interpretation is that DLS is more sensitive to the formation of aggregates in the proximity of LCST. The fraction of polymers with higher molecular mass undergoes LCST transition at lower temperatures. Accordingly, the entity of the differences between the two measurements of LCST could provide information on the polydispersity of PNVCL-COOH polymers. According to this interpretation, the polymer with highest polydispersity is PNVCL_610.

3.4 Molecular weight determination

3.4.1 Size exclusion chromatography

Two samples of PNVCL-COOH, PNVCL_244 and PNVCL_1220, were analysed with a triple detector size exclusion chromatography system (HP-SEC TDA) available at Istituto Ronzoni (Milano, IT). The experiment was originally intended to be performed using DMF as eluent. Unfortunately, this was not possible due to the incompatibility of the solvent with certain components of the TDA system. Samples loaded into the column for a test using an aqueous acetate buffer (0.3 M) as a solvent. The peak of the mobile phase was identified in the chromatogram, but no other component was found (Figure 25). It was

concluded that PNVCL-COOH is not able to elute from the column under these conditions. Therefore, the molecular weight could not be determined by GPC-SEC.

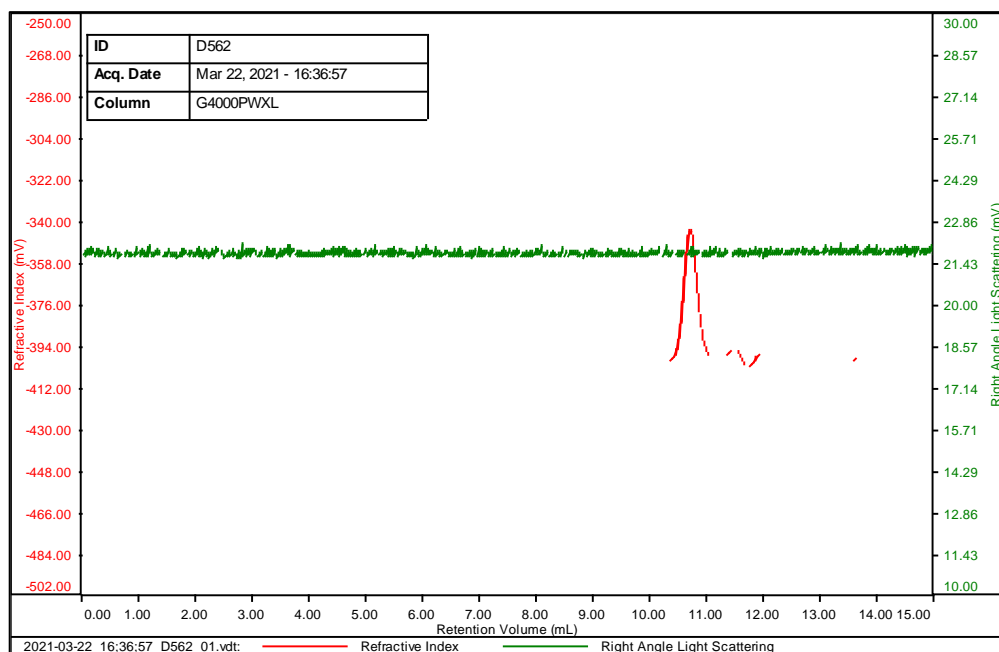


Figure 25 GPC-SEC chromatogram of PNVCL_244. The absence of the analyte peak shows that the sample was not able to elute from the column.

3.4.2 Dynamic light scattering

The molecular mass of the polymers has been estimated using DLS. All measurements were performed at 25 °C at a concentration of 5 mg/ml in water. As mentioned previously, DLS analyses provided a direct estimation of D_h of PNVCL_1220 and PNVCL_1690. The analysis of the other samples resulted in a bimodal distribution that resulted from the cumulate fitting of the autocorrelation curves. We evaluated the possibility that these peaks could originate from the presence of PNVCL-COOH in random coil conformation and the molecular mass was estimated from their corresponding D_h . The peaks were located between 5 and 30 nm, depending on the type of PNVCL-COOH under observation. Since the analysis were carried out below the LCST, PNVCL-COOH polymers had a random coil conformation. Accordingly, the radius of gyration R_g was obtained from the D_h of the polymer. In a random coil conformation, the ratio between R_g and D_h is 0.75. The average molecular mass of the polymers was obtained using the equation reported by Lau²¹¹:

$$R_g = 2.94 \cdot 10^{-2} M_w^{0.54} \quad (19)$$

Chapter 3: Synthesis and characterization of PNVCL-COOH polymers

The corresponding D_h values increased with the M/I of the polymer. The values are reported in Table 9. The standard deviation is referred to the position of the peak and it is not related to the polydispersity of the polymer. The analysis confirmed that the molecular mass increases as the M/I. The graph in Figure 26 represents the estimated molecular mass as a function of M/I.

Sample	Average D_h (nm)	D_h SD (nm)	R_g (nm)	R_g SD (nm)	M_w (KDa)
PNVCL_122	6.605	1.236	4.954	0.927	13.28±0.36
PNVCL_244	8.800	2.298	6.600	1.723	22.60±0.06
PNVCL_305	9.484	2.874	7.113	2.155	25.96±0.05
PNVCL_610	12.21	3.744	9.156	2.808	52.20±0.36
PNVCL_1220	17.36	7.568	13.02	5.676	79.54±0.25
PNVCL_1690	22.08	8.071	16.56	6.053	124.1±0.61

Table 9 Estimation of the molecular mass of PNVCL-COOH polymers based on DLS analysis of 5mg/ml solutions.

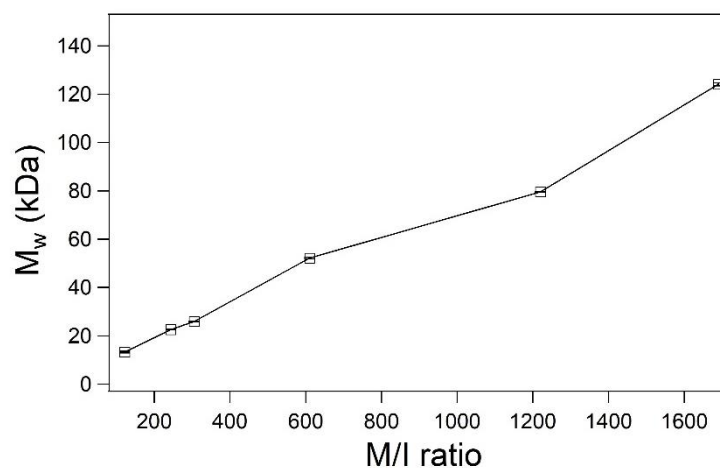


Figure 26 Estimated molecular mass reported as a function of M/I. The standard deviation is related to the values used for the estimation and not from the FWHM of the peaks in the distribution curves.

3.4.3 Viscosimetry

The viscosimetric molecular mass of PNVCL_244, PNVCL_305 and PNVCL_1220 mass was determined according to the procedure described in the “Materials and Methods” section. The values of reduced (η_{red}) and inherent viscosity (η_{inh}) were derived from the run time of polymer solution dissolved in distilled water at 25 °C and plotted as a function of the concentration in g/dl. The determination of M_η of PNVCL-COOH samples was carried out using a starting concentration of 2 mg/ml. Due to the low viscosity of the sample, the difference between the run times was very small. The total run time difference between the solvent and the concentrated solution was between 7 and 9 seconds. Consequently, dilutions lead to small variations that can lead to difficult data interpretation. However, the utilization of more concentrated solution was not possible due to the surfactant nature of the sample, that easily leads to the formation of foams at higher concentrations. The results of the measurements are reported in Tables 10, 11 and 12. Despite the small differences between the run times, a calibration line was drawn between 4 or 6 points depending on the sample, and the correlation value was considered acceptable. The values of in intrinsic viscosity $[\eta]$ was calculated at infinite dilution using the Huggins methods as reported by Equation 25 (see “Methods” section). Due to the very low values if η_{inh} , the Kraemer model (Equation 26) was not considered for the calculation of molecular masses. The average M_η was calculated by using two calibration lines per sample, one of which was obtained by excluding the values for the most diluted sample. The results are shown in Table 13. M_η was calculated in agreement to the Mark-Houwink-Sakurada equation (Equation 27). The calibration lines for both models are represented in Figure 27.

Dilution	Concentration (g/dL)	t (seconds)	Relative viscosity	Specific viscosity	Reduced viscosity (dL/g)	Inherent viscosity (dL/g)
0	0.2045	284.87	1.0249	0.02499	0.12219	0.12069
1	0.1887	284.30	1.0229	0.02294	0.12154	0.12017
2	0.1636	283.36	1.0196	0.01956	0.11959	0.11844
3	0.1291	282.09	1.0150	0.01500	0.11617	0.11531
4	0.0908	280.72	1.0101	0.01007	0.11084	0.11029

Table 10 Viscosimetric analysis of PNVCL_305.

Dilution	Concentration (g/l)	Average run time (seconds)	Relative viscosity	Specific viscosity	Reduced viscosity (dL/g)	Inherent viscosity (dL/g)
0	0.2270	285.50	1.02727	0.02727	0.12015	0.11854

Chapter 3: Synthesis and characterization of PNVCL-COOH polymers

1	0.2095	284.83	1.02485	0.02485	0.11860	0.11715
2	0.1816	283.81	1.02119	0.02119	0.11670	0.11548
3	0.1433	282.42	1.01617	0.01617	0.11281	0.11190
4	0.1008	280.89	1.01069	0.01069	0.10592	0.10536

Table 11 Viscosimetric analysis of PNVCL_244.

Dilution	Concentration (g/l)	Average run time (seconds)	Relative viscosity	Specific viscosity	Reduced viscosity (dL/g)	Inherent viscosity (dL/g)
0	0.2225	290.28	1.04448	0.04448	0.19992	0.19560
1	0.2054	289.09	1.04020	0.04020	0.19573	0.19190
2	0.1780	287.24	1.03353	0.03353	0.18840	0.18530
3	0.1405	285.11	1.02587	0.02587	0.18410	0.18176
4	0.0989	282.69	1.01715	0.01715	0.17347	0.17200
5	0.0685	281.03	1.01120	0.01120	0.16362	0.16272

Table 12 Viscosimetric analysis of PNVCL_1220.

PNVCL_244	
[η] – Huggins model	Molecular mass - M_{η}
9.5882	19.74 KDa
10.060	20.57 KDa
Average molecular mass M_{η}	19.74±1.12 kDa
PNVCL_305	
[η] – Huggins model	Molecular mass - M_{η}
10.248	21.25 KDa
10.588	22.50 KDa
Average molecular mass M_{η}	21.87±0.88 kDa
PNVCL_1220	
[η] – Huggins model	Molecular mass - M_{η}
15.014	41.52 kDa
15.560	44.32 kDa
Average molecular mass M_{η}	42.87±1.90 kDa

Table 13 Results of viscosimetric characterization of PNVCL-COOH.

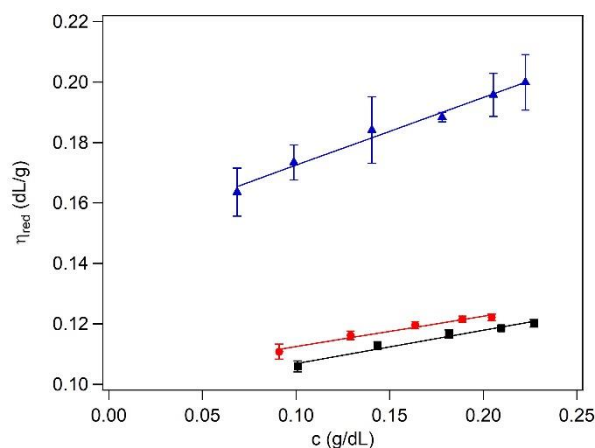


Figure 27 Linear fit of the results for the calculation of M_{η} of PNVCL_244 (black), PNVCL 305 (red) and PNVCL_1220 (blue) based on Huggins.

The results are in line with a type I thermoresponsive polymer behaviour. As the molecular mass increases, the LCST decreases. This behaviour is in accordance with the water mixing behaviour of PNVCL as previously reported by Meeussen¹⁵⁶ and Kirsh³³⁷. Molecular mass values obtained through viscosimetry were slightly lower than those obtained by interpreting DLS data with the model provided by Lau (Equation 19). Accordingly, scattering methods should be considered for the estimation of the molecular mass of PNVCL polymers with lower molecular mass, that are not suitable for viscosimetric analysis due to their low viscosity. PNVCL_244 and PNVCL_305 possess a molecular mass of around 20 kDa and exhibit LCST around 37.5 °C. In the study of Meeussen¹⁵⁶, the measured LCST for a diluted 20 kDa PNVCL solution is around 37 °C¹⁵⁶. Accordingly, the small difference between the calculated LCST may be related to the different end groups of the polymers under consideration. The presence of terminations or compounds that increase the hydrophilicity of PNVCL is known to increase the LCST¹⁹⁷. Furthermore, PNVCL-COOH polymers with a 32 °C LCST have been frequently used as starting polymers for the preparation of CP polymers and thermoresponsive particles^{91,93,99,104,185,223}. PNVCL_1220 shows similar properties as the LCST is close to 33 °C and has a M_{η} around 42 kDa. According to the relation between LCST and molecular mass, PNVCL-COOH requires a molecular mass higher than 42 kDa in order to exhibit LCST at 32 °C. However, this LCST value has been previously associated to the behavior of PNVCL-COOH polymers with a molecular weight of 1 kDa by means of GPC-SEC measurements in THF by Prabakaran⁹³. It can be concluded that the value reported by Prabakaran was incorrect. However, Prabakaran work is a point of reference for all CP-related studies. Due to the importance of that work for future developments on CP-based systems, it follows that this imprecision may have affected the reproducibility of subsequent studies^{91,99,108,185,223,303,304}. The molecular mass of the PNVCL has a central role in defining the thermoresponsive behaviour of nanoparticles, microgels, gels and other biocompatible release devices. Consequently, it is essential to correctly characterize the molecular mass with precise, standardised, and reproducible methods.

3.5 Differential Scanning Calorimetry

The DSC thermograms of NVCL monomer, PNVCL_610 and PNVCL_1690 are represented in Figure 28. The monomer exhibits an endothermic peak at 35.30 °C corresponding to its melting point, with a heat fusion of 135.6 J/g. In the thermogram of the polymers, it is observed a broad peak at 43.52 °C (24.96 J/g) and 48.39 °C (61.36 J/g)

for PNVCL_610 and PNVCL_1690, respectively. The peaks have been previously associated to the softening temperature of PNVCL polymers³³⁶.

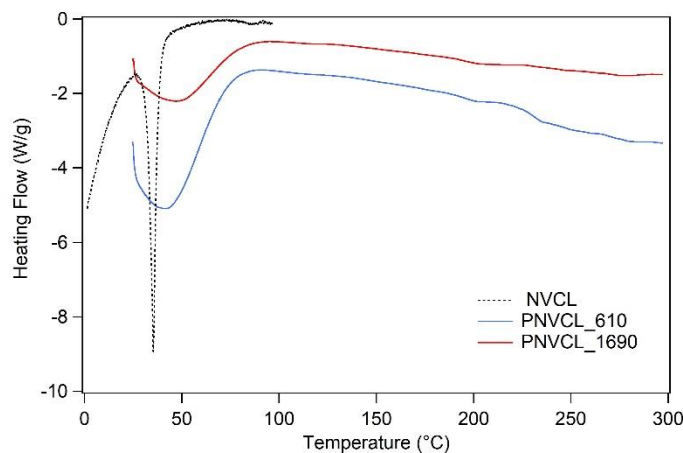


Figure 28 DSC thermograms of NVCL, PNVCL_610 and PNVCL_1690.

DSC was also used for the investigation of peaks related to LCST transition of PNVCL aqueous solution. However, results were poorly reproducible and in contrast with previous observations. Consequently, the LCST of PNVCL-COOH was not determined with DSC measurements.

3.5 Summary

In this chapter, the preparation of PNVCL-COOH linear thermoresponsive polymers with a LCST of between 33 and 42 °C was reported. The results contradict the established thesis that PNVCL has a characteristic LCST at 32 °C and exhibits a miscibility behavior similar to PNIPAM. The utilization of different ratios between monomer and initiator (M/I) allowed to lower the LCST by increasing the molecular mass of the polymer. Accordingly, the increase in molecular mass was associated with a decrease in terminal groups content that was observed in NMR spectroscopy and conductivity titration. Molecular mass characterization was approached with different methods and a comparison of the results was provided. While GPC-SEC has proven to be unreliable regarding the tendency of the polymer to adsorb on the column, DLS and viscosimetry proved to be simple and effective methods for the estimation of the molecular mass in simple aqueous solution. The behaviour of PNVCL-COOH was described according to its concentration and in the presence of different environments, such as aqueous buffers with different pH and the concentration of NaCl. The variability associated with the LCST values in the different

solutions demonstrated the importance in reporting the LCST of PNVCL polymers in relation to their concentration and molecular mass. In addition, the study demonstrates the importance of the screening of the behaviour of PNVCL polymers in biologically relevant environments (PBS, physiological solution). Accordingly, the LCST of PNVCL polymers for biological applications should be determined within these solutions in order to prevent cytotoxic effects due to the lowering of the LCST caused by the presence of ions and proteins in the aqueous environment.

Chapter 4: Characterization of chitosan

4.1 NMR characterization

In this work, two types of CS with different molecular weight and DDA were used (see “Materials and methods” section). Due to its high molecular weight, most CS solutions are highly viscous. In order to diminish the viscosity of the solution, ^1H NMR analysis were performed using a dilute solution of the polymer in glass tube at 70 °C, by dissolving 3 mg of the polymer in 600 μl of a 1% solution of $\text{D}_2\text{O}/\text{DCl}$ (5 mg/ml). When the solution temperature is risen, the viscosity is reduced, and the molecular mobility is increased. As molecular mobility increases, relaxation time T_1 increases^{338,339}. This results in the reduction of the spectral linewidth of the signals. The increase in temperature provides the displacement of the solvent peak from the integration area of the anomeric proton which is used for the calculation of the DDA. The DDA was calculated using three different equations (Equations 20-22) as reported in previous works^{299,340–343} for the physical characterization of CS with a high DDA (Table 14):

$$DDA(\%) = \left(\frac{H_1}{H_1 + H_{CH3}/3} \right) \quad (20)$$

$$DDA(\%) = [1 - (1/3H_{CH3})/(1/6H_{2-6})] \quad (21)$$

$$DDA(\%) = 1 - \frac{H_{1(Ac)}}{H_1} \quad (22)$$

Equation	LMW Chitosan (Sigma Aldrich)	HMC+ Chitosan-HCl
(21)	80.86%	96.65%
(22)	78.32%	99.91%
(23)	73.00%	92.60%
Total average	77.39%	96.4%

Table 14 Calculation of DDA of CS polymers based on their ^1H NMR spectra.

Chapter 4: Characterization of chitosan

The two polymers were characterized using a series of spectra, namely: ^1H , ^{13}C , 2D-COSY, 2D-HSQC, 2D-TOCSY, 2D-DOSY. Due to the lack of sensitivity, ^{13}C and HSQC analyses did not produce appreciable results. The proton assignments are reported in Table 15 and the two spectra are shown in Figure 29. The assignments of the carbon peaks were based on results that were previously reported in literature and the assignment were confirmed by CP-MAS analyses of CP derivatives (Figure 34).

Type of proton	Shift (ppm) at 70 °C	Shift (ppm) at 25 °C
H ₁	5.30-5.12	Hidden by H ₂ O solvent peak
H ₁ (Ac)	4.85-5.00	4.32-4.54
H ₂	3.44-3.60	2.90-3.15
H ₃ ,H ₄ ,H ₅ ,H ₆	3.80-4.35	3.20-4,.5
H _{CH₃}	2.30-2.42	1.82-2.00
Type of carbon	Shift (ppm)	
C ₁	102.38	
C ₂	54.84	
C ₃	72.48	
C ₄ -C ₅	80.68	
C ₆	58.57	

Table 15 ^1H and ^{13}C NMR assignments of CS polymers.

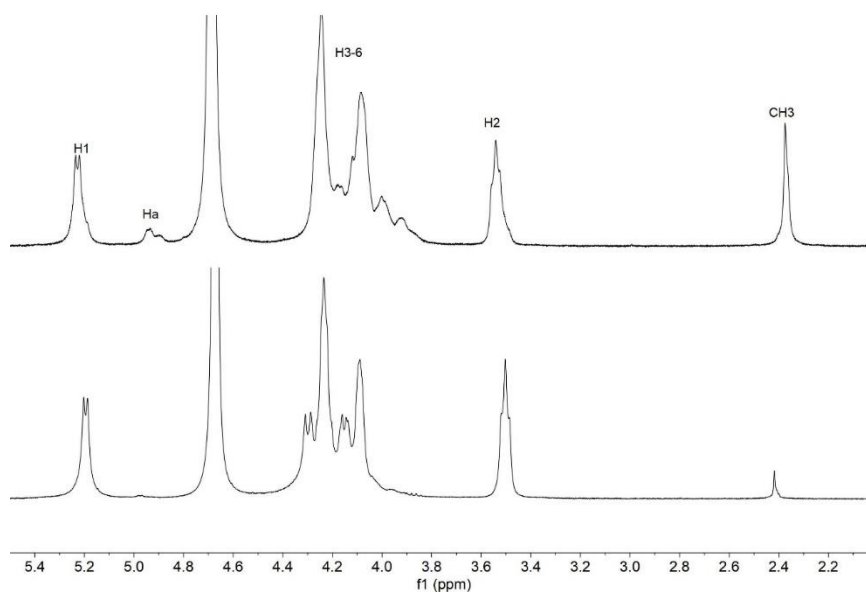


Figure 29 ^1H NMR spectra of +CS polymer (96.4% DDA, below) and CS (77.4% DDA, below) acquired at 70 °C.

4.2 Viscosimetric determination of the molecular weight

LMW CS (Sigma Aldrich, USA) viscosimetric molecular mass was measured according to the procedure described in the “Materials and Methods” section. The values of reduced (η_{red}) and inherent viscosity (η_{inh}) were derived from the run time of polymer solution dissolved in acetate buffer at 25 °C and plotted as a function of the concentration in g/dl.

Chapter 4: Characterization of chitosan

The result of the measurement is reported in Table 16. The values of intrinsic viscosity $[\eta]$ was calculated at infinite dilution using the Huggins and Kramer methods as reported by equation 25 and 26 (see “Methods” section). The calibration lines for both models are represented in Figure 30. The corresponding viscosity average molecular weight (M_η) of CS was calculated in agreement to the MHS equation (Equation 27), as reported in Table 17.

N°	Concentration (g/dl)	Average run time (seconds)	Relative viscosity	Specific viscosity	Reduced viscosity (dL/g)	Inherent viscosity (dL/g)
0	1000	506.40	1.7739	0.7739	7.7394	5.7320
1	0.9231	488.32	1.7106	0.7106	7.6984	5.8159
2	0.8000	459.56	1.6098	0.6098	7.6231	5.9518
3	0.6316	421.45	1.4763	0.4763	7.5425	6.1684
4	0.4444	377.96	1.3240	0.3240	7.2904	6.3151
5	0.3077	349.21	1.2233	0.2233	7.2569	6.5501

Table 16 Viscosimetric analysis of CS.

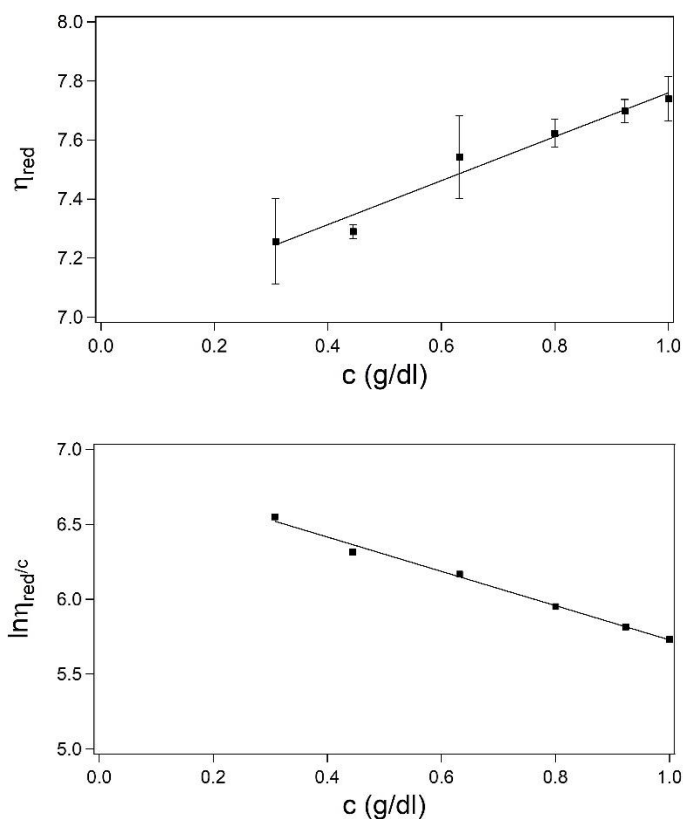


Figure 30 Linear fit of the results for the calculation of M_η based on Huggins (above) and Kraemer model (below).

$[\eta]$ – Huggins model	Molecular mass - M_η
701.62	223 kDa
$[\eta]$ – Kraemer model	Molecular mass - M_η
659.38	218 kDa

Average molecular mass M_{η}	220±3.52kDa
-----------------------------------	-------------

Table 17 Calculations of viscosimetric molecular mass based on Huggins and Kraemer models.

The results of demonstrated that the molecular mass of CS was significantly higher compared to the value declared by the producer, which had been previously estimated between 50 and 190 kDa. Accordingly, an incorrect estimation of the molecular mass of CS may results in scarce reproducibility of the results, since higher molecular masses have been frequently correlated with the formation of bigger and more polydisperse microgels and nanoparticles^{252,282,285}.

4.3 X-ray diffraction analysis

The crystallinity of CS and +CS were evaluated by wide angle X-ray diffraction analysis (XRD) using a Siemens/Bruker D5000 XRD apparatus. As of today, six polymorphs have been suggested for CS, namely: “1-2”, “L-2”, “tendon (hydrated)”, “annealed (anhydrous)”, “form-I” and “form-II”^{341,344}. In both form I and form II, CS molecule takes up a two-fold helical structure. Form I is orthorhombic and has cell unit of $a = 7.76$, $b = 10.91$, and $c = 10.30$ Å. The strongest reflection appears around $2\theta = 11^\circ$, which correspond to (100) reflection. Form II crystal is also orthorhombic with a unit cell of $a = 4.4$, $b = 10.0$, and $c = 10.3$ Å. The strongest reflection usually appears around $2\theta = 20^\circ$, which corresponds to the (100) crystal face³⁴⁴. CS and +CS are represented in Figure 31. CS with 78% DDA exhibits two broad peaks at $2\theta = 10.7^\circ$ and $2\theta = 19.9^\circ$, which correspond form I and form II crystal patterns. +CS with 96% DDA is totally amorphous as no peaks was found in the XRD spectrum.

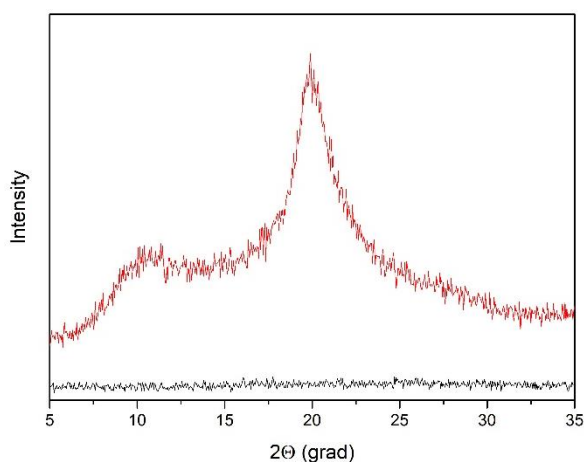


Figure 31 XRD profiles of CS (78% DDA, red) and +CS (96% DDA, black).

4.4 Summary

The characterization of two types of chitosan (CS and +CS) was performed by NMR, FT-IR, XRD spectroscopy and the molecular mass of CS was determined via viscosity. In this way, the molecular mass and the DDA of the polymers were calculated. These two properties affect the resulting microgels size and surface charge. In particular, the molecular mass affects the size of the microgels, thus defining their metabolic fate, while the DDA affects the surface charge, which defines the mechanism of interaction with biological barriers. Furthermore, the degree of deacetylation was used as a starting point to assess the degree of substitution of the chitosan copolymers after the grafting of PNVCL on the amino sites. The crystallinity of the polymers was assessed using XRD. The analyses revealed that CS has an orthorhombic structure, while +CS is amorphous.

Chapter 5: Synthesis and characterization of Chitosan-g-Poly-N-Vinylcaprolactam polymers

CS-g-PNVCL (CP) was prepared by the formation of an amidic bonds between the amino groups of CS and carboxyl groups of PNVCL-COOH (Figure 32). EDC and NHS were used as condensing agents. The two polymers were mixed in different ratio in order to provide different set of copolymers with different LCST. Reaction yields are reported in Table 18 along with their respective LCST.

<i>PNVCL/CS ratio</i>	<i>Sample</i>	<i>Yield (%)</i>	<i>LCST</i>
<i>1:2</i>	+CP122_12	45.42	-
	+CP244_12	39.79	-
	+CP305_12	20.41	-
	+CP610_12	35.42	-
	+CP1220_12	39.17	-
	+CP1690_12	38.33	-
<i>1:1</i>	+CP122_11	31.56	-
	+CP244_11	25.63	-
	+CP305_11	44.69	-
	+CP610_11	50.94	-
	+CP1220_11	42.19	-
	+CP1690_11	45.94	-
<i>2:1</i>	+CP122_21	50.20	~44
	+CP244_21	44.29	~49
	+CP305_21	59.37	~47
	+CP610_21	71.70	-
	+CP1220_21	49.79	-
	+CP1690_21	75.70	-
<i>4:1</i>	CP122_41	59.99	39.48±0.06
	CP244_41	83.77	37.59±0.08
	CP305_41	72.66	37.55±0.09
	CP610_41	85.70	34.01±0.19

Chapter 5: Synthesis and characterization of Chitosan-g-Poly-N-Vinylcaprolactam polymers

	CP1220_41	72.85	33.56±0.19
	CP1690_41	79.38	30.50±0.11
	+CP122_41	59.99	39.52±0.08
	+CP244_41	83.77	36.59±0.07
	+CP305_41	72.66	36.55±0.06
	+CP610_41	85.70	35.59±0.06
	+CP1220_41	72.85	34.50±0.11
	+CP1690_41	79.38	33.52±0.08
8:1	+CP122_81	56.35	41.48±0.08
	+CP244_81	98.72	38.43±0.02
	+CP305_81	75.56	38.33±0.09
	+CP610_81	72.47	36.48±0.09
	+CP1220_81	70.60	34.49±0.06
	+CP1690_81	97.34	33.52±0.08

Table 18 Results of the synthesis of CP and +CP polymers. The numeric values are referred to the ratio between PNVCL-COOH and CS used in the synthesis.

In this preparation, MES was used as a buffer in order to maintain pH at an optimal value of 5.5 during synthesis. Unlike acetate buffer, MES does not compete for the formation of the amide bond. PNVCL-COOH solutions were incubated overnight with EDC/NHS for the activation of carboxyl bonds. The reaction is illustrated in the Appendix section. Yield variations were mainly due to material losses during freeze-drying and dialysis. Due to the presence of PNVCL, CP samples tend to easily form foams that remains attached to the dialysis membranes. However, the lower yields observed in the first prepared samples (PNVCL/CS=1:1, 2:1 and 1:2) were related to incorrect handling during freeze-drying. During the sublimation of the solvent, frozen samples tend to expand during the process, and this led to the leakage of the powders. In order to reduce sample loss, the individual volumes contained within the falcons were reduced to less than half the volume of the falcons. In addition, the falcons were coated with a double layer of parafilm containing a layer of cotton inside. With this device, it was possible to increase the average process yield by about 20%.

5.1 Spectroscopic characterization

CP structural information were derived by FT-IR and NMR analyses. IR spectra of CP, PNVCL and +CS are shown in figure 25. The spectra of CP are generally dominated by the absorptions of PNVCL, but it is possible to identify the characteristic stretching vibration of the hydroxyl, aliphatic C–H, and acetylated amino groups from CS. The presence of terminal carboxyl group is also verified by the broad -OH peak between 3500 and 2600 cm^{-1} . The characteristic vibrations of PNVCL-COOH and CP are reported in Table 19. As the PNVCL/CS ratio changes, the ratio between the absorption bands changes and the intensity of the C=O band increase with increasing PNVCL/CS ratios. On the contrary, in

Chapter 5: Synthesis and characterization of Chitosan-g-Poly-N-Vinylcaprolactam polymers

^1H NMR spectra the signals related to the two different polymers are more easily distinguishable for higher PNVCL/CS ratios.

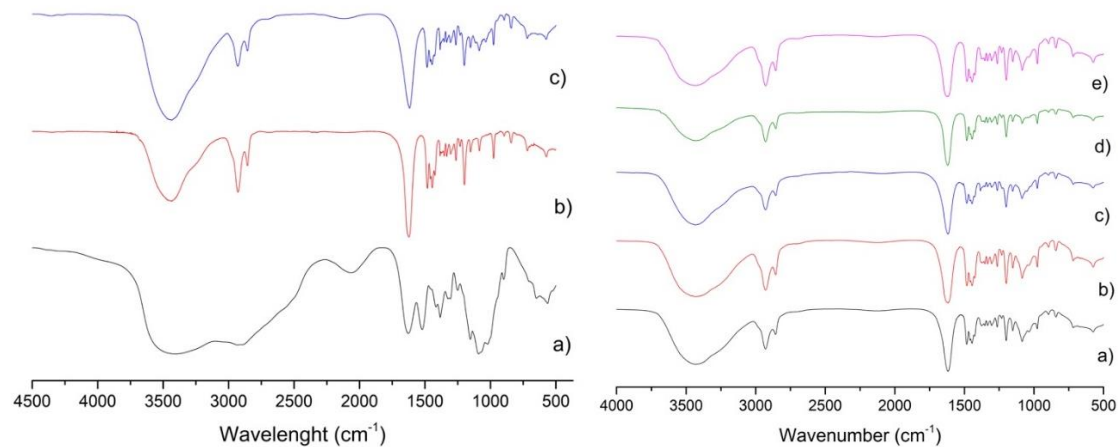


Figure 32 (left) IR spectra of a)+CS b)PNVCL_244 C)+CP244_41 (right) IR spectra of a)+CP305_11 a)+CP305_12 b)+CP305_11 a)+CP305_21 a)+CP305_41 and a)+CP305_81.

Chapter 5: Synthesis and characterization of Chitosan-g-Poly-N-Vinylcaprolactam polymers

<i>HMC+ Chitosan (+CS)</i>	
<i>Frequency (cm⁻¹)</i>	Group
3402	O-H and N-H stretching
2935	C-H asymmetric stretching
2890	C-H symmetric stretching
1628	N-H bending
1520	N-H bending (Amide II)
1423	C-N stretching
1375	C-N stretching
1325	C-N stretching (amide III)
1253	O-H bending
1157	Bridge -O stretching
1091	C-O stretching
897	C-H out of plane
650	N-H twist
<i>PNVCL-COOH</i>	
3416	O-H stretching (carboxylic acid)
2928	C-H asymmetric stretching
2858	C-H symmetric stretching
1622	N-H-C-O bending (amide I)
1482	C-N stretching
1441	C-H deformation
<i>CS-g-Poly-N-Vinylcaprolactam (CP)</i>	
3416	O-H stretching (alcoholic and carboxylic acid)
2928	C-H asymmetric stretching
2875	C-H symmetric stretching
1616	N-H-C-O bending (amide I)
1482	C-N stretching
1444	C-H deformation
1423	C-N stretching
1375	C-N stretching
1263	O-H bending
1153	Bridge-O-stretching
1084	C-O stretching
895	C-H out of plane

Table 19 FT-IR attributions for +CS, PNVCL-COOH and CP.

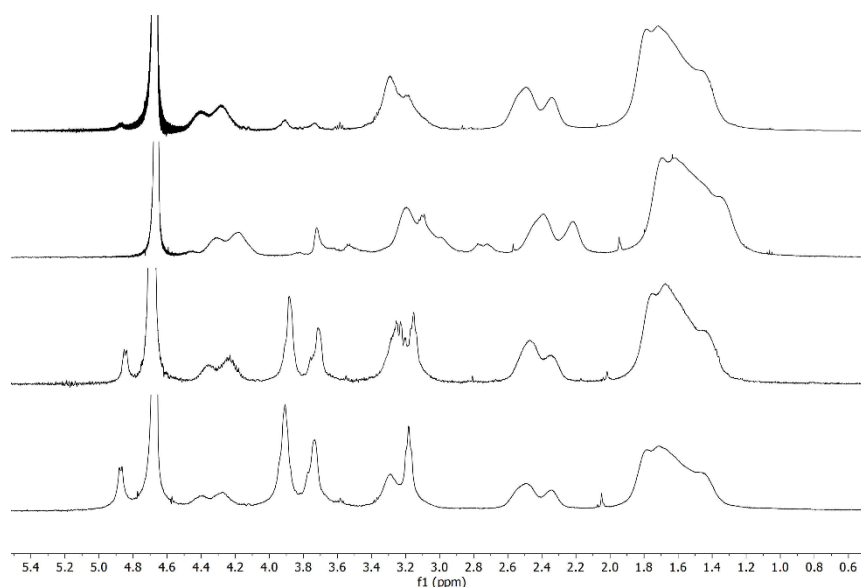


Figure 33 ¹H NMR spectra of +CP305_12, +CP305_21, +CP305_41 and +CP305_81. All spectra were recorded at 35 °C except CP305_41 (recorded at 25 °C) using a Varian 500 MHz spectrometer.

Chapter 5: Synthesis and characterization of Chitosan-g-Poly-N-Vinylcaprolactam polymers

NMR analysis of +CP_244_41 and +CP_305_41 polymers were performed with a Bruker 500 MHz available at Instituto Ronzoni (Milano, IT). Polymers were analysed using ^1H NMR, CP-MAS ^{13}C , HP-DEC CP-MAS ^{13}C and diffusion-ordered spectroscopy (DOSY). Due to the spectral linewidth of the polymer signals, ^1H NMR spectra showed similar characteristics of a mixture solution of CS and PNVCL. The utilization of DOSY was pivotal to establish the formation of CP polymer as well as to establish the presence of unreacted CS and PNVCL. DOSY analysis of +CP305_41 (Figure 35) allowed the recognition of the signals of three different species, distributed along the y-axis as a function of their diffusion coefficient. Unreacted PNVCL and CP were identified according to their proton signals. The value of the diffusion coefficient of each polymer was derived by using a three-component fitting model. Interestingly, the result showed that CP has a lower diffusion coefficient than PNVCL and CP. PNVCL and CS are linear polymers, and the different value of the diffusion coefficient can be related to their different molecular mass. On the contrary, CP is a grafted polymer and behaves differently in solution. Due to the presence of residual starting polymers, it was not possible to estimate the degree of substitution from the results of DOSY. CP-MAS ^{13}C and HP-DEC ^{13}C characterization (Figure 34) allowed to recognize the signals of the carbon relative to both PNVCL and CS. The results confirmed the presence of unreacted CS. By using the anomeric carbon (C_1 , 102.38 ppm) as a reference peak, it can be observed that the total integral of the CS signals (8.36) is higher than the expectation value (6). This accounts for the presence of unreacted CS.

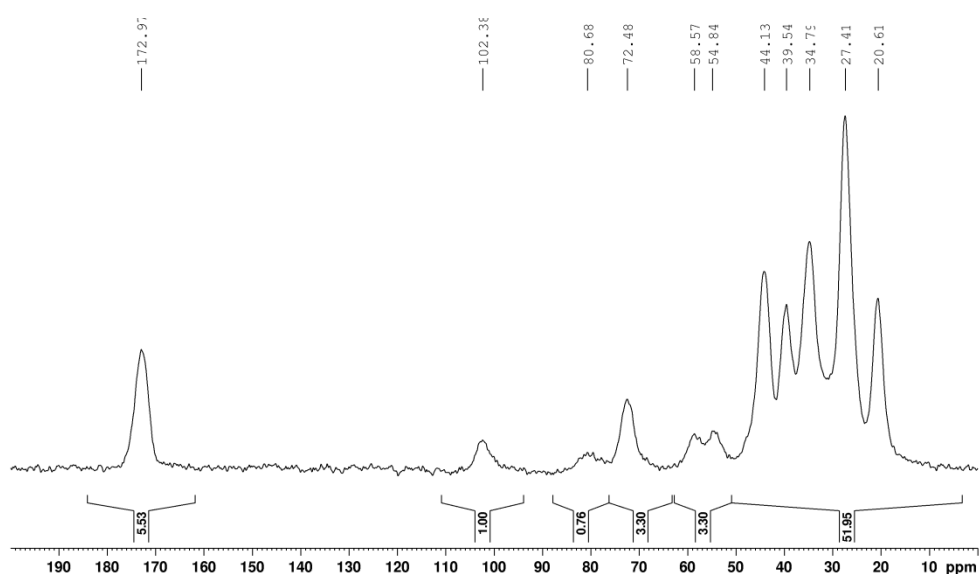


Figure 34 HP-DEC CP-MAS spectrum of +CP305_41.

Chapter 5: Synthesis and characterization of Chitosan-g-Poly-N-Vinylcaprolactam polymers

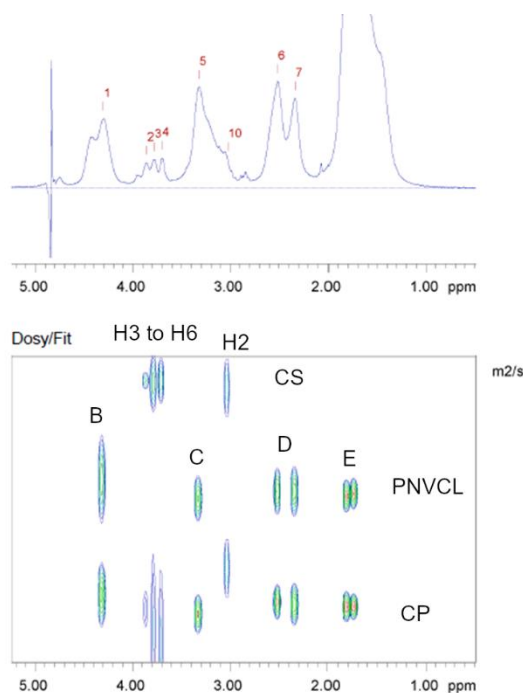


Figure 35 DOSY spectrum of +CP305_41.

Polymer	Diffusion coefficient (m ² /s)
+CS	$1.3 \cdot 10^{-11}$
PNVCL	$3.3 \cdot 10^{-11}$
+CP305_41	$7.8 \cdot 10^{-11}$

Table 20 Results on the analysis of DOSY spectrum of +CP305_41.

5.2 Estimation of the degree of substitution

Unreacted amino groups in CS are necessary for the formations of microgels with TPP during ionotropic gelation^{93,278,345}. NMR spectroscopy did not provide any information on the presence of N-H protons due to solvent exchange. The degree of substitution (DS) of CP_305_41 and CP_244_41 was estimated via conductimetric titration. The DDA of the copolymers was estimated from by the plateau present in the conductivity curve, by using the following equation³⁴⁶:

$$DDA(\%) = \frac{161[\text{base}](V_2 - V_1)}{m} \quad (23)$$

in which [base] is the concentration of the NaOH solution (in mol L⁻¹), V₁ and V₂ are the volume of NaOH (in mL) used in the titration, 161 is the molar mass of the repetitive unit and m is the mass of CS (in mg).

The DS was calculated by subtracting from the DDA of the CS the calculated DDA by conductivity.

The DS for CP_305_41 and CP_244_41 was estimated to be, respectively, 56.3% and 54.2%. It is possible that the DS value can be slightly overestimated due to the presence of residual unreacted CS, as demonstrated by DOSY. For the same reason, the grafting efficiency (GE) was not calculated as the value can be easily affected by the presence of polymer mixtures.

5.3 Analysis of the thermoresponsive behaviour

The goal of the synthesis of polymers of CP and +CP was to identify a family of thermoresponsive copolymers capable of exhibiting thermoresponsivity in a temperature range of between 37 and 42 °C. This range is ideal for delivery applications, as the fluidity of biological membranes is enhanced without inducing apoptosis of treated cells^{93-94, 104, 106-107}. The LCST of CP and +CP polymers was determined via UV-VIS spectroscopy. Polymers were analysed at a concentration of 5 mg/ml and a 5.5 pH. The LCST was determined from the inflection point of the sigmoidal curves that were used to fit the miscibility curves (Figure 36 and 37). The results showed that CP and +CP exhibit inferior LCST in respect to the related PNVCL polymers. Polymer LCST are reported in Table 18. In general, during the formation of these polymers the opposite behaviour is observed, and the amount of CS is decided in order to increase the LCST of the thermoresponsive polymer^{91,93,96,99,104,108}. However, the results obtained were reproducible. By using a PNVCL/CS ratio of 4 to 1, the LCST of PNVCL is generally decreased by ~1 °C. The decrease of the thermoresponsive portion results in the disappearance of the thermoresponsive behaviour. By using lower PNVCL/CS ratio, the transition was observed only with the use of PNVCL with lower molecular weight (+CP122_21, +CP244_21 and +CP305_41), where the conformational change required less energy. On the contrary, by increasing the degree of substitution (8:1), the LCST remained substantially identical as PNVCL. CP and +CP polymers that exhibited LCST between 35 and 42 °C were considered as possible materials for the preparation of thermoresponsive drug delivery vectors.

Chapter 5: Synthesis and characterization of Chitosan-g-Poly-N-Vinylcaprolactam polymers

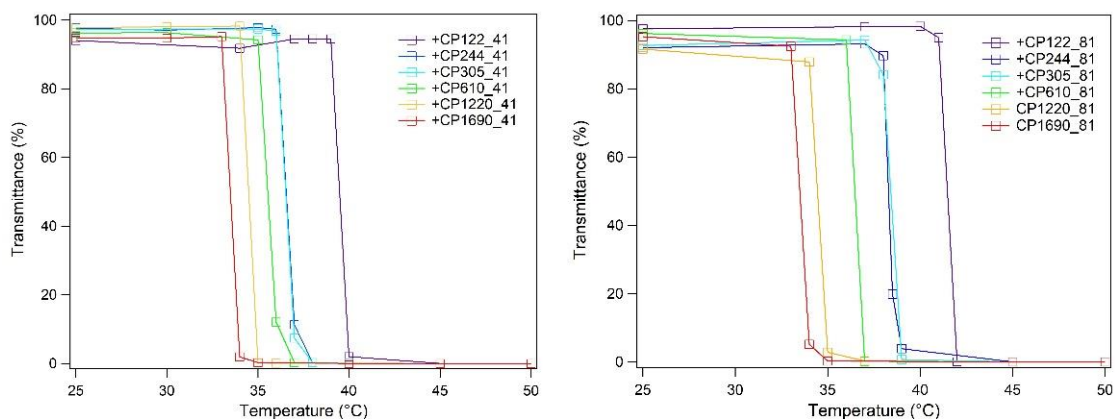


Figure 36 Solubility curves of +CP_41 (left) and +CP_81 (right) polymers.

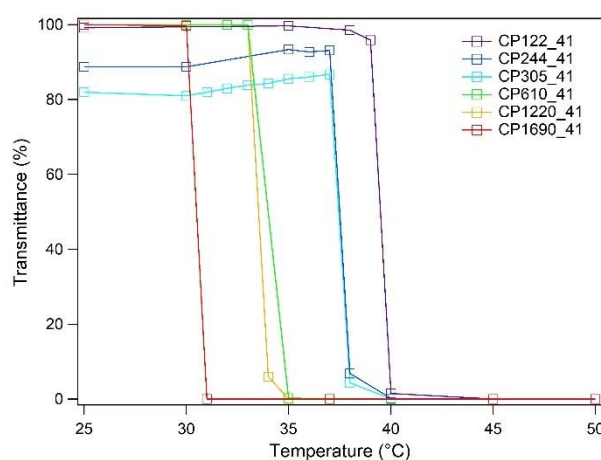


Figure 37 Solubility curves of CP_41 polymers.

The phase transition of CP41 (+CP305_41) was also observed through ^1H NMR spectroscopy by raising the temperature of a sample in D_2O from 25° to 70°C (Figure 38). At 25°C , the polymer is completely dissolved and both of PNVCL and CS signals are clearly visible. During the heating process, CS signals exhibited the expected behaviour of a polysaccharide in solution. As far as the temperature increases, the absorption signals related to CS protons are deshielded and the band width is reduced due to reduction in viscosity and desolvation. On the contrary, PNVCL exhibited the characteristic behaviour of a polymer undergoing LCST transition and the signal intensity disappeared and almost vanished at 70°C . A possible explanation to the phenomenon is that while CS becomes more desolvated as the temperature increases, while PNVCL becomes less soluble in water. The desolvation of CS results in the reduction of the spectral linewidth of the proton signals. On the contrary, the coil-to-globule transition “hides” the protons of the PNVCL inside the internal part of the globules.

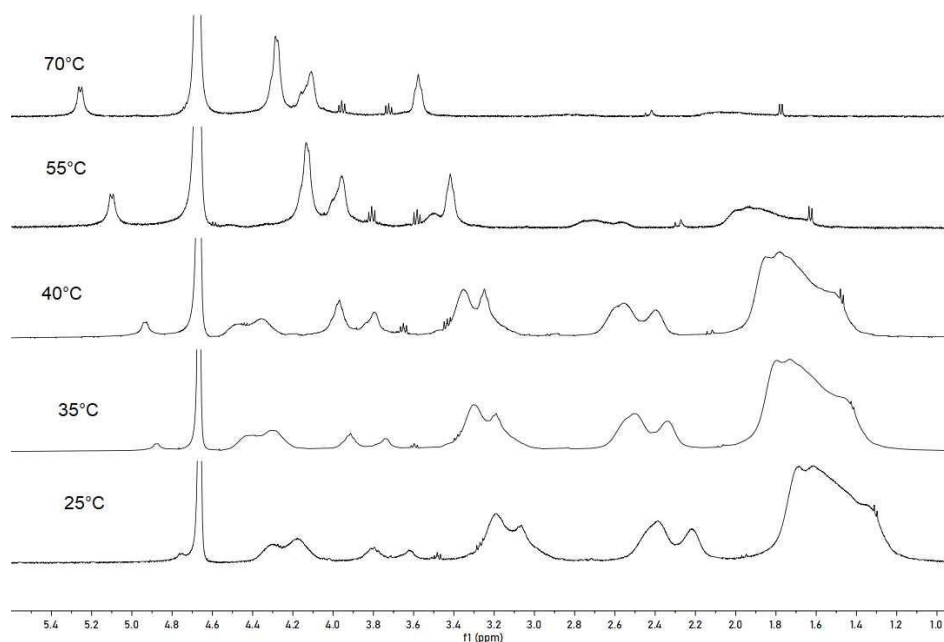


Figure 38 Phase transition behaviour of CP305_41 in the temperature range between 25 and 70 °C.

5.4 Summary

CP copolymers were synthesized using EDC and NHS as condensing agents. PNVCL and CS have been used in different ratios (1:2, 1:1, 2:1, 4:1 and 8:1) in order to obtain a set of polymers with different LCST. The LCST of the copolymers was determined by UV-VIS. CP and +CP exhibit inferior LCST in relation to their corresponding PNVCL polymers. By using lower PNVCL/CS ratio, the LCST rises. In this way, we selected a range of polymers with LCST ranging from 37 to 42 °C for the fabrication of thermoresponsive microgels. CP polymers were characterized by different mono- and two-dimensional NMR techniques and FT-IR spectroscopy. DOSY analysis showed the presence of unreacted PNVCL and chitosan. Consequently, the DS was not calculated via DOSY and the value was estimated using conductimetric titration.

Chapter 6: Preparation and characterization of chitosan microgels

6.1 Preparation and optimization

CS microgels were prepared by ionotropic gelation²⁸⁴ adding TPP (0.5 mg/ml) to a CS solution (1.25mg/ml) in the drop wise manner using a micropipette or a dripping funnel. For both type of CS, the formation of visible opalescent solution usually resulted in the formation of NPs with a big diameter (~500 nm) that exhibited poor stability. Flocculation was avoided in order to prepare stable suspensions. Samples with a diameter between 100 and 200 nm showed a weak opalescence, which was detected by pointing a light directly at the reaction flask. The process was optimized in order to reach a reproducible protocol for the formation of CS NPs with an average size around 200 nm. The preparation of the microgels was optimized by adjusting several parameters, including the duration of the reaction, CS concentration, pH, acetic acid concentration (0.05 %), temperature and CS/TPP mass ratio. The preliminary study on CS particles allowed to determine the experimental conditions for the preparation of CP particles. The best CS/TPP mass ratio depended on the type of CS used for NPs preparation. The utilization of +CS with lower molecular weight resulted in the formation of bigger particles. The suspensions were characterized in terms of size of particles and polydispersity (PDI).

6.1.1 Effect of polymer concentration

In the early stages of this study, CS microgels were prepared using CS and TPP solution at a concentration, respectively, of 0,5 mg/ml and 0,1 mg/ml. For most preparations, CS and TPP concentration were raised to 1,25 mg/m and 0,25 mg/ml. The utilization of more concentrated solution was evaluated. The utilization of CS and +CS solutions at a concentration of 2, 2,5 and 5 mg/ml led to the formation of unstable suspensions in the same experimental conditions. The correlation curves related to CS NPs prepared with different polymer concentrations are represented in Figure 39. Results are shown in Table 21. +CS NPs reported in the table were prepared using a 5:1 +CS/TPP ratio.

CS concentration	D_h	PDI
0,5	186±101	0.341
1,25	194±87	0.269
+CS concentration (mg/ml)	D_h	PDI
1,25	294±124	0.176
2	precipitation	-
2,5	precipitation	-
5	precipitation	-

Table 21 Effect of +CS concentration on NPs size distribution. NPs were analysed without dilution.

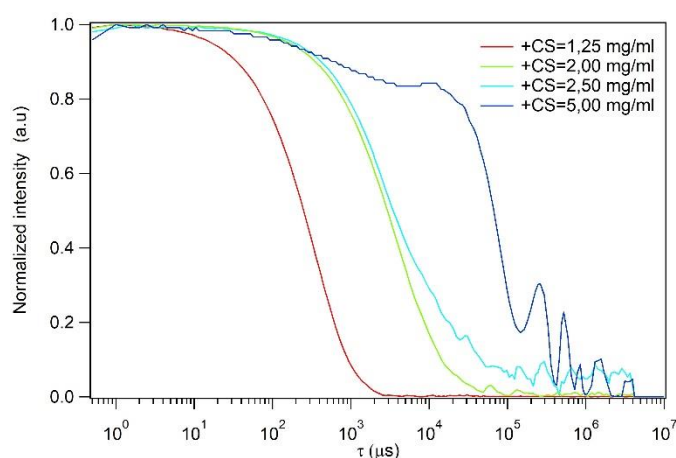


Figure 39 Correlation curves of +CS NPs prepared using different +CS concentration.

6.1.2 Effect of molecular weight and DDA

The utilization of two different types of CS polymers with different molecular mass and DDA led to the formation of nanoparticles with different chemico-physical properties. In the same preparation conditions, the utilization of +CS with lower molecular weight (128 kDa) led to the formation of larger particles (Table 22). This experimental result is in apparent contradiction to the principle for which the utilization of CS with lower molecular weight leads to the formation of smaller NPs. The preparation of stable suspensions of +CS NPs with a diameter between 150 nm and 300 nm was accomplished by using a different CS/TPP mass ratio. Both CS and +CS NPs have positive surface charge due to the presence of protonated amine groups. Due to their higher DDA, +CS particles have a higher positive surface charge (Table 22).

6.1.3 Effect of CS/TPP mass ratio

The optimal CS/TPP mass ratio for the formation of NPs with a 200 nm size was determined experimentally. The utilization of CS led to similar results to what has been previously reported in literature. The optimal CS/TPP value for the preparation of CS NPs

Chapter 6: Preparation and characterization of chitosan microgels

with a diameter around 200-250 nm was 5:1. On the contrary, the utilization of +CS required higher CS/TPP ratio (6:1 and 8:1) for the formation of NPs with similar sizes. Microgels formed with lower CS/TPP ratio exhibited lower surface charge as expected. This eventually led to particle destabilization due to the formation of intermolecular links between particles. Accordingly, the correlation curves were displaced to higher τ values (Figure 40). Results are shown in Table 22.

CS/TPP ratio	D _h (nm)	PDI	Z potential (mV)
19:1	116,9±99	0.183	46.6±5,79
9:1	358±212	0.374	45.8±4,88
6:1	268±126	0.410	44.6±4,15
5:1	194±87	0.269	42.4±4,95
4:1	181±86	0.302	41.7±5,22
3,33:1	335±182	0.374	40.7±5,83
+CS/TPP ratio	D _h (nm)	PDI	Z potential (mV)
8:1	550±207	0.241	53.2±4.27
6:1	309±123	0.226	46.3±3.69
5:1	566±275	0.263	52.7±3.32
4:1	410±217	0.243	39.7±3.19
3:1	Precipitation	-	-
2:1	Precipitation	-	-

Table 22 Particle size distribution and surface charge related to CS/TPP ratio. All preparations were prepared using 1,25 mg/ml CS solutions. NPs samples were analysed without dilution.

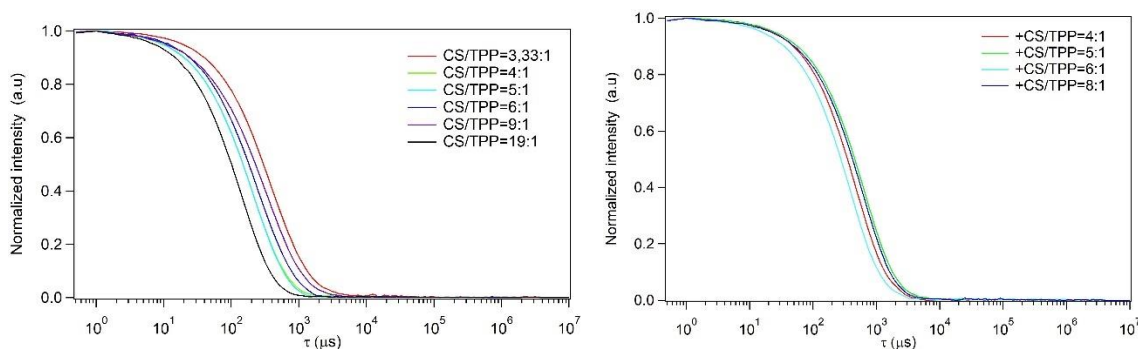


Figure 40 Displacement of DLS correlation curves in relation to different CS/TPP ratios. (left) CS NPs. (right) +CS NPs.

6.1.4 Effect of temperature

Fan *et al.* suggested that reducing the temperature of CS solution leads to the formation of monodisperse CS NPs²⁸⁶. CS NPs were prepared by using a CS and TPP solution and a magnetic bar that were kept at 4 °C overnight. The results (Table 23) showed that lowering the temperature resulted in little improvement in size distributions and PDI. For simplicity, most CS NPs were prepared by using solution at room temperature.

Chapter 6: Preparation and characterization of chitosan microgels

CS/TPP ratio	25 °C		4 °C	
	D _h (nm)	PDI	D _h (nm)	PDI
5:1	194±87	0.269	186±79	0.190
4:1	181±86	0.302	210±101	0.253
3,33:1	335±182	0.374	315±190	0.353

Table 23 Effects of temperature on size distribution. NPs samples were analysed without dilution.

6.1.5 Effect of NaCl concentration

Jonassen *et al.* suggested the utilization of medium ionic strength solvent for the formation of CS NPs with unimodal size distribution and small PDI^{278,283}. CS NPs were formed in presence of NaCl 0.05 and 0.15 M NaCl (Table 24). The polymer was dissolved in a solution containing acetic acid and NaCl. Our results are coherent with the findings of Jonassen *et al.* and showed a non-linear relationship between the ionic strength of the solvent and the average size of the NPs. The addition of NaCl provided a size-focusing effect and reduce the average size and the PDI of the particles. Furthermore, the presence of NaCl reduces the surface charge of the NPs. CS NPs prepared in the presence of NaCl 0.15 M showed greater stability than particles prepared using water as a solvent. CS NPs prepared in presence of NaCl showed no change in chemical-physical properties within 21 days (Figure 42).

Sample	[NaCl] (mol/l)	D _h (nm)	PDI	Type of distribution	Z potential (mV)
CS NPs (3.33/1)	0	358±212	0.374	bimodal	40,7±5,83
	0.05	138±85	0.271	unimodal	23.2±4.70
	0.15	141±83	0.240	unimodal	16.3±1.28
CS NPs (4/1)	0	181±86	0.302	unimodal	41,7±5,22
	0.05	142±88	0.279	unimodal	31.4±6.99
	0.15	116±53	0.191	unimodal	19.6±1.54
CS NPs (5/1)	0	186±101	0.341	unimodal	42,4±4,95
	0.5	123±57	0.235	unimodal	31.1±6.47
	0.15	113±50	0.183	unimodal	21.1±1.65

Table 24 Effects of NaCl on size distribution. NPs samples were analysed without dilution.

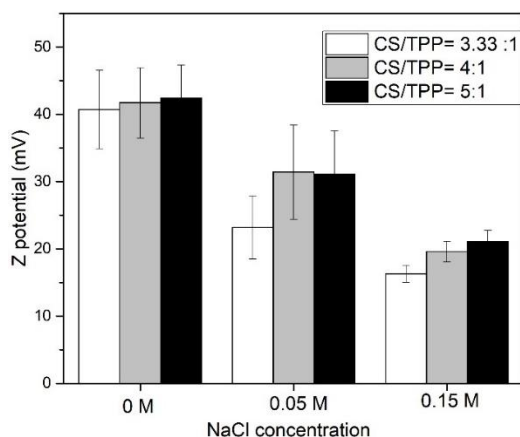


Figure 41 Effects of NaCl concentration on Z-potential values.

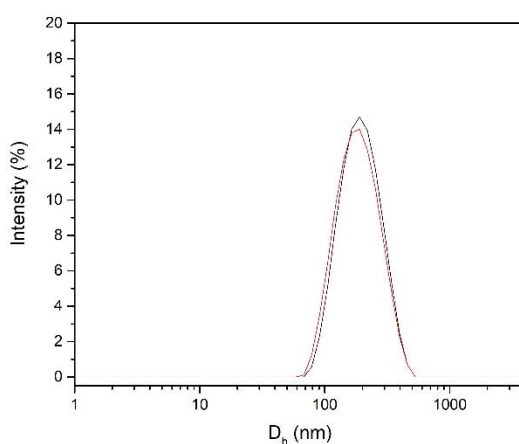


Figure 42 Size distribution by intensity of CS NPs (CS/TPP=5:1, 0.15 M NaCl) before (black) and after (red) 28 days of storage at 4 °C.

6.1.6 Optimization of DLS measurements

It is crucial to perform DLS analyses in a correct range of particle concentration. Concentrated samples can give rise to backscattering between nearby particles. In addition, if two particles are too close, they can be "seen" by the DLS as a larger aggregate. Since the intensity strongly depends on the size of the objects, these values can strongly influence the results of the analyses. However, although the experimental conditions of DLS analysis are adequately addressed in technical manuals, their importance is not usually addressed in scientific publications. In this work, many particles were analysed without dilution. NPs dispersion that exhibited narrow unimodal size distribution and low PDI showed no improvement upon dilution. However, it was observed that dilution has a stronger effect on dispersions containing a small amount of larger particles. The analysis of +CS samples with $D_h \sim 450$ nm showed that a 1:100 dilution results in a decrease of the average D_h value by almost 100 nm (Table 25). Accordingly, the correlation curves were displaced towards lower τ values.

Chapter 6: Preparation and characterization of chitosan microgels

+CS concentration (mg/ml)	Dilution factor (D)	D_h (nm)	PDI
0.625	1	448±212	0.248
0.3125	2	452±222	0.253
$6.25 \cdot 10^{-2}$	10	413±228	0.225
$6.25 \cdot 10^{-3}$	100	299±132	0.251
$6.25 \cdot 10^{-4}$	1000	-	-

Table 25 Effects of NPs concentration on DLS analysis of CS NPs (CS/TPP=8:1). Concentrated samples lead to the overestimation of D_h . Highly diluted samples are not suitable for DLS analysis.

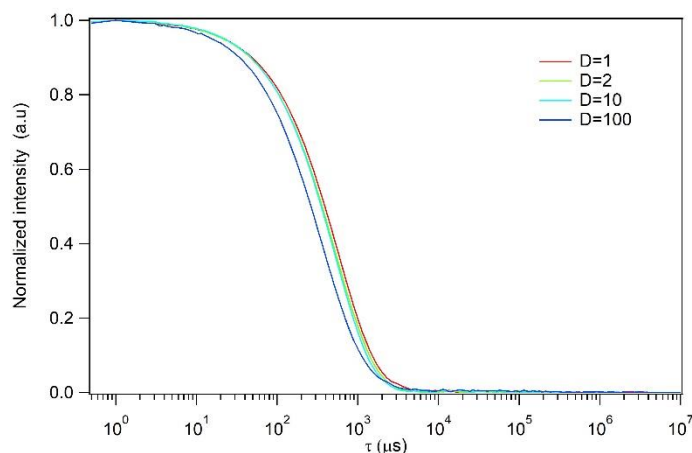


Figure 43 Correlation curves of the same sample +CS NPs (+CS/TPP=8:1) analysed at different concentrations.

6.2 Nanoparticle tracking analysis

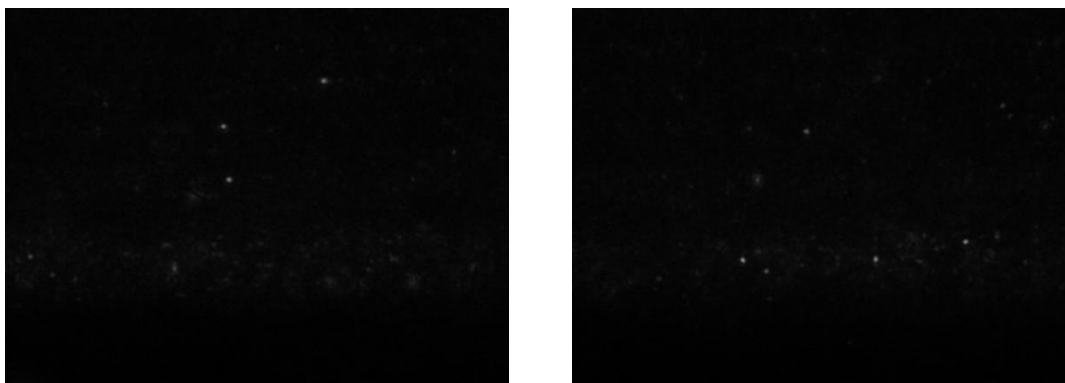


Figure 44 Frames of NTA of CS NPs.

The utilization of NTA as a complementary technique to DLS allowed to obtain further information on the distribution of CS particles. Unlike the DLS, the NTA is less affected by the presence of aggregates and allows more detailed analysis of multimodal distributions. In addition, NanoSight software, unlike Zetasizer software, offers the possibility to export the result of the analysis and to use an appropriate model depending on the sample under observation. Previous DLS analysis of CS particles (CS/TPP ratio = 5:1) showed a unimodal distribution with a main peak at 186 nm and a PDI of 0,352. NTA

analysis showed the presence of a multimodal distribution with five different peaks. The deconvolution of the curve was carried out in order to obtain five normal distributions in the range between 80 and 600 nm. Values below 80 nm were not considered in the fitting range as they were found to be below the reliability threshold of the instrument. The results showed the presence of three main populations at 156 nm, 216 and 256 nm (Figure 45, Table 26). The presence of two minority peaks at 399 and 100 nm suggested the necessity of purification techniques for the elimination of particles with a larger diameter. Particle concentration was not determined from the number of events as it required a calibration sample with similar size distribution and refractive index.

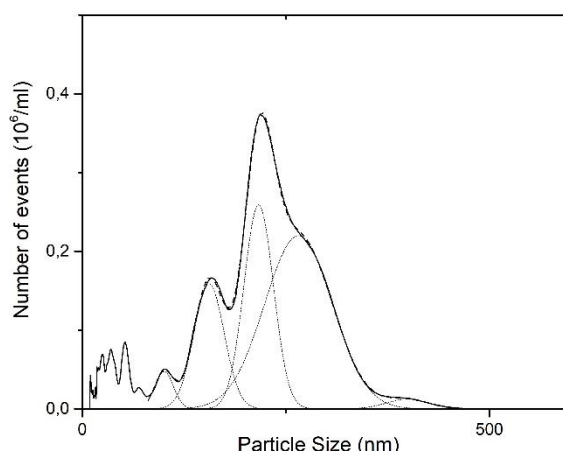


Figure 45 Results of NTA analysis of CS NPs (CS/TPP=5:1). Fit peaks and cumulative fit function are represented with dashed lines.

Peak position and FWHM	% of total fitted area
100±27	3.06%
156±44	16.75%
216±43	26.55%
256±98	51.84%
399±61	1.79%
r^2	0.99965

Table 26 Peak positions, FWHM and correlation value of the fitting function used for the interpretation of NTA results.

6.3 Purification method

NPs purification was approached through different methods. A widespread method is to perform a dialysis. NPs are commonly dialysed with distilled water, NaCl solutions or PBS in order to gradually disperse the NPs in a new environment. If the cutoff of the membrane (MWCO) is superior to the mass of CS, this method also allows the purification from non-reacted CS. Despite this, the utilization of membrane with a cutoff inferior to the mass of the polymer is a very common mistake that is reported in many preparation protocols^{93,99,106,185}. CS NPs particles were purified from the acetate buffer by dialysis for

Chapter 6: Preparation and characterization of chitosan microgels

two days against a solution of NaCl 0M, 0,05 M and 0,15 M. The suspensions obtained showed an increase in average size and PDI (Table 27) and precipitated in the fridge after few days of storage. The change in pH induced during dialysis resulted in irreversible aggregation.

Sample	D _h before dialysis	PDI	Type of distribution	D _h (main peak) after dialysis	PDI	Type of distribution
CS NPs (3.33/1)	358±212	0.374	unimodal	312±117	0.591	multimodal
CS NPs (4/1)	181±86	0.302	unimodal	515±202	0.702	multimodal
CS NPs (5/1)	186±101	0.341	unimodal	413±193	0.725	multimodal

Table 27 Comparison between size distribution of CS NPs before and after dialysis with distilled water for 2 days.

Another common method for CS NPs purification is centrifugation. The purification of CS NPs was initially approached through the method proposed by *Rampino et al.*³⁰⁷, in which it is suggested that centrifugation at 3270 g prevents the breakage of NPs during the process. However, this value should be recalculated according to the estimated average size of the NPs, the solvent used, their concentration and the molecular mass of CS. By using this method, no precipitates could be observed. The centrifugation rate was established experimentally. For each centrifugation attempt, the supernatant and the precipitate were measured using DLS (Table 28-29). The experiments allowed to determine suitable values for the NPs centrifugation. After the centrifugation rate was established (table 29), two methods were tested for particle purification. The conventional method is to centrifugate the NPs at a determined rate, re-suspend the pellet in water and discard the fraction that remains in the supernatant. The analyses of the individual fractions of a sample of +CS NPs are shown in Table 29. The results showed that the method is not reliable since the formation of aggregates was not totally predictable. In the case in which fractional separation was produced, it was observed a decrease in polydispersity in relation to the initial population and a slight increase in the average size in the precipitate fraction. After two centrifugations, the PDI of the supernatant had an overall decrease of 0,1. However, this method was not considered reliable due to the formation of irreversible aggregates and the lack of reproducibility. A second method consisted in centrifugating the NPs initially at lower rates (5000g, 10 min) in order to selectively precipitate the bigger NPs. After the aggregates are separated, the NPs were concentrated in a pellet (15000g, 10 min) and resuspended in water. The results of the application of this method are given in Table 30. Centrifugated NPs usually exhibited unimodal size distribution that with improved PDI in both fractions and higher average D_h in the pellet fraction. The second method confirmed the instability of the particles in respect to high centrifugation speeds.

Chapter 6: Preparation and characterization of chitosan microgels

+CS/TPP ratio	Supernatant D _h (nm)	PDI	Pellet D _h (nm)	PDI
4:1	448±212	0.248	aggregates	-
5:1	452±222	0.253	aggregates	-
6:1	330±138	0.225	aggregates	-
8:1	330±138	0.253	218±108	0.254

Table 28 CS NPs size distribution before and after centrifugation at 10000 g for 10 min.

Centrifugation rate	Time (min)	Supernatant D _h (nm)	PDI	Pellet D _h (nm)	PDI
5000g	10	336±143	0.312±0.004	404±169	0.279±0.006
10000g	10	310±170	0.334±0.048	338±191	0.260±0.018
15000g	10	283±170	0.295±0.007	340±181	0.267±0.028
Second centrifugation of pellet fraction					
10000g	10	227±103	0.164±0.017	aggregates	-
15000g	10	256±118	0.206±0.004	317±148	0.257±0.010
Third centrifugation of pellet fraction					
15000g	10	Aggregates	-	Aggregates	-

Table 29 Results of conventional method of NPs centrifugation. The pellet fraction was resuspended and purified through three centrifugation steps.

Step	Time (min)	Supernatant D _h (nm)	PDI	Pellet D _h (nm)	PDI
Initial	-	373±275	0,312±0,010	373±275	0,312±0.010
5000g	10	323±140	0,208±0,006	385±256	0,404±0.004
5000g	10	320±134	0,201±0,004	362±176	0,417±0.012
15000g	10	-	-	287±120	0,183±0.03

Table 30 Results of the second purification method. NPs were initially separated from the aggregates and concentrated in a pellet in the last centrifugation step. The initial size distribution is reported in the first line.

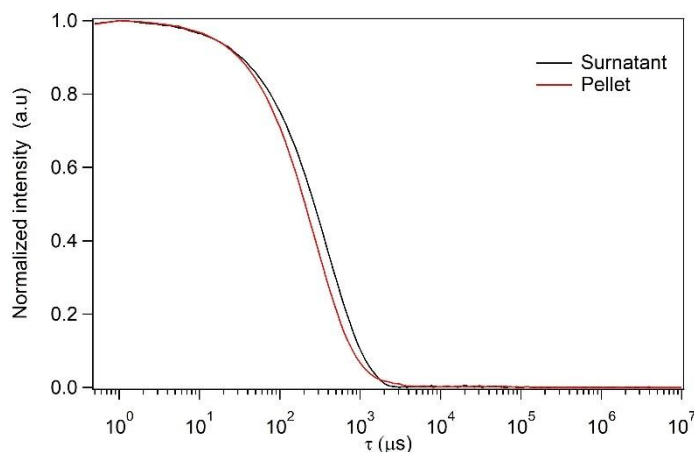


Figure 46 Comparison between the correlation curves of +CS NPs (+CS/TPP=8:1) present in the supernatant and the pellet.

A reliable protocol consisted in centrifugating the particle using a centrifugation rate between 500 and 2500 rpm to get rid of the bigger particles. The rate was decided on each case according to the initial size distribution. The yield of the purification process was not measured. In general, it was observed that NPs are not able to sustain more than two centrifugation cycles. The utilization of glycerol beads (about 5-10 μ l) deposited on the bottom of Eppendorf did not provide substantial improvements. The presence of glycerol

leads to changes in the local refractive index of the solvent. Consequently, DLS measurement can easily give rise to artifacts during size determination.

6.4 pH-responsivity

CS particles pH-responsivity were studied by measuring the correlation curves at different pH. CS microgels were prepared by using acetic acid solution at a 0,05% w/v concentration and buffered at 4.8 pH using NaOH solutions prior to the reaction. Our findings showed that the preparation of CS solutions showed similar size distribution if prepared in a range of pH between 4.8 and 5.5. TPP solutions were used at a concentration of 0,25 mg/ml at a pH of 9,74 and the addition of TPP did not cause any change in pH during particle formation. The results exclude a reversible pH-responsive behaviour. The behaviour of a sample of CS NPs (CS/TPP=4:1) in function of the pH is reported in Table 31. CS particles underwent aggregation once exposed to a pH superior to 6. By lowering the pH back to 5.5, it was not possible to redisperse the particles. Irreversible aggregation can still result in pH-triggered release, but the formation of aggregates is generally associated to cytotoxic effects. From a formal point of view, the appropriate description of the phenomenon is that pH-changes results in the destabilization of CS microgels suspensions (Figure 47). This is due to the deprotonation of amino sites, which results in the breaking of the ionic bond that holds together the meshes of microgels.

pH	D_h	PDI
4.8	264±109	0.201
5.5	273±104	0.199
6.0	329±132	0.317
6.5	1174±381	0.222
7.4	aggregation	-

Table 31 Effects of pH on size distribution. NPs samples were analysed without dilution.

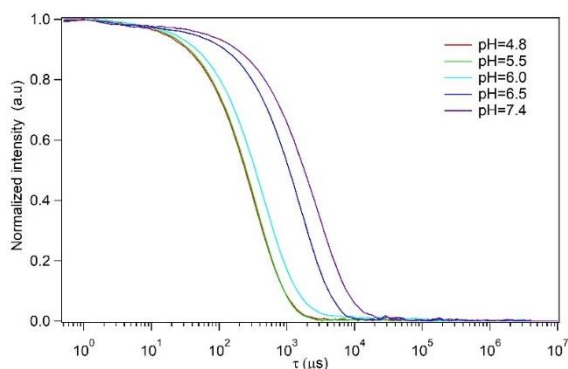


Figure 47 Correlation curves of CS NPs analysed at different pH.

6.5 Summary

Chitosan microgels were prepared by ionotropic gelation in order to define a reliable protocol for the preparation of particles with a size around 200 nm. The preparation of the microgels required the optimization of several parameters, including the ratio between CS and TPP, the duration of the reaction, CS concentration, pH and the concentration of acetic acid. Size distribution and zeta potential of microgel suspension were monitored in relation to every single parameter. NTA analysis provided a more detailed description of the polydispersity of the samples. The study confirmed the hypothesis that polydispersity and surface charge of CS microgels can be reduced by dissolving CS into NaCl solutions. The purification via centrifugation resulted in the formation of aggregates, but we managed to reduce polydispersity by excluding aggregates using low centrifugation rates. Finally, we ruled out the possibility that CS microgels were pH-responsive. The deprotonation of amine sites led to irreversible aggregation of samples.

Chapter 7: Preparation of chitosan-grafted-poly-N-vinylcaprolactam microgels

7.1 Preparation and optimization

CP microgels were prepared by ionotropic gelation according to the results observed during the preparation of CS NPs. However, the utilization of the same polymer/TPP ratio resulted in irreversible aggregation for most of +CP NPs. This is due to the fact that many amino sites are no longer available for the formation of ionic bonds after the synthesis of the copolymer. Consequently, CS/TPP ratio for the preparation of ~200 nm NPs were determined experimentally. It is important to notice that many works do not provide any information about the CP/TPP ratios that were used for the preparation of microgels, and this can account for lack of reproducibility. CP/TPP ratios were determined by working in-situ, by observing the variation of correlation curves in relation to the addition of different volumes of TPP solutions. In particular, the study was focused on polymers that showed an LCST in a range of temperatures of interest (37-42 °C) for possible physiological applications. In particular, CP particles were prepared using CP polymers with a PNVCL/CS ratio of 4:1 and 8:1, respectively. CP polymers that exhibited LCST with a lower PNVCL/CS ratio were not considered for the preparation of NPs. The values

Chapter 7: Preparation of chitosan-grafted-poly-N-vinylcaprolactam microgels

reported in Table 32 were acquired 5 minutes after the addition of TPP. The displacement of the correlation curves in relation to CP/TPP ratio is displayed in Figure 48 and 49.

Sample	CS/TPP ratio	Average D_h (nm)	PDI
CP244_41	19:1	multimodal	0.513±0.110
	15:1	46±25	0.391±0.016
	10:1	43±20	0.306±0.033
	8:1	53±25	0.244±0.003
	5:1	97±40	0.175±0.011
CP305_41	19:1	multimodal	-
	15:1	69±35	0.377±0.051
	10:1	55±23	0.273±0.030
	8:1	77±34	0.192±0.006
	5:1	147±57	0.173±0.005
+CP244_41	8:1	aggregates	-
	10:1	aggregates	-
	15:1	165±83	0.202±0.007
	19:1	180±78	0.207±0.019
+CP305_41	10:1	aggregates	-
	19:1	166±64	0.364±0.017
	25:1	128±57	0.365±0.013
	50:1	268±104	0.281±0.043
+CP244_81	19:1	157±96	0.305±0.027
+CP305_81	19:1	aggregates	-
	50:1	aggregates	-

Table 32 Size distribution values of CP and +CP nanoparticles related to their polymer/TPP ratio. All samples were diluted 1:10 with water before analysis.

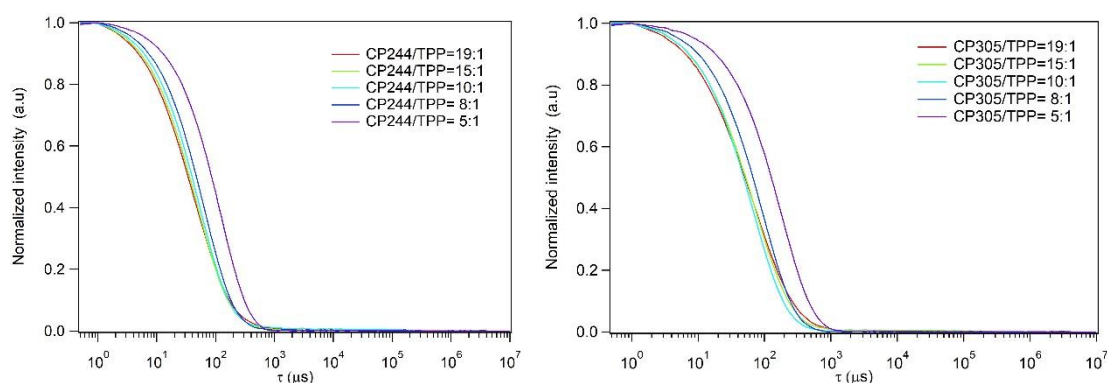


Figure 48 Displacement of correlation curves of CP244 (left) and CP305 (right) in relation to CP/TPP ratio

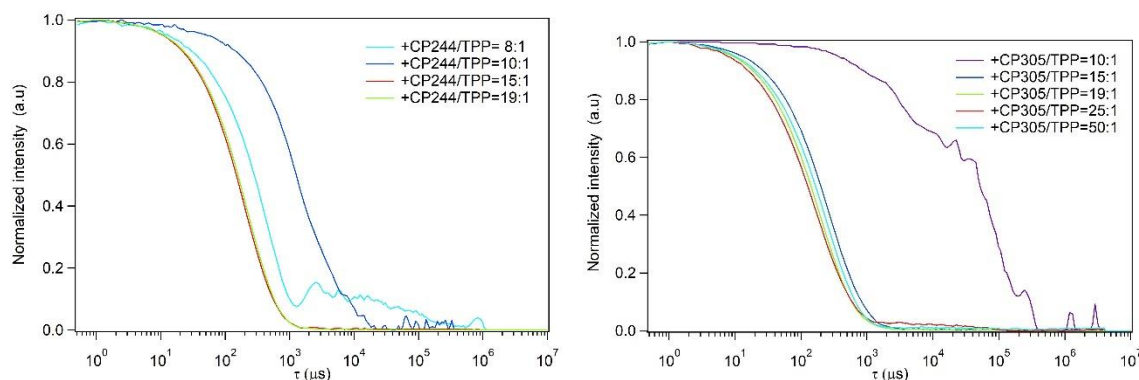


Figure 49 Displacement of correlation curves of +CP244 (left) and +CP305 (right) in relation to +CP/TPP ratio

7.1.1 Evolution of particle formation

Size distributions of CS and CP NPs samples were followed using DLS during 2 hours of formation (Figure 50). The particles were analysed at different times, by taking 1 ml of solution and analysing it without dilution. During the first two hours, the correlation curves were shifted to higher τ values. Consequently, particles average dimension and polydispersity rises fast during the first two hours. The common explanation is that CS chains initially fold upon interacting with TPP into very compact structure. This can be also defined as an initial “water-free” conformation. As the partial positive charge are neutralized by the anionic TPP, polymeric chains are rearranged in relation of their charge density and flexibility. After that, larger particles are formed and water is allowed to enter microgels structure, thereby dilatating their volume. In most cases, unimodal size distributions were observed by letting the solutions under agitation for a time period between 15 and 30 min. For shorter time intervals, a minor peak between 15 to 30 nm was usually observed due to the presence of unreacted copolymer. For longer time intervals, the precipitation of lesser stable samples is observed. This was the case of polymers prepared with CP1690_41. Average D_h values are reported in Table 33 as a function of the reaction time point. In this way, it was possible to prepare thermoresponsive particles in a temperature range between 36 and 43 °C, with an average size between 70 and 300 nm and positive surface potential.

Sample	Time (min)	Average D_h (main peak)	PDI	Type of distribution
CS	0	235±160	0.290±0.006	bimodal
	10	245±159	0.285±0.011	Broad unimodal
	20	233±154	0.307±0.041	Broad unimodal
	30	254±204	0.352±0.037	Broad unimodal
	60	225±134	0.296±0.016	bimodal
	120	218±162	0.281±0.006	bimodal
CS + NaCl 0.15 M	0	198±93	0.217±0.015	unimodal
	10	200±89	0.209±0.011	unimodal
	20	202±92	0.217±0.007	unimodal
	30	205±93	0.222±0.005	unimodal
	60	199±89	0.221±0.013	unimodal
	120	203±75	0.201±0.007	unimodal
CP305_41	0	88±45	0.258±0.030	unimodal
	10	93±50	0.261±0.017	unimodal
	20	107±65	0.276±0.015	unimodal
	30	113±67	0.270±0.018	unimodal
	60	120±71	0.268±0.016	unimodal

	120	156±143	0,279±0.023	Broad unimodal
CP610_41	0	103±47	0,229±0.008	unimodal
	10	162±78	0,221±0.011	unimodal
	20	265±136	0,201±0.007	unimodal
	30	337±223	0,250±0.016	unimodal
	60	309±97	0,248±0.005	unimodal
	120	350±204	0,263±0.007	unimodal
CP1690_41	0	193±68	0,209±0.024	unimodal
	10	254±127	0,253±0.010	Bimodal
	20	278±138	0,272±0.015	unimodal
	30	300±142	0,279±0.003	Bimodal
	60	385±134	0,335±0.053	bimodal
	120	547±246	0,457±0.007	Bimodal
	180	724±392	0,518±0.020	bimodal

Table 33 Evolution of size distributions during particle formation.

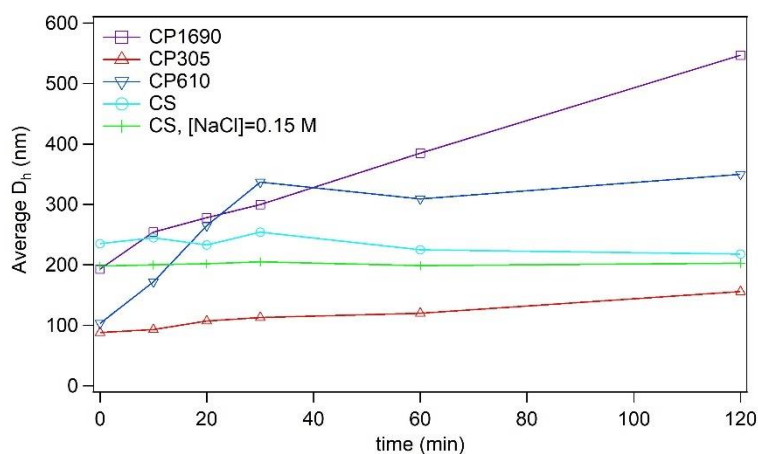


Figure 50 Evolution of particle size during formation. For bimodal distribution, the value of D_h is referred to the main peak. Peak standard deviations are reported in Table 33.

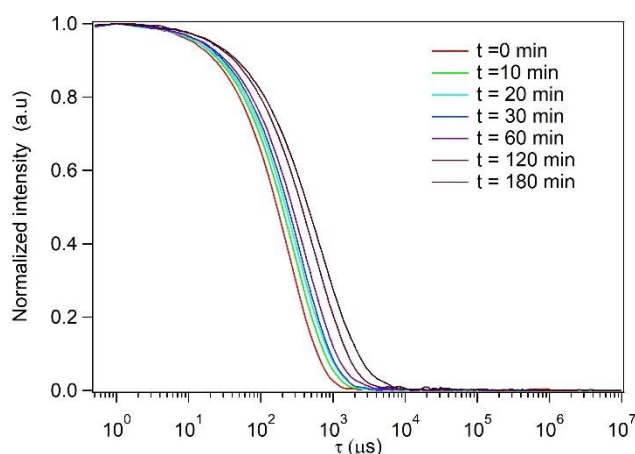


Figure 51 Displacement of CP1690 correlation curves during particle formation.

A summary of CP and CS NPs is reported in Table 34. It should be noted that the transition

temperature has been reported as VPTT. VPTT is referred to the behaviour of microgel particle structure in solution. However, according to the results of DOSY spectra of +CP polymers, the presence of unreacted PNVCL-COOH makes it impossible to establish whether the critical temperature value is entirely caused by the behaviour of CP microgels. In most cases, the measured VPTT is different from the LCST of the starting copolymers (Table 34). Consequently, it can be assumed that the presence of residual PNVCL-COOH is negligible and does not affect the behaviour of the microgels in solution. It was assumed that the low stability of +CP305_81 and CP1690_41 NPs was due to the presence of a higher percentage of unreacted PNVCL. The polymers were prepared under the same experimental conditions as those shown in Table 18. However, copolymers prepared with a higher PNVCL/CS ratio requires longer activation times due to higher number of carboxyl groups involved in the reaction. Accordingly, longer grafting reaction times are required in order to ensure the yield of the reaction. In a similar way, the presence of longer molecular chains in PNVCL1690 makes carboxyl groups terminal groups more difficult to access during the reaction with CS. The hypothesis that unreacted PNVCL-COOH lead to poor particle stability was verified by reversing the method of NPs preparation. Instead of preparing the CPs using CP as a starting material, PNVCL was grafted directly onto CS NPs, by activating the amino sites of the NPs using EDC/NHS. The reaction was performed using the same PNVCL/CS ratio. PNVCL was incubated overnight with EDC and NHS and CS particles were prepared 30min before preparation (CS/TPP = 5:1, 15 min reaction). The formation of aggregates was observed immediately after the addition of the PNVCL, and the solution was left under agitation for 24h. At the end of the reaction, DLS analysis confirmed that the presence of aggregated NPs. It was assumed that only small quantities of unreacted PNVCL were present in the more stable samples. CS grafted with shorter PNVCL chains showed a mixed behaviour. PNVCL lowers the positive charge of CS and nanoparticles with smaller sizes are formed. These particles are very stable to agitation but easily precipitate with the addition of TPP due to the presence of fewer unreacted amino sites. On the contrary, as already suggested by *Fan et Al.*²⁸⁶, CS microgels are extremely stable in presence of 0.15 NaCl and no substantial change in the average dimension is observed after 2h of reaction. In absence of NaCl, CS NPs evolves from unimodal to broad bimodal size distribution.

Chapter 7: Preparation of chitosan-grafted-poly-N-vinylcaprolactam microgels

Sample	Average D_h (nm)	PDI	ζ (mV)	VPTT (°C)
CS	205±93	0.222±0.005	42.4±4.95	-
CS + NaCl 0.15 M	205±93	0.222±0.005	21.1±1.65	-
+CS	299±132	0.251±0.007	53.2±4.27	-
+CP122_41	151±59	0.247±0.019	22.2±4.49	41 °C
+CP122_81	151±65	0.314±0.008	18.6±5.02	41 °C
CP244_41	153±63	0.173±0.012	12.1±3.28	39 °C
+CP244_41	180±78	0.207±0.019	25.5±5.36	39 °C
+CP244_81	157±96	0.305±0.027	22.3±5.08	38 °C
CP305_41	113±67	0.270±0.018	14.3±4.26	39 °C
CP305_41 + NaCl 0.15 M	172±56	0.100±0.011	5.81±3.17	41 °C
+CP305_41	166±64	0.364±0.017	23.1±3.46	38 °C
CP610_41	337±223	0.250±0.016	10.1±3.39	35 °C
+CP610_41	248±110	0.233±0.014	19.9±4.36	35 °C
+CP1220_41	172±68	0.253±0.014	19.3±4.18	34 °C
CP1690_41	300±142	0.279±0.003	13.7±4.12	33 °C

Table 34 Summary of size distribution and zeta potential of CS and CP microgels.

7.1.2 Particle purification

CP particles were purified by applying the same method used for +CS NPs. After each centrifugation, the precipitate was resuspended in 1ml of milliQ water, and the pellet and the supernatant were analysed with DLS in order to determine the optimal centrifugation rate experimentally. As a general method, in the presence of bimodal distributions, microgels were purified by centrifugation in a range between 500 and 5000 g in order to precipitate the bigger particles.

7.1.3 pH stability

CP_305_41 NPs were analysed with DLS at different pH to study their stability. Compared to CS particles, CP microgels exhibited improved stability towards pH changes and a small displacement in the correlation curve is observed at pH 6.5 (Figure 52). At physiological pH, the particles undergo rapid aggregation.

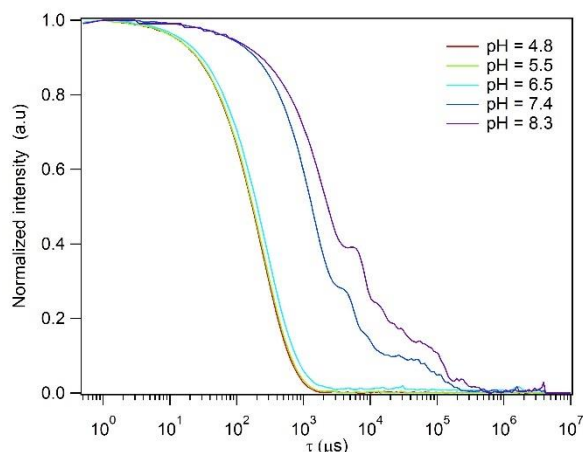


Figure 52 Displacement of CP305_41 NPs correlation curve at different pH.

7.2 Particle storage

The ability of a formulation to maintain its chemico-physical properties is fundamental for pharmaceutical applications. However, the interest towards ionotropic gelled particles is also due to the simplicity of the fabrication protocol as particles can be rapidly prepared according to the necessity. The maintenance of chemical-physical properties over time was monitored over 28 days (Figure 53, Table 35). The suspensions were kept at 4 °C inside sealed vials. The results showed that nanoparticles undergo only slight modifications during 21 days of storage. CS NPs prepared in the presence of concentrations of NaCl (0.15 M) exhibited remarkable maintenance of their physical properties. Despite the evolution of CP particles in the presence of NaCl has not been monitored, this result suggests the utilization of saline solutions, such as physiological solutions, for the conservation and the utilization of nanoparticles.

Sample	Storage days	Average D_h (main peak)	PDI
CS	0	254±204	0.352±0.037
	7	200±122	0.285±0.014
	14	225±158	0.274±0.010
	21	243±192	0.278±0.006
	28	236±153	0.276±0.001
CS + NaCl 0.15 M	0	205±93	0.222±0.005
	7	197±69	0.180±0.002
	14	198±74	0.183±0.003
	21	199±83	0.182±0.002
	28	197±76	0.176±0.008
CP305_41	0	113±67	0.270±0.018
	7	128±58	0.230±0.005

	14	130±60	0.224±0.007
	21	137±64	0.228±0.004
	28	154±66	0.232±0.009
CP610_41	0	337±223	0.250±0.016
	7	343±120	0.252±0.012
	14	446±240	0.266±0.013
	21	439±234	0.251±0.015
	28	428±174	0.207±0.027
CP1690_41	0	300±142	0.279±0.003
	7	780±426	0.710±0.052
	14	Aggregates	-
	21	Aggregates	1.000
	28	Aggregates	1.000

Table 35 Evolution of particle size during 28 days of storage at 4 °C.

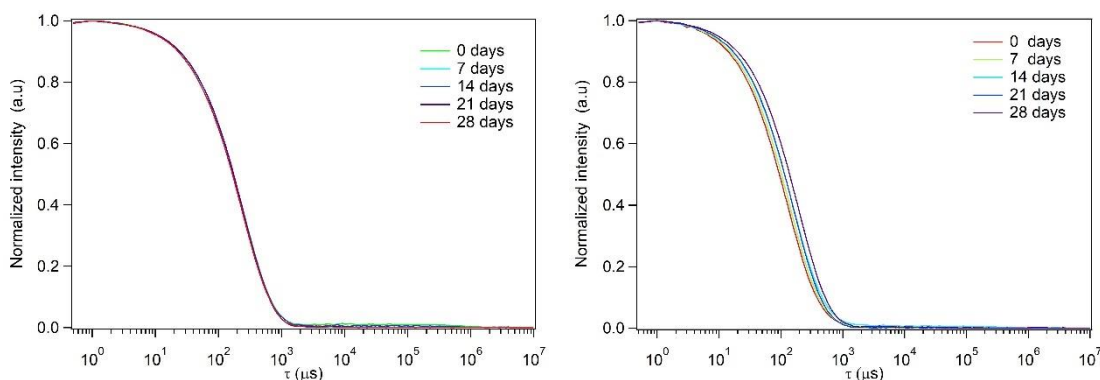


Figure 53 Variation of the correlation curves during 28 days of storage. (left) CS NPs prepared with NaCl 0.15 M, (right) CP305 NPs.

7.2.1 Lyophilization

Particle storage is critical for the maintenance of its properties over time. When an aqueous suspension of polymeric nanoparticles is stored, both the polymer and the drugs may undergo degradation. Likewise, the physical properties of nanoparticles can change dramatically. In addition to this, if the polymer matrix is soluble, the drug is leaked or desorbed. Lyophilization is one of the most useful methodologies for the conservation of hydrophilic polymers and polysaccharide formulations. As we already mentioned, despite freeze-drying of CS NPs formulations is a standard procedure, only few works focused on the importance of a proper protocol for the lyophilization of CS NPs. During the lyophilization process, the suspension is frozen (freeze step) and the water content is consequently removed by sublimation under reduced pressure (drying step). However, some formulations may be difficult to redisperse and exhibit very different chemico-physical properties. Earlier studies indicate that the particle size typically increases during the freezing step of the lyophilization process^{307,347}. Accordingly, both freezing and

dehydration processes can induce irreversible aggregation of nanoparticles. The formation of a crystal forces the nanoparticles to approach and reach the energy minimum of their interaction. This is particularly critical in absence of a steric stabilization agent which is covalently bound to the surface of the nanoparticles. Also, ice crystallization exercises a mechanical stress on nanoparticles which can lead to both fusion and particle breakage. The appropriate choice of a lyoprotective agent is important to prevent aggregation during the drying step of lyophilization³⁴⁸. The most common cryoprotectants for the freeze-drying of polymeric nanoparticles are sugars such as sucrose, glucose, mannitol and especially trehalose. Due to the high density of -OH groups, it is suggested that sugars can interact with polysaccharide NPs through hydrogen bonding^{349,350}. Since sugar-water systems forms an amorphous system which is characterized by a glass transition temperature, CS NPs are maintained in a “pseudo hydrated” state during dehydration which protected from damage during dehydration and subsequent rehydration³⁵¹. Furthermore, the amorphous matrix can protect them from aggregation and mechanical stress related to crystallization. Accordingly, CS and CP NPs were freeze-dried by using three differ cryoprotectors, namely sucrose, trehalose and mPEG-5000. Before freezing, cryoprotectants were added to NPs suspensions in order to reach 20% w/v concentration. Results showed that lyophilization resulted in irreversible aggregation (Figure 54) even with the utilization of cryoprotectors. TEM micrographs of freeze-dried samples showed that the particles aggregated into horizontal structures (Figure 55). FT-IR analyses of lyophilized samples showed no significant difference to CS. The characteristic downshift of 1628 and 1412 cm^{-1} NH_2 vibrations related to the interaction between the amine sites and TPP¹⁰⁹ were not observed.

Sample	Size	PDI	Type of distribution
CP305_41 solution	140±56	0,173±0.005	Unimodal
Lyophilized CP305_41	Aggregates	1.000	-
Lyophilized CP305_41 + sucrose	483±245	0.473±0.052	Bimodal
Lyophilized CP305_41 + mPEG500	512±319	0.489±0.0026	Bimodal
Lyophilized CP305_41 + trehalose	377±136	0.447±0.061	bimodal

Table 36 Comparison between size distribution of CP305_41 microgels before and after freeze-drying.

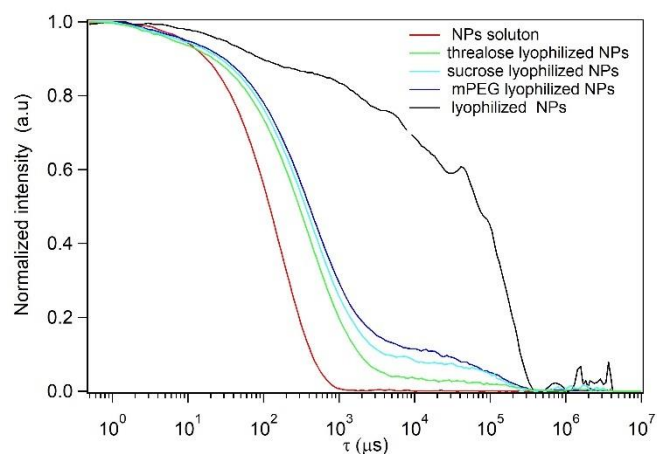


Figure 54 Comparison between CP305_41 NPs before and after freeze-drying with different cryoprotectors.

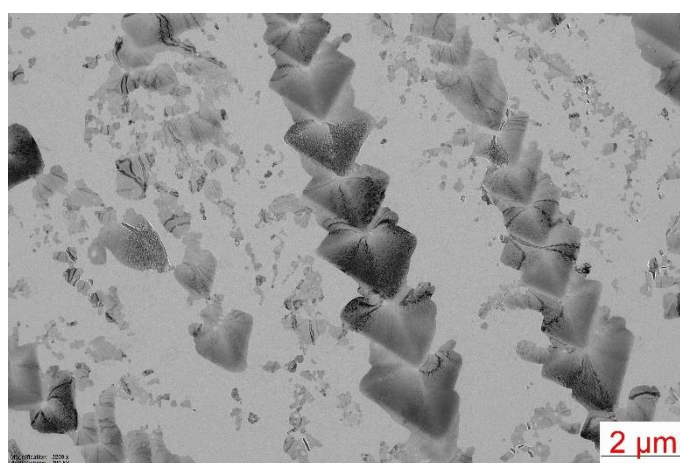


Figure 55 TEM micrographs of lyophilized CP NPs.

7.3 Nanoparticle tracking analysis

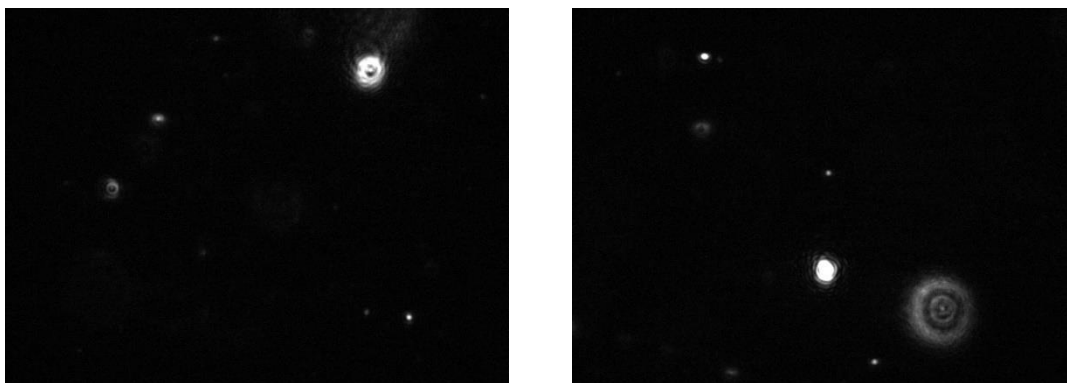


Figure 56 Frames of NTA of +CP244_41 (left) and +CP244_81(right) NPs.

+CP244_41 and +CP244_81 NPs were studied using NTA as a complementary technique to DLS in order to study size distribution. Both samples were prepared by using a CP/TPP ratio of 19:1 and leaving the solutions under agitation for 15 min. Samples were analysed in the same day of preparation without any purification step. Samples were diluted with milliQ water prior to analyses in order to reach optimal concentration for particle analysis. The analyses showed the presence of multimodal distribution in both samples. Size distributions were analysed in a size range between 50 and 700 nm in order to establish the position of the main peaks and peak areas. The analysis of +CP244_41 NPs showed the presence of three main populations at 140 nm, 216 and 268 nm and a small population related to the presence of bigger particles at 390 nm (Figure 57, left). +CP244_81 NPs exhibited the characteristic of a highly polydisperse sample (Figure 57, right). The deconvolution of the curve resulted in eight different population with a major peak at 100 nm. The results are reported in Table 37.

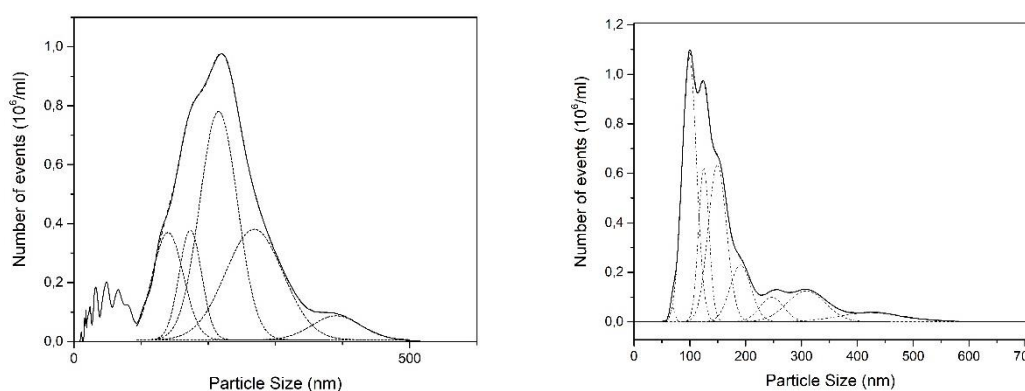


Figure 57 Results of NTA analysis of +CP244_41 (left) and +CP244_81 (right) NPs. Fit peaks and cumulative fit function are represented with dashed lines.

+CP244_41 NPs	
Peak position and FWHM	% of total fitted area
140±54	15.11%
173±39	11.25%
216±66	39.17%
269±41	29.08%
390±85	5.39%
r ²	0.99981
+CP244_81 NPs	
Peak position and FWHM	% of total fitted area
69±9	0.55%
100±30	32.00%
124±22	13.65%
149±39	24.21%
191±44	9.99%
246±50	4.88%
308±80	9.89%
425±134	4.83%
r ²	0.99993

Table 37 Size distribution of +CP244_41 and +CP244_81 NPs by NTA.

7.4 Transmission electron microscopy

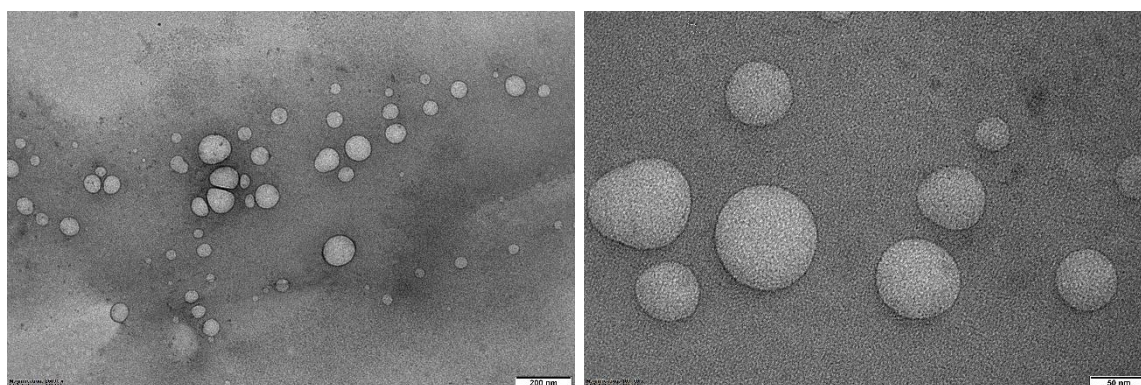


Figure 58 TEM micrographs of CP244_41 NPs.

CP NPs were observed at TEM to observe morphology and size (Figure 58). Previously, the TEM observations of CS particles were unsuccessful. For sample preparation, a protocol was considered in which paraformaldehyde is used to trap particles inside a viscous matrix. In this way, particles can be observed in a hydrated state using TEM³⁰⁷. However, due to instrument malfunctions, cancellation and postponements during the CoVid pandemic, it was not possible to observe the samples under these conditions. Consequently, CS NPs were observed in aqueous solutions that were left to evaporate on the grid overnight. TEM micrographs showed that most of the samples were in aggregate form due to solvent evaporation, but some isolated particles were observed. CP particles appeared as single isolated particles with a diameter around 30-40 nm and larger particles due to the aggregation of single small particles that aggregate into larger entities. The observed particles had a spherical shape and showed smaller size due to evaporation caused by the exposure of electron rays. During TEM analysis, the increase in

magnification resulted in nanoparticles aggregation. Particle fusion was promoted in a few minutes of observation. The heat of the ray promotes intermolecular links due to the present of aqueous environment inside the gel-network.

7.5 Thermoresponsive behaviour

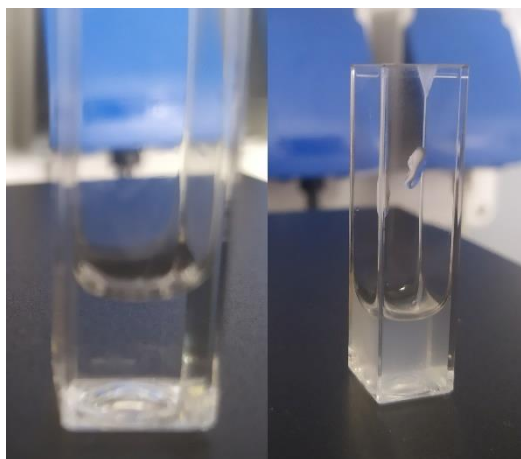


Figure 59 VPTT transition of +CP244_41 microgels. Picture were taken after incubation at 25 °C (left) and 39 °C (right), respectively.

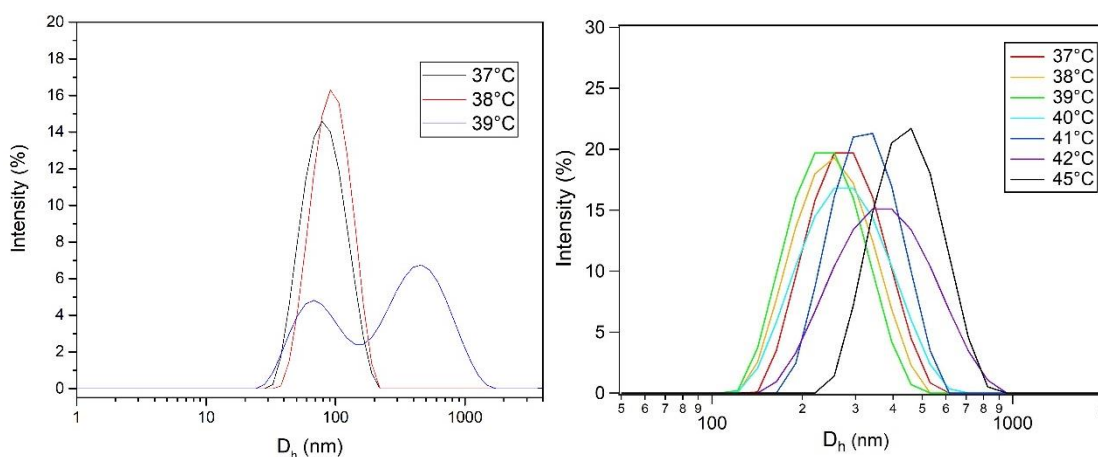


Figure 60 Size distribution of CP305_41 NPs at different temperatures at different concentration. Total CP concentration is 0.625 mg/ml (left) and 0.0625 mg/ml (right).

The thermoresponsivity of the particles was determined by acquiring the correlation curves of CP NPs at different temperature in a range between 25 and 50 °C. For each analysis, samples were incubated for 2 min at a specific temperature in the interval range. After each heating cycle, samples were incubated at 25 °C for 5 min to reverse the transition. When the VPTT was reached, the curve was displaced towards higher τ values. As a consequence, the main peak of the size distribution is shifted towards higher D_h values. In few samples, the distribution becomes bimodal as the original main peak is still present in the size distribution (Figure 60, left). This is indicative of a swelling of microgels, which

leads to the increase in the size of the average size. At higher temperatures, the peak at D_h values disappears. Another interpretation is that CP microgels undergo reversible aggregation. According to this hypothesis, the individual microgels would flocculate with the increase of temperature. On this basis, it would be more appropriate to define the critical temperature as LCST instead of VPTT. The observed behaviour would be due to the attraction between the thermoresponsive CP polymers instead of the swelling of the microgel networks. DLS data does not allow to discriminate between the two hypotheses. The correct way to discriminate between VPTT or LCST would be to use a technique that measure particle concentration. In the presence of LCST, a decrease in concentration is observed to the formation of irreversible aggregates, while microgels swelling do not change particle concentration. Unfortunately, the NanoSight at disposal did not allow reliable concentration estimates due to the absence of a calibration standard. For simplicity, VPTT was referred as the transition temperature of microgels in order to distinguish the behaviour of microgels from that of polymers. The study of CP NPs behaviour showed that VPTT depended on the concentration of particles. The values of VPTT reported in Table 34 were measured without diluting particle suspensions. At this concentration, the rapid increase in turbidity prevents to describe the behaviour of CP NPs in the entire temperature range. Moreover, a different dimensional distribution was observed once microgels were cooled back to 25 °C. In some cases, a multimodal distribution is observed, with the permanence of a size peak located at higher D_h values. However, by diluting microgels suspension using a dilution factor of 10, it was observed that the transition was completely reversible (Figure 60, right, Figures 61-67). This is indicative of particle swelling due to the enlargement of the microgel networks. In addition, it was observed that VPTT was shifted to higher values. In this way, it was also possible to observe the displacement of size distributions as a function of temperature. According to this observation, all prepared samples can exhibit VPTT in the desirable temperature range between 37 and 42 °C. The analyses of +CP610_41 and +CP1220_41 NPs behaviour demonstrated that dilution shifted VPTT towards 38 and 37 °C, respectively (Figure 67 and 68). In conclusion, it can be argued that microgels, under appropriate concentration conditions, exhibit a reversible thermoresponsive behaviour in the temperature range between 37 and 43 °C.

Chapter 7: Preparation of chitosan-grafted-poly-N-vinylcaprolactam microgels

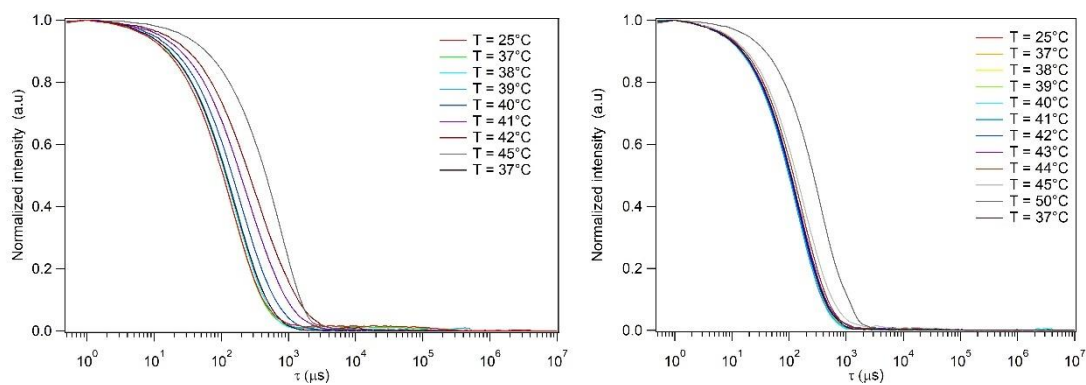


Figure 61 Displacement of undiluted (left) and diluted (right) +CP122_41 NPs at different temperatures.

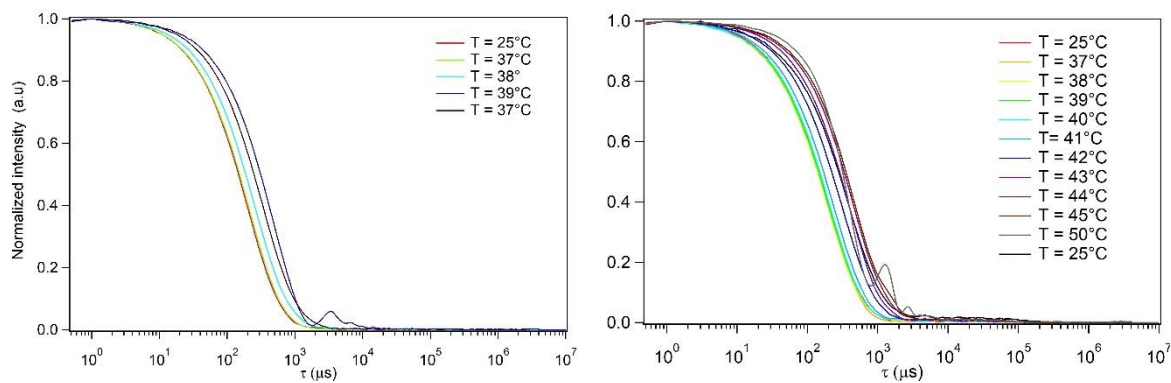


Figure 62 Displacement of undiluted (left) and diluted (right) +CP244_41 NPs at different temperatures.

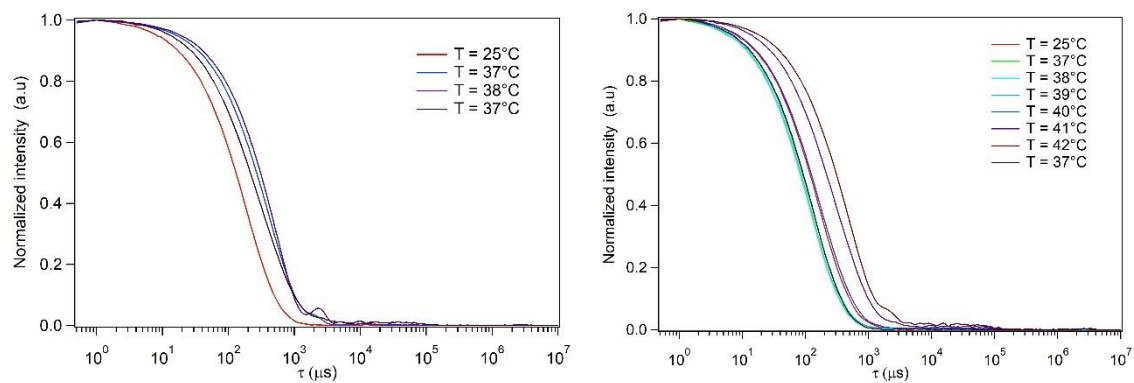


Figure 63 Displacement of undiluted (left) and diluted (right) +CP244_81 NPs at different temperatures.

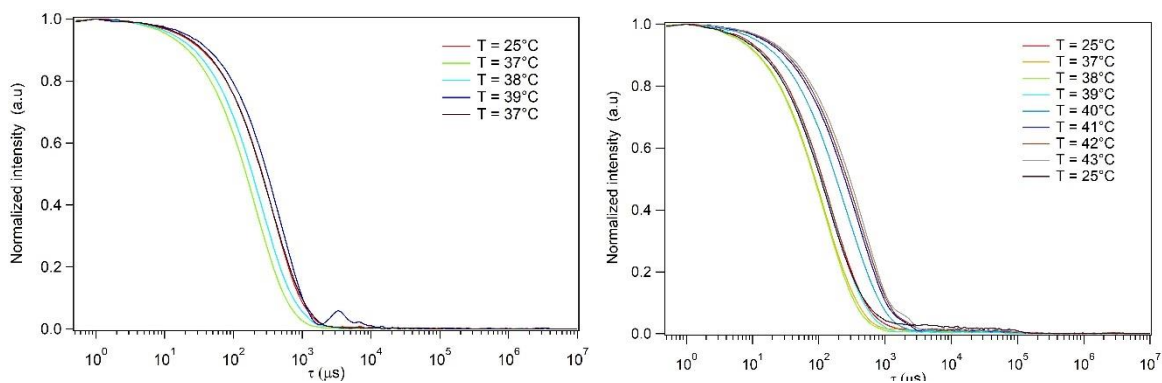


Figure 64 Displacement of undiluted (left) and diluted (right) +CP305_41 NPs at different temperatures.

Chapter 7: Preparation of chitosan-grafted-poly-N-vinylcaprolactam microgels

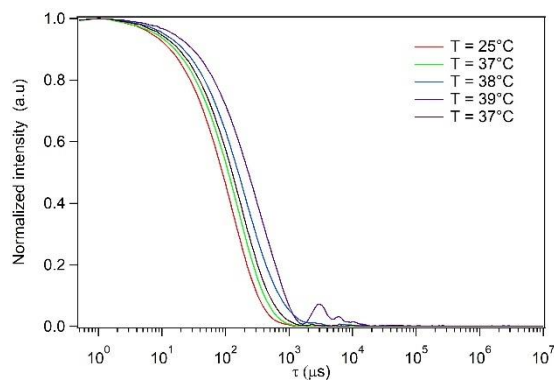


Figure 65 Displacement of undiluted (left) and diluted (right) +CP244_41 NPs at different temperatures.

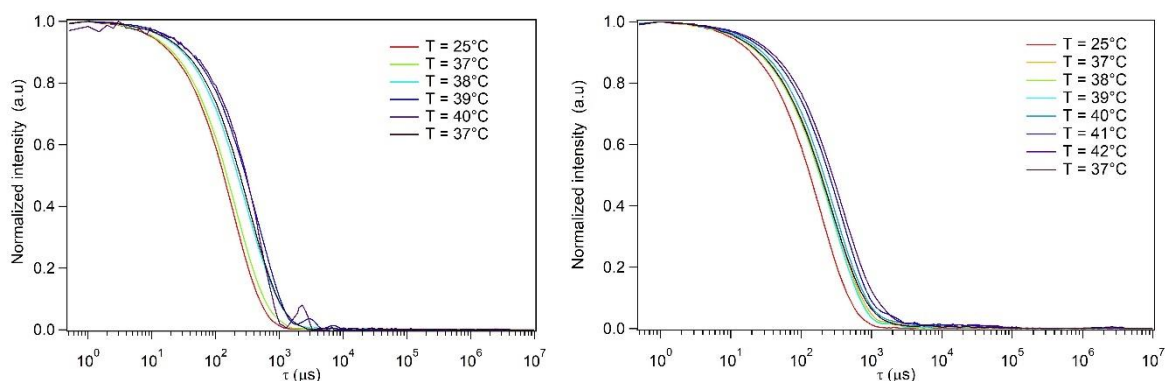


Figure 66 Displacement of undiluted (left) and diluted (right) CP305_41 NPs at different temperatures.

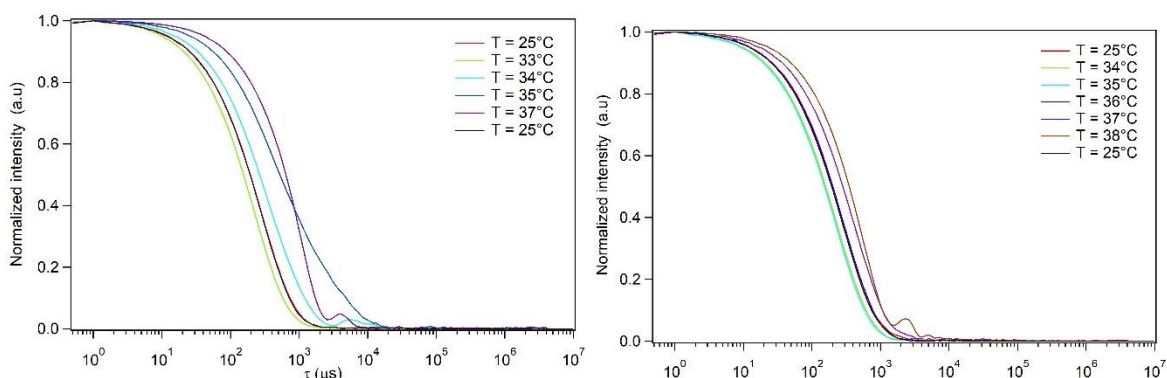


Figure 67 Displacement of undiluted (left) and diluted (right) +CP610_41 NPs at different temperatures.

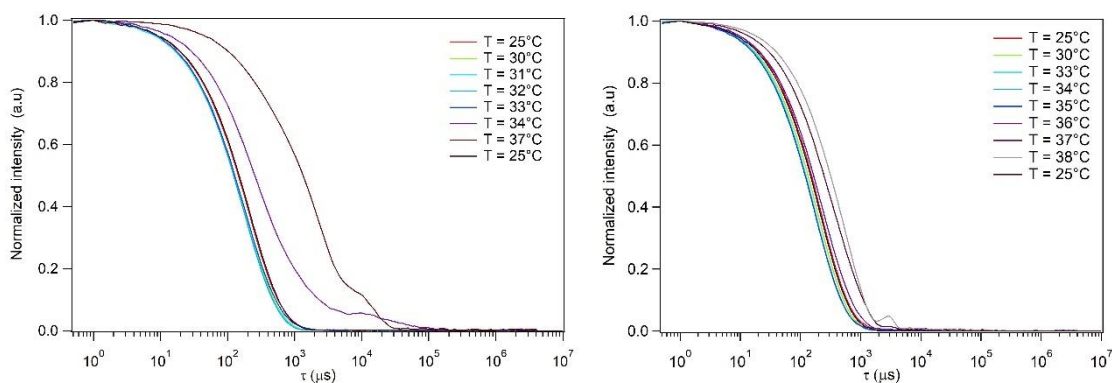


Figure 68 Displacement of undiluted (left) and diluted (right) +CP1220_41 NPs at different temperatures.

A further experiment was carried out by observing the behaviour of CP305_41 in the presence of NaCl 0.15 M (Figure 69). The presence of NaCl allows to increase the VPTT by about 2 °C (Table 34). In addition, under these conditions, microgels exhibited an effect of size focusing similar to that observed for CS particles. According to this result, it is possible to modify the responsivity of microgels by using or resuspension in saline solution. In addition, CP particles are suitable for administration and storage using physiological solutions.

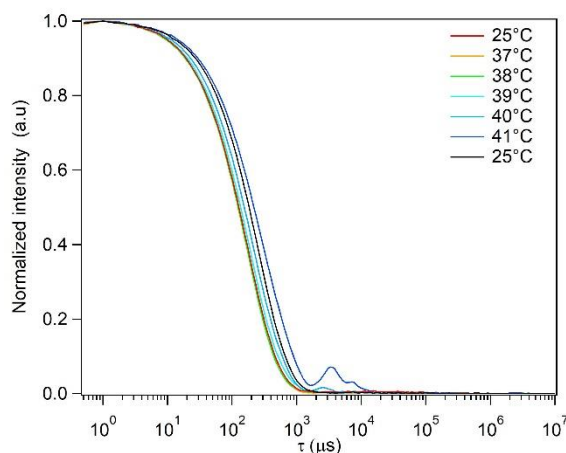


Figure 69 Displacement of CP305_41 NPs prepared with NaCl 0.15 M at different temperatures.

7.6 Summary

CP microgels were synthesized with ionic gelation and characterized using DLS, Zeta potential and NTA. Due to the diminishing of the available amino sites after the grafting of PNVCL, CP/TPP ratios were determined by working in-situ. Microgels were analysed with DLS after the addition of different volumes of TPP solutions. In this way, we defined a protocol for the fabrication of CP microgels with an average D_h between 110 and 180 nm and a VPTT between 37 and 42°C for drug delivery application. The thermoresponsive behaviour of several different samples of CP microgels were analysed by observing the change in size distribution at different temperatures. Upon heating, CP microgels can change their dimension in a reversible fashion. The study also demonstrated that the change is concentration dependent.

Chapter 8: Preparation and characterization of thermoresponsive magnetic microgels

In this chapter, the possibility of introducing superparamagnetic iron oxide nanoparticles (MNPs, or SPIONs) into CP microgels was evaluated. The fabrication of dual-responsive microgels would theoretically allow to control the release of DOX remotely. The fabrication process is based on the procedure that was previously illustrated by *Indulekha et al.*⁹⁹ The presence of MNPs inside the microgels is able to cause an increase in the local temperature increase during exposure to an alternating magnetic field. This induces the conformational change of the gel, which would eventually result in the release of the encapsulated drug. Since the VPTT transition of CP microgels is reversible, the presence of encapsulated MNPs would provide the ideal structural feature for remote control of drug delivery. The encapsulated drug would be delivered by simply activating and switching off the magnetic field. Magnetic CP microgels were prepared by simply dispersing MNPs into the TPP solution during their preparation. The suspensions exhibited poor stability were characterized using DLS, zeta potential and TEM.

8.1 Preparation and characterization of iron oxide magnetic nanoparticles

Iron oxide MNPs were synthesized in order to provide magnetic responsivity towards CP microgels nanocomposite. Furthermore, iron oxide MNPs are FDA-approved, and they have been studied for combinational cTACE treatments³³⁴. The particles have photothermal properties and because they are visible to both NRI and CT. MNPs were prepared by chemical precipitation method. The particles were synthesized without the use of any ligands for steric stabilization. After being redispersed to in ethanol, MNPs were dried in an oven at 50 °C without the utilization of inert atmosphere. MNPs exhibited strong magnetic properties as it the powder was easily aligned and manipulated under the application of a magnetic field. Since paramagnetic properties are usually exhibited when the diameter is less than the size of a singular magnetic domain (about 50 nm), MNPs size was measured by using TEM and DLS. DLS measurement were performed in ethanol, using suspensions at a concentration of 0.05 mg/ml. DLS size distribution by intensity was higher than expected but the results were consistent with values reported in literature⁹⁹. Iron oxide NPs have a big solvation shell that influences the measure of D_h . Furthermore,

size measurement by intensity is strongly influenced by the presence of redispersible flocculates in solution the intensity $I \propto r^6$ of the scattered particles. The results of DLS (Figure 70) and Z-potential analysis is reported in Table 38.

Dynamic light scattering	
D _h (nm) (by intensity)	129.7±52.72
D _h (nm) (by number)	18.17±4.53
PDI	0.099
TEM	
Average diameter (nm)	12.31±4.33
XRD	
Calculated diameter (nm)	7.02
Zeta potential	
Surface charge (mV)	+13.2±4.56

Table 38 Results of MNPs characterization.

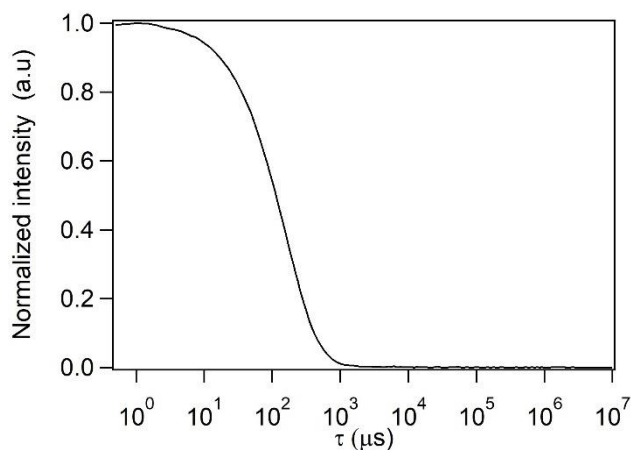


Figure 70 DLS correlation curve of MNPs.

TEM micrographs (Figure 71) showed the presence of pseudospherical nanoparticles with an average size between 10 and 20 nm with a good degree of crystallization. An additional index of crystallinity was demonstrated by the possibility of reaching almost atomic resolution of the photos due to the presence of Moire effect created by the proximity of crystalline samples³⁵².

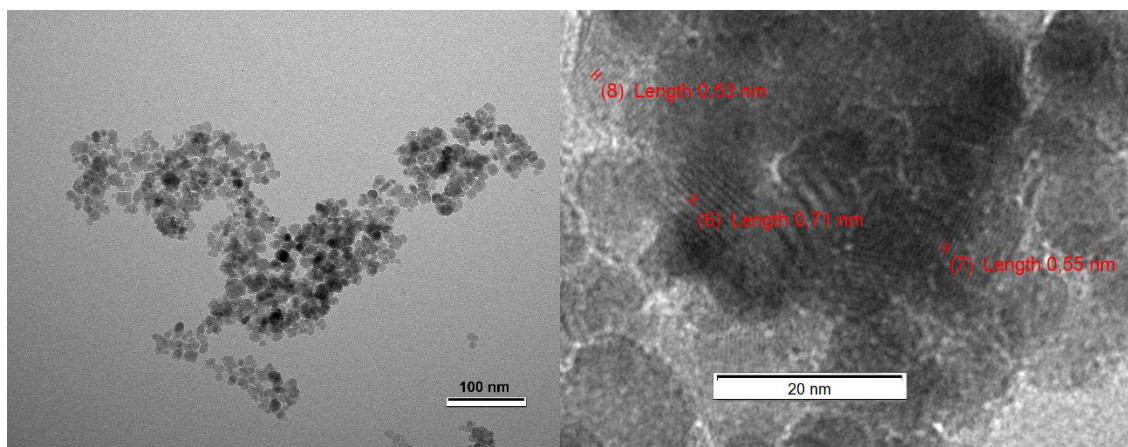


Figure 71 (left) TEM micrographies of MNPs. (right) Detail of MNPs crystal planes. The black lines correspond to lines of Fe atoms inside of a crystal face. Some of the distance between the atom planes are reported: 0,53 nm, 0,71 nm and 0,55 nm.

In a few cases (Figure 71, right), the distances between the atomic planes inside the crystal faces of the MNPs were measured. The magnetic deflection of the electrons of the sample resulted in the formation of characteristic white clouds that were observed in TEM micrographs. As the particles were almost spherical in shape, the diameter of the particle was estimated using the size distribution by number obtained using DLS. DLS size distribution by number provided comparable results to TEM size distribution (Table 38). Given the high degree of crystallinity of the particles, MNPs were studied with XRD (Figure 72). The spectrum exhibits the characteristic planes of magnetite (α - Fe_3O_4) NPs with face centred cubic (FCC) structure. The diameter of the particles was also estimated to be ~ 7 nm from the average size dimension of the crystallites to using the Debye-Scherrer equation³⁵³ (Equation 28, see “Methods” section).

However, recorded Z-potential values remains controversial. Despite the meticulousness of the purification process, MNPs exhibited positive Z-potential in both ethanol and H_2O . It was not possible to characterize the magnetic behaviour of MNPs with a magnetic hysteresis loop. Due to their small size, it was assumed that MNPs are able to give rise to anhysteretic magnetization curves due to their superparamagnetic behaviour. The crystalline index was estimated to be $\sim 52\%$ from the ratio between the sum of the area of the peaks and the total spectrum area.

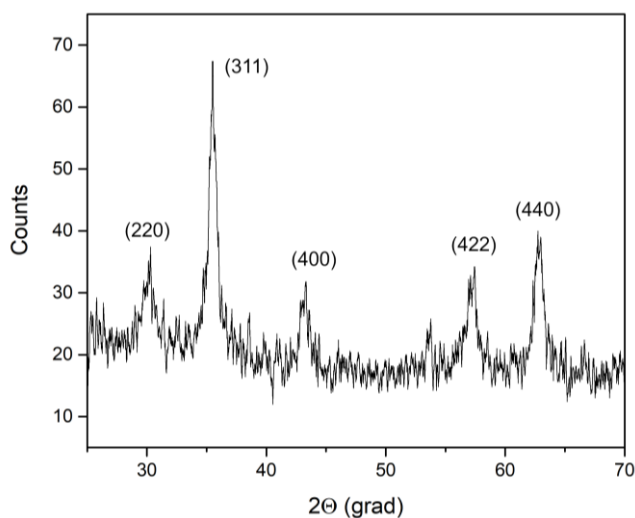


Figure 72 XRD spectrum of MNPs.

8.2 Preparation and characterization of CP magnetic nanoparticles

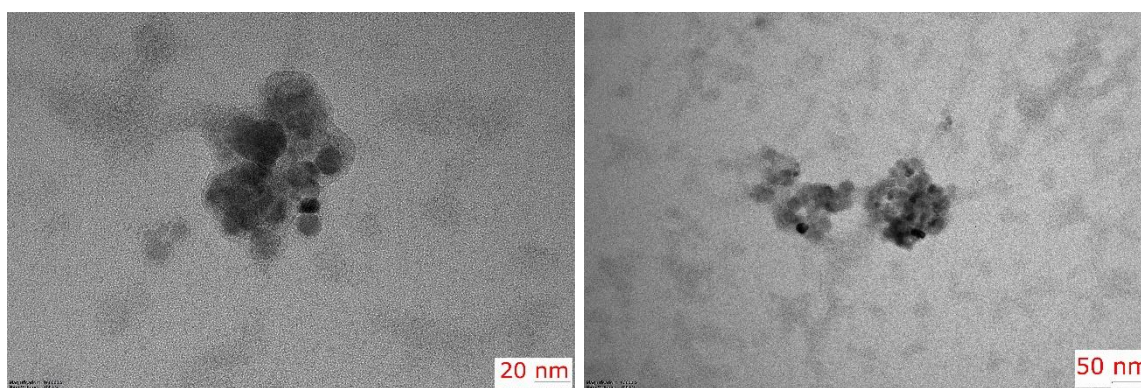


Figure 73 TEM micrographs of CP305_41 MNPs.

CP_305_41 magnetic microgels (CP305_41 MNPs) were prepared by dispersing MNPs into the TPP solution used for NPs fabrication. During the formation of NPs, the formation of a brown turbid solution was observed as MNPs particles were entrapped inside the polymeric network of the microgels. The hybrid particles showed magnetic properties as aggregation was induced by applying a magnetic field. The suspensions were filtered by magnetic filtration or centrifugation. Magnetic filtration proved to be ineffective as both naked MNPs and magnetic microgels were separated from the solution. Similarly, centrifugation resulted in the precipitation of aggregates. In general, it was observed that CP MNPs exhibited poor stability. To verify the encapsulation of MNPs, the supernatant of the centrifugated nanohybrid were observed at TEM. The micrographs showed the presence of MNPs particles inside a polymeric matrix (Figure 73). The small dimension of the NPs observed at TEM are coherent with the size contraction that was expected due to

solvent evaporation, as it was already observed for empty CP particles. DLS characterization was difficult as samples showed pattern of aggregation. The utilization of 450 nm filters allowed to isolate a small population of CP magnetic particles for a sufficient time to determine D_h and the zeta potential. However, zeta potential results were not considered reliable due to the poor stability of the sample. Results are reported in Table 39.

Sample	D_h (nm)	PDI	ζ (mV)
CP_305_41 MNPs	265±132	0.377±0,022	4.19±2.86

Table 39 Results of DLS and Zeta potential characterization of CP MNPs.

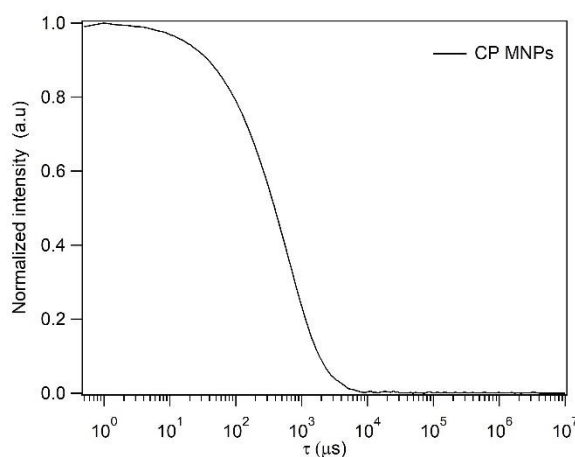


Figure 74 DLS correlation curve of filtrated CP MNPs.

8.3 Summary

MNPs were synthesized by using the coprecipitation method. Particles were characterized using DLS, Zeta potential, TEM and XRD. The comparison between DLS data and TEM micrographs showed that the average diameter is around 12 nm. Due to their size, MNPs are expected to exhibit superparamagnetism. The magnetic properties were verified with a magnetic rod and the magnetic deflection of electrons was observed with TEM. XRD analysis revealed that MNPs constituted by magnetite (α - Fe_3O_4) NPs with FCC structure. The good crystallinity degree was confirmed by XRD measurement and TEM observation. CP MNPs were prepared by introducing MNPs during ionotropic gelation. Magnetic microgels were characterized using DLS, Zeta potential and TEM. TEM micrographs showed the presence of MNPs enveloped in a polymeric matrix. The formulations exhibited magnetic properties, but all prepared suspensions exhibited poor stability..

Chapter 9: DOX loading and release

9.1 Encapsulation of DOX

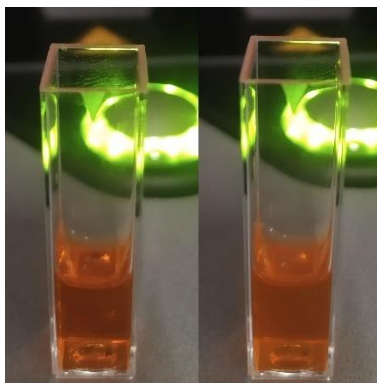


Figure 75 DOX/CP305_41 before and after 5 min incubation at 41 °C.

The preparation of DOX-loaded CP microgels was attempted by following a preparation protocol reported in many scientific works^{99,114,320–322,354}. According to these studies, DOX is trapped inside CP microgels during gelation due to the formation of CS-TPP crosslink around the molecule. However, due to poor interaction between DOX and CS, DOX is expected to remain in the external solution. According to *Janes et al.*³⁰⁶, DOX encapsulation is favoured by dissolving DOX in the TPP solution that is added to the polymeric solution. However, the basic environment of TPP solution accelerates the degradation of DOX molecule^{318,319}. Alternatively, small interactions between DOX and CS can be promoted by dissolving CS in the presence of DOX and leaving the solution under agitation overnight. The preparation of DOX loaded CP NPs was attempted by using both approaches. Microgels were prepared using different concentrations of DOX and results were evaluated in relation the DOX/CS ratios of the solutions. An overview of the results is reported in Table 40. Microgels were analysed using DLS and any changes in size and surface charge were evaluated due to the presence of the drug. The encapsulation efficacy (EE) was calculated by centrifugating the NPs and measuring the DOX concentration from the UV-VIS spectra using the $\pi \rightarrow \pi^*$ absorption band at 481 nm. Due to the elevated value of ϵ of the $\pi \rightarrow \pi^*$ band, DOX solution exhibit a characteristic intense orange-red colour at mild acidic pH (Figure 75). Thanks to this feature, effective encapsulation can be usually seen by the diminishing of the intensity of the solution colour. The results excluded the possibility that CS and CP microgels are able to trap the DOX due to the poor drug-polymer interaction³²¹. NPs centrifugation resulted in the formation of a white precipitate without any visible change in the DOX solution colour. This suggested

Chapter 9: DOX loading and release

that DOX remained outside CP NPs. The observation was confirmed by quantitative analysis performed using UV-VIS (Figure 76, Table 40) and DLS (Table 41). The measurement of DOX concentration in the supernatant provided average EE inferior to 1%. Results are reported in table 40. DSL characterization of CP NPs demonstrated that CP NPs prepared in presence of DOX exhibited similar chemical properties to empty CP NPs in terms of size and surface charge. Another possible interpretation is that CP NPs may break during centrifugation, thereby causing the leaking of encapsulated DOX. However, DOX encapsulation would result in the variation of the intensity of the solution that was not observed before centrifugation. In conclusion, it can be established that CP NPs can only entrap negligible amounts of DOX. The result is consistent with the low entity of DOX and CS interaction.

DOX/polymer	+CS NPS	CP244_41 NPs	CP305_41 NPs
1:1	0.00 %	2.78	1.21
1:2	1.20 %	1.73	0
1:5	0.50 %	2.50	2.13
Average EE	0.56 %	2.33 %	1,11 %

Table 40 Calculation of EE of CS, CP244_41 and CP305_41 NPs.

Sample	Dh (nm)	PDI	ζ (mV)
+CS NPs (empty)	340±105	0.333±0.025	55.9±4.16
+CS NPs + DOX	380±154	0.283±0.019	53.1±4.37
CP_244_41 NPs (empty)	165±54	0.128±0.017	11.9±3.91
CP_244_41 NPs + DOX	153±65	0.147±0.011	12.6±3.28
CP_305_41 NPs (empty)	97±35	0.184±0.021	13.3±4.26
CP_305_41 NPs + DOX	103±46	0.203±0.013	13.6±6.03

Table 41 Comparison between empty microgels and microgels prepared using DOX.

Chapter 9: DOX loading and release

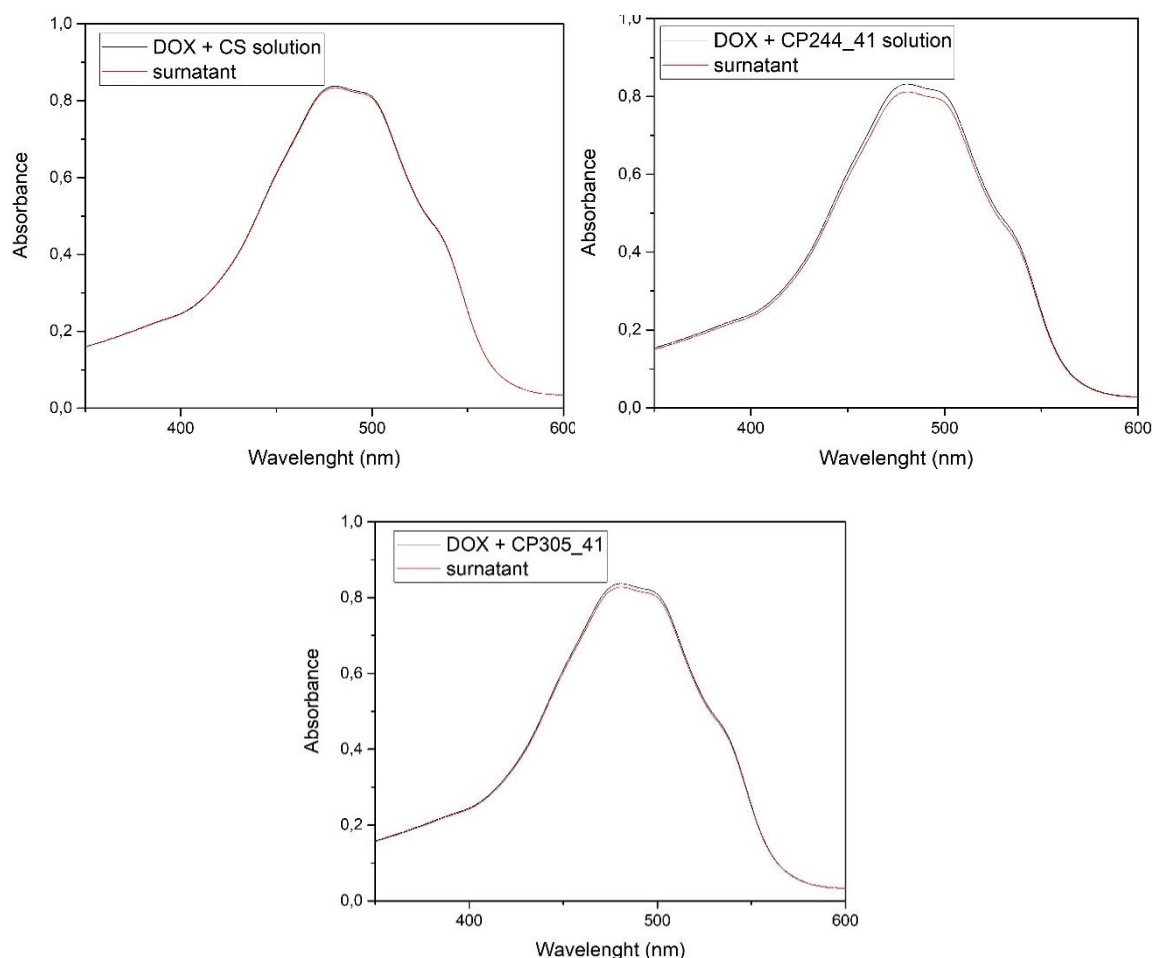


Figure 76 Comparison between UV-VIS spectra of DOX-polymer solutions (DOX/polymer=1:5) before gelation (black) and the supernatant of polymer NPs after centrifugation.

In the previous chapters, it was hypothesized that microgels aggregation may promote the encapsulation of DOX within microparticles. During microgels formation, local variations of viscosity within the particles can slow down the diffusion of the molecule in solution and facilitate drug encapsulation. Our hypothesis is that the concentration of the polymer was too low to promote the encapsulation of the drug. Furthermore, microgels may not have a sufficiently compact structure that can prevent the diffusion of the drug into the solution. DOX encapsulation was achieved by inducing the precipitation of CP244_41 in the presence of DOX. The precipitation was induced by raising the quantity of TPP up to a CP/TPP ratio of 3:1. During centrifugation, the formation of a purple precipitate was observed and the intensity of the colouration of the supernatant diminished. UV-VIS analysis showed that the process led to an encapsulation rate of about 78% (Figure 77). The analysis at the DLS did not allow to determine the particle size due to their micrometric size. The observation of the aggregates using optical (Figure 78) and fluorescence microscope (Figure 79) allowed to estimate the average size of the microgels

Chapter 9: DOX loading and release

around 5 micrometres. The observations confirmed the presence of DOX inside the mesh of the microgels.

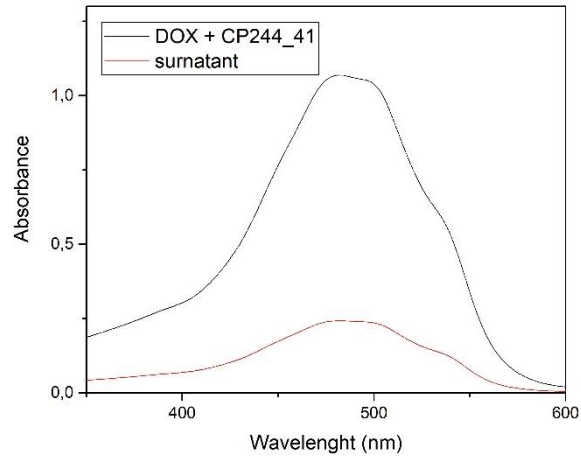


Figure 77 Comparison between UV-VIS spectra of DOX-CP244_41 solutions before gelation (black) and the supernatant of CP244_41 NPs after centrifugation.

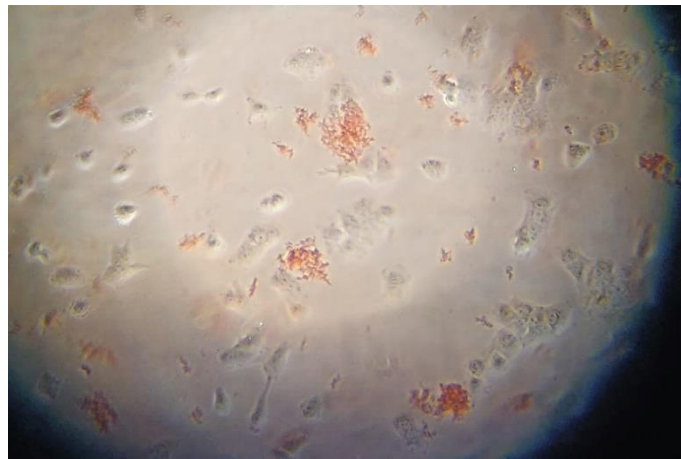


Figure 78 Microscope observation of DOX loaded CP244_41 in HUH7 cell lines using a 10x objective magnification. The orange colour is due to the localization of DOX inside the microparticles.

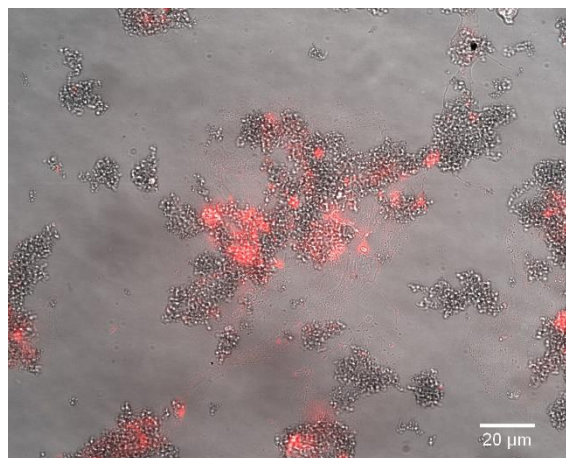


Figure 79 Fluorescence microscope observation of DOX loaded CP244_41 after 24 hours of HUH7 cell lines using a 40x objective magnification. The red fluorescence allowed to observe the localization of DOX.

9.1.1 Thermoinduced drug encapsulation

DOX encapsulation was attempted by inducing conformational change of microgels by increasing temperature. In the previous chapter, it was reported that the reversibility of the conformational change induced by VPTT is concentration dependent. In general, CP and +CP particles exhibited a small increase in the average size when the samples were cooled back to 25 °C. Consequently, it was observed that VPTT conformational change may induce aggregation patterns for longer periods of time. Accordingly, VPTT behaviour can be exploited to induce the uptake of the drug. CP244_41 and CP305_41 NPs fabricated with DOX were incubated at 41 °C for 5 min in order to promote DOX encapsulation. At the end of the process, microgels were centrifuged and the concentration of DOX was determined in the supernatant via UV-VIS spectroscopy (Figure 80, Table 42). The test was unsuccessful, and the percentage of EE was negligible. The study provided further confirmation that the dispersed microgels are unable to encapsulate the DOX due to the low affinity between CP polymers and DOX.

DOX/CP	CP244_41 NPs	CP305_41 NPs
1:1	0.71	1.15
1:2	2.23	0.87
1:5	0.42	0
Average EE	2.33 %	1.11 %

Table 42 Results of thermoinduced encapsulation of DOX at 41 °C.

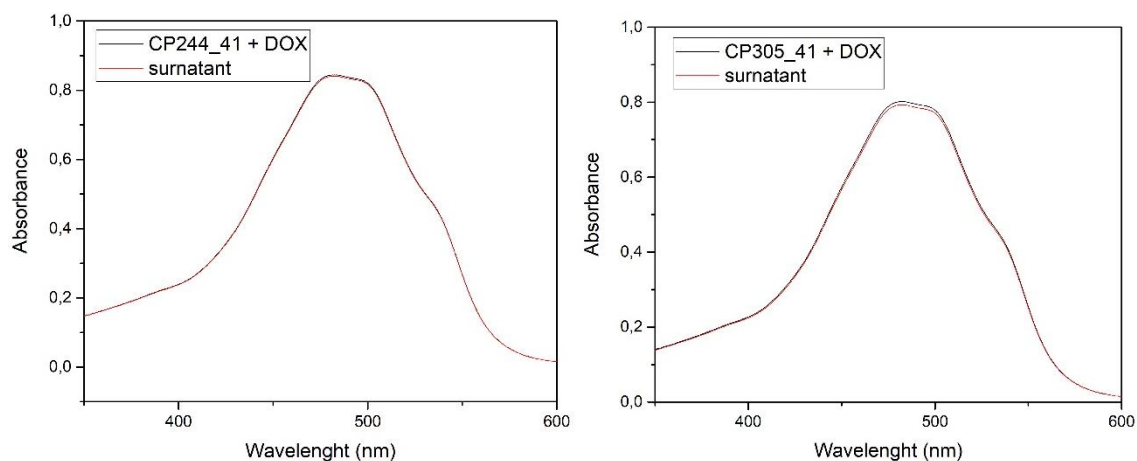


Figure 80 Comparison between UV-VIS spectra of DOX-CP244_41 solutions (DOX/CP=1:5) before gelation (black) and the supernatant of CP NPs after centrifugation.

9.2 DOX release and uptake

9.2.1 Cumulative release and uptake



Figure 81 Microgels precipitation inside Float-A-Lyzer™ device after 52h of release. The purple colour is related to the presence of DOX inside the polymer precipitate.

Cumulative release tests are performed without replacing the external buffer at each sampling point. Compared to conventional release tests, cumulative releases allow for the screening of particle behaviour by simplifying experimental protocol and data processing. The first cumulative tests highlighted the uptake behaviour of thermoresponsive CP305_41 and CP305_244_41 NPs at the VPTT (39 °C). CP305_41 exhibited radically different behaviour at 25 and 39 °C (Figure 82). At 39 °C, the drug is initially released faster due to thermal agitation. After 4 hours, the elution of the drug stopped, and the amount of drug released started to decrease. This behaviour is in accordance with an uptake mechanism of the drug by the CP microgels. The result is consistent with the expectation that the thermal transition can be exploited to induce the encapsulation of DOX inside CP particles. Over the next hours, the slow formation of purple aggregates was observed, and the colour of the solution decreased. The curves were analysed with different kinetic models. The n values obtained by fitting the data until 60% of the release at 25 °C with Korsmeyer-Peppas equation (Equation 55, see “Appendix II” section) is close to the 0.45 and accounts for Fickian diffusion from spherical geometries²⁹⁴. In addition, the curves at 25 °C and 39 °C were analysed with two different double exponential models (Equation 56 and 57) which allowed to include the calculation of parameter A. At 25 °C, the A parameter correspond to the value of VCs (saturation point) calculated using the first-order model (Equation 56). At 39 °C, the S parameter represents the maximum of the curve after which uptake is observed and k_2 represent the rate of DOX uptake (Equation 57). The pharmacokinetic parameters and their correlation coefficients are summarized in Table 43. As shown, the two double exponential models ($R^2 > 0.99$) best described DOX release at both temperatures. The fit allowed to calculate an asymptotic value of ~65%. The value indicates that the system reached saturation and sink conditions were not met. This is in accordance with the low correlation values achieved by applying Higuchi (Equation 54)

and Korsmeyer-Peppas models (Equation 55). At 25 °C, the similar values between the two kinetic constants k_1 and k_2 excluded the interpretation of a two-step mechanism based on polymer relaxation and diffusion. Consequently, release is diffusion-driven. The first constant was associated to the elution of free DOX and the second constant to a slower diffusion related to the system being close to the osmotic equilibrium. Accordingly, this interpretation is in line with the results of previous experiments, which excluded the possibility of DOX encapsulation at room temperature. At 39 °C, the difference between calculated A (or VC_s) and the final rate of released DOX allowed to estimate DOX loading around ~22%.

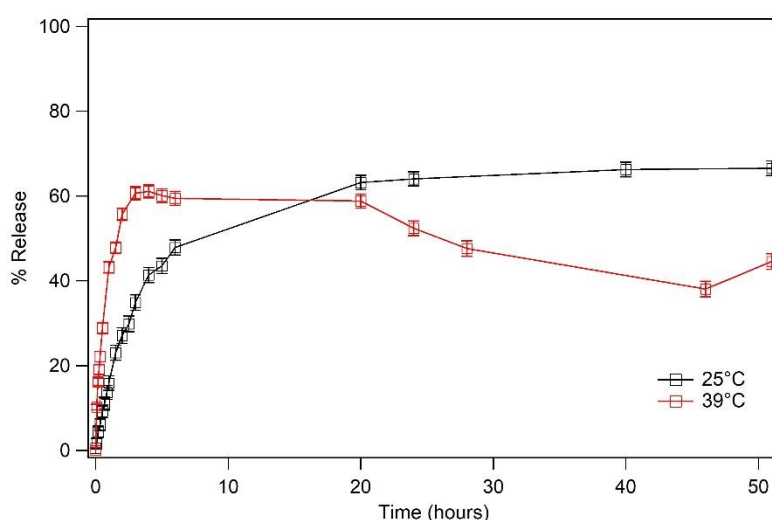


Figure 82 DOX release profile from CP305_41 NPs at 25 and 39 °C in PBS (0.1 M, pH = 7.4).

T	First-order		Higuchi		Korsmeyer-Peppas			Double exponential				
	K_o	R^2	VC_s	K_H	R^2	n	K_{KP}	R^2	K_1	K_2	R^2	A
25 °C	0.254	0.998	64.67	16.89	0.925	0.443	18.77	0.939	0.443	0.107	0.999	64.68
39 °C	1.711	0.951	55.47	32.029	0.457	0.338	38.51	0.570	0.008	1.256	0.991	64.71

Table 43 Pharmacokinetic parameters of DOX release from CP305_41 microgels.

9.2.2 DOX release and uptake

The utilization of dialysis membranes for conventional release tests resulted in poor reproducible data and experimental conditions. One of the main limits of the dialysis membranes is the variability in the surface area in contact with the buffer solution. Accordingly, DOX release tests were carried out using two different devices that are designed to ensure a fixed surface area in contact with the solution: MINI Slide-A-Lyzer™ (SAL) and Float-a-Lyzer™ (FAL). FAL devices consist in cylindrical floating tubes that

remain immersed in the buffer solution, while SAL devices have a cup-like shape with the bottom consisting in a dialysis membrane. SAL are directly applied on 50ml falcons under the falcon caps. Both devices remain perfectly sealed during the entire process and ensure that no variability in DOX concentration related to solvent evaporation. The tests were performed at 25 and 41 °C (2 °C above VPTT) using +CP244_41 and +CP305_41 NPs. The tests were carried out in sink conditions, calculating the amount of DOX in order to ensure that DOX remained below 20% of the solubility concentration. The release curves are represented in Figure 83 and 84. The sampling volumes were reduced to 300 µl in order to reduce errors related to external buffer dilution. The experiment confirmed that microgels are able to encapsulate and retain the drug if the temperature is kept above VPTT. The release curves of FAL devices at 41 °C showed uptake behaviour after 30 hours of incubation and were modelled successfully using double-exponential functions ($R^2 > 0.99$, Table 44-45). The uptake behaviour was less evident by using SAL devices in the same conditions. The formation of bigger particles prevented the elution of the DOX and the uptake behaviour was more evident after 40 h of elution. Accordingly, SAL release curves at 41 °C were best interpreted using first order kinetics (see Table 44-45). The difference observed between SAL and FAL devices at 41 °C were probably related to the difference in DOX concentration. SAL release tests were performed using twice the volume of the external buffer. The relatively high correlation values ($R^2 > 0.98$) obtained by fitting SAL curves at 25 °C with Higuchi and Korsmeyer-Peppas models are in accordance with the behaviour of a drug molecule released from a polymer matrix²⁹⁴ (Table 44-45). For all samples, the calculated n values accounts for non-Fickian transport governed by diffusion and swelling. Accordingly, microgels have a role in defining DOX transport even in the absence of effective DOX encapsulation. After 30 h, the aggregation of microgels was also observed at 25 °C. One of the possible explanations is that destabilization was induced by the elevated pH of the external buffer. At the end of the release process, a portion of micrometric aggregates was observed for both temperature conditions. The dark purple colour of the precipitates indicates that the drug was encapsulated in the polymer matrix (Figure 81). uptake percentage of the DOX was calculated for the samples by the peak point and the end point of the curve.

Chapter 9: DOX loading and release

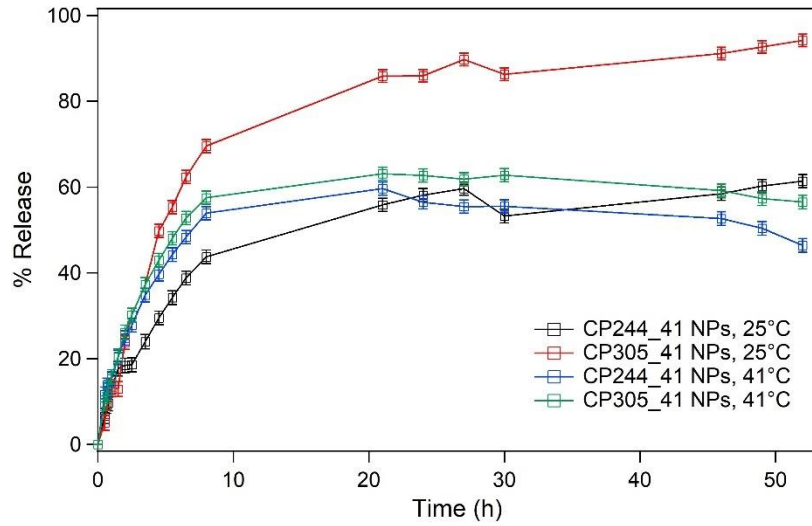


Figure 83 DOX release profile from +CP244_41 NPs at 25 and 41 °C in PBS (0.1 M, pH = 7.4).

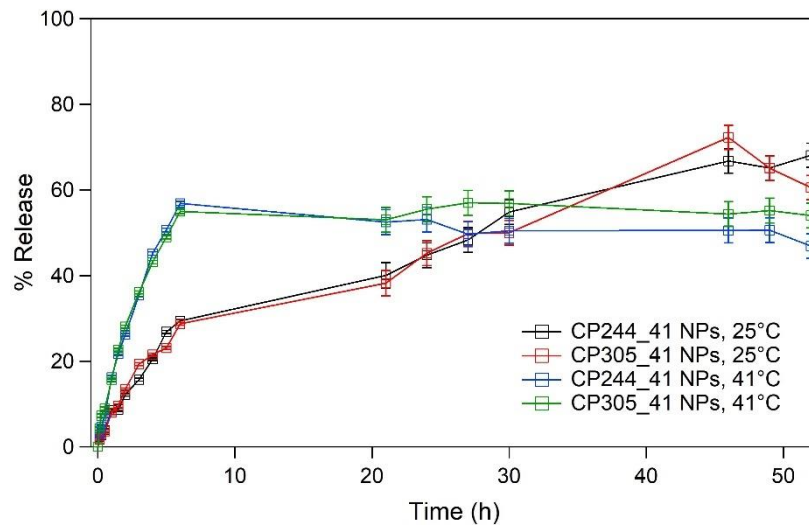


Figure 84 DOX release profile from +CP305_41 NPs at 25 and 41 °C in PBS (0.1 M, pH = 7.4).

Chapter 9: DOX loading and release

+CP244_41 NPs (Float-a-Lyzer™)												
T	First-order		Higuchi		Korsmeyer-Peppas			Double exponential				
	K _o	R ²	VC _s	K _H	R ²	n	K _{KP}	R ²	K ₁	K ₂	R ²	A
25 °C	0.173	0.995	58.03	13.41	0.950	0.485	13.79	0.952	0.169	0.029	0.990	61.52
41 °C	0.322	0.987	54.03	18.39	0.815	0.577	16.43	0.788	0.005	0.244	0.996	64.86

Table 44 Pharmacokinetic parameters of DOX release from +CP244_41 microgels.

+CP305_41 NPs (Float-a-Lyzer™)												
T	First-order		Higuchi		Korsmeyer-Peppas			Double exponential				
	K _o	R ²	VC _s	K _H	R ²	n	K _{KP}	R ²	K ₁	K ₂	R ²	A
25 °C	0.167	0.997	90.04	20.49	0.939	0.535	19.06	0.932	0.190	0.029	0.995	94.50
41 °C	0.299	0.996	67.49	19.60	0.848	0.619	16.48	0.812	0.008	1.256	0.999	64.71

Table 45 Pharmacokinetic parameters of DOX release from +CP305_41 microgels.

9.3 Summary

In this chapter, we evaluated the possibility of encapsulating DOX inside CP microgels with different approaches, including the fabrication of microgels in the presence of DOX and the incubation of the fabricated microgels above the VPTT. We concluded that CP microgels represent a poor substrate for DOX encapsulation due to weak interaction between the polymers and the drug. However, release tests showed that the uptake of OX can be induced after an incubation period of >4 h due to the destabilization of microgels above the VPTT. Release mechanisms at 25, 39, and 41 °C were interpreted with different mathematical models (first order, Higuchi, Korsmeyer-Peppas, double-exponential) and a double-exponential model was proposed for the interpretation of a release and uptake mechanism. Aggregated gels precipitated during the incubation were observed with a fluorescent microscope and exhibited a strong fluorescence signal caused by the presence of DOX inside the polymeric matrix.

Chapter 10: Assessment of biocompatibility

10.1 Determination of LCST in plasma

The critical miscibility behaviour of PNVCL-COOH was observed in human plasma to evaluate possible cytotoxic effects related to the utilization of the polymer in physiological fluids. Plasma represents 55% of the blood and consists mainly of water, dissolved ions, proteins and gases. Among the main proteins, albumin, fibrinogen and globulins are present, whose functional groups give rise to the intense visible bands in the region between 200 and 600 nm³⁵⁵. In both samples analysed, the peak at 576 nm and the shoulder at 540 nm are related to the presence of oxyhaemoglobin³⁵⁶ due to the haemolysis of residual erythrocytes. A first calibration of the matrix was performed on a pool of plasma realised from the union of samples taken from 12 healthy donors in a temperature range between 25 and 50 °C. The calibration excluded any spectral modification between 25 and 42 °C. Due to the complexity of the matrix, all solutions were analysed using milliQ water as a reference. The measurements of the LCST of PNVCL_122, PNVCL_244 and PNVCL_305 were provided by the analysis of the region devoid of amino acid signals, between 600 and 800 nm (Figures 85 and 86). Upon heating, the absorbance signal of the spectra was shifted towards higher values due to the conformational change of the polymers. The LCST was significantly lowered by about 10 °C and spectral changes were already observed at 28 °C.

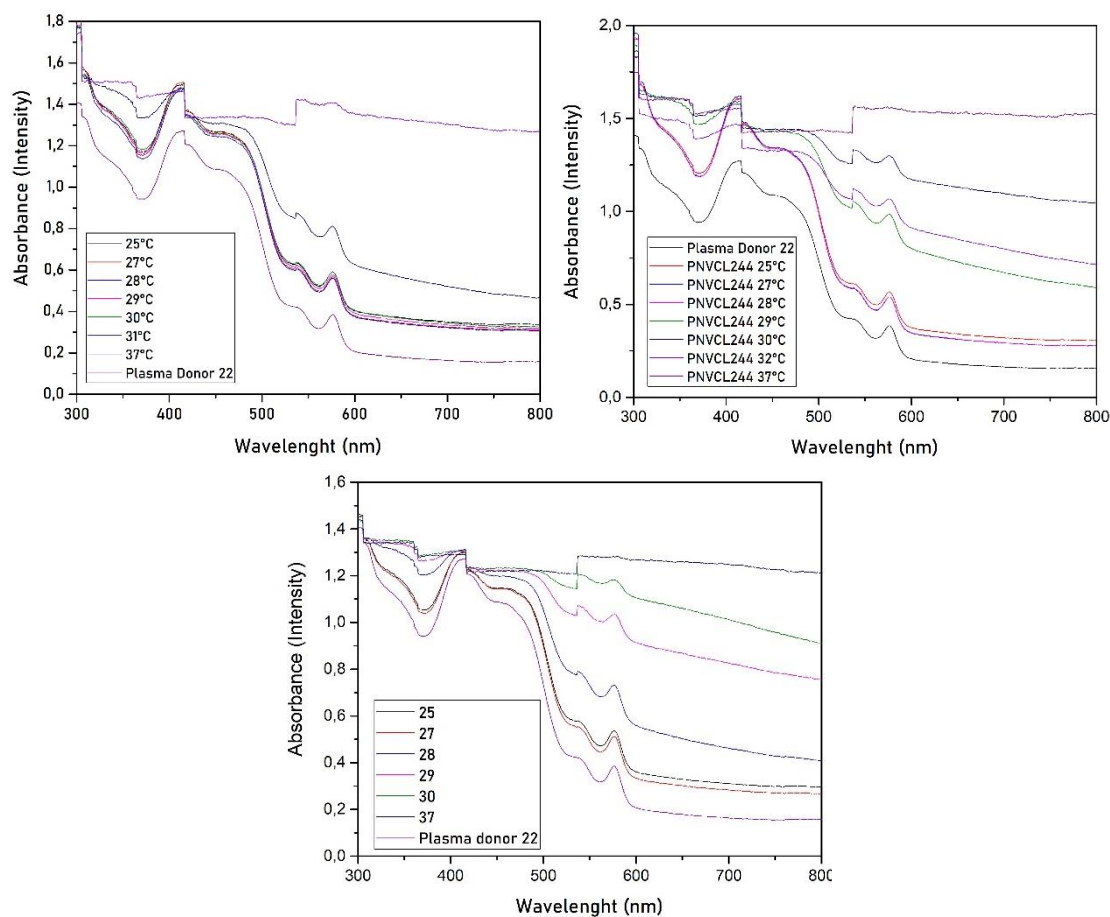


Figure 85 Evolution of UV-VIS spectrum of PNVL₁₂₂ (top left), PNVL₂₄₄ (top right) and PNVL₃₀₅ (below) as a function of temperature.

This is in line with the results of previous experiments, which have shown that LCST is affected by changes in ionic force, pH and concentration. By heating up the solution to 37 °C, the spectra change dramatically, and it was no longer possible to recognize any spectral information. The spectra of PNVL-plasma solution at different temperatures are reported in Figure 85. However, the change of the spectral properties was reversed by cooling the system down to 25 °C. Accordingly, the reversibility of PNVL-COOH thermoresponsivity is maintained within the plasma matrix. The comparison between the LCST of PNVL-COOH in water and plasma are reported in Table 46 along with the correlation value of the sigmoidal models that were used for the calculation of the LCST. It can be concluded that the polymer is not suitable for direct utilization within the plasma at the concentration of 5mg/ml. However, the reversibility of the transition could be an important starting point for future developments. According to the previously reported results, the LCST can be increased by simply decreasing the chain length by modifying the M/I ratio and by diminishing the concentration of the polymer³³⁵.

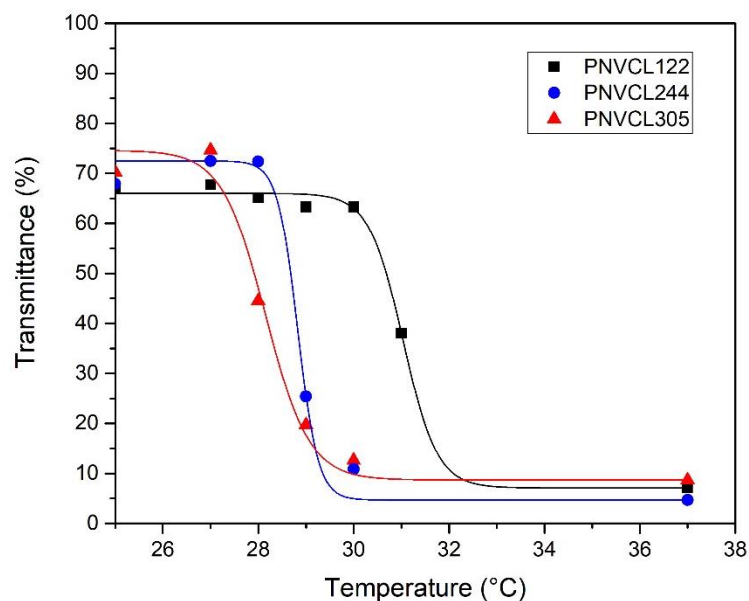


Figure 86 Fitting of the miscibility curves of PNVCL_122 (black squares), PNVCL_244 (blue circles) and PNVCL_305 (red triangles).

Campione	LCST (plasma)	LCST (H ₂ O)	r ₂
PNVCL_122	42 °C	31.04±0.05	0.99624
PNVCL_244	39 °C	28.09±0.15	0.97019
PNVCL_305	39 °C	28.82±0.19	0.98702

Table 46 Comparison between LCST of PNVCL-COOH in plasma and water at the concentration of 5mg/ml and correlation values of the sigmoidal models used for the fitting of transmission data.

10.2 In-vitro cytotoxicity assays

MTT and Cell-Titer viability assays were carried out on HUH7 cell lines in order to provide a preliminary evaluation of the biocompatibility of synthesized polymers and polymeric particles. Given the difficulties encountered in drug encapsulation, the aim of this study was to verify the potential applicability of CP microgels as embolic agent for TACE treatments of HCC. In TACE applications, the embolic agents are added to a drug solution and the mixture is simply agitated before administration. Accordingly, drug encapsulation is not strictly required as the local increase of drug concentration inside the tumour is provided by the formation of the embolus. The toxicity of DOX solution on HUH7 cells was compared with the toxicity of DOX/CP microgels solutions without calculating the percentage of encapsulation. Finally, MNPs particles were dispersed in DOX/CP solution for the evaluation on the toxicity of a magnetic-responsive formulation.

10.2.1 MTT test

+CS and PNVCL_244 were found to be non-toxic in HUH7 cell lines up to 0.635 mg/ml concentrations (Figure 87). At 0.635 mg/ml, CP244_41 and CP305_41 polymer concentration, only 78% and 65% of the cells are viable, respectively. The low survival rates show that polymers exhibit cytotoxic effect at low concentrations. One possible explanation is that the LCST of CP244 and CP305 is lowered by the cell culture environment to ≤ 37 °C. Consequently, CP polymers underwent a conformational change which resulted in reduced biocompatibility. The same effect is not visible for PNVCL244. In previous studies, it has been observed that the LCST of PNVCL_244 at a concentration of 0.5 mg/ml is ~ 41 °C. Accordingly, a difference of 4 °C between the cell culture and the LCST of the polymer is sufficient to prevent cytotoxic effect due to critical miscibility behaviour.

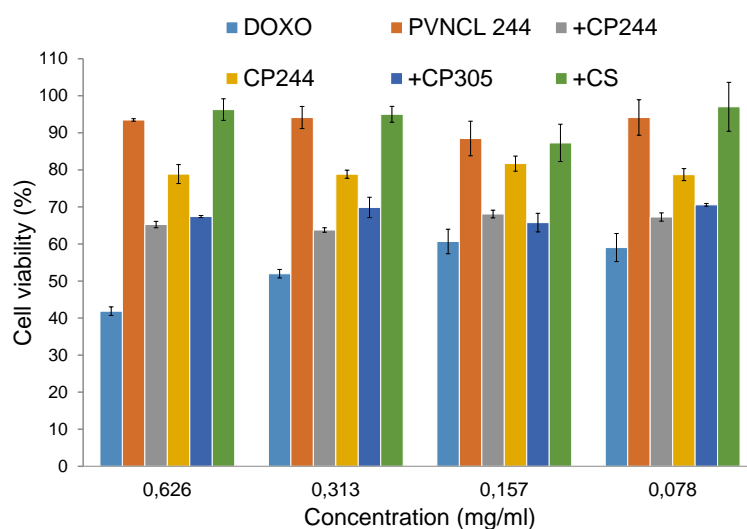


Figure 87 MTT assay of PNVCL and CP polymers in human hepatoma cell lines (HUH7).

In a similar way, bare CP microgels were found to be partially toxic due whereas cell survival rate was higher for +CS, CS and MNPs particles (Figure 88). At 0.626 mg/ml, +CP305_41 and +CP244 survival rate dropped to ~ 75 and $\sim 67\%$, respectively. A possible interpretation is that sample aggregation was largely promoted before administration during the purification step. The evaluation of CP244_41 and +CS particles with DLS prior to administration demonstrated that the suspensions were partially aggregated. Nonetheless, aggregated +CS microgels were found to be non-toxic. The reduction in cell survival was associated with the lowering of the VPTT due to cell culture medium.

Chapter 9: DOX loading and release

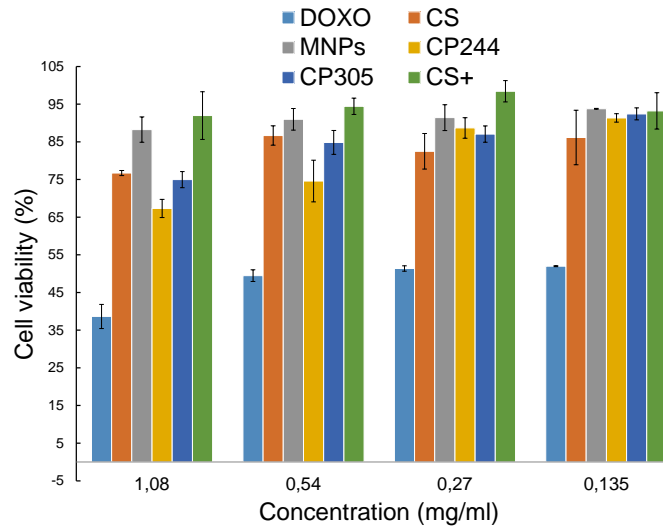


Figure 88 MTT assay of MNPs, CS, +CS and CP NPs in human hepatoma cell lines (HUH7).

The administration of DOX/CP formulation resulted in a significant increase in cell mortality (Figure 89). According to the previous results, the overall increase in drug toxicity is caused by the thermo-induced conformational change of CP microgels at 37 °C. The presence of MNPs did not exhibit any substantial change in DOX/CP toxicity. Accordingly, MNPS can be dispersed in DOX/CP formulations without affecting the biocompatibility of the drug-microgel suspension.

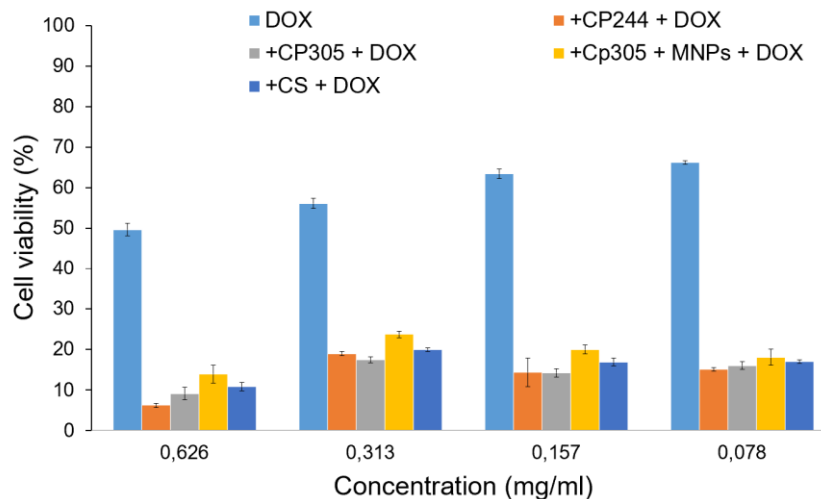


Figure 89 MTT assay DOX/CS, DOX/+CS and DOX/CP NPs in human hepatoma cell lines (HUH7).

10.2.2 Cell-Titer

The effect of administration of DOX/CP formulations on HUHT was evaluated using Cell-Titer assay in the same preparation conditions (Figure 90). Cell-Titer assay is based on a

different principle as survival rate is measured from the metabolic activity of the cultured cells. The results obtained are consistent with the observation of an increase in DOX toxicity due to the presence of polymeric particles that undergo conformational change at 37 °C due to cell environment. Compared to MTT, survival rates are significantly different at higher (0.625 mg/ml) and lower concentrations (0.078 mg/ml). At the highest concentration, the total disappearance of metabolically active cells is observed. At lower concentrations, the cytotoxic effect of CP/DOX suspensions is significantly lower than that recorded with MTT. resulted in a significant increase in cell mortality.

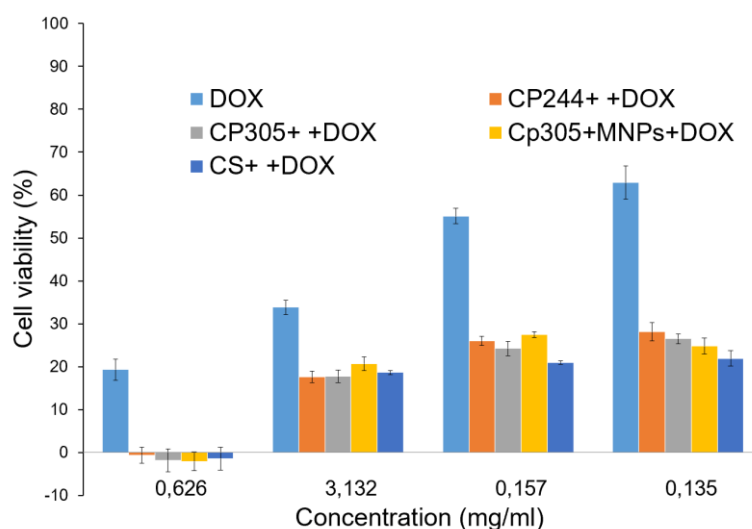


Figure 90 Cell-Titer assay DOX/CS, DOX/+CS and DOX/CP NPs in human hepatoma cell lines (HUH7).

10.2.3 Immunofluorescence

The subcellular localization of DOX within HUH7 cells was studied using immunofluorescence (IF). The images of HUH7 cells treated with different samples are represented in Figure 91-96. The technique allowed to observe the differences in morphology and DOX accumulation within HUH7 cell lines. Consistently with previous observations, DOX was not encapsulated into CP microgels. Consequently, there were not substantial differences between cells treated with DOX and cells treated with DOX/CP suspensions. A dramatical change was observed by treating HUH7 cells with aggregated CP244 microgels loaded with DOX. The administration of aggregated DOX-loaded microgels resulted in a strong increase in cell mortality. Accordingly, DOX-loaded CP micrometric particles are highly toxic due to their big dimension and the elevated concentration of DOX inside the polymer network. Due to its micrometric size, the system has potential for the development of a DEB-TACE therapy based on a thermoresponsive system. In a future perspective, the control of drug loading and size at the microscale is

fundamental requirement for the development of reliable TACE therapies based on CP polymers.

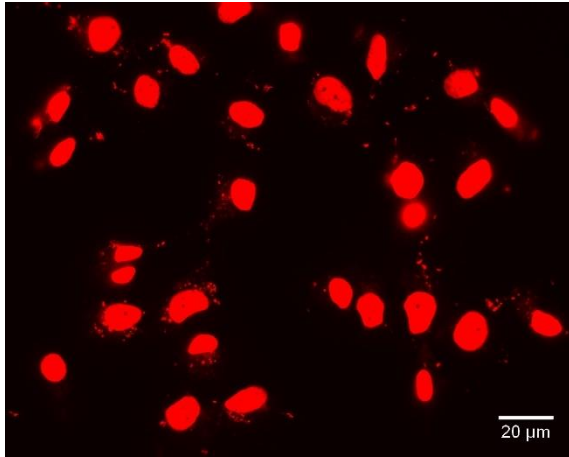


Figure 91 Fluorescence microscope image of HUH7 lines treated with DOX.

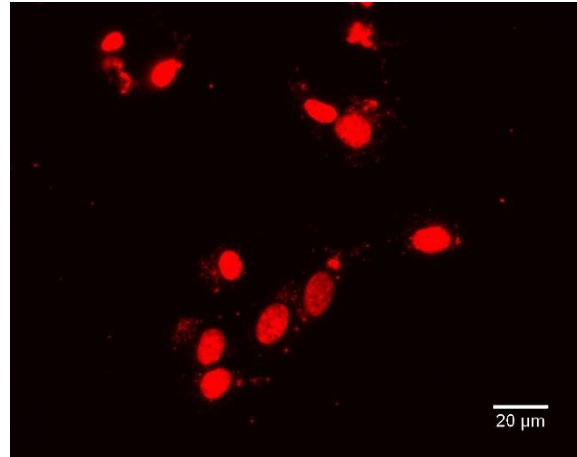


Figure 92 Fluorescence microscope image of HUH7 lines treated with CP244_41 NPs and DOX.

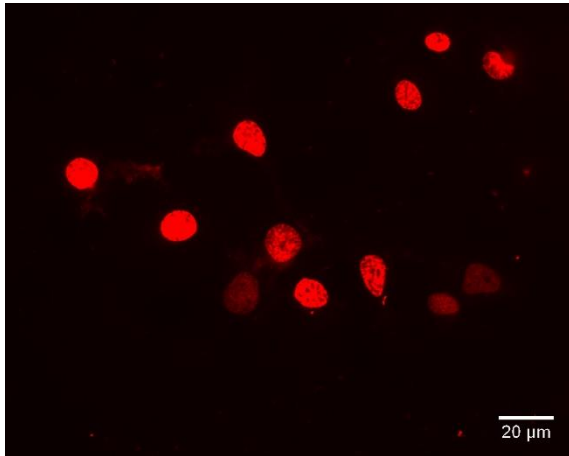


Figure 93 Fluorescence microscope image of HUH7 lines treated with CP305_41 NPs and DOX.

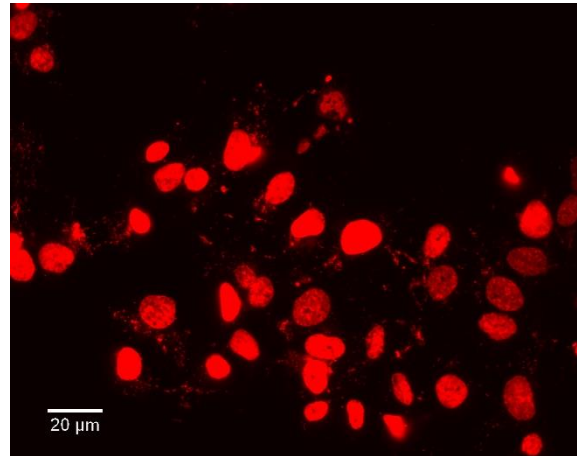


Figure 94 Fluorescence microscope image of HUH7 lines treated with +CP244_41 NPs and DOX.

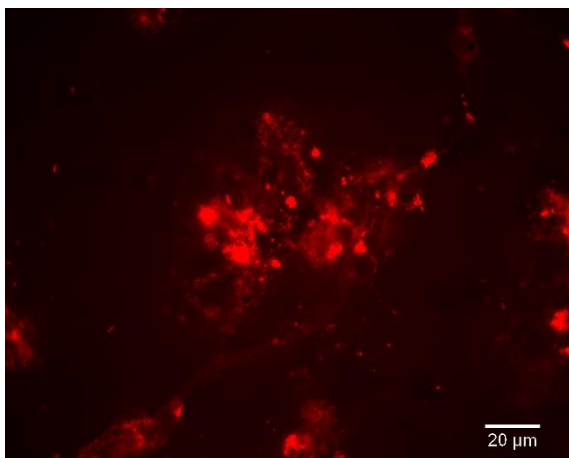


Figure 95 Fluorescence microscope image of HUH7 lines treated with aggregated CP244_41 NPs and DOX.

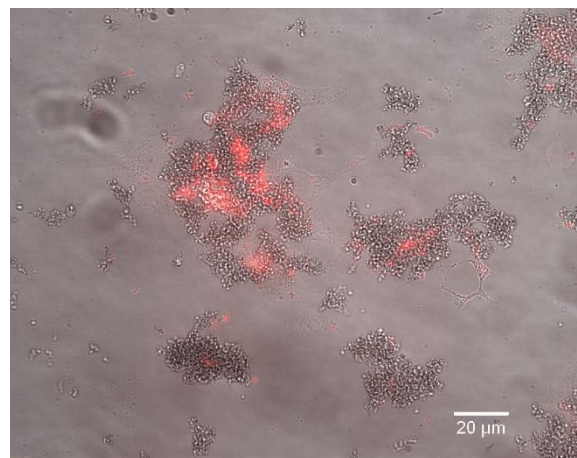


Figure 96 Merged pictures (TRITC/bright field) image of HUH7 lines treated with DOX.

10.4 Summary

In this chapter, a preliminary evaluation of the cytotoxicity of the synthesized polymers and CP microgels is provided. *In-vitro* tests (MTT, Cell Titer, immunofluorescence) were performed on HUH7 cells and both microgels and polymers exhibited mild toxicity. These preliminary results highlight the need to investigate further on the proper condition of utilization of the thermoresponsive devices. PNVCL and PNVCL-based particles, such as CP microgels, possess a critical transition temperature that is heavily influenced by environmental factors. The presence of ions and proteins dissolved in the solutions leads to the lowering of the LCST (or the VPTT), that may result in cytotoxic effects in physiological conditions. This hypothesis was confirmed by measuring the LCST of PNVCL-COOH polymers in human plasma. The presence of the biological fluid resulted in the lowering of the LCST by about 10 °C.

Chapter 11: Materials and methods

11.1 Materials

➤ *Polymers*: LMW Chitosan (50-190 KDa) (CS) was purchased from Sigma-Aldrich (St. Louis, MO, USA). Chitosan-HCl, 128 KDa, 95% deacetylated (+CS) was purchased from HMC+ Chitoceuticals (Heppe Medical Chitosan GmbH, Halle, DE). Methyl poly(ethylene glycol) ($M_w = 5$ kDa) was purchased from Fluka (Buchs, Switzerland).

➤ *Reagents*: N-Vinyl Caprolactam (NVCL), 2,2'-Azobis(2-methylpropionitrile) (AIBN), 3-mercaptopropionic acid (MPA), Iron (II) Oxide tetrahydrate ($FeCl_2 \cdot 4H_2O$), Iron (III) Oxide hexahydrate ($FeCl_3 \cdot 6H_2O$), Sodium acetate trihydrate, Trisodium citrate dihydrate, Citric acid monohydrate, 2-morpholin-4-ylethanesulfonic acid (MES), Sodium Chloride, Sodium Hydroxide, Potassium Chloride, Sucrose, Trehalose and Phosphate-buffered saline tablets were purchased from Sigma-Aldrich (St. Louis, MO, USA).

N-hydroxy succinimide (NHS) was purchased from Fluka (Buchs, Switzerland) and Sigma-Aldrich (St. Louis, MO, USA)

Sodium phosphate dihydrate, disodium phosphate dihydrate and potassium bromide were

purchased from Carlo Erba (Milano, IT).

Sodium tripolyphosphate (TPP) was purchased from Merck (Darmstadt, DE).

Doxorubicin 2mg/ml solution and Adryamicin[®] lyophilized powder were purchased from Pfizer (Brooklyn, NY, USA).

DMEM cell culture medium was purchased from Euroclone (Euroclone S.p.A., Pero, IT).

➤ *Solvents*: Anhydrous N,N-Dimethylformamide (DMF), Hexane, Diethyl ether, NH₄OH 25% solution, Glacial Acetic Acid, Acetone, Hydrochloric Acid, Dimethyl sulfoxide, Sulfuric Acid, Nitric Acid, Deuterium oxide (D₂O), Dimethyl sulfoxide-d₆, Deuterium Chloride 37% (DCI/D₂O) were purchased from Sigma-Aldrich.

Ethanol was purchased from Sigma Aldrich (St. Louis, MO, USA) and PanReach AppliChem (ITW reagents- AppliChem GmbH, Darmstadt, DE).

NaOH 1M solution was purchased from VWR Chemicals (Radnor, PA, USA).

➤ *Laboratory equipment*: Spectra/Por[™] Cellulose membrane tubing (1 KDa, 12-14 KDa MWCO), Slide-A-Lyzer[™] MINI Dialysis Device (20KDa MWCO, 2 mL), Vybrant MTT Cell Proliferation Assay Kit were purchased from Thermo Fisher Scientific (Waltham, MA, USA).

Millex 450 nm and 220 nm PES filters were purchased from Merck (Darmstadt, DE).

Spectra/Por[™] Cellulose membrane tubing (15KDa MWCO), Sterican Needles (0.80 x 120mm), 15 ml glass vials, 450 nm and 200 nm PTFE 13mm filter were purchased from VWR International (Radnor, PA, USA).

Neodymium-based cylinder magnet (1.2 T) was purchased from Webcraft GmbH (Gottmadingen, DE).

Headspace sealed vials, Pear-shaped evaporating flask, Rubber Septa, Float-A-Lyzer (20 KDa MWCO, 2 ml) were purchased from Sigma-Aldrich (St. Louis, MO, USA).

11.2 Preparation protocols

11.2.1 *Recrystallization of AIBN*

2.0 g of AIBN (12.2 mmol) were placed in a round bottomed flask equipped with a stirring bar and a condenser. The vacuum and a flow of Ar was alternated in the system for 3 times, to avoid any trace of oxygen. AIBN was dissolved in 5 ml of ethanol and the temperature was increased slowly to 50-55 °C. At this temperature, 2 ml of ethanol were

added to solubilize the product. The flask was then left to reach room temperature to allow crystallization. AIBN was stored at -20° C in the form of crystalline flakes.

11.2.2 *Synthesis of PNVCL-COOH*

PNVCL-COOH was synthesized by free radical polymerization. For all preparations, 5 mg of AIBN (0.304 mmol) and 28 μ l of MPA (3.278 mmol) were used. Prior to its utilization. The monomer was recrystallized from hexane before use, and MPA was transferred in a sealed vial that was deoxygenated with Ar prior to its utilization. Different molar ratio between NVCL and AIBN were used in order to obtain polymer with different molecular mass and LCST. The NVCL/AIBN molar ratio were, respectively, 122, 244, 305, 610, 1220 and 1690. DMF was deoxygenised with Ar for 15 min prior to the addition of the reagents. After the dissolution of the reagents, the reaction was carried out in sealed vials at 70 °C for 8 h. All sealed vials were dried overnight at 80 °C before the reaction. After the reaction, the solution was dialyzed in a cellulose membrane tubing (MWCO of 1-2 kDa) against distilled water for at least 2 days to remove impurities and unreacted materials. Finally, the frozen product was freeze-dried at -50 °C and 0.05 mbar and stored at 4 °C.

11.2.3 *Synthesis of Chitosan-g-PNVCL (CP)*

PNVCL-COOH was grafted onto CS using EDC and NHS as condensing agents at room temperature. All preparations were prepared in order to have different mass ratio between PNVCL and CS. The molar ratios were, respectively: 8:1,4:1, 2:1, 1:1 and 1:2. For all preparations, polymer solutions were prepared in order to have concentrations inferior to 5 mg/ml. First, a solution of PNVCL-COOH was prepared in MES buffer (0.1 M, pH = 5.5) with EDC and NHS in large excess to the number of carboxyl groups (at least ten times higher) and left stirring overnight for group activation. CS was dissolved in diluted HCl (0.1 M), filtered with a 0.45 μ m nitrocellulose filter and added to the PNVCL solution. After the addition of the CS solution, the reaction was allowed to continue for 24 h at room temperature under constant stirring. The solutions were dialyzed using cellulose membrane tubing (MWCO 12-14 kDa) for 2 d against distilled water and the product was freeze-dried.

11.2.3 Preparation of Fe₃O₄ magnetic nanoparticles (MNPs)

Fe₃O₄ MNPs were prepared by chemical precipitation method. Ferric and ferrous chlorides (1.9: 1 wt. ratio) were dispersed in aqueous medium and the solutions were deoxygenized by bubbling Ar for 15 min prior to the addition of the reagents. The mixture was stirred vigorously at 70 °C and co-precipitated by adding 25% ammonium hydroxide. The obtained black precipitate was separated using a magnet and purified three times with milliQ water. Finally, the particles were resuspended in ethanol and the suspensions were dried at 50 °C overnight.

11.2.4 Preparation of CP and CS microgels via ionotropic gelation

CS and CP microgels were prepared by ionotropic gelation. For a 5 ml polymer solution, 6.25 mg of CS or CP were weighed and dissolved in 250 µl of 1% CH₃COOH and then diluted twenty times to reach a final concentration of the polymer of 1.25 mg/ml. The pH was adjusted to 4.8 or 5.5 using a 1M NaOH solution. A TPP solution of 0.25 mg/ml were added dropwise to induce the formation of the microgels. All polymer solutions were filtered with a 450 nm filtered unit prior to utilization. TPP solution were filtered with a 220 nm filtered with a 220 nm filtered unit prior utilization. For the preparation of magnetic CP and CS microgels, MNPs inside the TPP solution (CP/MNP=3:1). The MNPs/TPP solution were sonicated for 15 min prior to the addition to the polymeric solutions.

11.3 Methods

11.3.1 UV-Visible spectroscopy

UV-VIS absorption measurements were performed on an Agilent Technologies Cary Series UV-VIS G9821A Spectrophotometer using QS 108002B-10-40 micro cell cuvettes. Temperature-dependent measurement were performed on a Shimadzu UV-visible spectrophotometer model UV-2450 equipped with a TCC-240A Thermoelectrically Temperature Controlled Cell Holder using a Hewlett-Packard (Palo Alto, CA, USA) 1000 QS cuvettes.

11.3.2 Fluorescence spectroscopy

Fluorescence emission measurements were performed on an Agilent Technologies Cary Eclipse Fluorescence Spectrophotometer using a QS 108-F-10-40 Semi-Micro cell cuvette (Hellma GmbH &Co, Mullheim, DE). DOX solution were excited at 497.80 nm using an

excitation and emission slit width of 5 nm. Emission spectra were recorded from 510 to 800 nm, with a scan rate of 120 nm/min and a data interval of 1.0 nm.

11.3.3 Calibration of DOX measurements

Adryamicine[®] and DOX-HCl concentration signal were calibrated using UV-VIS and fluorescence spectroscopy. DOX-HCl was calibrated with fluorescence signal in the range between 0 and $2,00 \cdot 10^{-4}$ M. Since self-association between DOX molecules due to $\pi - \pi$ stacking interactions³¹² results in fluorescence quenching³⁵⁷, UV-VIS spectroscopy was used for the calibration of solution with a concentration $>2,00 \cdot 10^{-4}$ M. The molar extinction coefficients ϵ was derived from the slope of the correlation lines. Statistical values and errors were calculated using the method of least squares. The values of the associated error were calculated using t student values related to N-2 degrees of freedom and a level of significance of 5%. The concentration range, molar extinction coefficient ϵ and correlation coefficient R^2 are reported in Table 47.

Sample	Technique	Concentration range (mol/l)	Molar extinction coefficient (ϵ)	Correlation coefficient (R^2)
Adryamicine [®]	UV-VIS	0 – $1,72 \cdot 10^{-4}$	1628 \pm 47	0,999752
DOX-HCl	Fluorescence	0 – $2,00 \cdot 10^{-4}$	10965 \pm 291	0,999646
DOX-HCl	UV-VIS	0 – $2,00 \cdot 10^{-5}$	3676148 \pm 117219	0,999195

Table 47 Calibration of DOX measurements.

11.3.3 UV-VIS determination of LCST

The critical miscibility behaviour temperature and absorbance measurements were carried out in a Shimadzu UV-visible spectrophotometer model UV-2450 equipped with a TCC-240A Thermoelectrically Temperature Controlled Cell Holder. For each temperature, the absorbance was recorded in the spectral range between 400 and 500 nm. The absorbance signals at 480 nm were converted into transmission for the realization of the miscibility curves. For plasma samples, spectra were recorded using the interval spectral range between 200 and 800 nm and the transmission was calculated from the signal at 800 nm. UV-Visible.

11.3.4 DLS determination of LCST/VPTT

The critical miscibility behaviour temperature of PNVCL-COOH polymers and the VPTT of CP NPs was determined using a Malvern Zetasizer Nano ZS90 (Malvern Panalytical S.R.L., Malvern, UK). Samples were analysed in a temperature range between 25 and 50 °C. For each temperature, the correlation curves were recorded and the cuvette were examined to check visible turbidity.

11.3.5 *Temperature dependent DOX release and uptake*

DOX release curves were built by measuring the intensity of the absorbance of the $\pi \rightarrow \pi^*$ band of DOX at 480 nm. The percentage of release was calculated as follows:

$$\% \text{ release} = \frac{A_t}{A_0} \cdot 100 \quad (24)$$

Where A_t is the absorbance of the external buffer solution at a specific timepoint and A_0 is the value of absorbance of a DOX solution with the same concentration of the initial DOX/NPs solution.

➤ *Cumulative drug release and uptake*: DOX release of CP305_41 NPs was performed in phosphate buffers (0.1 M, pH 7.4) at 25 °C and VPTT (39 °C). DOX/CP solutions were prepared by incubating DOX-HCl (2mg/ml) with TPP in order to promote a slight increase in DOX encapsulation as reported by *Janes et al.*³⁰⁶. 2 ml of freshly prepared CP305_41 NPs (CP 0.625 mg/ml, DOX 1,56 mg/ml) were placed inside a dialysis membrane (MWCO=12-14 KDa). The membrane was put into a beaker containing 25 ml buffer and left under moderate stirring for three days. For each point of the release curve, 1 ml of external buffer solution was analysed with UV-VIS and put back into the external buffer.

DOX release of CP305_41 and CP244_41 NPs was performed at 37 and 41 °C in a phosphate buffer solution (0.1 M, pH 7.4). 2 ml of freshly prepared NPs (CP 0,625 mg/ml, DOX 0,625 mg/ml) were placed inside a dialysis membrane (MWCO=12-14 KDa). The membranes were put into a sealed glass vials containing 10 ml of buffer and left under moderate stirring for 3 days. The test was performed at 37 °C and 41 °C (2° above the estimated VPTT of the microgels).

➤ *Drug release and uptake using Float-A-LyzerTM*: Dialysis membrane were activated before utilization using the following protocol. First, the devices were filled with 20% ethanol solutions and agitated in the same solutions for 30 min. Then, membranes were filled with milliQ water and agitated in milliQ water for 30 min. Finally, the membranes filled with the external buffer used for the experiment (PBS 0.1 M, pH=7.4) and left under agitation in the same solution overnight. 1 ml of freshly prepared NPs+CP244_41 and +CP305_41 NPs (CP 0.99 mg/ml, DOX 0.752 mg/ml) were dialysed against 20 ml of buffer using the Float-A-Lyzer plastic holder as a container for the external buffer under moderate stirring for 3 days. The test was performed at 25 °C and 41 °C (2° above the VPTT of the microgels).

➤ *Drug release and uptake using Slide-A-Lyzer™*: Slide-A-Lyzer™ devices were prepared by leaving the membrane in contact with the external buffer (PBS 0.1 M, pH=7.4) under agitation for 30 min. 1 ml of freshly prepared NPs+CP244_41 and +CP305_41 NPs (CP 0.99 mg/ml, DOX 0.752 mg/ml) were dialysed against 45 ml of buffer using the Float-A-Lyzer falcon as a container for the external buffer under moderate stirring for 3 days. The test was performed at 25 °C and 41 °C (2° above the VPTT of the microgels).

Drug release mechanism were analysed using first order, Higuchi²⁹³ (Equation 54, see Appendix II), Korsmeyer-Peppas²⁹²(Equation 55) and double exponential kinetic models^{294,358,359}(Equation 56-57).

11.3.6 FT-IR spectroscopy

The FT-IR spectra of the products were recorded with a double-beam Perkin Elmer System 2000 Ft-IR Spectrometer (Perkin Elmer, (Waltham, MA, USA) in the range of 4500–370 cm⁻¹ using KBr pellets.

11.3.7 NMR spectroscopy

NMR spectra were acquired using three different spectrometers: a Varian 400 MHz, a Varian 500 MHz spectrometer and a High-resolution 500 MHz Bruker NEOn500 Quadruple resonance (H/C/N/2H) equipped with a high-sensitivity TCI 5mm CryoProbe. 400 MHz Varian spectrometer was used for the acquisition of ¹H spectra operating at 25 °C with a minimum number of 16 scans, using a relaxation delay of 2s. PNVCL samples were analysed in D₂O with a concentration between 5 and 10 mg/ml. CS and CP samples were analysed in D₂O/DCl (1%) at a concentration of 5 mg/ml. All samples were analysed using a minimum volume of 600 µL.

500 MHz Varian was used for the acquisition of ¹H, ¹³C, 2D-HSQC, 2D-COSY and 2D-TOCSY spectra.

¹H spectra of PNVCL and CP were acquired at 25 °C and 35 °C depending on the sample, operating with a minimum number of 16 scans and a relaxation delay of 2s. NMR analyses of CS and +CS were performed at 70 °C. The analysis of the miscibility behaviour of CP was performed by acquiring different ¹H NMR spectra at 25 °C, 40 °C, 55 °C and 70 °C, respectively.

2D-COSY spectra were acquired at 25 °C, with a minimum number of 16 scans and a relaxation delay of 1s.

2D-TOCSY spectra were acquired at 25 °C, with a minimum number of 32 scans and a relaxation delay of 1s.

2D-HSQC spectra were acquired at 25 °C and a relaxation delay of 1s. PNVCL samples were analysed in D₂O with a concentration between 5 and 10 mg/ml. CS and CP samples were analysed in D₂O/DCl (1%) at a concentration of 5 mg/ml. All samples were analysed using a minimum volume of 600 µL.

500 MHz Bruker spectrometer was used for the acquisition of ¹H, ¹³C, 2D-HSQC, 2D-HSQC DEPT, DOSY, ¹³C-CP-MAS and ¹³C-HP-DEC. 55 °C and 70 °C, respectively. ¹H analyses were performed at 20 °C, operating with 32 scans and a pulse delay of 20s for CP samples and 20 scans and a pulse delay of 12s for PNVCL samples. 2D-DOSY analyses were performed at 20 °C, operating with 16 scans and a pulse delay of 12s. ¹³C analyses of PNVCL samples were performed at 25 °C, operating with 10'000 scans and a pulse delay of 1s.

HSQC and HSQC-DEPT analyses of PNVCL samples were performed at 25 °C, operating with 24 scans, a pulse delay of 2s. Spectra were collected as TD 1024/320 experiments. PNVCL samples were analysed at a concentration of 25 mg/ml, CP samples were analysed at a concentration of 8,33 mg/ml. All liquid sample were analysed using a minimum volume of 600 µL.

Solid state NMR analyses were performed at 25 °C using a High Resolution 500 MHz Bruker Advance HD solid state probe – MASSB-DR-BB/1H&19F-3.2mm using a spin rate of 22 kHz. CP-MAS spectrum was acquired using 4000 scans and a relaxation time of 8s, HPDEC was acquired using 16000 scans and a relaxation time of 2s.

11.3.8 *Size exclusion chromatography*

High Performance Size Exclusion Chromatography Triple Detector Array (HP-SEC-TDA) Size was performed with a Viscotek TDA 302 (HP-SEC-TDA, Viscotek, USA) consisting of an online two channel degasser, a high pressure pump, an autosampler (all parts integrated in the GPCmax, Viscotek, USA), a 0.5 mm stainless steel in-line filter with a nylon membrane, two serially connected ViscoGEL columns (TSKgel G4000PWXL, 7.8x300 mm), a temperature controlled triple detector array (TDAmx 305, Viscotek, USA) with a differential refractometer at λ=660 nm (RID 3580), a right angle (90°) light scattering detector (RALS) and a low angle (7°) light scattering detector (LALS 270-03) with a semiconductor laser diode at λ=670 nm and a Anton Paar MCR92 viscometer. The SEC conditions were as follows: a degassed 0.3 M CH₃COOH/0.3 M CH₃COONa buffer (pH = 4.5) was used as solvent, PNVCL₂₄₄ concentration was 4 mg/ml and PNVCL₁₂₂₀ concentration was 2 mg/ml. The injection volume was 100 µL, flow rate

was maintained at 0.6 ml/min, and the column and detectors temperature were kept at 25 °C. Before injection, PNVCL-COOH solutions were filtered through a 0.45 µm cellulose nitrate disposable membrane. The eluent was filtrated through a 16–40 µm glass filter to ensure a low light scattering noise level. A polyethyleneoxide standard ($M_w = 22,411$, $[\eta] = 0.384$ dL/g, $M_w/M_n = 1.03$) was used to normalize the viscometer and the light scattering detectors. Data acquisition and processing were carried out by use of OmniSEC 4.1 software (Viscotek Corporation). A dn/dc of 0.1700 was used for the M_w calculation⁷. The combination of online viscometer and light scattering detector provides essential information on the R_h of polymers in solution according to Einstein-Stokes' equation (Equation 39).

11.3.9 Viscosimetry

The intrinsic viscosity $[\eta]$ of CS was measured at 25 °C by means of a CT 1150 Schott Geräte automatic measuring apparatus and a Schott capillary viscometer as reported by P. Sacco *et al.*²⁵², using acetate buffer (20mM, pH 4.5, NaCl 100 mM) as a solvent³⁶⁰. PNVCL-COOH polymers $[\eta]$ was measured at 25 °C using water as a solvent. Polymers were filtered prior to the analysis through 0.45 µm nitrocellulose filters (Millipore, Germany). $[\eta]$ was calculated from the polymer concentration dependence of the reduced specific viscosity, η_{sp}/c , and of the reduced logarithm of the relative viscosity (inherent viscosity), $\ln(\eta_{rel})/c$. Reduced specific viscosity and inherent viscosity calculation was achieved using the Huggins (25) and Kraemer (26) equations, respectively:

$$\eta_{red} = \frac{\eta_{sp}}{c} = [\eta] + k[\eta]^2c \quad (25)$$

$$\eta_{inh} = \frac{\ln\eta_{rel}}{c} = [\eta] - k'[\eta]^2c \quad (26)$$

where k and k' are the Huggins and Kraemer constants, respectively. $[\eta]$ was calculated as an average of the values calculated by applying both equations. The corresponding viscosity average molecular weight (M_η) of CS was calculated in agreement to the MHS equation (27).

$$[\eta] = K \cdot M_\eta^\alpha \quad (27)$$

For CS, K and parameters are 8.43×10^3 and 0.92, respectively³⁶⁰.

The intrinsic viscosity of PNVCL-COOH was calculated by applying the Huggins

equation. M_η was calculated using the MHS equation using K and a parameters value of 35 and 0.57, respectively¹⁹⁰.

11.3.10 X-Ray Diffraction (XRD)

X-ray diffraction patterns were obtained using a Bruker Siemens D5000 powder X-ray diffractometer. The samples were placed in a plastic holder and scanned over a 2θ range using a Bragg-Bentano geometry with a $\theta:2\theta$ scan, with a sample rotation of $0.30^\circ/\text{min}$. The crystallite size of MNPs was calculated using the Debye-Scherrer's formula as follows³⁵³:

$$d \text{ (nm)} = \frac{0,9 \cdot \lambda_{Cu-K\alpha}}{\beta \cdot \cos\theta} \quad (28)$$

In which β was obtained by the FWHM of the (311) peak.

11.3.11 Differential Scanning Calorimetry (DSC)

Thermal properties of the polymers were analysed by using TA Instrument Q100 Differential Scanning Calorimeter (TA Instruments, New Castle, DE, USA). Polymers were encapsulated in a pan and put together with a reference pan on a thermoelectric disk surrounded by a furnace. The differential heat flow between the sample and the reference pan was measured by area thermocouples according to the following equation:

$$q = -\frac{\Delta}{R_r} - \Delta T_0 \left(\frac{R_r - R_s}{R_r R_s} \right) + (C_r - C_s) \frac{d}{dt} - C_r \frac{d\Delta T}{dt} \quad (29)$$

In which ΔT is the difference between sample temperature (T_s) and reference temperature, ΔT_0 is the difference between the base temperature of the sensor (T_0) and T_s , R_r is the thermal resistance of the reference sensor, R_s is the thermal resistance of the sample sensor, C_r is the reference sensor heat capacity and C_s the sample sensor heat capacity. All measurements were performed under N_2 atmosphere with a $10^\circ\text{C}/\text{min}$ heating rate.

11.3.12 Dynamic Light Scattering (DLS)

Dynamic Light Scattering, also known as Photon Correlation Spectroscopy (PCS) or Quasi-Elastic Light Scattering, is a technique that measures Brownian motion and relates it to the size of particles. The instrument measures the speed of particle diffusion by measuring the rate of which the intensity of the scattered light fluctuates. The intensity of the scattered light is measured at a single given angle (90°) and the time fluctuation of the intensity of the scattered radiation is analysed. If the size of the particles is small compared

to the incident wavelength, the scattering is isotropic (Rayleigh Scattering). According to the Rayleigh approximation, the intensity of the scattered light I is proportional to d^6 and to λ^4 . Consequently, larger particles are likely to hide the signal contributions of smaller particles. In the case of nanosystems, the size of the particles is generally comparable to the size of the incident wavelength. In this condition, the scattered light undergoes constructive and destructive interference in space, determining a scattering intensity pattern at different angles. The analysis of such pattern can provide information on the shape and the size particle distribution. DLS are equipped with laser source that provide monochromatic and coherent radiation. Accordingly, DLS analyses allow to see time-dependent fluctuation in the scattering intensity. These fluctuations are related to the fact that the distance between the scatterers constantly changes with time due to particles undergoing Brownian motion. The dynamic information of the particles is derived from an autocorrelation of the intensity trace recorded during the experiment. The second order autocorrelation curve ($g^2(q, t)$) is generated from the intensity trace as follows:

$$g^2(q, t) = \frac{\langle I(t)I(t + \tau) \rangle}{\langle I(t) \rangle^2} \quad (30)$$

where $g^2(q, t)$ is the autocorrelation function at a particular wave vector, q , and delay time, τ , and I is the intensity. $g^2(q, t)$ is related to relates the first order autocorrelation function $g^1(q; \tau)$ according to Siegert's equation as follows:

$$g^2(q, t) = 1 + \beta [g^1(q, t)]^2 \quad (31)$$

where the parameter β is a correction factor that depends on the geometry and alignment of the laser beam in the light scattering setup. At short time delays, the correlation is high because the particles do not have a chance to move to a great extent from the initial state that they were in. The two signals are thus essentially unchanged when compared after only a very short time interval. As the time delays become longer, the correlation starts to exponentially decay to zero. This means that for longer time delays there is no correlation between the scattered intensity of the initial and final states. The exponential decay is related to the motion of the particles and, more specifically, to the diffusion coefficient D . The correlation function decay can be fitted with different numerical methods based on calculations of assumed distributions. If the sample is monodispersed, the decay is a single exponential. The fitting of the correlation function allows the determination of size distribution and polydispersity. DLS analyses are facilitated when particles do not interact through collisions or electrostatic forces between ions. Particle-particle collisions can be

suppressed by dilution, and charge effects are reduced with the utilization of salts to collapse the electrical double layer. The simplest approach, which represent the standard procedure on Zetasizer software, is to treat the first order autocorrelation function as a single exponential decay. This is appropriate for a monodisperse population. Accordingly, the first autocorrelation function can be rewritten as follows:

$$g^1(q, t) = \exp(-\Gamma t) \quad (32)$$

Where Γ is the decay rate. The translational diffusion coefficient D can be derived at a single angle or at a range of angles depending on the scattering wave vector q .

$$\Gamma = q^2 D \quad (33)$$

The diffusion coefficient D provides access to the hydrodynamic radius (R_H) for isotropic particles through the Stokes-Einstein relationship:

$$D = \frac{k_B T}{6\pi\eta R_H} \quad (34)$$

where η is the solvent viscosity and k_B the Boltzmann constant. It is important to note that the size determined by DLS is the size of a sphere that moves in the same manner as the scatterer. If the scatterer is a random coil polymer, the determined size is not the same as the radius of gyration determined by static light scattering. It is also useful to point out that the obtained size will include any other molecules or solvent molecules that move with the particle. In most cases, samples are polydisperse. Thus, the autocorrelation function is a sum of the exponential decays corresponding to each of the species in the population. One of the most common methods to fit DLS autocorrelation functions is the Cumulant method, from which in addition to the sum of the exponentials above, more information can be derived about the polydispersity of the system as follows:

$$g^1(q, t) = \exp(-\Gamma t) \left(1 + \frac{\mu_2}{2!} + \frac{\mu_3}{3!} + \dots \right) \quad (35)$$

Particle size distribution was measured using a Malvern Zetasizer Nano ZS90 (Malvern Panalytical S.R.L., Malvern, UK) with a 90° scattering detector angle, equipped with a 4mW He-Ne laser (λ 632.8 nm). Measurements were performed at different temperature and concentrations using Sarstedt PMMA cuvette (45x12 mm, 4ml). Values reported are average between three analyses, each of which included between 11 and 17 measurements.

11.3.13 *Zeta potential*

Zeta potential measurements were carried out using a Malvern Zeta Malvern Zetasizer Nano ZS90 (Malvern Panalytical S.R.L., Malvern, UK) using DTS1070 folded capillary cells. Values reported were obtained from 100 measurements for each sample.

11.3.14 *Nanoparticle tracking analysis (NTA)*

Nanoparticle Tracking Analysis (NTA) allows for the determination of particle size and particle size distribution in a range between 10 and 200 nm^{361,362}. The method is also referred as Particle Tracking (PT) or Single Particle Tracking (SPT). NTA is based on the analysis of the Brownian motion of investigated particles. The system is composed by a measurement cell, a microscopic objective and a light source. An improved version of the equipment allows for the utilization in fluorescent mode. NTA measurements consist in the recording of videos of particles undergoing Brownian motions in a liquid solution³⁶². Particles are illuminated by laser light and usually appears as white dots floating on a black screen. The identification and determination of the trajectory of the recorded particles in the measurement window (frame) allows for the creation of a particle size distribution. Particle tracking parameters such as track length can be adjusted manually in order to eliminate artifacts caused by scattered light created by bigger particles³⁶³. The diffusion coefficient (D) of each particle is calculated from the recorded particle trajectory. The system analyses the mean square displacement (x^2) in a specified time interval (t):

$$\langle x^2 \rangle = 2kDt \quad (37)$$

Where the value of k refers to the dimensionality of Brownian motions³⁶⁴. The calculated average diffusion coefficient D_{NTA} is independent on the molar concentration of the investigated components and is provided by:

$$D_{NTA} = \frac{\sum D_i N_i}{\sum N_i} \quad (38)$$

Where D_i and N_i are diffusion coefficients and concentrations, respectively. Finally, the hydrodynamic diameter (D_h) is determined from the Stokes-Einstein equation for a known solvent viscosity and temperature (Equation 34).

Compared to DLS, in which the particle size is directly estimated by the intensity of the scattering signal, NTA is more suitable for the analysis of polydisperse systems. The signal has a lower dependency on the size of the particles and is suitable for the recognition of aggregates within monodisperse populations³⁶⁵. Similarly, the technique is more suitable for the analysis of large particles (~500nm) while it is less sensitive for populations below

100 nm. Since particle tracking is derived from the recording, the ability of the software to elaborate accurate information depends on the number of spots analysed in the frames. Consequently, particle concentration has a strong impact on the quality of the measurements. A recommended protocol is to adjust particle concentration in order to reduce the number of particles per frame between 20 and 60. NTA analysis collects data of the concentration versus particle size, particle size versus surface, particle size versus volume and diffusion coefficient versus concentration³⁶⁵.

The instrument used for the analysis was the NanoSight LM10 (NanoSight Ltd, UK) equipped with a PL L 20/0.40 objective, a 655 nm 50 mW laser and a Scientific Marlin F-033B ASG CCD Camera (Allied Vision Technologies GmbH, Germany). The video data for the NTA measurements were collected for 60 seconds (1800 frames), which was repeated three times for each sample. Acquired video data was processed by the software NanoSight NTA version 2.0 to acquire tracks. During the process, the detection threshold was set to an optimal value depending on the nominal particle size and the concentration, while the value was used for the three runs of each sample condition. The recognition radius, or the max jump distance in the NTA software, varied from 6 to 30 pixels, corresponding to a range of 1.1 to 5.4 μm . The recognized tracks produced by the NTA software were used for the determination of the particle size distribution.

11.3.15 *MTT test*

Cytotoxicity of CP microgels was assessed by using the MTT assay. The human liver cell line, HUH7, was cultured DMEM medium at 37 °C and 5% CO₂. HUH7 cells were added (5000 cells per well) in a 96-well plate and were treated in relation to the concentration of DOX (0, 25, 50, 100 and 200 μmol) for 48 h. After that, 10 μL of fresh media and 10 μL of MTT solution was added to the cells and incubated for 4 h at 37 °C. After discarding 85 μL of the culture medium, 50 μL of dimethyl sulfoxide (DMSO) was added to dissolve the precipitates and the plate was left for 10 min at 37°. The absorbance was measured at 570 nm with a Tecan Infinite F200 Pro (Tecan Group Ltd., Männedorf, CH), which determined the measure of viable cells in the plate. Cell viability was calculated in percentage as follow:

$$Viability (\%) = \frac{A_t}{A_c} \cdot 100 \quad (39)$$

where A_t is the absorbance of cells treated with sample and A_c is the absorbance of untreated cells. Statistical analysis was performed by ANOVA followed by Student t-test. Differences with $p < 0.05$ were considered statistically significant.

11.3.16 Cell Titer

The CellTiter-Glo[®] Luminescent Cell Viability Assay is a homogeneous method for the determination cell survival based on ATP quantification. The signal is related to the presence of metabolically active cells. The assay relies on the mono-oxygenation of luciferin catalysed by a thermostable luciferase (Ultra-Glo[™] Recombinant Luciferase) (Figure 97).

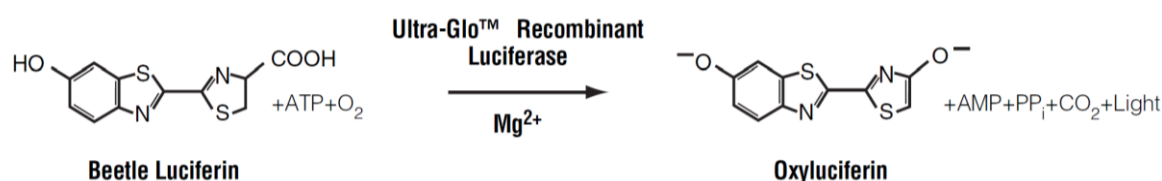


Figure 97 Mono-oxygenation of luciferin catalysed by luciferase in presence of ATP, O₂ and Mg²⁺.

The luminescence of oxyluciferin is proportional to ATP concentration. In this way, the results provide an estimation of cell survival based on the number of metabolically active cells. Due to the intensity and the stability of the signal, the assay can be performed in a wide range of conditions. Cell viability assay was performed on HUH7 cell lines using 2,500 cells per well in a 96-well plate. HUH7 cells were treated according to the following protocol:

1. 100 μ l of HUH7 cells in culture medium were put on opaque-walled multiwell plates (96x). 100 μ l of culture medium were used as a control for the calculation of background luminescence.
2. DOX/CP microgels and DOX solutions were added to the wells and HUH7 cells were incubated at 37 °C.
3. The plate was equilibrated at room temperature for 30 minutes and 100 μ l of CellTiter-Glo[®] Reagent solution was added to the wells.
4. The contents were shaken for 2 minutes on an orbital shaker for the induction of cell lysis. After that, the plate was allowed to incubate at room temperature for 10 minutes to stabilize the luminescent signal.

5. The emission signal of oxyluciferin was recorded at 570 nm using a fluorescence spectrometer.

11.3.17 Immunofluorescence

To visualize the subcellular localization of DOX, HUH7 cell lines treated with DOX, CP and CS NPs were placed on glass slides (25'000 cells for glass slide) and were observed using a fluorescence microscope after 24 h. Glass slides were washed with H₂O and EtOH and left to dry on paper. After that, the slides were treated with 400 µl poly-D-lysine (100 µg/ml) for 5 minutes and washed three times with milliQ water. The washed slides were dried in an incubator for 2-3 h. After that, the cells were detached and were placed into the slides in 1ml of total soil. The cells were allowed to grow at 37 °C, the culture medium was removed. A total of seven slides were prepared that contained, respectively:

- µl of DOX 1 µm + 950 µl soil
- 20 µl of CP305 +and CP244 + 980 µl of soil
- CP244, +CP305, +CP244 and +CS 100 µl sample + 900 µl soil
- 1 ml of soil (control)

All samples were incubated at 37 °C for 24h. At the end of the incubation, 2 images for each slide were acquired using 20x magnification in light field and TRITC (B filter of the microscope) to see the fluorescent signal of the DOX. The culture medium was removed and washed two times with PBS (without Ca/Mg). The cells were attached by using 4% paraformaldehyde PBS solution for 11 min. After that, the cells were washed two times for 5 min with PBS (with Ca/Mg), one time with 0.1 M glycine for 3 min and, finally, three times for 5 min with PBS (with Ca/Mg). After that, another 2 images were taken for each slide in light field and TRITC. Finally, the slides were washed again with H₂O and EtOH and dried on paper. The solution was dripped on the slide and rinsed quickly in H₂O to remove the remaining PBS and was placed it on the upright of the microscope with the cells facing the solution. The upright was allowed to dry for 1-2 h at room temperature. After that, the glasses were sealed and stored at 4 °C. Finally, three images for each slide were acquired in the light field and TRITC using a 40x magnification lens.

11.3.18 Optical microscopy

HUH7 cell lines were observed during treatment using Leitz Diavert inverted optical Microscope (Leica Microsystems GmbH, Wetzlar, Germany).

11.3.19 Fluorescence microscopy

DOX cell intercalation fluorescence was cell lines treatment using Nikon Eclipse TI Fluorescence Microscope (Nikon Corporation, Minato, JP). The inverted microscope is equipped with an OKOLAB H101 stage-top incubator with CO₂, humidity and temperature control for the imaging of cell cultures. High quality fluorescence images are obtained with a Nikon Plan Apo 60x 1.4NA oil immersion objective. DOX fluorescence was detected using a TRITC filter (bandpass windows from 545 to 565 nm), using a 130W mercury lamp as fluorescent light source. The image capture is performed by a sensitive monochrome Hamamatsu Orca R2 CCD camera with active cooling.

11.3.20 Transmission electron microscopy

The micrographs were acquired using a Philips EM 208 microscope Transmission Electron Microscope (Philips, Amsterdam, NL). Samples were exposed to high energy electrons (up to 100 KeV) that were transmitted to a fluorescent screen and converted by a Quemesa CCD camera (Olympus Soft Imaging Solutions GmbH, Muenster, DE) into a larger image file. Image acquisition was performed using RADIUS Software. All samples for TEM were prepared by putting a single drop onto a carbon-covered 200-mesh copper grid. After air-drying overnight at room temperature, both particle and raw materials were observed.

Chapter 12: Conclusions

In the present thesis, a protocol was developed for the fabrication of CP thermoresponsive microgels by ionotropic gelation for the treatment of HUH7 cell lines with DOX. The work used a bottom-up approach, that started from two simple elements: NVCL, the monomer for the polymerization of thermoresponsive PNVCL, and CS. During the three years of studies, the issues were addressed primarily from the chemico-physical point of view. In particular, the critical points were related to the poor reproducibility of the published studies CP nanosystems and the encapsulation of the DOX within CS-based polymer vectors.

Polymerization of PNVCL-COOH polymers was achieved by FRP, using AIBN as initiator and MPA to obtain carboxyl group terminations that were necessary for subsequent condensation reactions. The non-reproducibility of the procedures used confirmed the hypothesis that the LCST of PNVCL depends on the molecular mass. This observation is in strong contrast to the statement that PNVCL, like PNIPAM, has a LCST at 32° C that is independent of its molecular mass. As we previously mentioned, this information was

erroneously reported by a variety of scientific publications^{91,93,99,104,108,185,223,303-305}. The hypothesis of mass-dependent LCST was first supported by the comparison of ¹³C NMR spectra of different PNVCL-COOH, assessing the variation of the signals related to the terminations as a function of the NVCL/AIBN ratio that were used for the synthesis. Finally, the determination of the viscosimetric mass demonstrated that the LCST of PNVCL-COOH is inversely proportional to the molecular mass. LCST was characterized using UV-VIS and LCST at a concentration of 5 mg/ml. The critical miscibility behaviour was also observed in relation to the concentration of the polymer, NaCl and three different buffers: citrate (pH 3), acetate (pH 5) and phosphate (pH 7). In particular, it was observed that it is possible to increase LCST by decreasing PNVCL-COOH concentration, while the presence of salts, in particular phosphate, allows to significantly lower the LCST. This observation is particularly useful for physiological applications, since the polymers undergoing LCST form aggregates that are potentially cytotoxic. In-vitro evaluation tests on HUH7 cells excluded the toxicity of PNVCL244 up to a concentration of about ~1 mg/ml. It was that the LCST is required to be at least 4 °C higher (≥ 41 °C) than the cell incubation temperature to prevent cytotoxic effects.

The critical miscibility behaviour of three PNVCL samples (122, 305 and 1220) were observed in human plasma at the concentration of 5 mg/ml. According to the previous observations, the results showed that the plasma matrix, due to the presence of salts and proteins, leads to a drop in temperature of about 10 °C.

For the synthesis of CP polymers, two different types of CS with different molecular weight and DDA. CP polymers were synthesized by condensation with EDC/NHS. For the synthesis of polymers, different CS/PNVCL ratios were used in order to obtain different LCST depending on the degree of substitution. The results showed that CP polymers exhibit higher LCSTs in relation to the corresponding PNVCL polymers. Preliminary evaluations on HUH7 cell lines showed partial biocompatibility of polymers due to their insolubility and lowering of LCST due to cell culture conditions.

The method for the preparation of CP microgels was developed by initially working on CS particles. The procedure was optimised by studying the variation of particle properties in relation to polymer concentration, polymer-TPP ratio, reaction temperature and pH. The utilization of NaCl aqueous solution allowed to reduce particle size and polydispersity. In this way, it was possible to obtain particles with a size between 150 and 300 nm with a high surface charge (>30 mV). The analysis of the behaviour of the particles as a function of pH allowed to exclude that CS microgels are pH responsive. Formulations exhibited

poor stability for pH above 6.

The preparation of thermoresponsive CP microgels was realized via ionotropic gelation, by redefining the amounts of CP/TP due to the decrease of the available amino groups on the copolymer particles. In this way, it was possible to prepare CP NPs with a D_h between 150 and 170 nm and a surface charge between 13 and 15 mV. The particles showed stability up to a pH of 6.5 and their conservation was studied. The suspensions retained their properties for a period of 28 days at 4° C, but their lyophilization lead to the formation of irreversible aggregates.

The preparation of magneto-thermoresponsive microgels (CP MNPs) was achieved by dispersing MNPs particles with a size around 12 nm into the structure of the microgels. The formulations of CP MNPs were very unstable and the presence of MNPs within the polymer was confirmed by TEM micrographs.

Due to their fragility, CP microgels were considered suitable for precipitation a purification procedure composed centrifugation and resuspension. The particles were purified by using centrifugations at low rates in order to selectively precipitate the aggregates.

The possibility to encapsulate DOX inside CP microgels was studied through different procedures, including the fabrication of particles in the presence of DOX and the incubation at $T > VPTT$ in order to induce the uptake of DOX. DOX release tests showed that uptake can be induced after a minimum incubation period of 4 h due to particle destabilization induced by the conformational change. The release mechanisms at 25, 39, and 41 °C were interpreted by using several mathematical models, including a double-exponential model for the description of a release mechanism followed by uptake. Similarly, micrometric particles were prepared by precipitating the copolymer in the presence of DOX.

DOX-loaded particles were observed under the fluorescent microscope and showed a size between 1 and 40 μm and a strong fluorescence signal caused by the presence of DOX. Their utilization on HUH7 cells minimum cell survival rate.

Accordingly, CP micro- and nanogels prepared with ionotropic gelation does not to have great potential for drug-delivery applications of small drugs such as DOX. Due to their extreme fragility, the particles are easily subjected to the formation of aggregates under centrifugation, and this compromise the ability to separate them from non-encapsulated drug. In addition, the copolymeric particles have a limited range of pH and temperature application. However, micrometric systems ($>1 \mu\text{m}$) have potential for HCC treatment by

Appendices

TACE. Up to this date, thermoresponsive delivery systems have not yet been applied for HCC system. In the future, further investigation is required in order to provide the conditions for the utilization of CP polymers. According to preliminary observations, the utilization of copolymers that exhibit a $VPTT > 41$ °C may avoid cytotoxic effects at 37 °C. Furthermore, since DOX encapsulation was achieved within aggregated CP microgels, the low stability of magnetic microgels does not necessarily represent a limitation for the fabrication of magneto-responsive micrometric DOX-eluting microparticles. In this way, it is possible to develop a new type of DEB-TACE, based on the release of DOX by exposing them to alternating magnetic fields^{99,104,108}. In the future, this would require the determination of appropriate conditions for the synthesis of microparticles with a specific size.

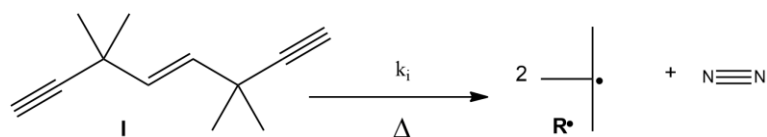
Appendices

I: Free radical polymerization of PNVCL

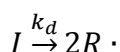
To date, free radical polymerisation (FRP) represents the most largely used pathway to synthesise polymers in academic facilities and industry^{366,367}. FRP is a chain growth polymerisation technique in which monomer concentration decreases rapidly as the polymerisation proceeds. Consequently, FRP can provide high molecular weight polymers at low conversion. FRP is commonly used for a wide range of vinyl monomers and is highly regarded for its versatility in respect to a variety of functional groups. Unlike ionic or coordination polymerization, FRP is tolerant of impurities and can be carried out over a wide temperature range (-80 to 250 °C)³⁶⁸. In addition, FRP can be conducted in organic or aqueous solutions, in suspension, in emulsion or in bulk. During the reaction, the presence of highly reactive free radicals allows to produce high molecular weight polymer in short reaction times. It has been estimated that the lifetime of a propagating chain in FRP is approximately one second³⁶⁹. However, due to the high reactivity of the free radicals, FRP is not suitable for the control of molecular length, polydispersity and polymer architecture³⁷⁰. FRP is commonly described as a three-step process which include initiation, propagation and termination. The formation of the free radical initiating species is usually generated from the thermal decomposition of an azo or peroxide compound. Electromagnetic radiation can be also used to irradiate these compounds to fragment them into radical species. Other radical sources can initiate provide the formation of free radicals

Appendices

via electrolysis or the utilization of ionizing radiation (α , β , γ , x-rays) or redox initiation³⁷¹. The polymerization of PNVCL is initiated by the thermal decomposition of AIBN on the C-N monomer.

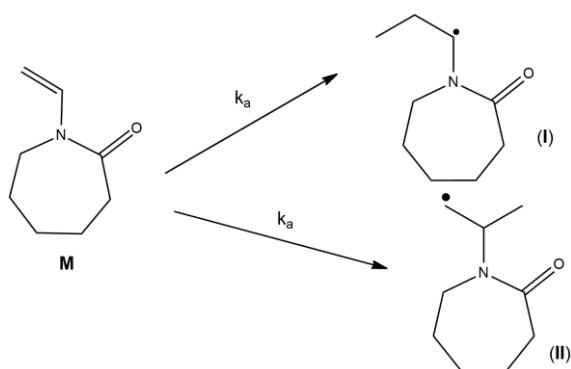


In FRP, the rate controlling step is the decomposition of radical initiator (R_d):



$$R_d = \frac{-d[I]}{dt} = k_d[I] \quad (40)$$

This generates a radical that attack the monomer molecule, NVCL, on the C=C bond of a vinyl monomer. This generates a propagating radical capable of attacking other NVCL molecules. The addition can occur at both the vinylic carbons:



The rate of initiation (R_i) can be described as:

$$R_i = \frac{d[M \cdot]}{dt} = k_i[I][M] \quad (41)$$

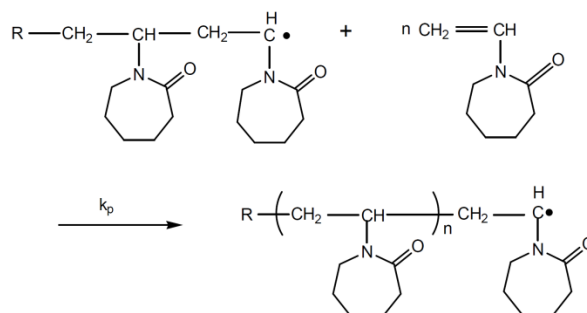
and:

$$R_i = 2k_d f [I] \quad (42)$$

Where f is efficiency of the initiator. Typical values are between 0.3 – 0.8³⁷². The efficiency is reduced by the occurring of side reaction that involves the initiator, such as primary recombination or induced decomposition. Induced composition occurs when a radical reacts with an unreacted initiating compound and generate inactive species. Since the reaction leads to the formation of the most stable product, the formation is radical (I) is favoured. Also, the formation of radical (I) is favoured due to the resonance effects of the substituent³³⁶. The propagation rate constant is generally considered to be independent from the length of the molecular chains.

Appendices

During the propagation step, the growing polymer reacts with the monomer several times and the length of the chain increases.



The rate of polymerisation (R_p) can be written as:

$$R_p = \frac{-d[M]}{dt} = k_d[M][M \cdot] \quad (43)$$

The rate of propagation can be described by this equation:

$$R_p = k'[M][I]^{1/2} \quad (44)$$

Where

$$k' = \left(\frac{k_p^2 k_{df}}{k_t}\right)^{1/2}. \quad (45)$$

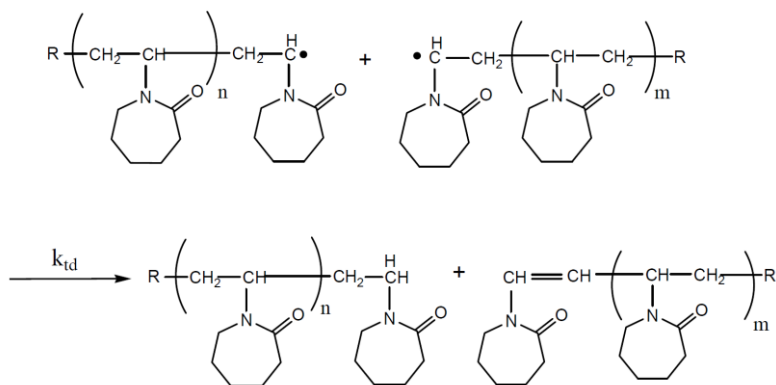
Consequently, the rate of polymerisation is proportional to the concentration of monomer and to the square root of the concentration of the initiator. The growth of the polymer chain is stopped by the termination reaction. The termination reaction can through combination and disproportionation. Combination occurs when two radicals form a covalent bond and form a single chain.

The rate of termination (R_t) due to coupling of polymer chains is given by:

$$R_t = \frac{-d[M \cdot]}{dt} = 2k_t[M \cdot]^2 \quad (46)$$

When disproportionation occurs, a hydrogen atom is transferred by a free radical from an active chain and a double carbon bond is formed.

Appendices



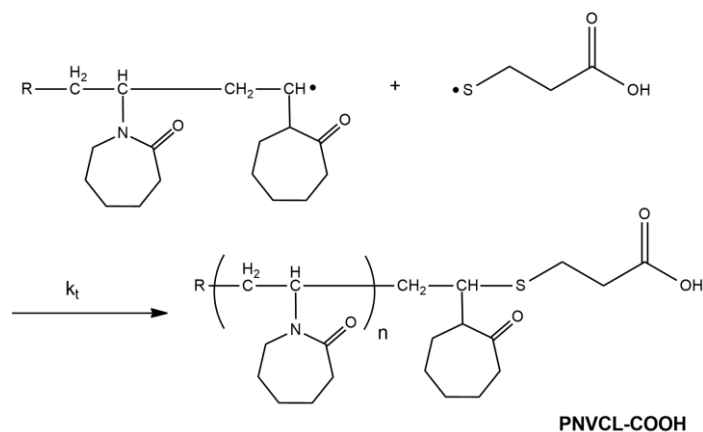
The rate of termination (R_{td}) due to disproportionation is given by:

$$R_{td} = 2k_d[M \cdot]^2 \quad (47)$$

The overall rate of termination is given by:

$$R_T = 2k_d f [I] \quad (48)$$

The presence of MPA in excess prevents the formation of species C and D and favours the formation of sulfanylpropionic acid derivative (PNVCL-COOH). Since the rate of termination is only by the initiator radical, the presence of a termination agent does not affect the rate of the reaction.



II: Polymer conjugation with EDC/NHS

Due to its ability to form conjugates between two protein or polymer molecules, EDC represent the most popular zero-length crosslinker for biochemical conjugations. Direct EDC mediated crosslinking is achieved without EDC becoming part of the final amide bond between the target molecules. EDC has the advantage of being water soluble and it has been extensively used as it dissolves in aqueous buffer solutions that are commonly use for the preparation biological macromolecules solution. The reaction by-product, isourea, is dissolved into the reaction medium allowing easy purification of the crosslinked product.

Appendices

The solutions are usually purified with dialysis, precipitation, chromatography, or ultrafiltration.

NHS or its water-soluble analog (Sulfo-NHS), are commonly used in conjunction with EDC as they provide higher coupling efficiency and more stable amine-reactive intermediates. The first step of the reaction consists in the activation of carboxyl groups by EDC which results in the formation of an amine reactive O-acylisourea intermediate. The intermediate reacts spontaneously with primary amines to form an amide bond and an isourea by-product. Due to the instability of the O-acylisourea intermediate in water, the failure of the reaction will provoke the hydrolysis of the intermediate, thus regenerating of the carboxyl groups and releasing an N-substituted urea. A common procedure is to quench the activation of EDC with a thiol such as 2-mercaptoethanol. The addition of NHS induces the coupling between EDC couples and NHS carboxyls. This provide the formation of an NHS ester that is significantly more stable than the O-acylisourea intermediate and allows for efficient conjugation to primary amines at buffer pH.

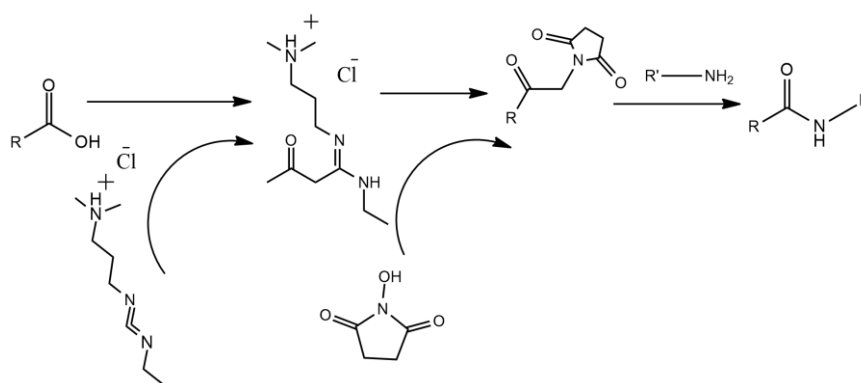


Figure 98 Mechanistic steps for EDC/NHS mediated coupling of carboxylic acids and amides under acidic conditions.

III: Mathematical models for drug release

Mathematical models describe the dependence of drug release in function of time. In this section, a brief explanation of the models used for the interpretation of the data is provided.

III.1 Zero order kinetics

For zero-order kinetics, the release of a therapeutic is only a function of time. Drug release takes place at a constant rate that is independent of active agent concentration. Zero order drug delivery systems are of particular interest from the pharmaceutical point of view as the drug versus time relationship is ideal for sustained drug release³⁷³. The fraction of drug release f_t is provided by the equation as follows:

$$f_t = K_0 t \quad (49)$$

III.II First order kinetics

In non-Fickian diffusion, drug release can be affected by several factors. First order kinetics have been used to describe absorption or elimination from a porous matrix. Drug released is proportional to the amount of drug that remains inside the matrix. Consequently, the rate of release tends to decrease over time. The variation of solute passing to the solution dW/dt is provided by the following equation, as proposed by Hixson and Cromwell²⁹⁴:

$$\frac{dW}{dt} = k(V C_s - W) \quad (50)$$

Where V is the volume and C_s is the equilibrium solubility. After integration, the equation that results is:

$$W = V C_s (1 - e^{-kt}) \quad (51)$$

The equation is transformed by applying decimal logarithms in the following form:

$$\log(V C_s - W) = \log V C_s - \frac{kt}{2.303} \quad (52)$$

Since $V_s - W$ is equal to the mass Q, the equation is usually applied as follows:

$$\log Q_t = \log Q_0 + \frac{kt}{2.303} \quad (53)$$

In the present thesis, data were interpreted using the form of Equation 52. The value of $V C_s$ provided the asymptotic value of the exponential curve.

III.III Higuchi model

The mathematical model proposed by Higuchi in 1961 is one of the most applied equation for the interpretation of the release rate of drugs from porous matrices^{293,294}. The equation describes the behaviour drug particles dispersed in a uniform matrix that behaves as the diffusion media and it has been applied extensively to planar systems, such as hydrogels. The simplified form of Higuchi model, which relates the concentration of active agent to the square root of time³⁷³. These conditions are met if the swelling and the dissolution of the matrix are negligible, the drug has a constant diffusivity and perfect sink conditions are attained²⁹⁴. The equation is usually applied as follows:

$$\frac{Q_t}{Q_\infty} = K_H t^{0.5} \quad (54)$$

Where Q_t/Q_∞ is the percentage of drug released at a specific timepoint.

III.IV Korsmeyer-Peppas model

Korsmeyer and Peppas is a semi-empirical power law model that describes drug release from a polymeric system. The fraction of released drug as a function of time is provided as follows:

$$\frac{Q_t}{Q_\infty} = K_{KP}t^n \quad (55)$$

The equation is useful to study systems where the release mechanism is not known³⁷³. In general, the release mechanism is provided by a combination of different processes: diffusion, relaxation and drug transport. The value of n establishes a classification according to the geometry of the delivery system and the mechanism model. The classification allows to establish if the behaviour is Fickian or non-Fickian. In the case of spherical NPs, the value of n for Fickian behaviour is 0.43. Fickian behaviour are governed by diffusion. Depending on the n value, there are three types of non-Fickian behaviour: case II, anomalous transport and super case II). When $n=1$, the model corresponds to zero-order kinetics and the driving mechanism is the swelling or the relaxation of the polymeric network. When $0.43 < n < 0.85$, the model is anomalous transport and drug release is driven by both swelling and diffusion. Finally, the super case II model ($n > 0.85$) is an extreme form of transport that is characterized by the breaking of the polymer or solvent crazing²⁹⁴.

III.V Double exponential models

In this thesis, two different types of double exponential models were applied for the interpretation of experimental results. Double exponential functions are not commonly used for the interpretation of drug kinetics. This type of models is most commonly applied in the field of physical or surface chemistry. For example, double exponentials are used to describe the saturation of a surface or the experimental behaviour of flash signal³⁷⁴. In general, a double exponential model allows to interpret a phenomenon as the combination of two kinetic events characterized by two different rates. In this thesis, the following exponential model was proposed for the interpretation of a system reaching saturation:

$$f_t = A + Be^{k_1t} + Ce^{k_2t} \quad (56)$$

In drug release mechanism, A represents the amount of drug required to reach saturation C_sV . Accordingly, the equation is analogous to first order kinetics. The two models usually provide similar correlation values for the interpretation of the same data. The first k_1 usually has a higher value and can be easily correlated to the fraction of the drug that is not bound to the polymer, while k_2 is associated to the slower process that leads to equilibrium.

Appendices

When $k_2 > k_1$, the second event is faster. In this case, the release behaviour is best described by a power law.

Some systems can exhibit radical change of behaviour over time. If slope of the release function df_i/dt becomes negative, a possible interpretation is that the polymer starts encapsulating the drug. If the release curve has a positive slope in the initial phase and a negative slope a second phase, the following double-exponential model can be applied:

$$f_t = A(e^{-k_1 t} - e^{-k_2 t}) \quad (57)$$

In which A represent the maximum of the curve and, k_1 describes the release rate and k_2 the rate of the uptake that occurs during the conformational change of the polymer.

References

1. Melchiorre, F. *et al.* DEB-TACE: A standard review. *Future Oncology* (2018) doi:10.2217/fon-2018-0136.
2. Lencioni, R. Management of hepatocellular carcinoma with transarterial chemoembolization in the era of systemic targeted therapy. *Critical Reviews in Oncology/Hematology* (2012) doi:10.1016/j.critrevonc.2011.10.008.
3. Sergio, A. *et al.* Transcatheter arterial chemoembolization (TACE) in hepatocellular carcinoma (HCC): The role of angiogenesis and invasiveness. *Am. J. Gastroenterol.* **103**, 914–921 (2008).
4. Fuchs, K. *et al.* Drug-eluting embolic microspheres for local drug delivery – State of the art. *Journal of Controlled Release* (2017) doi:10.1016/j.jconrel.2017.07.016.
5. Huang, K., Zhou, Q., Wang, R., Cheng, D. & Ma, Y. Doxorubicin-eluting beads versus conventional transarterial chemoembolization for the treatment of hepatocellular carcinoma. *J. Gastroenterol. Hepatol.* **29**, 920–925 (2014).
6. Kim, D.-H. & Larson, A. C. Nanocomposite Carriers for Transarterial Chemoembolization of Liver Cancer. *Interv. Oncol.* **360** **4**, E173–E182 (2016).
7. Cortez-Lemus, N. A. & Licea-Claverie, A. Poly(N-vinylcaprolactam), a comprehensive review on a thermoresponsive polymer becoming popular. *Prog. Polym. Sci.* **53**, 1–51 (2016).
8. Mohammed, M. N., Bin Yusoh, K. & Shariffuddin, J. H. B. H. Poly(N-vinyl caprolactam) thermoresponsive polymer in novel drug delivery systems: A review. *Mater. Express* **8**, 21–34 (2018).
9. Tiwari, G. *et al.* Drug delivery systems: An updated review. *Int. J. Pharm. Investig.* (2012) doi:10.4103/2230-973x.96920.
10. Kreuter, J. & Speiser, P. P. In vitro studies of poly(methyl methacrylate) adjuvants. *J. Pharm. Sci.* (1976) doi:10.1002/jps.2600651115.
11. Vert, M. *et al.* Terminology for biorelated polymers and applications (IUPAC recommendations 2012). *Pure Appl. Chem.* (2012) doi:10.1351/pac-rec-10-12-04.
12. Lee, B. K., Yun, Y. H. & Park, K. Smart nanoparticles for drug delivery: Boundaries and opportunities. *Chem. Eng. Sci.* (2015) doi:10.1016/j.ces.2014.06.042.
13. Navya, P. N. *et al.* Current trends and challenges in cancer management and therapy using designer nanomaterials. *Nano Convergence* (2019) doi:10.1186/s40580-019-0193-2.
14. Xin, Y., Yin, M., Zhao, L., Meng, F. & Luo, L. Recent progress on nanoparticle-based drug delivery systems for cancer therapy. *Cancer Biology and Medicine* (2017) doi:10.20892/j.issn.2095-3941.2017.0052.
15. Hartshorn, C. M. *et al.* Nanotechnology Strategies to Advance Outcomes in Clinical Cancer Care. *ACS Nano* (2018) doi:10.1021/acsnano.7b05108.
16. Parvanian, S., Mostafavi, S. M. & Aghashiri, M. Multifunctional nanoparticle developments in cancer diagnosis and treatment. *Sensing and Bio-Sensing Research* (2017) doi:10.1016/j.sbsr.2016.08.002.
17. Park, W., Heo, Y. J. & Han, D. K. New opportunities for nanoparticles in cancer immunotherapy. *Biomaterials Research* (2018) doi:10.1186/s40824-018-0133-y.

References

18. Buabeid, M. A., Arafa, E. S. A. & Murtaza, G. Emerging Prospects for Nanoparticle-Enabled Cancer Immunotherapy. *Journal of Immunology Research* (2020) doi:10.1155/2020/9624532.
19. Rocha, M., Chaves, N. & Bào, S. Nanobiotechnology for Breast Cancer Treatment. in *Intech* vol. i 411–432 (2017).
20. Hervault, A. & Thanh, N. T. K. Magnetic nanoparticle-based therapeutic agents for thermo-chemotherapy treatment of cancer. *Nanoscale* **6**, 11553–11573 (2014).
21. Rink, J. S., Plebanek, M. P., Tripathy, S. & Thaxton, C. S. Update on current and potential nanoparticle cancer therapies. *Current Opinion in Oncology* (2013) doi:10.1097/CCO.000000000000012.
22. Abadeer, N. S. & Murphy, C. J. Recent Progress in Cancer Thermal Therapy Using Gold Nanoparticles. *Journal of Physical Chemistry C* (2016) doi:10.1021/acs.jpcc.5b11232.
23. Amreddy, N., Babu, A., Muralidharan, R., Munshi, A. & Ramesh, R. Polymeric Nanoparticle-Mediated Gene Delivery for Lung Cancer Treatment. *Top. Curr. Chem.* **375**, (2017).
24. Nichols, J. W. & Bae, Y. H. EPR: Evidence and fallacy. *J. Control. Release* **190**, 451–464 (2014).
25. Danhier, F. To exploit the tumor microenvironment: Since the EPR effect fails in the clinic, what is the future of nanomedicine? *J. Control. Release* **244**, 108–121 (2016).
26. Chadha, N. *et al.* Engineered nanoparticles associated metabolomics. *J. Hazardous, Toxic, Radioact. Waste* **20**, (2016).
27. Pucci, C., Martinelli, C. & Ciofani, G. Innovative approaches for cancer treatment: Current perspectives and new challenges. *ecancermedicalscience* (2019) doi:10.3332/ecancer.2019.961.
28. Greten, T. F., Wang, X. W. & Korangy, F. Current concepts of immune based treatments for patients with HCC: From basic science to novel treatment approaches. *Gut* (2015) doi:10.1136/gutjnl-2014-307990.
29. Taieb, J., Barbare, J. C. & Rougier, P. Medical treatments for hepatocellular carcinoma (HCC): What's next? *Ann. Oncol.* **17**, x308–x314 (2006).
30. L. Simel, D. Approach to the Patient: Hystory and Physical Esamination. in *Goldman-Cecil Medicine* (eds. Goldman, L. & I. Schafer, A.) 1166–1195 (Elsevier, 2019).
31. Franks, T. What Is Standard Therapy in Cancer Treatment? *Translational Drug Development* [https://www.td2inc.com/news/what-is-standard-therapy-in-cancer-treatment#:~:text=Standard therapies for treating cancer,they are contained or localized.](https://www.td2inc.com/news/what-is-standard-therapy-in-cancer-treatment#:~:text=Standard%20therapies%20for%20treating%20cancer,they%20are%20contained%20or%20localized.) (2016).
32. National Cancer Institute. Types of Cancer Treatment. <https://www.cancer.gov/about-cancer/treatment/types>.
33. Medline Plus. Cancer treatments. <https://medlineplus.gov/ency/patientinstructions/000901.htm> (2019).
34. Malhotra, V. & Perry, M. C. Classical chemotherapy: mechanisms, toxicities and the therapeutic window. *Cancer biology & therapy* (2003) doi:10.4161/cbt.199.
35. Ventola, C. L. Progress in nanomedicine: Approved and investigational nanodrugs. *P T* (2017).
36. Martins, J. P. *et al.* The solid progress of nanomedicine. *Drug Deliv. Transl. Res.* (2020)

References

- doi:10.1007/s13346-020-00743-2.
37. Hare, J. I. *et al.* Challenges and strategies in anti-cancer nanomedicine development: An industry perspective. *Adv. Drug Deliv. Rev.* **108**, 25–38 (2017).
 38. Wang, R., Billone, P. S. & Mullett, W. M. Nanomedicine in action: An overview of cancer nanomedicine on the market and in clinical trials. *Journal of Nanomaterials* (2013) doi:10.1155/2013/629681.
 39. Greish, K., Mathur, A., Bakhiet, M. & Taurin, S. Nanomedicine: Is it lost in translation? *Ther. Deliv.* **9**, 269–285 (2018).
 40. Sarmiento, B. Have nanomedicines progressed as much as we'd hoped for in drug discovery and development? *Expert Opinion on Drug Discovery* (2019) doi:10.1080/17460441.2019.1621286.
 41. Wicki, A., Witzigmann, D., Balasubramanian, V. & Huwyler, J. Nanomedicine in cancer therapy: Challenges, opportunities, and clinical applications. *J. Control. Release* **200**, 138–157 (2015).
 42. Krishnamachari, Y., Geary, S. M., Lemke, C. D. & Salem, A. K. Nanoparticle delivery systems in cancer vaccines. *Pharmaceutical Research* (2011) doi:10.1007/s11095-010-0241-4.
 43. Shafei, A. *et al.* A review on the efficacy and toxicity of different doxorubicin nanoparticles for targeted therapy in metastatic breast cancer. *Biomedicine and Pharmacotherapy* (2017) doi:10.1016/j.biopha.2017.09.059.
 44. Resnik, D. B. & Tinkle, S. S. Ethical issues in clinical trials involving nanomedicine. *Contemp. Clin. Trials* (2007) doi:10.1016/j.cct.2006.11.001.
 45. Thorn, C. F. *et al.* Doxorubicin pathways: Pharmacodynamics and adverse effects. *Pharmacogenet. Genomics* (2011) doi:10.1097/FPC.0b013e32833ffb56.
 46. Tacar, O., Sriamornsak, P. & Dass, C. R. Doxorubicin: An update on anticancer molecular action, toxicity and novel drug delivery systems. *Journal of Pharmacy and Pharmacology* (2013) doi:10.1111/j.2042-7158.2012.01567.x.
 47. Gallagher, J. G. Diarrhea. in *Supportive Care in Cancer: A Handbook for Oncologists* (1999). doi:10.5124/jkma.1999.42.3.298.
 48. Benson, A. B. *et al.* Recommended guidelines for the treatment of cancer treatment-induced diarrhea. *Journal of Clinical Oncology* (2004) doi:10.1200/JCO.2004.04.132.
 49. Karakunnel, J. & Modi, A. A. Diarrhea and constipation. in *Cancer Supportive Care: Advances in Therapeutic Strategies* (2008). doi:10.1016/b978-1-4160-4698-1.50049-7.
 50. Batchelor, D. Hair and cancer chemotherapy: Consequences and nursing care - A literature study. *Eur. J. Cancer Care (Engl)*. (2001) doi:10.1046/j.1365-2354.2001.00272.x.
 51. Trusson, D. & Pilnick, A. The role of hair loss in cancer identity. *Cancer Nurs.* (2017) doi:10.1097/NCC.0000000000000373.
 52. Botchkarev, V. A. Molecular mechanisms of chemotherapy-induced hair loss. in *Journal of Investigative Dermatology Symposium Proceedings* (2003). doi:10.1046/j.1523-1747.2003.12175.x.
 53. Richardson, J. L., Marks, G. & Levine, A. The influence of symptoms of disease and side effects of treatment on compliance with cancer therapy. *J. Clin. Oncol.* (1988) doi:10.1200/JCO.1988.6.11.1746.
 54. Minami, M., Matsumoto, S. & Horiuchi, H. Cardiovascular side-effects of modern cancer

References

- therapy. *Circulation Journal* (2010) doi:10.1253/circj.CJ-10-0632.
55. Epstein, J. B. *et al.* Oral complications of cancer and cancer therapy: From cancer treatment to survivorship. *CA Cancer J. Clin.* (2012) doi:10.3322/caac.21157.
 56. de Golian, E., Kwong, B. Y., Swetter, S. M. & Pugliese, S. B. Cutaneous Complications of Targeted Melanoma Therapy. *Current Treatment Options in Oncology* (2016) doi:10.1007/s11864-016-0434-0.
 57. Goldinger, S. M. *et al.* Cytotoxic cutaneous adverse drug reactions during anti-PD-1 therapy. *Clin. Cancer Res.* (2016) doi:10.1158/1078-0432.CCR-15-2872.
 58. Wang, D. Y., Okoye, G. D., Neilan, T. G., Johnson, D. B. & Moslehi, J. J. Cardiovascular Toxicities Associated with Cancer Immunotherapies. *Current Cardiology Reports* (2017) doi:10.1007/s11886-017-0835-0.
 59. Brannon-Peppas, L. & Blanchette, J. O. Nanoparticle and targeted systems for cancer therapy. *Adv. Drug Deliv. Rev.* **56**, 1649–1659 (2004).
 60. Gaumet, M., Vargas, A., Gurny, R. & Delie, F. Nanoparticles for drug delivery: The need for precision in reporting particle size parameters. *Eur. J. Pharm. Biopharm.* **69**, 1–9 (2008).
 61. Rink, J. S., Plebanek, M. P., Tripathy, S. & Thaxton, C. S. Update on current and potential nanoparticle cancer therapies. *Curr. Opin. Oncol.* **25**, 646–651 (2013).
 62. Theek, B. *et al.* Characterizing EPR-mediated passive drug targeting using contrast-enhanced functional ultrasound imaging. *J. Control. Release* (2014) doi:10.1016/j.jconrel.2014.03.007.
 63. Kunjachan, S. *et al.* Passive versus active tumor targeting using RGD- and NGR-modified polymeric nanomedicines. *Nano Lett.* (2014) doi:10.1021/nl404391r.
 64. Jokerst JV, Lobovkina T, Zare RN, G. S. Nanoparticle PEGylation for imaging and therapy. **5**, 379–390 (2010).
 65. Lee, C. C. *et al.* A single dose of doxorubicin-functionalized bow-tie dendrimer cures mice bearing C-26 colon carcinomas. *Proc. Natl. Acad. Sci. U. S. A.* **103**, 16649–16654 (2006).
 66. Liu, F. Controlling Amphiphilic Functional Block Copolymers' Self-Assembly: From Structure to Size. *Glob. J. Nanomedicine* **1**, 1–4 (2018).
 67. Miao, T., Wang, J., Zeng, Y., Liu, G. & Chen, X. Polysaccharide-Based Controlled Release Systems for Therapeutics Delivery and Tissue Engineering: From Bench to Bedside. *Advanced Science* (2018) doi:10.1002/advs.201700513.
 68. Oberdorster, G., Ferin, J. & Lehnert, B. E. Correlation between particle size, in vivo particle persistence, and lung injury. in *Environmental Health Perspectives* (1994). doi:10.1289/ehp.102-1567252.
 69. Oberdörster, G. *et al.* Extrapulmonary translocation of ultrafine carbon particles following whole-body inhalation exposure of rats *J Toxicol Environ Health A* **65** (20): 1531–1543. *Find this Artic. online* (2002).
 70. Kreyling, W. G. *et al.* Translocation of ultrafine insoluble iridium particles from lung epithelium to extrapulmonary organs is size dependent but very low. *J. Toxicol. Environ. Heal. - Part A* (2002) doi:10.1080/00984100290071649.
 71. Pant, K. *et al.* Surface charge and particle size determine the metabolic fate of dendritic polyglycerols. *Nanoscale* (2017) doi:10.1039/c7nr01702b.
 72. Capolla, S. *et al.* Targeted tumor imaging of anti-CD20-polymeric nanoparticles developed

References

- for the diagnosis of B-cell malignancies. *Int. J. Nanomedicine* **10**, 4099–4109 (2015).
73. Kirpotin, D. B. *et al.* Antibody targeting of long-circulating lipidic nanoparticles does not increase tumor localization but does increase internalization in animal models. *Cancer Res.* (2006) doi:10.1158/0008-5472.CAN-05-4199.
74. Bartlett, D. W., Su, H., Hildebrandt, I. J., Weber, W. A. & Davis, M. E. Impact of tumor-specific targeting on the biodistribution and efficacy of siRNA nanoparticles measured by multimodality in vivo imaging. *Proc. Natl. Acad. Sci. U. S. A.* (2007) doi:10.1073/pnas.0707461104.
75. Roduner, E. Size matters: Why nanomaterials are different. *Chem. Soc. Rev.* (2006) doi:10.1039/b502142c.
76. Hernando, A., Crespo, P. & García, M. A. Metallic magnetic nanoparticles. *ScientificWorldJournal*. **5**, 972–1001 (2005).
77. Sun, Y., Gray, S. K. & Peng, S. Surface chemistry: A non-negligible parameter in determining optical properties of small colloidal metal nanoparticles. *Physical Chemistry Chemical Physics* (2011) doi:10.1039/c1cp20265k.
78. G., N., Casals, E., Ojea, I., Varon, M. & Puentes, V. The Reactivity of Colloidal Inorganic Nanoparticles. in *The Delivery of Nanoparticles* (eds. Dr. Abbass & A. Hashim) 377–400 (InTech, 2012). doi:10.5772/35238.
79. Choi, H. S. *et al.* Design considerations for tumour-targeted nanoparticles. *Nat. Nanotechnol.* (2010) doi:10.1038/nnano.2009.314.
80. Du, B., Yu, M. & Zheng, J. Transport and interactions of nanoparticles in the kidneys. *Nature Reviews Materials* (2018) doi:10.1038/s41578-018-0038-3.
81. Hainfeld, J. F., Slatkin, D. N. & Smilowitz, H. M. The use of gold nanoparticles to enhance radiotherapy in mice. *Phys. Med. Biol.* (2004) doi:10.1088/0031-9155/49/18/N03.
82. Lankveld, D. P. K. *et al.* The kinetics of the tissue distribution of silver nanoparticles of different sizes. *Biomaterials* (2010) doi:10.1016/j.biomaterials.2010.07.045.
83. Choi, H. S. *et al.* Rapid translocation of nanoparticles from the lung airspaces to the body. *Nat. Biotechnol.* (2010) doi:10.1038/nbt.1696.
84. Kumar, A. *et al.* Multifunctional magnetic nanoparticles for targeted delivery. *Nanomedicine Nanotechnology, Biol. Med.* (2010) doi:10.1016/j.nano.2009.04.002.
85. Durkut, S. Thermoresponsive poly (N-vinylcaprolactam)-g-galactosylated chitosan hydrogel: synthesis, characterization, and controlled release properties. *Int. J. Polym. Mater. Polym. Biomater.* **68**, 1034–1047 (2019).
86. Kean, T. & Thanou, M. Biodegradation, biodistribution and toxicity of chitosan. *Adv. Drug Deliv. Rev.* **62**, 3–11 (2010).
87. Duong, H. T. T. *et al.* Functionalizing biodegradable dextran scaffolds using living radical polymerization: New versatile nanoparticles for the delivery of therapeutic molecules. *Mol. Pharm.* **9**, 3046–3061 (2012).
88. Fernández-Quiroz, D. *et al.* Effect of the molecular architecture on the thermosensitive properties of chitosan-g-poly(N-vinylcaprolactam). *Carbohydr. Polym.* **134**, 92–101 (2015).
89. Gandhi, A., Paul, A., Sen, S. O. & Sen, K. K. Studies on thermoresponsive polymers: Phase behaviour, drug delivery and biomedical applications. *Asian J. Pharm. Sci.* **10**, 99–107 (2015).
90. Schmaljohann, D. Thermo- and pH-responsive polymers in drug delivery. *Adv. Drug Deliv.*

References

- Rev. (2006) doi:10.1016/j.addr.2006.09.020.
91. Indulekha, S., Arunkumar, P., Bahadur, D. & Srivastava, R. Thermoresponsive polymeric gel as an on-demand transdermal drug delivery system for pain management. *Mater. Sci. Eng. C* **62**, 113–122 (2016).
 92. Tian, Y., Bromberg, L., Lin, S. N., Alan Hatton, T. & Tam, K. C. Complexation and release of doxorubicin from its complexes with pluronic P85-b-poly(acrylic acid) block copolymers. *J. Control. Release* (2007) doi:10.1016/j.jconrel.2007.05.010.
 93. Prabakaran, M., Grailer, J. J., Steeber, D. A. & Gong, S. Stimuli-responsive chitosan-graft-Poly(N-vinylcaprolactam) as a promising material for controlled hydrophobic drug delivery. *Macromol. Biosci.* **8**, 843–851 (2008).
 94. Park, W. *et al.* Acidic pH-Triggered Drug-Eluting Nanocomposites for Magnetic Resonance Imaging-Monitored Intra-Arterial Drug Delivery to Hepatocellular Carcinoma. *ACS Appl. Mater. Interfaces* **8**, 12711–12719 (2016).
 95. Swamy, B. Y., Chang, J. H., Ahn, H., Lee, W. K. & Chung, I. Thermoresponsive N-vinyl caprolactam grafted sodium alginate hydrogel beads for the controlled release of an anticancer drug. *Cellulose* **20**, 1261–1273 (2013).
 96. Chauhan, D. S. *et al.* NIR light-triggered shrinkable thermoresponsive PNVCL nanoshells for cancer theranostics. *RSC Adv.* **7**, 44026–44034 (2017).
 97. Kawaguchi, H. Thermoresponsive microhydrogels: Preparation, properties and applications. *Polym. Int.* **63**, 925–932 (2014).
 98. Wust, P. *et al.* Hyperthermia in combined treatment of cancer. *Lancet Oncology* (2002) doi:10.1016/S1470-2045(02)00818-5.
 99. Indulekha, S., Arunkumar, P., Bahadur, D. & Srivastava, R. Dual responsive magnetic composite nanogels for thermo-chemotherapy. *Colloids Surfaces B Biointerfaces* **155**, 304–313 (2017).
 100. Luckanagul, J. A. *et al.* Chitosan-based polymer hybrids for thermo-responsive nanogel delivery of curcumin. *Carbohydr. Polym.* **181**, 1119–1127 (2018).
 101. Wedel, B., Zeiser, M. & Hellweg, T. Non NIPAM based smart microgels: Systematic variation of the volume phase transition temperature by copolymerization. *Zeitschrift fur Phys. Chemie* **226**, 737–748 (2012).
 102. Cazares-Cortes, E. *et al.* Doxorubicin Intracellular Remote Release from Biocompatible Oligo(ethylene glycol) Methyl Ether Methacrylate-Based Magnetic Nanogels Triggered by Magnetic Hyperthermia. *ACS Appl. Mater. Interfaces* **9**, 25775–25788 (2017).
 103. Nayak, S., Gan, D., Serpe, M. J. & Lyon, L. A. Hollow thermoresponsive microgels. *Small* **1**, 416–421 (2005).
 104. Sanoj Rejinold, N. *et al.* Curcumin-loaded biocompatible thermoresponsive polymeric nanoparticles for cancer drug delivery. *J. Colloid Interface Sci.* **360**, 39–51 (2011).
 105. Pitakchatwong, C. & Chirachanchai, S. Thermo-Magneto-responsive Dual Function Nanoparticles: An Approach for Magnetic Entrapable-Releasable Chitosan. *ACS Appl. Mater. Interfaces* **9**, 10398–10407 (2017).
 106. Sadighian, S., Rostamizadeh, K., Hosseini, M. J., Hamidi, M. & Hosseini-Monfared, H. Magnetic nanogels as dual triggered anticancer drug delivery: Toxicity evaluation on isolated rat liver mitochondria. *Toxicol. Lett.* **278**, 18–29 (2017).
 107. May, J. P. & Li, S. D. Hyperthermia-induced drug targeting. *Expert Opinion on Drug Delivery* (2013) doi:10.1517/17425247.2013.758631.

References

108. Rejinold, N. S. *et al.* Breast tumor targetable Fe₃O₄ embedded thermo-responsive nanoparticles for radiofrequency assisted drug delivery. *J. Biomed. Nanotechnol.* **12**, 43–55 (2016).
109. Jaiswal, M. K., Banerjee, R., Pradhan, P. & Bahadur, D. Thermal behavior of magnetically modalized poly(N-isopropylacrylamide)-chitosan based nanohydrogel. *Colloids Surfaces B Biointerfaces* **81**, 185–194 (2010).
110. Patra, J. K. *et al.* Nano based drug delivery systems: recent developments and future prospects. *J. Nanobiotechnology* (2018) doi:10.1186/s12951-018-0392-8.
111. Rizvi, S. A. A. & Saleh, A. M. Applications of nanoparticle systems in drug delivery technology. *Saudi Pharmaceutical Journal* (2018) doi:10.1016/j.jsps.2017.10.012.
112. Salouti, M. & Ahangari, A. Nanoparticle based Drug Delivery Systems for Treatment of Infectious Diseases. in *Application of Nanotechnology in Drug Delivery* (2014). doi:10.5772/58423.
113. Salehi, R., Rasouli, S. & Hamishehkar, H. Smart thermo/pH responsive magnetic nanogels for the simultaneous delivery of doxorubicin and methotrexate. *Int. J. Pharm.* **487**, 274–284 (2015).
114. Sun, J., Gui, R., Jin, H., Li, N. & Wang, X. CuS nanocrystal@microgel nanocomposites for light-regulated release of dual-drugs and chemo-photothermal synergistic therapy in vitro. *RSC Adv.* **6**, 8722–8728 (2016).
115. Alberts, B. Impact factor distortions. *Science (80-.)*. **340**, 787 (2013).
116. Paulus, F. M., Cruz, N. & Krach, S. The impact factor fallacy. *Front. Psychol.* **9**, 1–7 (2018).
117. Callaway, E. Publishing elite turns against impact factor. *Nature* **535**, 210–211 (2016).
118. Kumar, M. The import of the impact factor: fallacies of citation-dependent scientometry. *Bull. R. Coll. Surg. Engl.* (2010) doi:10.1308/147363510x481647.
119. Leydesdorff, L., Bornmann, L., Comins, J. A. & Milojević, S. Citations: Indicators of Quality? The Impact Fallacy. *Front. Res. Metrics Anal.* (2016) doi:10.3389/frma.2016.00001.
120. de Moraes Porto, I. C. C. Polymer Biocompatibility. in *Polymerization* (2012). doi:10.5772/47786.
121. Anusavice, K. J. *Phillip's Science of Dental Materials*. (Saunders, 2003).
122. Williams, D. F. On the mechanisms of biocompatibility. *Biomaterials* (2008) doi:10.1016/j.biomaterials.2008.04.023.
123. Schmalz, G. Materials science: Biological aspects. *J. Dent. Res.* **81**, 660–663 (2002).
124. Anderson, J. M. Biological responses to materials. *Annu. Rev. Mater. Sci.* (2001) doi:10.1146/annurev.matsci.31.1.81.
125. Xu, L. C., Bauer, J. W. & Siedlecki, C. A. Proteins, platelets, and blood coagulation at biomaterial interfaces. *Colloids Surfaces B Biointerfaces* (2014) doi:10.1016/j.colsurfb.2014.09.040.
126. Loureiro dos Santos, L. A. Natural Polymeric Biomaterials: Processing and Properties ☆. *Ref. Modul. Mater. Sci. Mater. Eng.* 1–6 (2017) doi:10.1016/b978-0-12-803581-8.02253-0.
127. Aminabhavi, T. M. & Deshmukh, A. S. *Polymeric Hydrogels as Smart Biomaterials*. *Polymer and Composite Materials* (2016).

References

128. Kohane, D. S. & Langer, R. Polymeric biomaterials in tissue engineering. *Pediatric Research* (2008) doi:10.1203/01.pdr.0000305937.26105.e7.
129. Teo, A. J. T. *et al.* Polymeric Biomaterials for Medical Implants and Devices. *ACS Biomaterials Science and Engineering* (2016) doi:10.1021/acsbiomaterials.5b00429.
130. Seal, B. L., Otero, T. C. & Panitch, A. Polymeric biomaterials for tissue and organ regeneration. *Materials Science and Engineering: R: Reports* (2001) doi:10.1016/S0927-796X(01)00035-3.
131. Griffith, L. G. Polymeric biomaterials. *Acta Mater.* (2000) doi:10.1016/S1359-6454(99)00299-2.
132. George, A., Sanjay, M. R., Srisuk, R., Parameswaranpillai, J. & Siengchin, S. A comprehensive review on chemical properties and applications of biopolymers and their composites. *Int. J. Biol. Macromol.* **154**, 329–338 (2020).
133. Gribova, V., Crouzier, T. & Picart, C. A material's point of view on recent developments of polymeric biomaterials: Control of mechanical and biochemical properties. *Journal of Materials Chemistry* (2011) doi:10.1039/c1jm11372k.
134. Hoffman, A. S. *Synthetic Polymer Biomaterials in Medicine — a Review. Macromolecules* (International Union of Pure and Applied Chemistry, 1982). doi:10.1016/b978-0-08-026226-0.50027-0.
135. Schmitt, E. E. & P. R. A. Surgical sutures. US patent 3297033 (10 January 1967). (1967).
136. Nair, L. S. & Laurencin, C. T. Biodegradable polymers as biomaterials. *Prog. Polym. Sci.* **32**, 762–798 (2007).
137. Vihola, H. *Studies on Thermosensitive Poly(N-vinylcaprolactam) Based Polymers for Pharmaceutical Applications. Faculty of Pharmacy* (2007). doi:952-10-0386-3.
138. Dubovik, A. S., Makhaeva, E. E., Grinberg, V. Y. & Khokhlov, A. R. Energetics of cooperative transitions of N-vinylcaprolactam polymers in aqueous solutions. *Macromol. Chem. Phys.* (2005) doi:10.1002/macp.200400554.
139. van Dijk, E., Hoogeveen, A. & Abeln, S. The Hydrophobic Temperature Dependence of Amino Acids Directly Calculated from Protein Structures. *PLoS Comput. Biol.* (2015) doi:10.1371/journal.pcbi.1004277.
140. KOZANOĞLU, S. Polymerization and characterization of N-Vinylcaprolactam. (Middle East Technical University, 2008).
141. Doberenz, F., Zeng, K., Willems, C., Zhang, K. & Groth, T. Thermoresponsive polymers and their biomedical application in tissue engineering-A review. *J. Mater. Chem. B* **8**, 607–628 (2020).
142. Somcynsky, T. The lower critical solution temperature (LCST) of non-polar polymer solutions: An introduction. *Polym. Eng. Sci.* **22**, 58–63 (1982).
143. Seuring, J. & Agarwal, S. Polymers with upper critical solution temperature in aqueous solution. *Macromolecular Rapid Communications* (2012) doi:10.1002/marc.201200433.
144. Seuring, J. & Agarwal, S. Polymers with upper critical solution temperature in aqueous solution: Unexpected properties from known building blocks. *ACS Macro Lett.* (2013) doi:10.1021/mz400227y.
145. Snyder, P. W. *et al.* Mechanism of the hydrophobic effect in the biomolecular recognition of arylsulfonamides by carbonic anhydrase. *Proc. Natl. Acad. Sci. U. S. A.* (2011) doi:10.1073/pnas.1114107108.

References

146. Cheng, Y. K. & Rossky, P. J. Surface topography dependence of biomolecular hydrophobic hydration. *Nature* (1998) doi:10.1038/33653.
147. Setny, P., Baron, R. & McCammon, J. A. How can hydrophobic association be enthalpy driven? *J. Chem. Theory Comput.* (2010) doi:10.1021/ct1003077.
148. Flory, P. J. Thermodynamics of high polymer solutions. *J. Chem. Phys.* **10**, 51–61 (1942).
149. Huggins, M. Thermodynamic Properties of Solutions of Long-Chain Compounds. *Ann. N. Y. Acad. Sci.* **43**, 1–32 (1942).
150. Gooch, J. W. Flory-Huggins Theory. in *Encyclopedic Dictionary of Polymers* (2011). doi:10.1007/978-1-4419-6247-8_5128.
151. Gooch, J. W. Theta solvent. in *Encyclopedic Dictionary of Polymers* (ed. Gooch, J. W.) (Springer, 2011). doi:https://doi.org/10.1007/978-1-4419-6247-8.
152. Wolf, B. A. Making Flory–Huggins Practical: Thermodynamics of Polymer-Containing Mixtures. 1–66 (2010) doi:10.1007/12_2010_84.
153. Delmas, G., Patterson, D. & Somcynsky, T. Thermodynamics of Polyisobutylenen-Alkane Systems. **57**, 79–98 (1962).
154. Schäfer-Soenen, H. *et al.* Zero and off-zero critical concentrations in systems containing polydisperse polymers† with very high molar masses. 2. The system water-poly(vinyl methyl ether). *Macromolecules* **30**, 410–416 (1997).
155. Moerkerke, R. *et al.* Phase transitions in swollen networks. 3. Swelling behavior of radiation cross-linked poly(vinyl methyl ether) in water. *Macromolecules* **31**, 2223–2229 (1998).
156. Meeussen, F. *et al.* Phase behaviour of poly(N-vinyl caprolactam) in water. *Polymer (Guildf)*. **41**, 8597–8602 (2000).
157. Šolc, K., Dušek, K., Koningsveld, Ro. & Berghmans, H. ‘Zero’ and ‘Off-Zero’ Critical Concentrations in Solutions of Polydisperse Polymers with Very High Molar Masses. *Collect. Czechoslov. Chem. Commun.* **60**, 1661–1688 (1995).
158. De Sousa, H. C. & Rebelo, L. P. N. Continuous polydisperse thermodynamic algorithm for a modified Flory-Huggins model: the (polystyrene + nitroethane) example. *J. Polym. Sci. Part B Polym. Phys.* (2000) doi:10.1002/(SICI)1099-0488(20000215)38:4<632::AID-POLB15>3.0.CO;2-Q.
159. Seuring, J. & Agarwal, S. Non-ionic homo- and copolymers with H-donor and H-acceptor units with an UCST in water. *Macromol. Chem. Phys.* (2010) doi:10.1002/macp.201000147.
160. Costa, R. O. R. & Freitas, R. F. S. Phase behavior of poly (N-isopropylacrylamide) in binary aqueous solutions. *Polymer (Guildf)*. **43**, 5879–5885 (2002).
161. Hoogenboom, R. *et al.* A schizophrenic gradient copolymer: Switching and reversing poly(2-oxazoline) micelles based on UCST and subtle solvent changes. *Soft Matter* (2009) doi:10.1039/b912491h.
162. Chua, G. B. H., Roth, P. J., Duong, H. T. T., Davis, T. P. & Lowe, A. B. Synthesis and thermoresponsive solution properties of poly[oligo(ethylene glycol) (meth)acrylamide]s: Biocompatible PEG analogues. *Macromolecules* (2012) doi:10.1021/ma202700y.
163. Boyko, V., Lu, Y., Richter, A. & Pich, A. Preparation and Characterization of Acetoacetoxyethyl Methacrylate-Based Gels. *Macromol. Chem. Phys.* (2003) doi:10.1002/macp.200350058.

References

164. Gelbrich, T., Feyen, M. & Schmidt, A. M. Magnetic thermoresponsive core-shell nanoparticles. *Macromolecules* (2006) doi:10.1021/ma060006u.
165. Yamauchi, H. & Maeda, Y. LCST and UCST behavior of poly(N-isopropylacrylamide) in DMSO/water mixed solvents studied by IR and micro-Raman spectroscopy. *J. Phys. Chem. B* (2007) doi:10.1021/jp072438s.
166. Ueki, T., Watanabe, M. & Lodge, T. P. Doubly thermosensitive self-assembly of diblock copolymers in ionic liquids. *Macromolecules* (2009) doi:10.1021/ma802443b.
167. Ueki, T. *et al.* UCST phase transition of azobenzene-containing random copolymer in an ionic liquid. *Macromolecules* (2011) doi:10.1021/ma2014244.
168. Wohlfarth, C. Lower critical (LCST) and/or upper critical (UCST) solution temperatures of aqueous polymer solutions. in *CRC Handbook of Chemistry and Physics* (ed. Lide, D. R.) 2205–2222 (CRC Press, 2010).
169. Buscall, R. & Corner, T. The phase-separation behaviour of aqueous solutions of polyacrylic acid and its partial sodium salts in the presence of sodium chloride. *Eur. Polym. J.* (1982) doi:10.1016/0014-3057(82)90084-2.
170. Sund-Levander, M., Forsberg, C. & Wahren, L. K. Normal oral, rectal, tympanic and axillary body temperature in adult men and women: A systematic literature review. *Scand. J. Caring Sci.* (2002) doi:10.1046/j.1471-6712.2002.00069.x.
171. Ramos, J., Imaz, A. & Forcada, J. Temperature-sensitive nanogels: Poly(N-vinylcaprolactam) versus poly(N-isopropylacrylamide). *Polym. Chem.* **3**, 852–856 (2012).
172. Ward, M. A. & Georgiou, T. K. Thermoresponsive polymers for biomedical applications. *Polymers (Basel)*. **3**, 1215–1242 (2011).
173. Lambermont-Thijs, H. M. L. *et al.* Solubility behavior of amphiphilic block and random copolymers based on 2-ethyl-2-oxazoline and 2-nonyl-2-oxazoline in binary water-ethanol mixtures. *J. Polym. Sci. Part A Polym. Chem.* (2009) doi:10.1002/pola.23168.
174. Wu, G., Chen, S. C., Zhan, Q. & Wang, Y. Z. Well-defined amphiphilic biodegradable comb-like graft copolymers: Their unique architecture-determined LCST and UCST thermoresponsivity. *Macromolecules* (2011) doi:10.1021/ma102588k.
175. Guo, X., Wang, L., Wei, X. & Zhou, S. Polymer-based drug delivery systems for cancer treatment. *J. Polym. Sci. Part A Polym. Chem.* **54**, 3525–3550 (2016).
176. Cao, P. F., Mangadlao, J. D. & Advincula, R. C. Stimuli-Responsive Polymers and their Potential Applications in Oil-Gas Industry. *Polym. Rev.* **55**, 706–733 (2015).
177. Weng, L. & Xie, J. Smart Electrospun Nanofibers for Controlled Drug Release: Recent Advances and New Perspectives. *Curr. Pharm. Des.* **21**, 1944–1959 (2015).
178. Seuring, J. & Agarwal, S. First example of a universal and cost-effective approach: Polymers with tunable upper critical solution temperature in water and electrolyte solution. *Macromolecules* **45**, 3910–3918 (2012).
179. Shimada, N. *et al.* Ureido-Derivatized Polymers Based on Both Poly(allylurea) and Poly(L-citrulline) Exhibit UCST-Type Phase Transition Behavior under Physiologically Relevant Conditions. *Biomacromolecules* **12**, 3418–3422 (2011).
180. Lutz, J. F. Polymerization of oligo(ethylene glycol) (meth)acrylates: Toward new generations of smart biocompatible materials. *J. Polym. Sci. Part A Polym. Chem.* **46**, 3459–3470 (2008).
181. Zheng, J. Y., Tan, M. J., Thoniyot, P. & Loh, X. J. Unusual thermogelling behaviour of poly[2-(dimethylamino)ethyl methacrylate] (PDMAEMA)-based polymers polymerized in

References

- bulk. *RSC Adv.* **5**, 62314–62318 (2015).
182. Hoogenboom, R. & Schlaad, H. Thermoresponsive poly(2-oxazoline)s, polypeptoids, and polypeptides. *Polym. Chem.* **8**, 24–40 (2017).
183. Uyama, H. & Kobayashi, S. A Novel Thermo-Sensitive Polymer. Poly(2- iso -propyl-2-oxazoline) . *Chem. Lett.* (1992) doi:10.1246/cl.1992.1643.
184. Halperin, A., Kröger, M. & Winnik, F. M. Poly(N-isopropylacrylamide) Phase Diagrams: Fifty Years of Research. *Angew. Chemie - Int. Ed.* (2015) doi:10.1002/anie.201506663.
185. Chauhan, D. S. *et al.* NIR light-triggered shrinkable thermoresponsive PNVCL nanoshells for cancer theranostics. *RSC Adv.* **7**, 44026–44034 (2017).
186. Heskins, M. & Guillet, J. E. Solution Properties of Poly(N-isopropylacrylamide). *J. Macromol. Sci. Part A - Chem.* (1968) doi:10.1080/10601326808051910.
187. Shostakovskii, M. F. & Sidel'kovskaya, F. P. Investigation of lactones and lactams Communication 14. Synthesis of n-vinylcaprolactam by the indirect-vinylation method. *Bull. Acad. Sci. USSR Div. Chem. Sci.* (1959) doi:10.1007/BF00915915.
188. Makhaeva, E. E., Thanh, L. T. M., Starodoubtsev, S. C. & Khokhlov, A. R. Thermoshrinking behavior of poly(vinylcaprolactam) gels in aqueous solution. *Macromol. Chem. Phys.* (1996) doi:10.1002/macp.1996.021970616.
189. Kozanoğlu, S., Özdemir, T. & Usanmaz, A. Polymerization of N-vinylcaprolactam and characterization of poly(N-vinylcaprolactam). *J. Macromol. Sci. Part A Pure Appl. Chem.* **48**, 467–477 (2011).
190. Kirsh, Y. E., Yanul, N. A. & Kalninch, K. K. Structural transformations and water associate interactions in poly-N-vinylcaprolactam-water system. *Eur. Polym. J.* (1999) doi:10.1016/S0014-3057(98)00114-1.
191. Lozinsky, V. I. *et al.* Synthesis of N-vinylcaprolactam polymers in water-containing media. *Polymer (Guildf).* (2000) doi:10.1016/S0032-3861(99)00844-7.
192. Cheng, S. C. *et al.* Radiation polymerization of thermo-sensitive poly (N-vinylcaprolactam). *Radiat. Phys. Chem.* (2002) doi:10.1016/S0969-806X(01)00638-7.
193. Solomon, O. F., Corciovei, M., Ciută, I. & Boghină, C. Properties of solutions of poly-N-vinylcaprolactam. *J. Appl. Polym. Sci.* (1968) doi:10.1002/app.1968.070120804.
194. Tager, A. A., Safronov, A. P., Sharina, S. V. & Galaev, I. Y. Thermodynamic study of poly(N-vinyl caprolactam) hydration at temperatures close to lower critical solution temperature. *Colloid Polym. Sci.* (1993) doi:10.1007/BF00652769.
195. Laukkanen, A., Valtola, L., Winnik, F. M. & Tenhu, H. Formation of colloiddally stable phase separated poly(N-vinylcaprolactam) in water: A study by dynamic light scattering, microcalorimetry, and pressure perturbation calorimetry. *Macromolecules* **37**, 2268–2274 (2004).
196. Medeiros, S. F., Barboza, J. C. S., Ré, M. I., Giudici, R. & Santos, A. M. Solution polymerization of N-vinylcaprolactam in 1,4-dioxane. Kinetic dependence on temperature, monomer, and initiator concentrations. *J. Appl. Polym. Sci.* (2010) doi:10.1002/app.32204.
197. Shao, L., Hu, M., Chen, L., Xu, L. & Bi, Y. RAFT polymerization of N-vinylcaprolactam and effects of the end group on the thermal response of poly(N-vinylcaprolactam). *React. Funct. Polym.* (2012) doi:10.1016/j.reactfunctpolym.2012.04.002.
198. Shostakovskiy, M. F., Sidelkovskaya, F. P. & Zelenskaya, M. G. Synthesis and transformations of vinylcaprolactam Part 1. Polymerization in presence of hydrogen peroxide. *Bull. Acad. Sci. USSR Div. Chem. Sci.* (1952) doi:10.1007/BF01164930.

References

199. Eisele, M. & Burchard, W. Hydrophobic water-soluble polymers, 1. Dilute solution properties of poly(1-vinyl-2-piperidone) and poly(N-vinylcaprolactam). *Die Makromol. Chemie* (1990) doi:10.1002/macp.1990.021910114.
200. Kalugin, D. I., Talyzenkov, Y. A. & Lachinov, M. B. Radical polymerization of N-vinylcaprolactam in benzene solutions in a wide conversion range. *Polym. Sci. - Ser. B* (2008) doi:10.1134/S1560090408110018.
201. Makhaeva, E. E., Tenhu, H. & Khokhlov, A. R. Conformational changes of poly(vinylcaprolactam) macromolecules and their complexes with ionic surfactants in aqueous solution. *Macromolecules* (1998) doi:10.1021/ma980158s.
202. Zhang, L., Liang, Y. & Meng, L. Thermo-sensitive amphiphilic poly(N-vinylcaprolactam) copolymers: Synthesis and solution properties. *Polym. Adv. Technol.* (2010) doi:10.1002/pat.1495.
203. Singh, P., Srivastava, A. & Kumar, R. Synthesis of amphiphilic poly(N-vinylcaprolactam) using ATRP protocol and antibacterial study of its silver nanocomposite. *J. Polym. Sci. Part A Polym. Chem.* (2012) doi:10.1002/pola.25911.
204. Van Nieuwenhove, I. *et al.* RAFT/MADIX polymerization of N-vinylcaprolactam in water-ethanol solvent mixtures. *Polym. Chem.* (2017) doi:10.1039/c6py02224c.
205. Schild, H. G. & Tirrell, D. A. Microcalorimetric detection of lower critical solution temperatures in aqueous polymer solutions. *J. Phys. Chem.* (1990) doi:10.1021/j100373a088.
206. Chilkoti, A., Dreher, M. R., Meyer, D. E. & Raucher, D. Targeted drug delivery by thermally responsive polymers. *Advanced Drug Delivery Reviews* (2002) doi:10.1016/S0169-409X(02)00041-8.
207. Shtanko, N. I., Lequieu, W., Goethals, E. J. & Du Prez, F. E. PH- and thermo-responsive properties of poly(N-vinylcaprolactam-co-acrylic acid) copolymers. *Polym. Int.* (2003) doi:10.1002/pi.1347.
208. Kirsh, I. E. (ĪUriĪ E. *Water-soluble poly-N-vinylamides : synthesis and physicochemical properties.* (Wiley, 1998).
209. Wu, J. Y., Liu, S. Q., Heng, P. W. S. & Yang, Y. Y. Evaluating proteins release from, and their interactions with, thermosensitive poly (N-isopropylacrylamide) hydrogels. *J. Control. Release* (2005) doi:10.1016/j.jconrel.2004.10.008.
210. Maeda, Y., Nakamura, T. & Ikeda, I. Hydration and phase behavior of poly(N-vinylcaprolactam) and poly(N-vinylpyrrolidone) in water. *Macromolecules* (2002) doi:10.1021/ma011034+.
211. Lau, A. C. W. & Wu, C. Thermally Sensitive and Biocompatible Poly(N-vinylcaprolactam): Synthesis and Characterization of High Molar Mass Linear Chains. *Macromolecules* (1999) doi:10.1021/ma980850n.
212. Lebedev, V. *et al.* Polymer hydration and microphase decomposition in poly(N-vinylcaprolactam)-water complex. in *Journal of Applied Crystallography* (2003). doi:10.1107/S0021889803008422.
213. Chee, C. K., Rimmer, S., Soutar, I. & Swanson, L. Fluorescence investigations of the conformational behaviour of Poly(N-vinylcaprolactam). *React. Funct. Polym.* (2006) doi:10.1016/j.reactfunctpolym.2005.07.007.
214. Guan, Y. & Zhang, Y. PNIPAM microgels for biomedical applications: From dispersed particles to 3D assemblies. *Soft Matter* (2011) doi:10.1039/c0sm01541e.

References

215. Lanzalaco, S. & Armelin, E. Poly(N-isopropylacrylamide) and Copolymers: A Review on Recent Progresses in Biomedical Applications. *Gels* (2017) doi:10.3390/gels3040036.
216. Vihola, H., Laukkanen, A., Valtola, L., Tenhu, H. & Hirvonen, J. Cytotoxicity of thermosensitive polymers poly(N-isopropylacrylamide), poly(N-vinylcaprolactam) and amphiphilically modified poly(N-vinylcaprolactam). *Biomaterials* (2005) doi:10.1016/j.biomaterials.2004.09.008.
217. Imaz, A., Miranda, J. I., Ramos, J. & Forcada, J. Evidences of a hydrolysis process in the synthesis of N-vinylcaprolactam-based microgels. *Eur. Polym. J.* **44**, 4002–4011 (2008).
218. Enomoto, Y., Kamitakahara, H., Takano, T. & Nakatsubo, F. Synthesis of diblock copolymers with cellulose derivatives. 3. Cellulose derivatives carrying a single pyrene group at the reducing-end and fluorescent studies of their self-assembly systems in aqueous NaOH solutions. *Cellulose* (2006) doi:10.1007/s10570-005-9005-4.
219. Shah, S., Pal, A., Gude, R. & Devi, S. Synthesis and characterization of thermo-responsive copolymeric nanoparticles of poly(methyl methacrylate-co-N-vinylcaprolactam). *Eur. Polym. J.* (2010) doi:10.1016/j.eurpolymj.2010.01.005.
220. Ainara, I. & Jacqueline, F. N-vinylcaprolactam-based microgels for biomedical applications. *J. Polym. Sci. Part A Polym. Chem.* (2010).
221. BASF. Luviskol ® Plus technical information. (2011).
222. Makhaeva, E. E., Tenhu, H. & Khokhlov, A. R. Behaviour of poly(N-vinylcaprolactam) macromolecules in the presence of organic compounds in aqueous solution. *Polymer (Guildf)*. (2000) doi:10.1016/S0032-3861(00)00258-5.
223. Rejinold, N. S., Chennazhi, K. P., Nair, S. V., Tamura, H. & Jayakumar, R. Biodegradable and thermo-sensitive chitosan-g-poly(N-vinylcaprolactam) nanoparticles as a 5-fluorouracil carrier. *Carbohydr. Polym.* **83**, 776–786 (2011).
224. Markvicheva, E. A. *et al.* Gel-immobilized enzymes as promising biocatalysts: Results from Indo-Russian collaborative studies. in *Pure and Applied Chemistry* (2005). doi:10.1351/pac200577010227.
225. Galaev, I. Y. & Mattiasson, B. Affinity thermoprecipitation of trypsin using soybean trypsin inhibitor conjugated with a thermo-reactive polymer, poly(N-vinyl caprolactam). *Biotechnol. Tech.* (1992) doi:10.1007/BF02439325.
226. Markvicheva, E. *et al.* Immobilized enzymes and cells in poly (N-vinyl caprolactam)-based hydrogels. *Appl. Biochem. Biotechnol.* (2000).
227. Shakya, A. K., Holmdahl, R., Nandakumar, K. S. & Kumar, A. Polymeric cryogels are biocompatible, and their biodegradation is independent of oxidative radicals. *J. Biomed. Mater. Res. - Part A* (2014) doi:10.1002/jbm.a.35013.
228. Markvicheva, E. A. *et al.* Proteases Entrapped in Polymer Composite Hydrogels : Preparation Methods and Applications. *Vestn. Mosk. Univ. Khimiya* (2000).
229. Barclay, T. G., Day, C. M., Petrovsky, N. & Garg, S. Review of polysaccharide particle-based functional drug delivery. *Carbohydr. Polym.* **221**, 94–112 (2019).
230. Alcázar-Alay, S. C. & Meireles, M. A. A. Physicochemical properties, modifications and applications of starches from different botanical sources. *Food Sci. Technol.* (2015) doi:10.1590/1678-457X.6749.
231. Singh, A. K., Bhadauria, A. S., Kumar, P., Bera, H. & Saha, S. Bioactive and drug-delivery potentials of polysaccharides and their derivatives. in *Polysaccharide Carriers for Drug Delivery* (2019). doi:10.1016/B978-0-08-102553-6.00002-7.

References

232. Singh, A. K., Bhadauria, A. S., Kumar, P., Bera, H. & Saha, S. *Bioactive and drug-delivery potentials of polysaccharides and their derivatives. Polysaccharide Carriers for Drug Delivery* (Elsevier Ltd., 2019). doi:10.1016/B978-0-08-102553-6.00002-7.
233. Yadav, H. & Karthikeyan, C. Natural polysaccharides: Structural features and properties. in *Polysaccharide Carriers for Drug Delivery* (eds. Maiti, S. & Jana, S.) 1–17 (Woodhead Publishing, 2019). doi:10.1016/B978-0-08-102553-6.00001-5.
234. Li, J. & Mooney, D. J. Designing hydrogels for controlled drug delivery. *Nature Reviews Materials* (2016) doi:10.1038/natrevmats.2016.71.
235. Liu, D., Yang, F., Xiong, F. & Gu, N. The smart drug delivery system and its clinical potential. *Theranostics* (2016) doi:10.7150/thno.14858.
236. Wen, Y. & Oh, J. K. Recent strategies to develop polysaccharide-based nanomaterials for biomedical applications. *Macromolecular Rapid Communications* (2014) doi:10.1002/marc.201400406.
237. Miao, T., Wang, J., Zeng, Y., Liu, G. & Chen, X. Polysaccharide-Based Controlled Release Systems for Therapeutics Delivery and Tissue Engineering: From Bench to Bedside. *Adv. Sci.* **5**, (2018).
238. Danhauser-Riedl, S. *et al.* Phase I clinical and pharmacokinetic trial of dextran conjugated doxorubicin (AD-70, DOX-OXD). *Invest. New Drugs* **11**, 187–195 (1993).
239. Kim, J. K. *et al.* Long-term clinical outcome of phase IIb clinical trial of percutaneous injection with holmium-166/chitosan complex (milican) for the treatment of small hepatocellular carcinoma. *Clin. Cancer Res.* **12**, 543–548 (2006).
240. Pinnix, C. *et al.* Topical hyaluronic acid vs. standard of care for the prevention of radiation dermatitis after adjuvant radiotherapy for breast cancer: Single-blind randomized phase III clinical trial. *Int. J. Radiat. Oncol. Biol. Phys.* (2012) doi:10.1016/j.ijrobp.2011.09.021.
241. Calando Pharmaceuticals. Safety Study of CALAA-01 to Treat Solid Tumor Cancers. <https://clinicaltrials.gov/ct2/show/NCT00689065>.
242. Tan, P. L. Company profile: Tissue regeneration for diabetes and neurological diseases at living cell technologies. *Regen. Med.* **5**, 181–187 (2010).
243. Prabakaran, M. & Jayakumar, R. Polymeric Bionanocomposites as Promising Materials for Controlled Drug Delivery. in *Chitosan for Biomaterials II* (eds. Jayakumar, R., Prabakaran, M. & Muzzarelli, Riccardo, A. A.) 1–18 (Springer, Berlin, Heidelberg, 2011). doi:<https://doi.org/10.1007/978-3-642-24061-4>.
244. Bellich, B., D'Agostino, I., Semeraro, S., Gamini, A. & Cesàro, A. 'The good, the bad and the ugly' of chitosans. *Marine Drugs* vol. 14 (2016).
245. Clark, G. L. & Smith, A. F. X-ray diffraction studies of chitin, chitosan, and derivatives. *J. Phys. Chem.* (1936) doi:10.1021/j150376a001.
246. Shukla, S. K., Mishra, A. K., Arotiba, O. A. & Mamba, B. B. Chitosan-based nanomaterials: A state-of-the-art review. *Int. J. Biol. Macromol.* **59**, 46–58 (2013).
247. Wang, Q. Z. *et al.* Protonation constants of chitosan with different molecular weight and degree of deacetylation. *Carbohydr. Polym.* (2006) doi:10.1016/j.carbpol.2006.01.001.
248. Casettari, L. *et al.* PEGylated chitosan derivatives: Synthesis, characterizations and pharmaceutical applications. *Prog. Polym. Sci.* **37**, 659–685 (2012).
249. Ho, T. H., Le, T. N. T., Nguyen, T. A. & Dang, M. C. Poly(ethylene glycol) grafted chitosan as new copolymer material for oral delivery of insulin. *Adv. Nat. Sci. Nanosci. Nanotechnol.* **6**, (2015).

References

250. Rampino, A. Polysaccharide-based nanoparticles for drug delivery. (Università degli studi di Trieste, 2011).
251. Felt, O., Buri, P. & Gurny, R. Chitosan: A unique polysaccharide for drug delivery. *Drug Dev. Ind. Pharm.* **24**, 979–993 (1998).
252. Sacco, P., Cok, M., Asaro, F., Paoletti, S. & Donati, I. The role played by the molecular weight and acetylation degree in modulating the stiffness and elasticity of chitosan gels. *Carbohydr. Polym.* **196**, 405–413 (2018).
253. Ways, T. M. M., Lau, W. M. & Khutoryanskiy, V. V. Chitosan and its derivatives for application in mucoadhesive drug delivery systems. *Polymers* (2018) doi:10.3390/polym10030267.
254. Henriksen, I., Skaugrud & Karlsen, J. Use of chitosan and chitosan malate as an excipient in wet granulation of three water soluble drugs. *Int. J. Pharm.* **98**, 181–188 (1993).
255. Gåserød, O., Jolliffe, I. G., Hampson, F. C., Dettmar, P. W. & Skjåk-Bræk, G. The enhancement of the bioadhesive properties of calcium alginate gel beads by coating with chitosan. *Int. J. Pharm.* (1998) doi:10.1016/S0378-5173(98)00277-4.
256. Shafabakhsh, R. *et al.* Chitosan: A compound for drug delivery system in gastric cancer-a review. *Carbohydr. Polym.* **242**, (2020).
257. Fu, S., Xia, J. & Wu, J. Functional chitosan nanoparticles in cancer treatment. *J. Biomed. Nanotechnol.* **12**, 1585–1603 (2016).
258. Sonia, T. A. & Sharma, C. P. Chitosan and Its Derivatives for Drug Delivery Perspective. in *Chitosan for Biomaterials I* (eds. Jayakumar, R., Prabakaran, M., Muzzarelli, M. & Riccardo, A. A.) 23–53 (Springer-Verlag Berlin Heidelberg, 2011). doi:10.1007/978-3-642-23114-8.
259. A. D. McNaught and A. Wilkinson. Definitions of terms relating to the structure and processing of sols, gels, networks, and inorganic-organic hybrid materials. in *IUPAC. Compendium of Chemical Terminology* 1801 (Blackwell Scientific Publications, 2007).
260. Blanco, E., Shen, H. & Ferrari, M. Principles of nanoparticle design for overcoming biological barriers to drug delivery. *Nature Biotechnology* (2015) doi:10.1038/nbt.3330.
261. Storm, G., Belliot, S., Daemenb, T. & Lasic, D. D. Surface modification of nanoparticles to oppose uptake by the mononuclear phagocyte system. (1995).
262. Klibanov, A. L., Maruyama, K., Torchilin, V. P. & Huang, L. Amphipathic polyethyleneglycols effectively prolong the circulation time of liposomes. **268**, 235–237 (1990).
263. Karg, M. *et al.* Nanogels and Microgels: From Model Colloids to Applications, Recent Developments, and Future Trends. *Langmuir* **35**, 6231–6255 (2019).
264. Brannon-Peppas, L. Recent advances on the use of biodegradable microparticles and nanoparticles in controlled drug delivery. *International Journal of Pharmaceutics* (1995) doi:10.1016/0378-5173(94)00324-X.
265. Rao, K. V. R. & Buri, P. A novel in situ method to test polymers and coated microparticles for bioadhesion. *Int. J. Pharm.* (1989) doi:10.1016/0378-5173(89)90229-9.
266. Yang, J. *et al.* Microfluidic liposomes-anchored microgels as extended delivery platform for treatment of osteoarthritis. *Chem. Eng. J.* (2020) doi:10.1016/j.cej.2020.126004.
267. Silva, A. C., González-Mira, E., Lobo, J. M. & Amaral, M. H. Current Progresses on Nanodelivery Systems for the Treatment of Neuropsychiatric Diseases: Alzheimer's and Schizophrenia. *Curr. Pharm. Des.* (2013) doi:10.2174/138161281941131219123329.

References

268. Tao, J. *et al.* Polydiacetylene-Nanoparticle-Functionalized Microgels for Topical Bacterial Infection Treatment. *ACS Macro Lett.* (2019) doi:10.1021/acsmacrolett.9b00196.
269. Schwendener, R. A. Liposomes as vaccine delivery systems: A review of the recent advances. *Therapeutic Advances in Vaccines* (2014) doi:10.1177/2051013614541440.
270. Polack, F. P. *et al.* Safety and Efficacy of the BNT162b2 mRNA Covid-19 Vaccine. *N. Engl. J. Med.* (2020) doi:10.1056/nejmoa2034577.
271. Bao, H., Li, L., Leong, W. C. & Gan, L. H. Thermo-responsive association of chitosan-graft -poly(N -isopropylacrylamide) in aqueous solutions. *J. Phys. Chem. B* **114**, 10666–10673 (2010).
272. Jaiswal, M. K., Mehta, S., Banerjee, R. & Bahadur, D. A comparative study on thermoresponsive magnetic nanohydrogels: Role of surface-engineered magnetic nanoparticles. *Colloid Polym. Sci.* **290**, 607–617 (2012).
273. Constantin, M., Cristea, M., Ascenzi, P. & Fundueanu, G. Lower critical solution temperature versus volume phase transition temperature in thermoresponsive drug delivery systems. *Express Polym. Lett.* **5**, 839–848 (2011).
274. Grobelny, S. *et al.* Conformational changes upon high pressure induced hydration of poly(N-isopropylacrylamide) microgels. *Soft Matter* (2013) doi:10.1039/c3sm27653h.
275. Suzuki, D., Nagase, Y., Kureha, T. & Sato, T. Internal structures of thermosensitive hybrid microgels investigated by means of small-angle X-ray scattering. *J. Phys. Chem. B* (2014) doi:10.1021/jp410983x.
276. Sreekumar, S., Goycoolea, F. M., Moerschbacher, B. M. & Rivera-Rodriguez, G. R. Parameters influencing the size of chitosan-TPP nano- and microparticles. *Sci. Rep.* **8**, 1–11 (2018).
277. Alonso, M. J., Calvo, P. & Remun, C. Novel Hydrophilic Chitosan – Polyethylene Oxide Nanoparticles as Protein Carriers. 125–132.
278. Jonassen, H., Kjønksen, A. L. & Hiorth, M. Effects of ionic strength on the size and compactness of chitosan nanoparticles. *Colloid Polym. Sci.* **290**, 919–929 (2012).
279. Desai, K. G. H. Chitosan nanoparticles prepared by ionotropic gelation: An overview of recent advances. *Crit. Rev. Ther. Drug Carrier Syst.* **33**, 107–158 (2016).
280. Ajun, W., Yan, S., Li, G. & Huili, L. Preparation of aspirin and probucol in combination loaded chitosan nanoparticles and in vitro release study. *Carbohydr. Polym.* (2009) doi:10.1016/j.carbpol.2008.08.019.
281. Pan, Y. *et al.* Bioadhesive polysaccharide in protein delivery system: chitosan nanoparticles improve the intestinal absorption of insulin in vivo. *Int. J. Pharm.* **249**, 139–47 (2002).
282. Huang, Y. & Lapitsky, Y. Monovalent salt enhances colloidal stability during the formation of chitosan/tripolyphosphate microgels. *Langmuir* **27**, 10392–10399 (2011).
283. Jonassen, H., Kjønksen, A. L. & Hiorth, M. Stability of chitosan nanoparticles cross-linked with tripolyphosphate. *Biomacromolecules* **13**, 3747–3756 (2012).
284. Calvo P., Remuñan-López C., Vila-Jato J. L., A. M. J. Chitosan and Chitosan/Ethylene Oxide-Propylene oxide Block Copolymer Nanoparticles as Novel Carriers for Proteins and Vaccines. (1997).
285. Zhang, H., Oh, M., Allen, C. & Kumacheva, E. Monodisperse chitosan nanoparticles for mucosal drug delivery. *Biomacromolecules* **5**, 2461–2468 (2004).
286. Fan, W., Yan, W., Xu, Z. & Ni, H. Formation mechanism of monodisperse, low molecular

References

- weight chitosan nanoparticles by ionic gelation technique. *Colloids Surfaces B Biointerfaces* **90**, 21–27 (2012).
287. Tsai, M. L., Bai, S. W. & Chen, R. H. Cavitation effects versus stretch effects resulted in different size and polydispersity of ionotropic gelation chitosan-sodium tripolyphosphate nanoparticle. *Carbohydr. Polym.* (2008) doi:10.1016/j.carbpol.2007.06.015.
288. Horinek, D. DLVO Theory. in *Encyclopedia of Applied Electrochemistry* (eds. Kreysa, G., Ota, K. & Savinell, R. F.) 343–346 (Springer New York, 2014). doi:10.1007/978-1-4419-6996-5_7.
289. Russel, W. B., Saville, D. A. & Schowalter, W. R. Polymeric stabilization. in *Colloidal Dispersions* 310–328 (Cambridge University Press, 1989). doi:10.1017/CBO9780511608810.012.
290. Wang, M. *et al.* Preparation and Properties of Chitosan-Poly (N- isopropylacrylamide) Semi-IPN Hydrogels. 474–481 (1999).
291. Berger, J. *et al.* Structure and interactions in covalently and ionically crosslinked chitosan hydrogels for biomedical applications. *European Journal of Pharmaceutics and Biopharmaceutics* (2004) doi:10.1016/S0939-6411(03)00161-9.
292. Korsmeyer, R. W., Gurny, R., Doelker, E., Buri, P. & Peppas, N. A. Mechanisms of solute release from porous hydrophilic polymers. *Int. J. Pharm.* **15**, 25–35 (1983).
293. Higuchi, T. Mechanism of sustained-action medication. Theoretical analysis of rate of release of solid drugs dispersed in solid matrices. *J. Pharm. Sci.* **52**, 1145–1149 (1963).
294. Bruschi, M. L. 5 - Mathematical models of drug release. in *Strategies to Modify the Drug Release from Pharmaceutical Systems* (ed. Bruschi, M. L.) 63–86 (Woodhead Publishing, 2015). doi:https://doi.org/10.1016/B978-0-08-100092-2.00005-9.
295. Rao, K., Rao, K. & Ha, C.-S. Stimuli Responsive Poly(Vinyl Caprolactam) Gels for Biomedical Applications. *Gels* **2**, 6 (2016).
296. Prabakaran, M. & Mano, J. F. Stimuli-responsive hydrogels based on polysaccharides incorporated with thermo-responsive polymers as novel biomaterials. *Macromol. Biosci.* **6**, 991–1008 (2006).
297. Chen, J. P. & Cheng, T. H. Thermo-responsive chitosan-graft-poly(N-isopropylacrylamide) injectable hydrogel for cultivation of chondrocytes and meniscus cells. *Macromol. Biosci.* (2006) doi:10.1002/mabi.200600142.
298. Malhotra, M., Lane, C., Tomaro-Duchesneau, C., Saha, S. & Prakash, S. A novel method for synthesizing PEGylated chitosan nanoparticles: strategy, preparation, and in vitro analysis. *Int. J. Nanomedicine* **6**, 485–494 (2011).
299. Hirai, A., Odani, H. & Nakajima, A. Determination of degree of deacetylation of chitosan by 1H NMR spectroscopy. *Polym. Bull.* **26**, 87–94 (1991).
300. Xu, Y. & Du, Y. Effect of molecular structure of chitosan on protein delivery properties of chitosan nanoparticles. *Int. J. Pharm.* (2003) doi:10.1016/S0378-5173(02)00548-3.
301. Ugelstad, J. MONODISPERSE POLYMER PARTICLES AND DISPERSIONS THEREOF. *US Patent* (1984).
302. Shao, L., Hu, M., Chen, L., Xu, L. & Bi, Y. RAFT polymerization of N-vinylcaprolactam and effects of the end group on the thermal response of poly(N-vinylcaprolactam). *React. Funct. Polym.* **72**, 407–413 (2012).
303. Sanoj Rejinold, N. *et al.* Anti-cancer, pharmacokinetics and tumor localization studies of pH-, RF- and thermo-responsive nanoparticles. *Int. J. Biol. Macromol.* **74**, 249–262 (2015).

References

304. Rejinold, N. S. *et al.* Radio frequency triggered curcumin delivery from thermo and pH responsive nanoparticles containing gold nanoparticles and its in vivo localization studies in an orthotopic breast tumor model. *RSC Adv.* **4**, 39408–39427 (2014).
305. Rejinold, N. S. *et al.* Retraction: Radio frequency triggered curcumin delivery from thermo and pH responsive nanoparticles containing gold nanoparticles and its: In vivo localization studies in an orthotopic breast tumor model (RSC Advances (2014) 4 (39408–39427) DOI: 10.1039/C. RSC Adv. **10**, 28483 (2020).
306. Janes, K. A., Fresneau, M. P., Marazuela, A., Fabra, A. & Alonso, M. J. Chitosan nanoparticles as delivery systems for doxorubicin. *J. Control. Release* (2001) doi:10.1016/S0168-3659(01)00294-2.
307. Rampino, A., Borgogna, M., Blasi, P., Bellich, B. & Cesàro, A. Chitosan nanoparticles: Preparation, size evolution and stability. *Int. J. Pharm.* **455**, 219–228 (2013).
308. Hermosillo-Ochoa, E., Picos-Corrales, L. A. & Licea-Claverie, A. Eco-friendly flocculants from chitosan grafted with PNVCL and PAAc: Hybrid materials with enhanced removal properties for water remediation. *Sep. Purif. Technol.* **258**, 118052 (2021).
309. Niu, S. *et al.* A chitosan-based cascade-responsive drug delivery system for triple-negative breast cancer therapy. *J. Nanobiotechnology* **17**, 1–18 (2019).
310. De Campos, A. M., Diebold, Y., Carvalho, E. L. S., Sánchez, A. & Alonso, M. J. Chitosan nanoparticles as new ocular drug delivery systems: In vitro stability, in vivo fate, and cellular toxicity. *Pharm. Res.* (2004) doi:10.1023/B:PHAM.0000026432.75781.cb.
311. Medical University of South Carolina. NCT03712371: Study of Chitosan for Pharmacologic Manipulation of AGE (Advanced Glycation Endproducts) Levels in Prostate Cancer Patients. <https://clinicaltrials.gov/ct2/show/NCT03712371> (2018).
312. Menozzi, M., Valentini, L., Vannini, E. & Arcamone, F. Self-association of doxorubicin and related compounds in aqueous solution. *J. Pharm. Sci.* (1984) doi:10.1002/jps.2600730615.
313. Martin, H. Tetracyclines and daunorubicin. *Met. Ions Biol. Syst.* **19: Antibi**, 19–52 (1985).
314. Daugherty, J. P., Hixon, S. C. & Yielding, K. L. Direct in vitro photoaffinity labeling of DNA with daunorubicin, adriamycin, and rubidazone. *BBA Sect. Nucleic Acids Protein Synth.* (1979) doi:10.1016/0005-2787(79)90079-0.
315. Thoma, K., Stritmatter, T. and Steinbach, D. Untersuchungen zur photoinstabilität von antibiotika. *Acta Pharm. Technol.* **26**, 269–272 (1980).
316. TAVOLONI, N., GUARINO, A. M. & BERK, P. D. Photolytic degradation of adriamycin. *J. Pharm. Pharmacol.* (1980) doi:10.1111/j.2042-7158.1980.tb13094.x.
317. Arcamone, F. Daunomycin and related antibiotics. *Top. Antibiot. Chem.* **2**, 99–239 (1978).
318. Beijnen, J. H., van der Houwen, O. A. G. J. & Underberg, W. J. M. Aspects of the degradation kinetics of doxorubicin in aqueous solution. *Int. J. Pharm.* **32**, 123–131 (1986).
319. Beijnen, J. H., Wiese, G. & Underberg, W. J. M. Aspects of the chemical stability of doxorubicin and seven other anthracyclines in acidic solution. *Pharm. Weekbl. Sci. Ed.* **7**, 109–116 (1985).
320. Janes, K. A., Fresneau, M. P., Marazuela, A., Fabra, A. & Alonso, M. J. Chitosan nanoparticles as delivery systems for doxorubicin. *J. Control. Release* **73**, 255–267 (2001).
321. Sanyakamdhorn, S., Agudelo, D. & Tajmir-Riahi, H. A. Encapsulation of antitumor drug doxorubicin and its analogue by chitosan nanoparticles. *Biomacromolecules* **14**, 557–563 (2013).

References

322. Karnati, K. R. & Wang, Y. Understanding the co-loading and releasing of doxorubicin and paclitaxel using chitosan functionalized single-walled carbon nanotubes by molecular dynamics simulations. *Phys. Chem. Chem. Phys.* **20**, 9389–9400 (2018).
323. Yang, G., Wang, X., Fu, S., Tang, R. & Wang, J. pH-triggered chitosan nanogels via an ortho ester-based linkage for efficient chemotherapy. *Acta Biomater.* **60**, 232–243 (2017).
324. Almeida, A. *et al.* Novel amphiphilic chitosan micelles as carriers for hydrophobic anticancer drugs. *Mater. Sci. Eng. C* (2020) doi:10.1016/j.msec.2020.110920.
325. Eliaz, R. E. & Szoka, J. Liposome-encapsulated doxorubicin targeted to CD44: A strategy to kill CD44-overexpressing tumor cells. *Cancer Res.* **61**, 2592–2601 (2001).
326. Etrych, T., Chytil, P., Jelínková, M., Říhová, B. & Ulbrich, K. Synthesis of HPMA copolymers containing doxorubicin bound via a hydrazone linkage. Effect of spacer on drug release and in vitro cytotoxicity. *Macromol. Biosci.* **2**, 43–52 (2002).
327. Subr, V., Strohalm, J. & Ulbrich, K. Polymer containing enzymatically degradable bonds, XII. Effect of spacer structure on the rate of release of daunomycin and adriamycin from poly. *J. Control. release* **8**, 123–132 (1992).
328. Torre, L. A., Siegel, R. L., Ward, E. M. & Jemal, A. Global cancer incidence and mortality rates and trends - An update. *Cancer Epidemiology Biomarkers and Prevention* (2016) doi:10.1158/1055-9965.EPI-15-0578.
329. El-Serag, H. B., Davila, J. A., Petersen, N. J. & McGlynn, K. A. The continuing increase in the incidence of hepatocellular carcinoma in the United States: an update. *Ann. Intern. Med.* (2003) doi:10.7326/0003-4819-139-10-200311180-00009.
330. Ahmed, M. & Goldberg, S. N. Thermal ablation therapy for hepatocellular carcinoma. *Journal of Vascular and Interventional Radiology* (2002) doi:10.1016/s1051-0443(07)61791-6.
331. Lencioni, R., Petruzzi, P. & Crocetti, L. Chemoembolization of hepatocellular carcinoma. *Semin. Intervent. Radiol.* (2013) doi:10.1055/s-0033-1333648.
332. Kim, K. M. *et al.* Reappraisal of repeated transarterial chemoembolization in the treatment of hepatocellular carcinoma with portal vein invasion. *J. Gastroenterol. Hepatol.* (2009) doi:10.1111/j.1440-1746.2008.05728.x.
333. Choi, J. W. *et al.* Doxorubicin-loaded poly(lactic-co-glycolic acid) microspheres prepared using the solid-in-oil-in-water method for the transarterial chemoembolization of a liver tumor. *Colloids Surfaces B Biointerfaces* (2015) doi:10.1016/j.colsurfb.2015.05.037.
334. Yuan, H., Li, X., Tang, J., Zhou, M. & Liu, F. Local application of doxorubicin-loaded Iron oxid nanoparticles and the vascular disrupting agent via the hepatic artery: Chemoembolization-photothermal ablation treatment of hepatocellular carcinoma in rats. *Cancer Imaging* (2019) doi:10.1186/s40644-019-0257-x.
335. Marsili, L. *et al.* Characterization of thermoresponsive poly-N-Vinylcaprolactam polymers for biological applications. **4**, 1–15 (2021).
336. Kozanoğlu, S., Özdemir, T. & Usanmaz, A. Polymerization of N-vinylcaprolactam and characterization of poly(N-vinylcaprolactam). *J. Macromol. Sci. Part A Pure Appl. Chem.* **48**, 467–477 (2011).
337. Kirsh, Y. E. Water soluble poly-N-vinylamides: synthesis and physicochemical properties. *Chicester John Wiley Sons. Inc* 240 (1998) doi:10.1002/(sici)1097-0126(199905)48:5<426::aid-pi163>3.0.co;2-#.
338. Kasaai, M. R. Determination of the degree of N-acetylation for chitin and chitosan by

References

- various NMR spectroscopy techniques: A review. *Carbohydr. Polym.* **79**, 801–810 (2010).
339. Fernandez-Megia, E., Novoa-Carballal, R., Quiñoá, E. & Riguera, R. Optimal routine conditions for the determination of the degree of acetylation of chitosan by ¹H-NMR. *Carbohydr. Polym.* (2005) doi:10.1016/j.carbpol.2005.04.006.
340. Lavertu, M. *et al.* A validated ¹H NMR method for the determination of the degree of deacetylation of chitosan. *J. Pharm. Biomed. Anal.* **32**, 1149–1158 (2003).
341. Kumirska, J. *et al.* Application of spectroscopic methods for structural analysis of chitin and chitosan. *Mar. Drugs* **8**, 1567–1636 (2010).
342. Tan, S. C., Khor, E., Tan, T. K. & Wong, S. M. The degree of deacetylation of chitosan: Advocating the first derivative UV-spectrophotometry method of determination. in *Talanta* (1998). doi:10.1016/S0039-9140(97)00288-9.
343. Vårum, K. M., Antohansen, M. W., Grasdalen, H. & Smidsrød, O. Determination of the degree of N-acetylation and the distribution of N-acetyl groups in partially N-deacetylated chitins (chitosans) by high-field n.m.r. spectroscopy. *Carbohydr. Res.* **211**, 17–23 (1991).
344. Ioelovich, M. Crystallinity and Hydrophilicity of Chitin and Chitosan Crystallinity and Hydrophilicity of Chitin and Chitosan. (2016).
345. Ahirrao, S. P., Gide, P. S., Shrivastav, B. & Sharma, P. Ionotropic Gelation: A Promising Cross Linking Technique for Hydrogels. *J. Pharm. Nanotechnol.* **2**, 1–6 (2013).
346. de Alvarenga, E. S. Characterization and Properties of Chitosan. in *Biotechnology of Biopolymers* (2011). doi:10.5772/17020.
347. Abdelwahed, W., Degobert, G., Stainmesse, S. & Fessi, H. Freeze-drying of nanoparticles: Formulation, process and storage considerations. *Adv. Drug Deliv. Rev.* **58**, 1688–1713 (2006).
348. Abdelwahed, W., Degobert, G. & Fessi, H. A pilot study of freeze drying of poly(epsilon-caprolactone) nanocapsules stabilized by poly(vinyl alcohol): Formulation and process optimization. *Int. J. Pharm.* (2006) doi:10.1016/j.ijpharm.2005.10.003.
349. Imamura, K. *et al.* Characteristics of hydrogen bond formation between sugar and polymer in freeze-dried mixtures under different rehumidification conditions and its impact on the glass transition temperature. *J. Pharm. Sci.* (2008) doi:10.1002/jps.21066.
350. Taylor, L. S. Sugar-polymer hydrogen bond interactions in lyophilized amorphous mixtures. *J. Pharm. Sci.* (1998) doi:10.1021/js9800174.
351. Chang, L. *et al.* Mechanism of protein stabilization by sugars during freeze-drying and storage: Native structure preservation, specific interaction, and/or immobilization in a glassy matrix? *J. Pharm. Sci.* (2005) doi:10.1002/jps.20364.
352. Williams, D. B. & Carter, C. B. *Transmission electron microscopy: A textbook for materials science. Transmission Electron Microscopy: A Textbook for Materials Science* (2009). doi:10.1007/978-0-387-76501-3.
353. Holzwarth, U. & Gibson, N. The Scherrer equation versus the ‘Debye-Scherrer equation’. *Nat. Nanotechnol.* **6**, 534 (2011).
354. Di Martino, A., Kucharczyk, P., Capakova, Z., Humpolicek, P. & Sedlarik, V. Chitosan-based nanocomplexes for simultaneous loading, burst reduction and controlled release of doxorubicin and 5-fluorouracil. *Int. J. Biol. Macromol.* **102**, 613–624 (2017).
355. Morgner, F. *et al.* Terbium to quantum dot FRET bioconjugates for clinical diagnostics: Influence of human plasma on optical and assembly properties. *Sensors* (2011) doi:10.3390/s111009667.

References

356. Zijlstra, W. G. & Buursma, A. Spectrophotometry of hemoglobin: Absorption spectra of bovine oxyhemoglobin, deoxyhemoglobin, carboxyhemoglobin, and methemoglobin. *Comp. Biochem. Physiol. - B Biochem. Mol. Biol.* (1997) doi:10.1016/S0305-0491(97)00230-7.
357. Watanabe, A. *et al.* A Simple and Easy Method of Monitoring Doxorubicin Release from a Liposomal Drug Formulation in the Serum Using Fluorescence Spectroscopy. **67**, 367–371 (2019).
358. Siepmann, J. & Siepmann, F. Mathematical modeling of drug delivery. *Int. J. Pharm.* **364**, 328–343 (2008).
359. Sing Mahat, B. Mathematical models used in the drug release studies. 0–26 (2009).
360. Berth, G. & Dautzenberg, H. The degree of acetylation of chitosans and its effect on the chain conformation in aqueous solution. *Carbohydr. Polym.* (2002) doi:10.1016/S0144-8617(00)00343-X.
361. Śliwa, T., Jarzębski, M. & Szutkowski, K. Nanoparticle Tracking Analysis of Latex Standardized Beads. *Curr. Top. Biophys.* (2015) doi:10.2478/ctb-2014-0074.
362. NanoSight. *NTA 2.0 analytical software, operating manual.* (NanoSight Ltd., 2010).
363. Filipe, V., Hawe, A. & Jiskoot, W. Critical Evaluation of Nanoparticle Tracking Analysis (NTA) by NanoSight for the Measurement of Nanoparticles and Protein Aggregates. **27**, 796–810 (2010).
364. Isa, L., Jung, J. M. & Mezzenga, R. Unravelling adsorption and alignment of amyloid fibrils at interfaces by probe particle tracking. *Soft Matter* (2011) doi:10.1039/c1sm05602f.
365. Jarzębski, M. *et al.* Particle tracking analysis in food and hydrocolloids investigations. *Food Hydrocoll.* **68**, 90–101 (2017).
366. Matyjaszewski, K. *Advances in Controlled / Living Radical Polymerization*,. (ACS, 2003).
367. Braun, D. Origins and development of initiation of free radical polymerization processes. *International Journal of Polymer Science* (2009) doi:10.1155/2009/893234.
368. Braun, D. *Polymer Syntheses.* (Academic Press, 1974).
369. Braunecker, W. A. & Matyjaszewski, K. Controlled/living radical polymerization: Features, developments, and perspectives. *Progress in Polymer Science (Oxford)* (2007) doi:10.1016/j.progpolymsci.2006.11.002.
370. Wang, J. S. & Matyjaszewski, K. Controlled/“Living” Radical Polymerization. Atom Transfer Radical Polymerization in the Presence of Transition-Metal Complexes. *J. Am. Chem. Soc.* (1995) doi:10.1021/ja00125a035.
371. Johnson, I. J. Synthesis and Characterisation of Polymeric Materials via RAFT Polymerisation. 332 (2013).
372. Young, R. J. & Lovell, P. A. *Introduction to Polymers.* (CRC Press, 2011).
373. Gokhale, A. Achieving zero-order release kinetics using multi-step diffusion-based drug delivery. *Pharm. Technol. Eur.* **38**, (2014).
374. Potenza, M. *et al.* Graphene nanoplatelets: Thermal diffusivity and thermal conductivity by the flash method. *AIP Adv.* **7**, (2017).